UNIVERSITY OF OKLAHOMA

GRADUATE COLLEGE

INFLUENCE OF HYDRAULIC HYSTERESIS ON THE MECHANICAL BEHAVIOR OF UNSATURATED SOILS AND INTERFACES

A DISSERTATION

SUBMITTED TO THE GRADUATE FACULTY

in partial fulfillment of the requirements for the

Degree of

DOCTOR OF PHILOSOPHY

By

CHARBEL N. KHOURY
Norman, Oklahoma
2010

INFLUENCE OF HYDRAULIC HYSTERESIS ON THE MECHANICAL BEHAVIOR OF UNSATURATED SOILS AND INTERFACES

A DISSERTATION APPROVED FOR THE
SCHOOL OF CIVIL ENGINEERING AND ENVIRONMENTAL SCIENCE

BY

_____
Dr. Gerald A. Miller, Chair

_____
Dr. Kanthasamy K. Muraleetharan

_____
Dr. Kianoosh A. Hatami

_____
Dr. Tohren C. Kibbey

_____
Dr. James D. Baldwin

This Dissertation is dedicated to my beloved

Mom and Dad (Isabelle & Najib), Sister (Andree) and Brothers (George, Dany & Naji)

Whose Love and Support Contributed to this Achievement

ACKNOWLEDGMENTS

I would like to express my sincere gratitude to my supervisor, Professor Gerald A. Miller for his continuous guidance, patience, and support during this study. Appreciation is expressed to him particularly for his valuable discussion and revision of the materials contained in this Dissertation. Special thanks are given to my committee members, Dr. Kanthasamy K. Muraleetharan, Dr. Kianoosh Hatami, Dr. Tohren C. Kibbey and Dr. James D. Baldwin for their valuable comments that helped improve the quality of this work and completion of the Dissertation.

I would also like to thank all the Staff at the School of Civil Engineering and Environmental Science, specifically, Mrs. Audre Carter, Mrs. Brenda Clouse, Ms. Molly Smith, Mrs. Susan Williams, and Ms. Dianne Wishard for their help and for making this Department feel like home. Special thanks and appreciation go to Mr. Mike Schmitz for his valuable assistance in the laboratory, and particularly for his exceptional skills in the fabrication of some of the unsaturated testing apparatus used in this study. I would like to thank my brother Dr. Naji Khoury for his overwhelming support and assistance throughout all these years.

I dedicate this work to my best friends, who were of good acquaintance to me, and to my family, especially to my mother, father, sister and brothers. Without their understanding, love and support, this research would have become impossible to accomplish.

TABLE OF CONTENTS

LIST OF TABLES

LIST OF FIGURES

ABSTRACT:

Unsaturated soils are commonly widespread around the world, especially at shallow depths from the surface. The mechanical behavior of this near surface soil is influenced by the seasonal variations such as rainfall or drought, which in turn may have a detrimental effect on many structures (e.g. retaining walls, shallow foundations, mechanically stabilized earth walls, soil slopes, and pavements) in contact with it. Thus, in order to better understand this behavior, it is crucial to study the complex relationship between soil moisture content and matric suction (a stress state variable defined as pore air pressure minus pore water pressure) known as the Soil Water Characteristic Curve (SWCC). This relationship is hysteretic, i.e., at given suction the moisture content differs depending on the drying and wetting paths. This hysteretic behavior is also referred to as hydraulic hysteresis.

The behavior of the SWCC has been widely studied and various models have been developed to capture this hysteretic behavior, but limited experimental data are available under different applied stresses (or at different void ratios) and do not include secondary dyring or scanning curves. The lack of SWCC experimental data is due to the long testing time of unsaturated soils. To this end, a new procedure was developed to shorten equilibrium time and obtain SWCC data as practically fast as possible. This new approach was used and SWCC tests under different stress states on silty soil specimens under drying, wetting, secondary drying, and along scanning curves were performed. Results from this study helped improve and validate existing models such as the elastoplastic constitutive model reported by Miller et al. (2008).

In addition, the influence of hydraulic hysteresis on the behavior of unsaturated soils, soil-structure interaction (i.e. rough and smooth steel interfaces, soil-geotextile interfaces) and pavement subgrade (depicted herein mainly by resilient modulus, M_r) was also studied. To this end, suction-controlled direct shear tests were performed on soils, rough and smooth steel interfaces and geotextile interface under drying (D) and wetting after drying (DW). The shearing behavior is examined in terms of the two stress state variables, matric suction and net normal stress. Results along the D and DW paths indicated that peak shear strength increased with suction and net normal stress; while in general, the post peak shear strength was not influenced by suction for rough interfaces and no consistent trend was observed for soils and soil-geotextiles interfaces. Contrary to saturated soils, results during shearing at higher suction values (i.e. 25 kPa and above) showed a decrease in water content eventhough the sample exhibited dilation. A behavior postulated to be related to disruption of menisci and/or non-uniformity of pore size which results in an increase in localized pore water pressures. Interestingly, wetting after drying (DW) test results showed higher peak and post peak shear strength than that of the drying (D) tests. This is believed to be the result of many factors such as: 1) cyclic suction stress loading, 2) water content (less on wetting than drying), and 3) type of soil. The cyclic suction loading may have induced irrecoverable plastic strains, resulting in stiffer samples for wetting tests as compared to drying. Additionally, water may be acting as a lubricant and thus resulting in lower shear strength for test samples D with higher water contents than DW samples.

Furthermore, various shear strength models were investigated for their applicability to the experimental data. Models were proposed for the prediction of shear strength with

suction based on the SWCC. The models are able to predict the shear strength of unsaturated soil and interfaces due to drying and wetting (i.e. hydraulic hysteresis) by relating directly to the SWCC. The proposed models were used and partly validated by predicting different test results from the literature. In addition, an existing elastoplastic constitutive model was investigated and validated by comparing the predicted and experimental (stress-displacement, volume change behavior) results obtained from rough and geotextile interface tests.

This study also explores the effect of hydraulic hysteresis on the resilient modulus (M_r) of subgrade soils. Suction-controlled M_r tests were performed on compacted samples along the primary drying, wetting, secondary drying and wetting paths. Two test types were performed to check the effect of cyclic deviatoric stress loading on the results. First, M_r tests were performed on the same sample at each suction (i.e. 25, 50, 75, 100 kPa) value along all the paths (drying, wetting etc.). A relationship between resilient modulus (M_r) and matric suction was obtained and identified as the resilient modulus characteristic curve (MRCC). MRCC results indicated that M_r increased with suction along the drying curve. On the other hand, results on the primary wetting indicated higher M_r than that of the primary drying and the secondary drying. The second type of test was performed at selected suction without subjecting the sample to previous M_r tests. Results indicated that M_r compared favorably with the other type of test (i.e. with previous M_r testing), which indicates that the cyclic deviatoric stress loading influence was not as significant as the hydraulic hysteresis (i.e. cyclic suction stress loading). A new model to predict the MRCC results during drying and wetting (i.e., hydraulic hysteresis) is

proposed based on the SWCC hysteresis. The model predicted favorably the drying and then the wetting results using the SWCC at all stress levels.

CHAPTER 1: INTRODUCTION

1.1 INTRODUCTION

It has been commonly recognized that saturated soil mechanics is not always the realistic approach to use in many geotechnical engineering applications. Many structures such as retaining walls, shallow foundations, mechanically stabilized earth (MSE) walls, reinforced soil slopes (RSS), landfill liners, tunnels, pavements and others, are frequently constructed in contact with unsaturated soils and subject to variations of moisture content due to climate changes. This variation of moisture content can greatly influence the mechanical behavior of soil. One important relationship is that between soil moisture content and suction (i.e. matric suction, defined as u_a - u_w, where u_a is pore air pressure and u_w pore water pressure) as reflected in the Soil Water Characteristic Curve (SWCC).

Results of research presented in this dissertation addresses three important aspects of soil behavior related to the SWCC. First, SWCC hysteretic behavior and influence of soil state; second, effect of the SWCC hysteresis on unsaturated soils and interfaces; and finally, the effect of SWCC hysteresis on resilient modulus of soils.

1.1.1 Soil Water Characteristic Curve Hysteresis and Influence of Soil State

The SWCC has been a fundamental component in predicting the shear strength, volume change, and hydraulic conductivity of unsaturated soils (Freedlund and Rahardjo 1993, Fredlund et al. 1994, Vanapalli et al. 1996, 1999). However, the SWCC shows a hysteretic behavior where different values of moisture content (e.g. due to climate changes) can correspond to the same suction depending on the drying and wetting paths. The hysteretic behavior of the SWCC has been widely studied, and various models (e.g. Wheeler et al. 2003, Pham et al. 2005, Wei and Dewoolkar 2006, Li 2007a&b, Sun et al.

2007a, Muraleetharan et al. 2008, and Miller et al. 2008) have been developed to capture this behavior. While major progress has been made, it is shown below that further research is needed to improve and validate existing models. There are limited experimental data available addressing the hysteretic behavior of SWCC under different applied stresses (or at different void ratios). For example, some recent data incorporating hysteresis do exist (e.g. Ng and Pang 2000, Tarantino and Tombolato 2005, Ho et al. 2006); however, the data typically does not include secondary drying or scanning curves. Since matric suction and water content impact the soil skeleton stress, the mechanical behavior of unsaturated soil is thus strongly dependent on the SWCC hysteresis. Thus, laboratory tests of SWCCs under different stresses on silty soil specimens under drying, wetting, secondary drying, and along scanning curves were performed and presented herein. Part of the results of the SWCC obtained in this study were presented and used to improve and validate an elastoplastic constitutive model as reported by Miller et al. (2008). The influence of the SWCC hysteresis behavior on two important geotechnical engineering problems, mainly unsaturated interfaces and resilient modulus, are also studied and presented.

1.1.2 Influence of Hydraulic Hysteresis on the Behavior of Unsaturated Interfaces

Soil-structure interaction, a common problem in geotechnical engineering, has been widely studied in an attempt to obtain better and more realistic solutions. Typical examples of such structures include pile foundations, retaining structures, mechanically stabilized earth (MSE) walls, reinforced soil slopes (RSS), and liners for landfills and tunnels. Deep foundations (piles) have been used extensively for the support of buildings, bridges, and other structures **(**Bradshaw and Baxter 2006) and often these piles penetrate

a zone of unsaturated soil. Yet, no systematic approaches to designing piles in unsaturated soil are widely adopted. Another important example of interfaces in unsaturated soil includes retaining structures, which have been used for bridge abutments, slope stabilization, and many other applications. As reported by Elias et al. (2001), retaining walls are essential for almost every highway design. According to Elias et al. (2001), the use of the new innovative methods (i.e. MSE and RSS), which are cost effective and can tolerate larger settlements than reinforced concrete walls, has drastically increased worldwide and specifically in the United States. For instance, on average more than 850,000 m^2 of MSE and 190,000 m^2 of RSS are constructed every year in the United States (Berg et al. 2009). Therefore, it is crucial to understand the behavior of these structures. Their design is often dominated by the shear strength of the interface between reinforcement layers and soil. Herein, an interface is defined as the contact zone between soil and the other material such as steel, concrete, or geosynthetic.

Since most of these structures are built in unsaturated soil conditions, one main concern in stability analysis and design is the reduction of the soil interface shear strength as a result of wetting. Factors such as seasonal precipitation and variation of ground water table can significantly alter the soil moisture condition and suction, and thus the interface behavior. As a result, the influence of soil suction on the shearing response of unsaturated interfaces should be investigated.

Numerous studies have been carried out to assess the interface behavior between soil and other construction materials. A few studies involving interfaces include work by Desai et al. (1986), Fakharian and Evign (1996), and Hu and Pu (2004) among others. A variety of equipment has been used to study interface behavior such as simple shear

(Kishida and Uesugi 1987), direct shear (Potyondy 1961), and torsion (Yoshimi and Kishida 1981) devices, among others. While previous studies provided important information on which to build, they did not address interface behavior in unsaturated soil.

To the authors' knowledge, Hamid (2005) and Miller and Hamid (2007), were among the first to conduct a systematic study of unsaturated interfaces. They designed and constructed a new apparatus for testing of interfaces between unsaturated soil and steel. The device is able to control the matric suction in the soil while shearing against a steel plate. It was reported that the maximum shear stress of interfaces between unsaturated soil and steel is a function of net normal stress and suction. In their study, suction was controlled following a drying path on the soil water characteristic curve (SWCC). While Hamid (2005) and Miller and Hamid (2007) paved the road for unsaturated interface behavior, further research is needed to study the effect of hysteresis on the interface strength parameters. To this end, the effect of hysteresis on unsaturated interfaces was investigated and will be presented in this dissertation. Furthermore, the interface shearing behavior is examined in terms of matric suction and net normal stress. Various shear strength models are investigated for their applicability to the experimental data. The influence of hysteresis on shear strength will be considered by incorporating SWCCs into prediction models. In addition, investigation and validation of the elastoplastic constitutive model developed by Hamid and Miller (2008) is conducted by comparing prediction results to laboratory results obtained on a different soil type and using a different interface, specifically geotextile.

1.1.3 Influence of Hydraulic Hysteresis on the Resilient Modulus of Fine-Grained Soil

Pavement structures have been a vital part in the economic growth of the nation. However, this economic growth requires significant investment to build and maintain the highway infrastructure. Research that leads to improved longer lasting pavements is crucial to maximize the benefit of this investment. One issue that deserves attention, as reported by the AASHTO design guide, is the Resilient Modulus (M_r) of subgrade soil. Although numerous related studies have been conducted on resilient modulus over the past years (e.g., Khoury and Zaman 2004, Kung et al. 2006, Liang et al. 2007, Khoury and Khoury 2009, Khoury et al. 2009), no research has been conducted to address the effect of suction hysteresis on resilient modulus of subgrade soils. In a pavement structure, changes in moisture content can significantly influence the subgrade layer and hence, its carrying capacity (AASHTO 2007). For this reason the new Mechanistic-Empirical Pavement Design Guide (MEPDG) includes provisions to predict the variation of resilient modulus (M_r) of pavement subgrades with moisture changes due to seasonal variations. While this is a very important step towards better pavement performance, there is still much research to be done to fully understand the role of moisture content changes (e.g. suction hysteresis) in subgrade behavior and pavement performance. Since the mechanical properties of fine-grained soils are strongly dependent on the matric suction, it is critical to understand the influence of suction and its hysteretic behavior on Resilient Modulus (M_r). This study assessed the effect of soil suction hysteresis on the resilient modulus of subgrade soils. Findings were used to develop and modify existing models to predict the resilient modulus (M_r) by incorporating the effect of the SWCC hysteresis.

1.2 OBJECTIVES AND SCOPE OF RESEARCH

It is hypothesized that the stress path (i.e. hysteresis) relative to the SWCC will have a significant influence on the shearing behavior of unsaturated soils/interfaces and on the resilient modulus (M_r) of subgrade soils, particularly fine-grained soils. By significant influence, it is meant that results will be outside the range of experimental errors which will be based mainly on repeated tests. To this end, the objectives of this research are to: (1) study and investigate the SWCC hysteresis as a function of stress state, (2) examine methods to decrease testing time for SWCC with hysteresis, (3) investigate the effect of SWCC hysteresis on the shearing behavior of unsaturated soils (steel interfaces and geosynthetics), and (4) investigate the effect of SWCC hysteresis on the resilient modulus of subgrade soils.

In order to achieve the aforementioned objectives, the scope of this research can be summarized as follows:

(1) Conduct a series of SWCC tests on different types of soils (mainly Sil-Co-Sil (SCS), a mixture of SCS and glass beads) and different sample heights to investigate methods to decrease SWCC testing time.

(2) Obtain a series of SWCCs with hysteresis (drying, wetting, and scanning curves) under different stress path history (i.e. under different normal stresses).

(3) Use the experimental results of SWCC hysteresis to validate an existing model (as shown by Miller et al. 2008).

(4) Conduct interface (i.e. steel interfaces) tests with suction control in unsaturated soil.

(5) Conduct suction-controlled soil-geotextile interface tests in unsaturated soil.

(6) Perform unsaturated interface testing following the SWCC hysteresis path and evaluate its effect on the shear strength results.

(7) Modify/develop models (e.g. Vanapalli et al., 1996) to predict the unsaturated shear strength of soils and interfaces (steel and geosynthetic interfaces) that captures the influence of hydraulic hysteresis by making use of the SWCC.

(8) Validate and improve the model by Hamid & Miller (2008) that accounts for the effect of suction and net normal stress of unsaturated interfaces by predicting the experimental results on different kind of soils and different interfaces such as steel and geotextiles.

(9) Perform resilient modulus (M_r) tests following different stress paths (drying/wetting, as reflected by the SWCC hysteresis) on a silty soil, and evaluate the effect of hysteresis on the results.

(10) Develop a relationship between resilient modulus and matric suction hysteresis known as Resilient Modulus Characteristic Curve (MRCC).

(11) Modify/Develop a model to predict the resilient modulus (M_r) hysteretic behavior from the experimental results by relating it to the SWCC hysteresis.

1.3 DISSERTATION OUTLINE

The Dissertation is divided into five chapters with mainly 3 subjects. Chapter 1 presents the introduction, which also includes the objectives and scope of research. Chapter 2 presents the first subject which is the Soil Water Characteristic Curve (SWCC) hysteresis. Chapter 3 presents the second subject on shearing behavior of unsaturated soils and interfaces (rough and smooth steel and geotextiles) as influenced by hydraulic

hysteresis. Chapter 4 presents the third subject related to unsaturated resilient modulus and suction hysteresis. Each of the three latter chapters includes various sections: a) literature review, b) materials/sample preparation and testing equipment, c) experimental test procedures, d) test results and discussions, and e) modeling. Finally, Chapter 5 consists of the conclusions and recommendations for future research.

CHAPTER 2: SOIL WATER CHARACTERISTIC CURVE

2.1 INTRODUCTION

The soil water characteristic curve (SWCC) is defined as the relationship between soil suction and water content (typically gravimetric or volumetric). This curve represents basic characteristics of unsaturated soils, from which many engineering properties (e.g. hydraulic conductivity, shear strength) have been determined. Thus, it is crucial to accurately obtain the SWCC of soils under different conditions. While major progress has been made to measure the SWCC, there are limited experimental data available on the hysteretic behavior of the SWCC under different stress states. The lack of SWCC hysteresis results (i.e. beyond primary drying and wetting curves) is largely due to the enormous testing time required for unsaturated soils. In this study, a new approach was developed and used to evade this problem to some extent by using an artificial soil and reducing the sample height of the soil sample to shorten equilibrium time. First, a series of tests was conducted to optimize the testing geometry while shortening the equilibrium time. Then, laboratory tests to determine SWCCs at different stresses and initial conditions (i.e. initially saturated and as compacted) under drying, wetting, secondary drying, and along scanning curves were performed on the silty soil and selected sample height. Some existing functional form models were used to fit part of the experimental data; the fitting model parameters obtained are key parameters used to predict the shear strength of unsaturated soils and interfaces with suction. In addition, the SWCC hysteresis results from this study were used to validate an elastoplastic constitutive model (developed by Muraleetharan et al. 2008) reported by Miller et al. (2008) and presented again in this study. The experimental approach and data obtained demonstrate the

significant contribution to the forward progression of constitutive modeling (e.g. by using the results to validate existing models).

2.2 LITERATURE REVIEW

2.2.1 Matric Suction

Before discussing the importance and complexity of the SWCC, it is instructive to look at a simple physical explanation of matric suction. Matric suction is associated with air-water menisci, which develops due to capillary action of water in the unsaturated soil pores. The interaction between solid particles, air, and water results in a thin layer (i.e. contractile skin) at the air-water interface. Due to the difference in pressure between air and water (i.e. u_a-u_w, defined as matric suction) and the presence of surface tension, the contractile skin is curved and forms a meniscus, as shown in Figure 2.1.

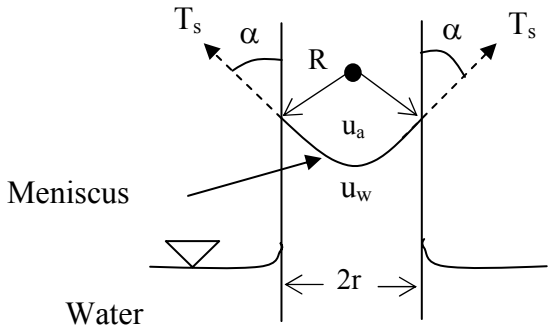

Figure 2.1- Illustration of a Capillary Tube Immersed in Water

As shown in Figure 2.1, water rises in a capillary tube immersed in water, similarly to the air and water in pores of the soil, where the pressure difference across the meniscus results in the following relation:

$$(u_a - u_w) = 2T_s / R \qquad \textbf{(2.1)}$$

where, u_a = air pressure; u_w = water pressure; T_s = surface tension of water, R = r/cos α = radius of curvature of meniscus, r = radius of tube (similar to radius of pores in soil), and α = contact angle.

This phenomenon is analogous to water in soil pores where R is a function of pores shape, size and particle minerology. The smaller the pore radius, the higher the soil suction. This indicates that the SWCC relation differs from one soil to another. The smaller voids in clayey soils are one of the reasons for higher suction than in granular soils. As the soil de-saturates and water recedes into smaller pores, the radius of curvature (R) of the meniscus decreases, and thus leads to an increase in matric suction. Similarly, suction decreases when water content increases.

2.2.2 Aspects of the Soil Water Characteristic Curve

A typical SWCC is shown in Figure 2.2, from which it is clear that this relationship is not unique even for the same soil; for a given suction value the moisture content varies depending on the drying and wetting paths (hysteresis behavior). The reasons for SWCC hysteresis have been investigated by many researchers (e.g. Bear, 1972, Adamson, 1990, Lu and Likos, 2004). Several factors contribute to the SWCC hysteresis such as a) contact angle variation during the wetting and drying process, b) non-uniformity of pore size in soil (ink bottle effect), and c) entrapped air in soil. During wetting the contact angle (θ_1) is larger than the one (θ_2) during drying as shown in Figure 2.3. Contact angle (θ_1) is known as the advancing contact angle moving on a surface during wetting while θ_2 is the receding contact angle. The difference in the contact angle may contribute to the SWCC hysteresis where the suction, according to Equation (2.1), is higher during drying (lower contact angle θ_1) than wetting (larger contact angle) at a given water content

value. The ink bottle effect is explained by the non-uniformity of pore size in soils. Pores (radius R_1) are usually larger than their openings (radius r_1), as shown in Figure 2.4 (Marshal et al. 1996). During wetting, which is an upward capillary flow, the capillary rise (h_w) is controlled by the radius opening (small r_1). However, during drying, which is the case where the capillary tube is initially filled with water, the capillary rise (h_d) is beyond the larger pore radius (R_1). The capillary rise represents suction and is related to pore radius as presented by Equation (2.1). On this basis, at a given suction (capillary rise) the water content of the drying pore exceeds that of the wetting as seen in Figure 2.2 and Figure 2.4.

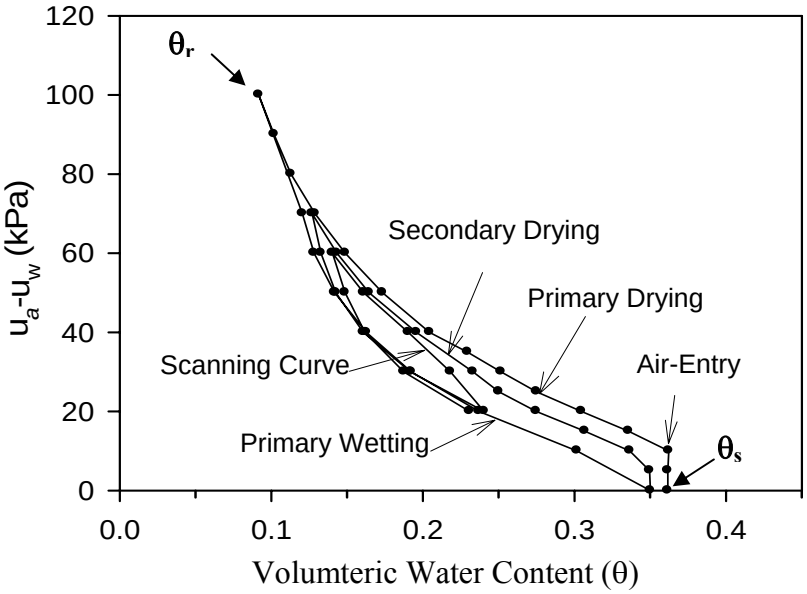

Figure 2.2- Typical Soil Water Characteristic Curve

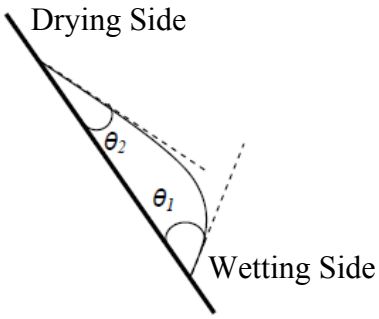

Figure 2.3- Illustration of Contact Angle for Advancing (θ1, wetting) and Receding (θ2, drying) Meniscus

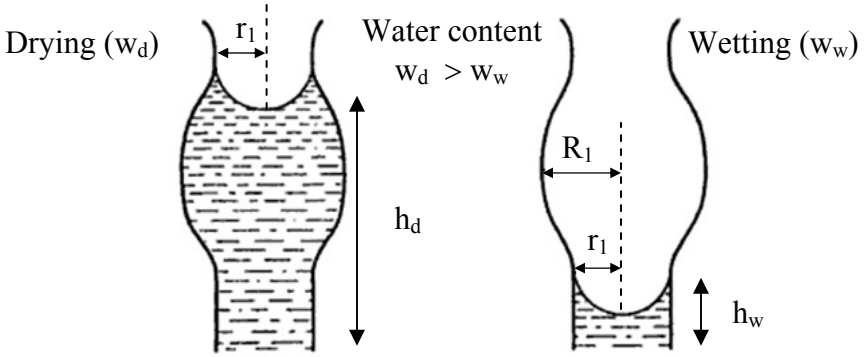

Figure 2.4- Illustration of Pore Non-Uniformity Effect on SWCC Hysteresis (After Marshal et al. 1996)

The different paths on the SWCC (Figure 2.2) are defined as the primary drying, primary wetting, secondary drying and secondary wetting curves, and the scanning curves, which are the curves that initiate inside the primary wetting and the secondary drying curves. Another important parameter shown in Figure 2.2 is the air entry value that is defined as the pressure (i.e. suction) after which air starts to fully penetrate into the pores of the soil during initial drainage.

The SWCC has been extensively studied (e.g. Fredlund and Xing 1994, Barbour 1998, Leong and Rahardjo 1997, Feng and Fredlund 1999, Vanapalli et al. 2001) and has been used as a basic function to predict, for example, the shear strength, and hydraulic conductivity of unsaturated soils (Fredlund et al. 1994, Vanapalli et al. 1996, 1999). But

since the SWCC is hysteretic, recent studies have been conducted to capture such behavior and incorporate it into mathematical models (e.g. Wheeler et al. 2003, Gallipoli et al. 2003, Yang et al. 2004a, Pham et al. 2005, Wei and Dewoolkar 2006, Li 2007a&b, Sun et al. 2007a, Kohgo 2008, Muraleetharan et al. 2008, and Miller et al. 2008 among others). There are limited experimental data available on the hysteretic behavior of SWCCs under different externally applied stress or different void ratios (e.g. Romero et al. 1999, Karube and Kawai 2001, Tarantino and Tombolato 2005, Ho et al. 2006). Data from these studies reveal that samples were prepared at different initial void ratios and thus differences in behavior may originate from variations in fabric/structure caused during sample preparation and not variations in void ratio caused by externally applied stress. In addition, SWCC data typically includes results of primary drying and wetting curves (i.e. no secondary drying/wetting or scanning curves), which is largely due to the long time requirements for unsaturated soil testing (a problem that was reduced to an extent in this study as discussed in later sections).

SWCC tests (following the primary drying/wetting, secondary drying and scanning curves) were thus obtained in this study for different stress histories (i.e. under different normal stresses) and were used to validate an existing model as shown by Miller et al. (2008).

2.3 MATERIALS, SAMPLE PREPARATION AND TESTING EQUIPMENT

2.3.1 Soil Material and Sample Preparation

Excessively long periods have been necessary to produce experimental data for unsaturated soils, particularly if wetting and drying cycles (i.e., hysteresis) are involved. Thus, a manufactured soil that provides levels of matric suction consistent with a silty

soil, but with considerably greater hydraulic conductivity (6 x 10^{-5} cm/sec) than most natural soils with similar suction ranges is used in this study in order to obtain experimental results in a reasonable amount of time.

The artificial soil used is a mixture of two commercially available manufactured soils, Sil-Co-Sil 250 (SCS), with nominal particle size range of 0.002 to 0.212 mm, manufactured by U.S. Silica Company and Glass Beads, Size BT-9 (nominal particle size range = 0.127 to 0.178 mm), manufactured by Zero Products. The soil mixture consists of 75% ground silica and 25% glass beads. The mixture has a grain size distribution (Figure 2.5) similar to that of fine sandy silt having about 48% fine sand (0.075-0.25 mm), 46% silt (0.002-0.075 mm), and 6% clay size material ($\leq$ 0.002 mm). Based on standard compaction tests, the soil mixture has a maximum dry unit weight (γ_d) of 16.3 kN/m^3 (103.6 pcf) and optimum moisture content (OMC) of 16.5%.

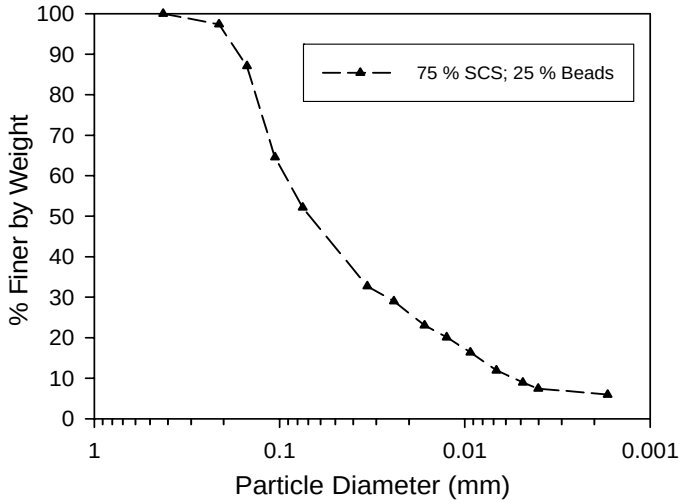

Figure 2.5- Grain Size Distribution of the Soil Mixture Used in this Study

The soil specimens prepared in this study, for all tests, were compacted to an initial dry unit weight of 15.4 kN/m^3 and at a moisture content of 17.2 $\pm$ 1%. Soil is mixed to

the desired moisture content and compacted to the required density by moist tamping (i.e. volume-based compaction) inside the test cell device (Section 2.3.2).

2.3.2 SWCC Testing Device

A custom made test cell was designed and built at the University of Oklahoma to obtain different sets of Soil Water Characteristic Curves (SWCC). Schematic and photographic views of the test cell are shown in Figure 2.6. The pore-water and pore-air pressures are digitally controlled using two commercially available high precision motorized piston pumps, which can accurately control pressure and volume changes to a resolution on the order of 1 kPa and 1 mm^3, respectively. The water is transmitted to the soil via a high air entry porous disc (HAEPD) having an air entry value of 3 bar.

The experimental apparatus allows for continuous control and measurement of the pore air pressure (u_a) and pore water pressure (u_w) throughout testing. Different cells were fabricated to obtain SWCCs with and without vertical net normal stress. One test cell was fabricated to fit into a one dimensional consolidation apparatus as shown in Figure 2.6b and Figure 2.6c, so that incremental vertical loading can be externally applied while independently controlling u_a and u_w in the soil sample. A vertical normal stress is applied to the sample through a stainless steel piston acting against the rigid top platen above the sample and linear variable differential transformers (LVDTs) are used to measure the vertical deformation of the sample during the test. For the SWCC tests, the LVDT resolution was estimated at approximately 1.68×10^{-4} mm. The experimental apparatus allows for independent control/measurement of suction (i.e. difference between air pressure and water pressure) and vertical net normal stress throughout testing so that a variety of loading sequences can be investigated.

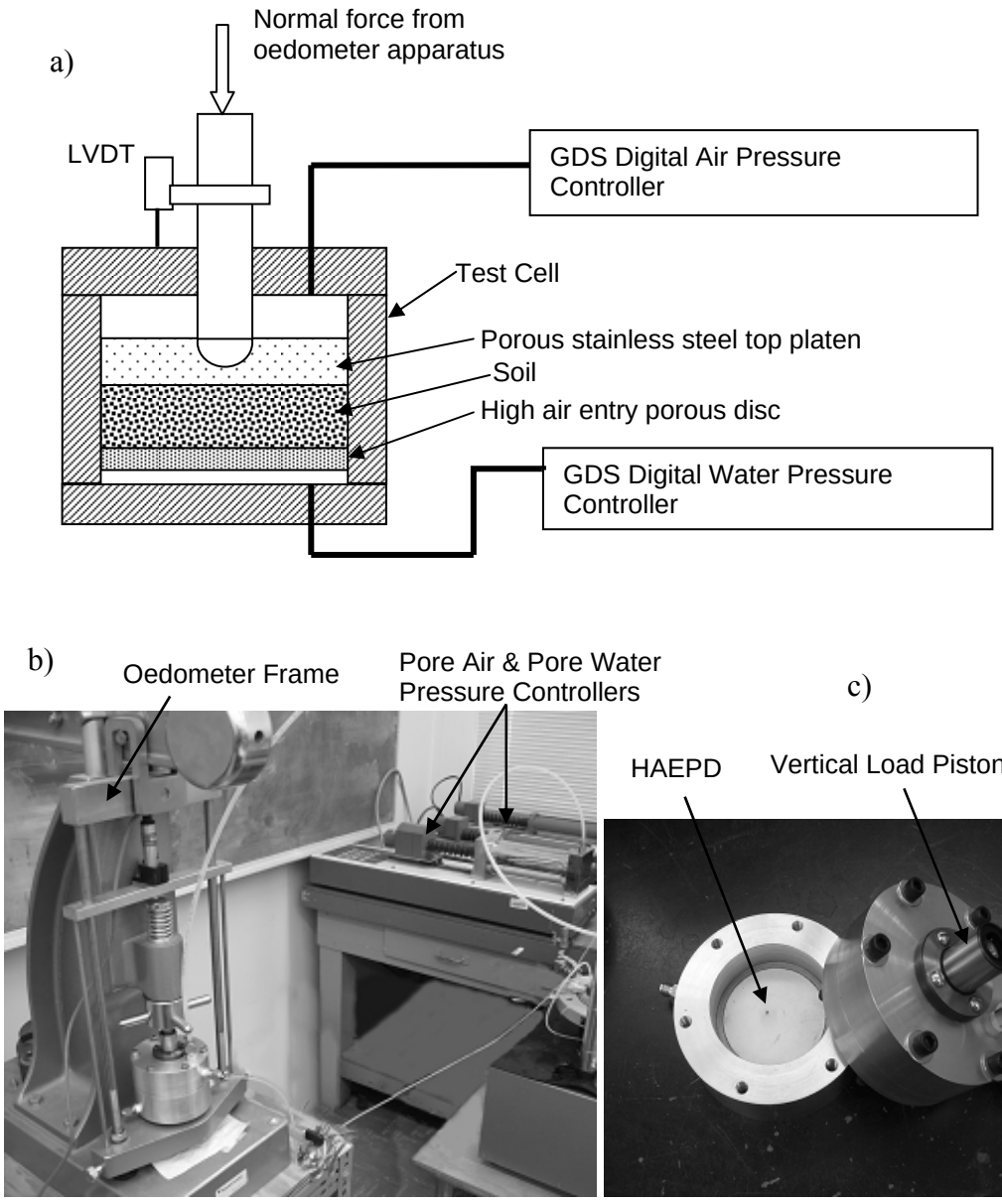

Figure 2.6- a) Schematic of the Test Cell Cross-section and Measurement System, b) Modified Oedometer Setup and c) Photo of Test Cell

2.4 EXPERIMENTAL TEST METHODOLOGIES

Soil Water Characteristic Curves (SWCCs) were experimentally determined using the device described previously in Section 2.3.2. Samples were prepared by moist tamping (i.e. volume-based compaction) the soil directly into the test cell on top of the pre-conditioned high air entry porous disc. The test cell was then placed in the oedometer

frame and a seating load (5-35 kPa) was applied to assure a good contact between the top cap and the soil.

Two different type of SWCC tests were performed in this study. The first was to saturate the soil and then conduct the SWCC test. This type of test was conducted by first filling the cell with water on top of the soil specimen. Water was then forced, under low pressure, through the sample by increasing the air pressure above the water in the cell. This process continues until a minimum of three pore volumes of water flow through the sample to remove the entrapped air in the soil pores. Following saturation, samples were loaded incrementally to the desired vertical normal stress, after which the drying (increase of suction by increasing u_a, air pressure) and wetting cycles were initiated. The second type of test was performed on samples without saturation; in other words, samples were compacted into the cell (Figure 2.6c) at the desired target unit weight of 15.4 kN/m^3 and moisture content of 17.2%. Samples were then loaded incrementally to the desired vertical normal stress, as described above, after which drying and wetting cycles for SWCCs were initiated without saturation. For this type of test, it is important to obtain the initial (as-compacted) suction value. To this end, a new testing procedure was developed and used as follows. The sample was first compacted on top of the HAEPD of the test cell (Figure 2.6), while the tube connected to the water controller piston is closed with a valve. Then, a minimal air pressure (u_a) was applied on top of the sample while maintaining a zero water volume change ($\Delta V_w = 0$) by setting the precision pumps to volume control. After u_a application the water valve connected to the tube was opened and the test started by recording the change in pore water pressure (u_w) due to the target air pressure value, while maintaining a zero water volume change. Higher air pressure u_a

was applied, and the corresponding change in u_w was recorded. After reaching equilibrium (i.e. no more change in u_w) for each target u_a, initial suction of the sample was thus estimated as the difference between the target u_a and measured u_w values. This difference (u_a - u_w) was nearly constant for all u_a increments.

Throughout testing of SWCC, suction was controlled during testing by using the axis translation method whereby the air pressure was increased while maintaining a constant water pressure of zero kPa or minimal pressure using the precision pumps described in section 2.3.2. To maintain constant net normal stress during an increase in air pressure the axial normal force exerted by the oedometer was adjusted slightly to compensate for the air pressure acting on the portion of the axial load piston inside the air chamber.

As previously mentioned, time required for completing the SWCC test may be the main reason for the lack of reported hysteretic data; thus, reducing testing time will encourage more extensive testing to fully define hysteretic behavior of the SWCC. This was precisely the motivation for an investigation to determine the minimum height of soil sample that could be used while practically achieving results similar to samples with heights more typical of one dimensional testing. The goal was to optimize the testing geometry while shortening the equilibrium time. To this end, a set of experimental results is presented and discussed in section 2.5.

2.5 TEST RESULTS AND DISCUSSION

2.5.1 Influence of Sample Height on the SWCC Equilibrium Time

Mainly SWCC tests were first performed on SCS soil samples with heights of 1" (25.4 mm), then on samples with ¼" (6.35 mm), which was the smallest practical height that could be compacted. Plots of the Soil Water Characteristic Curves (SWCCs, matric

suction (u_a-u_w) versus gravimetric water content) for tests having heights of 25.4 mm and 6.35 mm are presented in Figure 2.7 and Figure 2.8, respectively. Each data point in these figures represents an increment of suction and corresponding water content at equilibrium. Equilibrium was assumed to occur when negligible water volume change occurred for each suction increment. In Figure 2.9 an example of water volume change versus time for primary drying of the 25.4 mm sample height is shown; water volume changed fairly rapidly following application of an increment of suction followed by a more gradual change until equilibrium was observed.

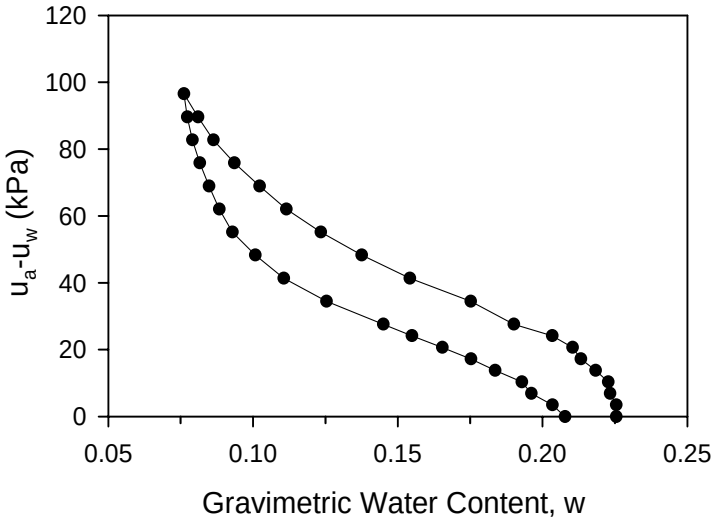

Figure 2.7- SWCC for Sample height of 25.4 mm

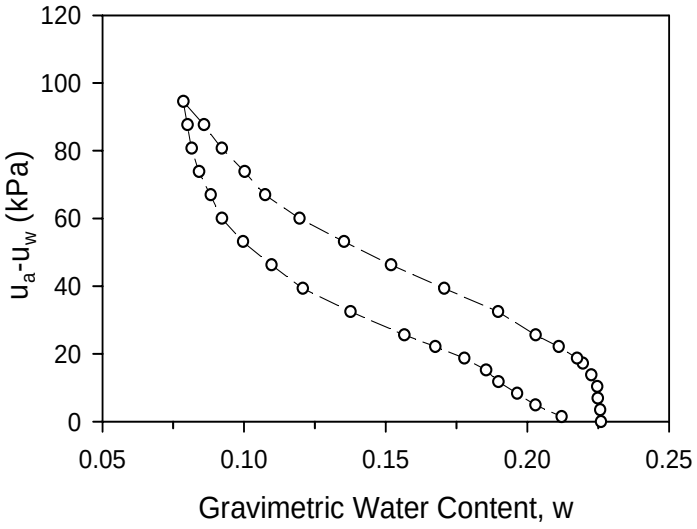

Figure 2.8- SWCC for Sample height of 6.35 mm

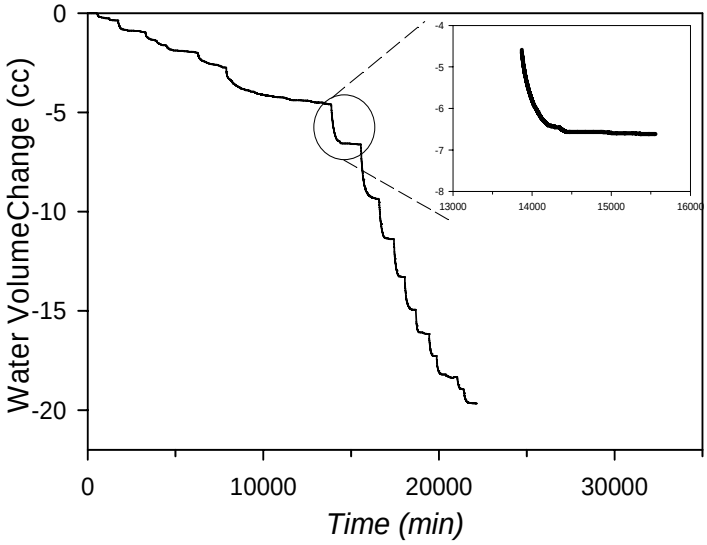

Figure 2.9- Water Volume Change versus Time for Primary Drying during Testing for 25.4 mm Height

In Figure 2.10, a comparison of the primary drying and primary wetting curves for each (25.4 mm and 6.35 mm sample height) test is shown. In examining Figure 2.10 it is apparent that the SWCCs for both sample heights were practically the same.

Figure 2.11 shows a comparison of water volume change versus total test time for both sample heights. The total time for testing, including primary drying and primary wetting curves for the 25.4 mm height was about 25 days compared to 10 days for the reduced sample height (6.35 mm). It can be noted that the time required to complete testing was reduced by more than 50% when the sample height was reduced from 25.4 mm to 6.35 mm. Results indicate that a reduction in sample height can be an effective way of achieving considerably faster equilibrium test times. However, other considerations remain when reducing the test specimen height, such as sample uniformity, and minimum vertical deformations required for accurate measurements on the specimen under vertical loading (i.e. for a given strain shorter heights mean smaller displacements). That said, the vertical deformations measured for the minimum height (6.35 mm) used in this study were reasonable given the accuracy of measurement devices.

In addition, previous to conducting a test on the smaller height sample a repeat test was conducted for the 1" (25.4 mm) sample height to investigate experimental variability. Figure 2.12 shows the comparison of results from the two nominally identical tests. Results of the duplicate test demonstrate that the SWCC is reproducible to reasonable accuracy.

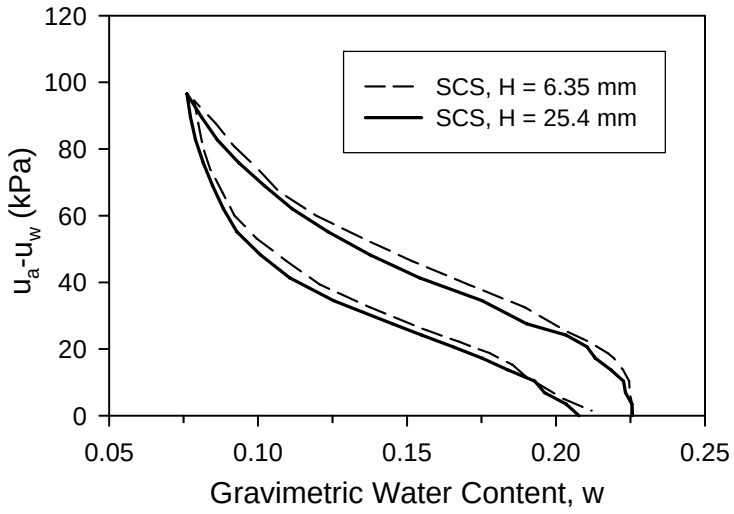

Figure 2.10- SWCC Comparison for the both Sample Heights (25.4 and 6.35 mm)

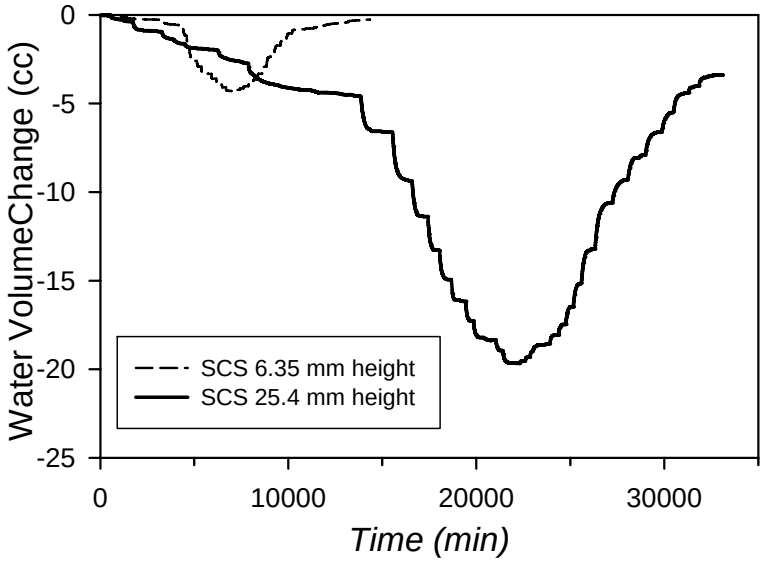

Figure 2.11- Water Volume Change versus Time for 25.4 mm and 6.35 mm Sample Height

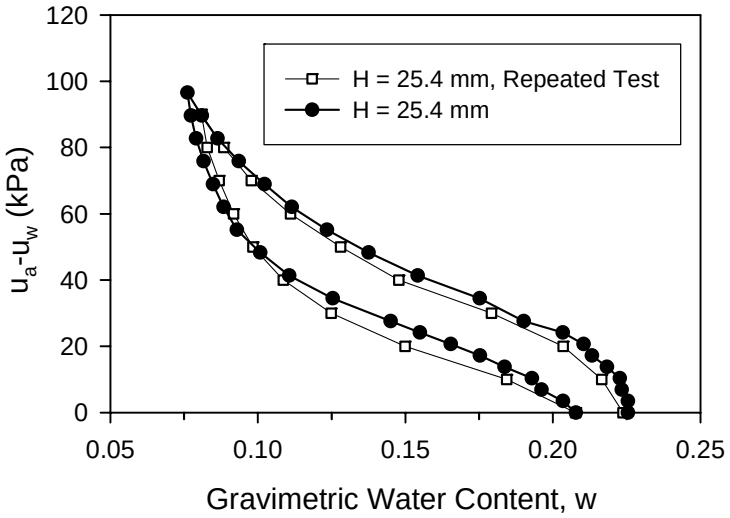

Figure 2.12- Comparison of SWCC Results for Two Nominally Identical Samples with a Height of 25.4 mm

The reduction in testing time gained by reducing the sample height to ¼" (6.35 mm) was a major achievement in that it allowed obtaining, in a reasonable time frame, a complete set of SWCCs including the hysteretic behavior; this included primary drying, primary wetting, secondary drying and scanning curves, which were thus performed on sample heights of ¼" (6.35 mm) as presented in Sections 2.5.2 and 2.5.3.

2.5.2 Initially Saturated Samples

Results in this section represent tests performed on the soil mixture (75 % SCS and 25 % Glass Beads) with sample heights of ¼" (6.35 mm), where samples were saturated before initiation of Soil Water Characteristic Curves (SWCCs). Initially saturated SWCCs, denoted by (IS-SWCC) were conducted under three different (0, 10 and 200 kPa) net normal stresses (σ_n-u_a). IS-SWCCs results for net normal stresses of 10 and 200 kPa are presented in Figure 2.13 and Figure 2.14, where matric suction is u_a-u_w, and θ_w is the volumetric water content (volume of water/total volume). The data points in these

figures represent the increments of suction and corresponding measurements of water volume at equilibrium. Similarly to previous tests, equilibrium was also assumed to occur when negligible water volume and total volume change occurred following application of a new suction increment. In Figure 2.15 an example of water volume change (*w* is gravimetric water content) versus time for primary drying at 200 kPa normal stress is shown. Based on Figure 2.15, the time to complete primary drying was about 18 days, which demonstrates the relatively fast equilibrium times that were achieved using the artificial soil and smaller sample heights.

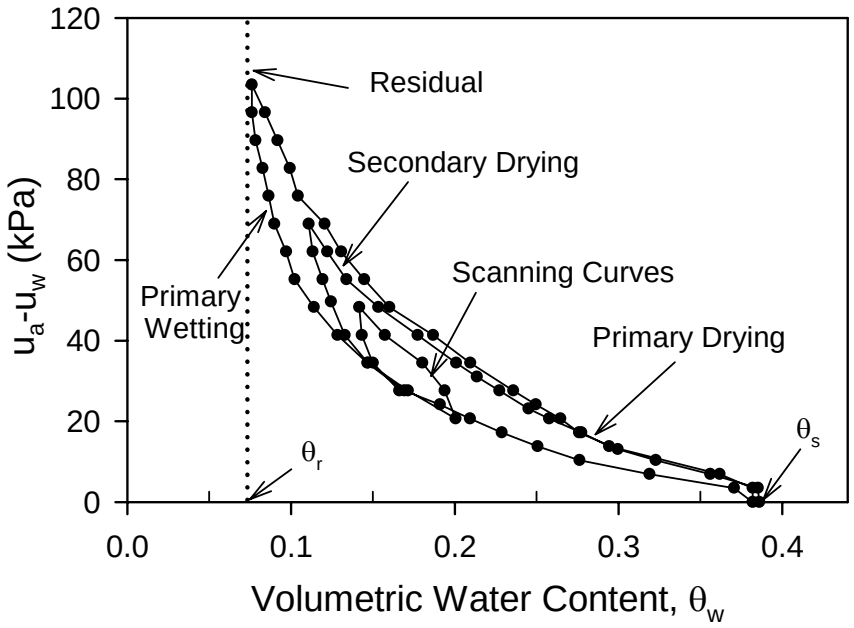

Figure 2.13- SWCC for Net Normal Stress of 10 kPa

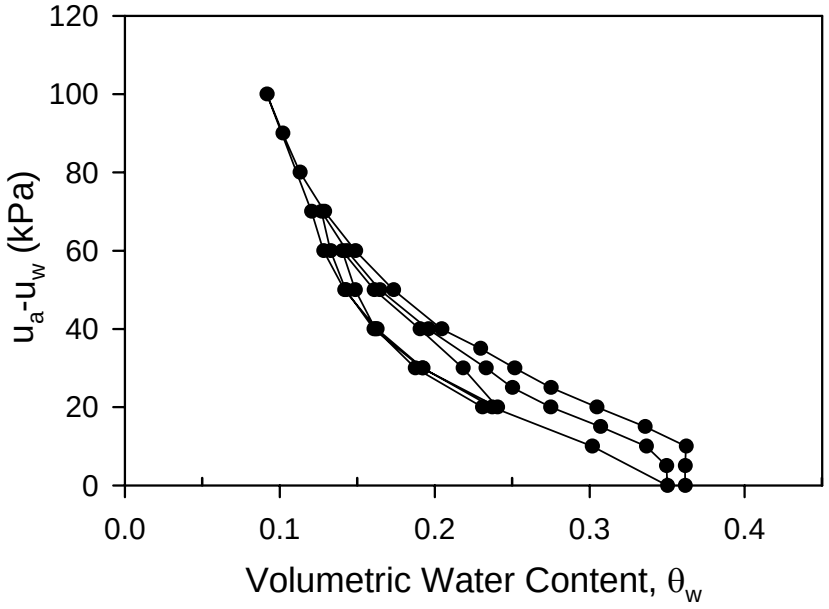

Figure 2.14- SWCC for Net Normal Stress of 200 kPa

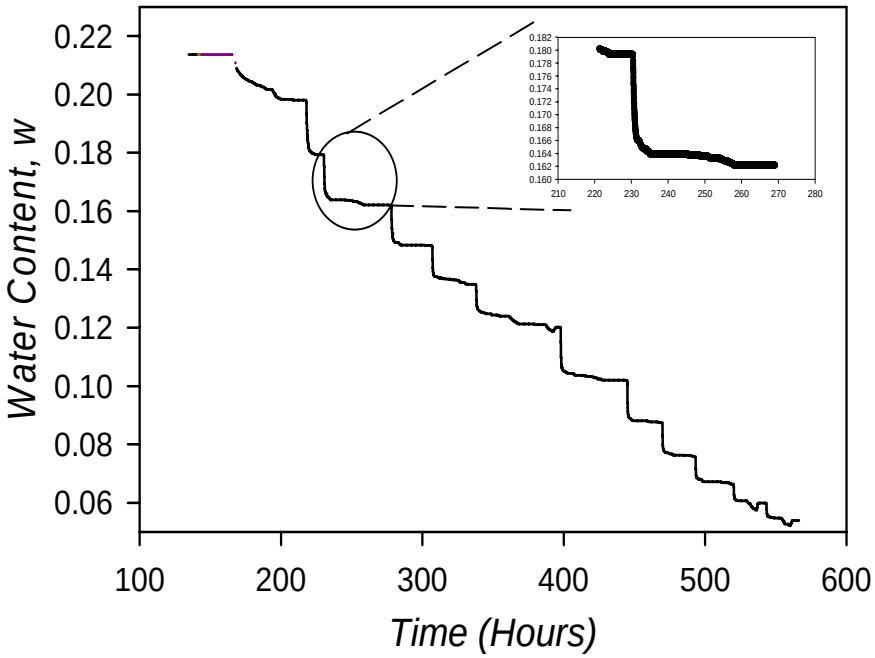

Figure 2.15- Water Volume Change versus Time for Primary Drying during Testing for Net Normal Stress of 200 kPa

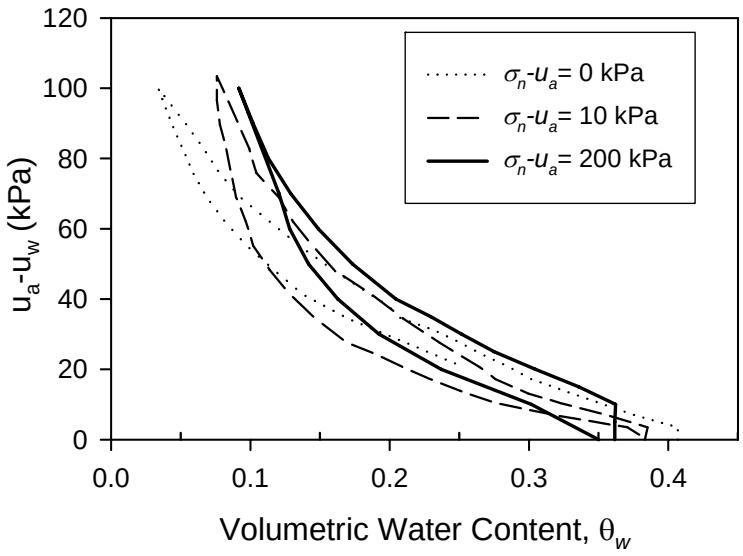

Figure 2.16- Comparison of SWCCs at Net Normal Stresses of 0, 10 and 200 kPa

In Figure 2.16, a comparison of the primary drying and primary wetting curves for each test is shown. Note that for 0 kPa normal stress, only the primary drying and a portion of the primary wetting curve were obtained because the test had to be terminated prematurely; these are shown for comparison to the 10 and 200 kPa normal stress curves.

In examining Figure 2.13, Figure 2.14 and Figure 2.16 some interesting observations are made:

1) For the 10 and 200 kPa normal stresses, the scanning curves are bounded by the secondary drying and primary wetting curve.
2) The initial volumetric water content decreases with increasing normal stress as expected since the void ratio (e) decreases more during application of higher normal stress.
3) Generally, the air entry value increases with increasing normal stress, again as expected due to the lower void ratio. However, the difference between the air

entry value for 0 and 10 kPa normal stress is negligible, probably because the change in void ratio from 0 to 10 kPa is relatively small compared to the difference between normal stress of 10 and 200 kPa. The air entry value is the matric suction necessary for air to penetrate the void space when the soil is initially saturated.

4) Generally, the slope of the SWCC is flatter at lower normal stress and becomes steeper with increasing normal stress; it is especially apparent as the curves approach the lower residual saturation moisture contents. This observation is reasonable because the pore channels in soil with lower void ratio would be smaller relative to higher void ratio soil. Thus, the lower void ratio soil would generate higher capillary pressure than a higher void ratio (i.e. matric suction) at the same volumetric water content. Also, the residual moisture contents appear to increase with increasing normal stresses.

In addition, the SWCC test at 200 kPa normal stress was repeated to investigate the experimental repeatability. Figure 2.17 shows the comparison of results from the two nominally identical tests. For the repeat test, only the primary drying and a portion of the primary wetting curve were obtained because the system developed a leak that could not be repaired during testing. Nevertheless, the comparison of the SWCC curves is favorable, as is the volume change behavior represented by specific volume (1+e) data presented in Figure 2.18. While the number of repeat tests was limited, the results for duplicate tests demonstrate that the SWCC is reproducible to reasonable accuracy.

For the 10 and 200 kPa normal stress SWCC tests, vertical displacements were recorded throughout testing beginning with the saturation process and continuing through

the saturated compression and SWCC testing. In Figure 2.18, a comparison of specific volume versus normal stress curves is presented. These curves represent compression starting from the compacted state, followed by wetting induced compression during saturation at a constant total stress, and subsequent compression under saturated conditions to reach the starting point of the SWCC tests. Although the curves exhibit some slight differences, they are generally similar and express similar soil behavior. Since samples were prepared in nearly identical fashion, similar behavior was expected. Interestingly, the samples showed considerable wetting-induced compression under a very low normal stress; the change in specific volume due to wetting represents a volumetric strain of about 1.5%. This collapse may be partly attributed to the relatively loose initial state of the sample following compaction and the significant angularity of the crushed silica particles. Both of these factors contribute to an open soil structure susceptible to collapse.

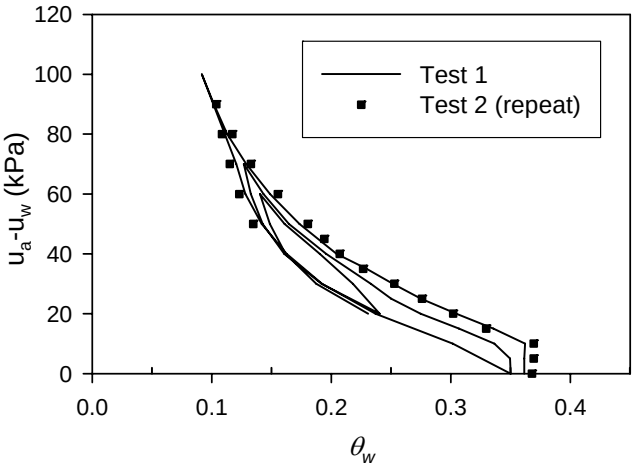

Figure 2.17- Comparison of SWCC Results for Two Nominally Identical Samples at σ_n-u_a of 200 kPa

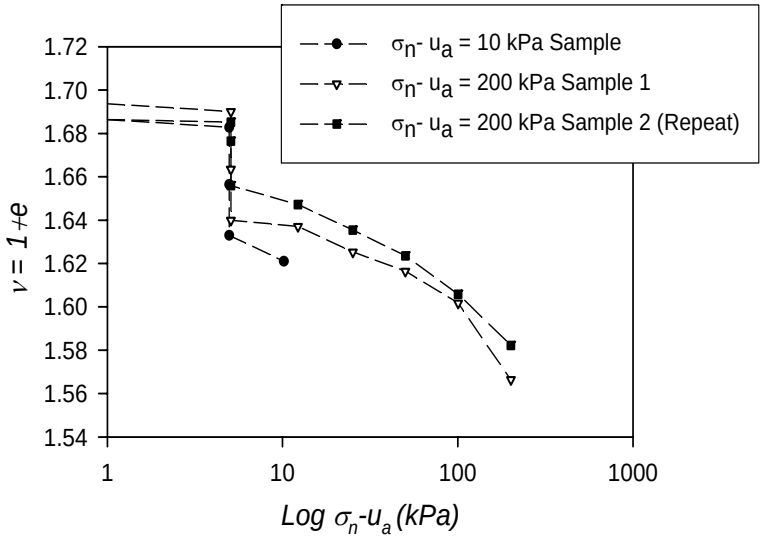

Figure 2.18- Specific Volume (1+e) versus Net Normal Stress of the Three Identically Prepared SWCC Specimens

During incremental loading the samples behaved similarly as evidenced by the similar slopes of each curve. Comparison of the specific volumes at 10 kPa and 200 kPa net normal stresses indicates that significant compression, about 4 to 5% volumetric strain, occurred during incremental loading up to 200 kPa. This account for the differences in the initial volumetric water content for corresponding SWCCs. Figure 2.19 shows a plot of void ratio (e) versus suction during SWCC drying-wetting cycles. During the SWCC testing, the volume change (or change in void ratio) as determined from LVDT measurements of vertical deformation was practically negligible with a maximum volumetric strain (due to suction change beginning from the start of the SWCC) of about 0.75%, for both the 10 and 200 kPa normal stress specimens. While small, the volume change was included in the computation of volumetric water content. This small volume change due to suction was initially observed during drying, but then ceased during wetting/drying cycles.

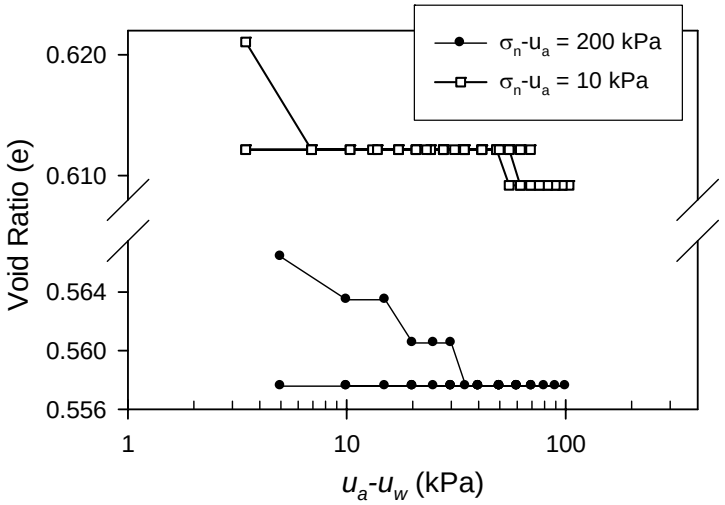

Figure 2.19- Void Ratio versus Suction during SWCC Drying-Wetting Cycles

2.5.3 As-Compacted Samples

This type of SWCC (as-compacted) test was performed on samples without initial saturation. Samples were first loaded incrementally (in an oedometer setup, as discussed in Section 2.4) to the desired vertical normal stress after which drying and wetting cycles were initiated.

This set of SWCCs was used to simulate as close as possible a similar stress path performed for direct shear tests and resilient modulus tests conducted in this study. Where, for example, a seating load was first applied to the direct shear test samples without saturation, after which suction and net normal stresses were applied and samples were then tested.

The as-compacted SWCC tests were conducted under net normal stresses (σ_n-u_a) of 0 and 150 kPa; results are presented in Figure 2.20 and Figure 2.21, respectively. Note this range of σ_n-u_a (0-150kPa) was selected because it covers the same range that direct shear tests and resilient modulus tests were subjected to.

Similar to the initially saturated SWCC (IS-SWCC) test results (Section 2.5.2), Figure 2.20, Figure 2.21 and Figure 2.22 showed that: a) the scanning curves are bounded by the secondary drying and primary wetting curve, b) the initial volumetric water content decreases slightly with increasing normal stress, a behavior however not as pronounced as for the IS-SWCC, c) the slope of the SWCC is flatter at 0 kPa normal stress and became steeper at higher normal stress (150 kPa). Again, an expected behavior because the pore channels in soil with lower void ratio (150 kPa net normal stress) would be smaller relative to higher void ratio soil (0 kPa net normal stress), d) also the residual moisture contents appear to increase with increasing normal stresses, for the same reasoning in c).

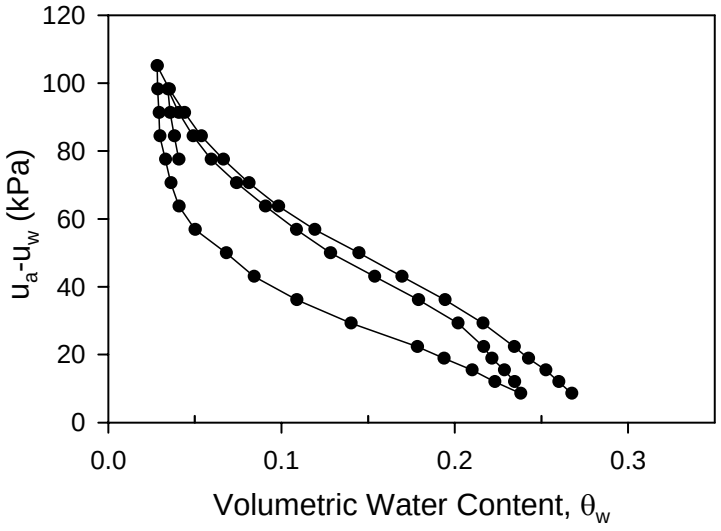

Figure 2.20- SWCC for As-Compacted Sample at Net Normal Stress of 0 kPa

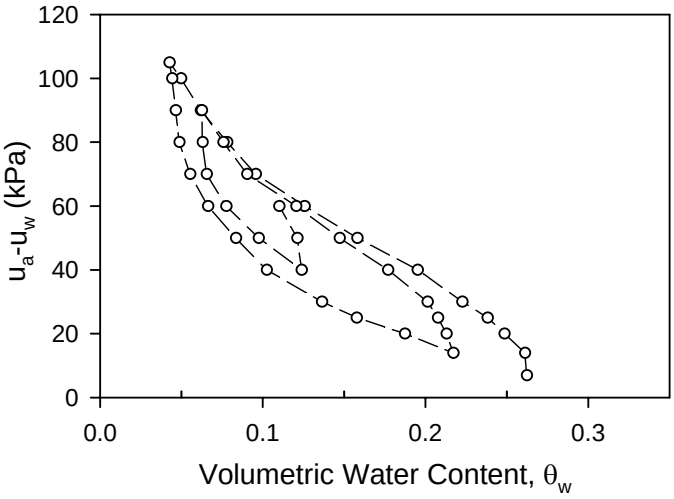

Figure 2.21- SWCC for As-Compacted Sample at Net Normal Stress of 150 kPa

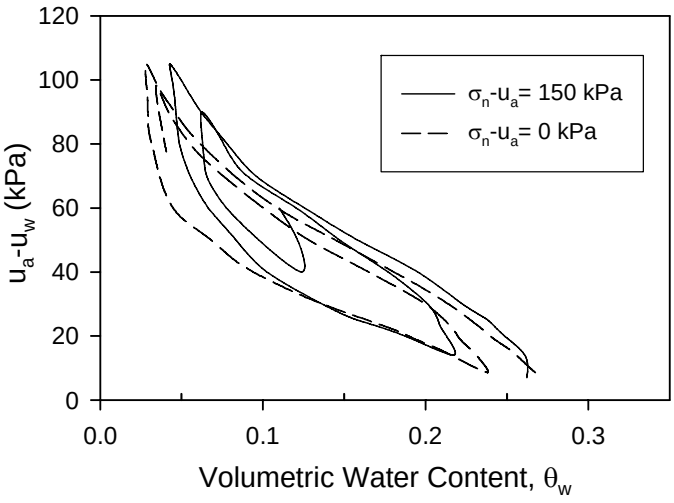

Figure 2.22- Comparison of SWCC for As-Compacted Sample at Net Normal Stress of 0 and 150 kPa

Consolidation of the sample at net normal stress of 150 kPa indicates approximately 2% volumetric strain during incremental loading as shown in Figure 2.23. A plot of void ratio (e) versus suction during SWCC drying-wetting cycles is shown in Figure 2.24. This change in void ratio (corresponding to a volumetric strain of approximately 0.2 %) was determined from LVDT measurements of vertical deformation during SWCCs, and

although it is very small, was included in the computation of volumetric water content. It is noted, that this small volume change due to suction was initially observed during early drying increments, but then ceased completely during further wetting/drying cycles.

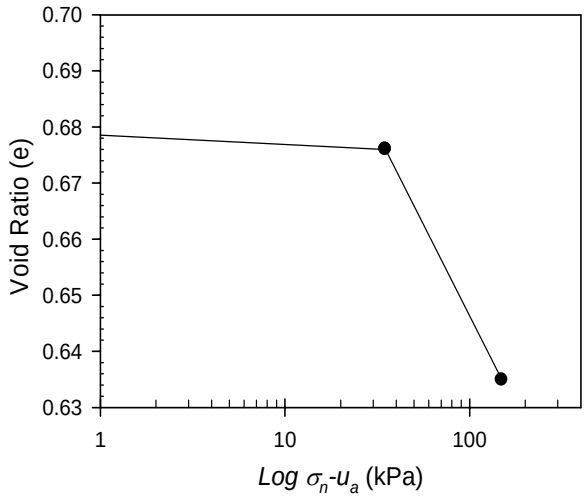

Figure 2.23- Void Ratio (e) versus Net Normal Stress of the SWCC Specimen at σ_n-u_a of 150 kPa

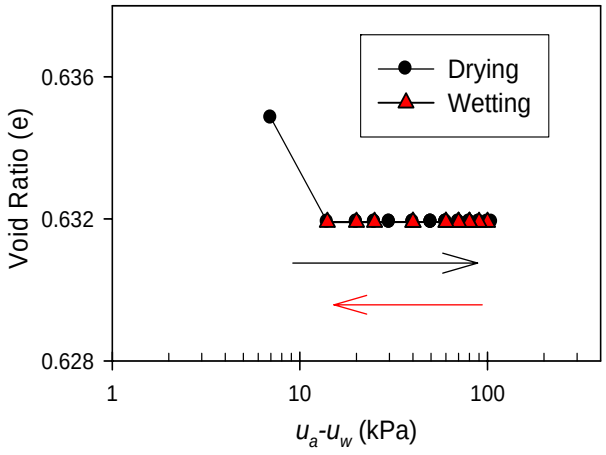

Figure 2.24- Void Ratio versus Suction during SWCC Drying-Wetting Cycles

2.6 MODELING OF THE SWCC

The SWCC has been extensively studied, and some early researchers proposed functional models to describe a single (primary drying) SWCC as follows:

Brooks and Corey (1964),

$$\theta = \theta_r + (\theta_s - \theta_r)(a \times \psi^n) \quad \textbf{(2.2)}$$

Van Genuchten (1980),

$$\theta = \theta_r + \frac{(\theta_s - \theta_r)}{\left[1 + (a \times \psi^n)\right]^m} \quad \textbf{(2.3)}$$

Fredlund and Xing (1994),

$$\theta = \theta_s \left[1 - \frac{\ln(1 + \psi/\psi_r)}{\ln(1 + 10^6/\psi_r)}\right] \left[\frac{1}{\left\{\ln\left[e + (\psi/a)^n\right]\right\}^m}\right] \quad \textbf{(2.4)}$$

Feng and Fredlund (1999),

$$\theta = \frac{\theta_s + \theta_r \left(\frac{\psi}{a}\right)^m}{1 + (\frac{\psi}{a})^m} \quad \textbf{(2.5)}$$

Where, θ = volumetric water content; θ_s = saturated volumetric water content; θ_r = residual volumetric water content; ψ = matric suction; ψ_r = matric suction at residual water content; e = base of natural logarithm = 2.71828; and a, m, n = are fitting parameters that describe the shape of the SWCC.

These models are essentially curve fitting equations, found through best fit of test data. Others have proposed models for hysteretic SWCCs such as Wheeler et al. (2003), Gallipoli et al. (2003), Yang et al. (2004a), Wei and Dewoolkar 2006, Li (2007a&b), Kohgo (2008), and Muraleetharan et al. (2008).

However, in this study the functional model by Fredlund and Xing (1994) and Feng and Fredlund (1999) will be used to fit the primary drying and primary wetting curves as presented in Section 2.6.1. The resulting fit parameters will be used for prediction of shear strength and resilient modulus with suction.

On the other hand, SWCC tests (following the primary drying/wetting, secondary drying and scanning curves) obtained in this study for different stress histories (i.e. under different normal stresses) were used to validate the Muraletharan et al. (2008) model presented in Miller et al. (2008), as presented in Section 2.6.2.

2.6.1 Functional Form Models

The models, Equations 2.4 and 2.5, by Fredlund and Xing (1994) and Feng and Fredlund (1999) are used to fit the primary drying and primary wetting curves, respectively. Comparison between experimental and fitting model results are shown in Figure 2.25 though Figure 2.31. The resulting fit parameters for each set of SWCC data (i.e. different net normal stresses and different initial conditions) obtained in this study are shown in Table 2.1 and some of which (i.e. the one corresponding to the same initial conditions) were used to predict the shear strength of unsaturated soils/interfaces and the resilient modulus of subgrade soil as presented in Sections 3.8.1.2, 3.8.2.2 and 4.5, respectively.

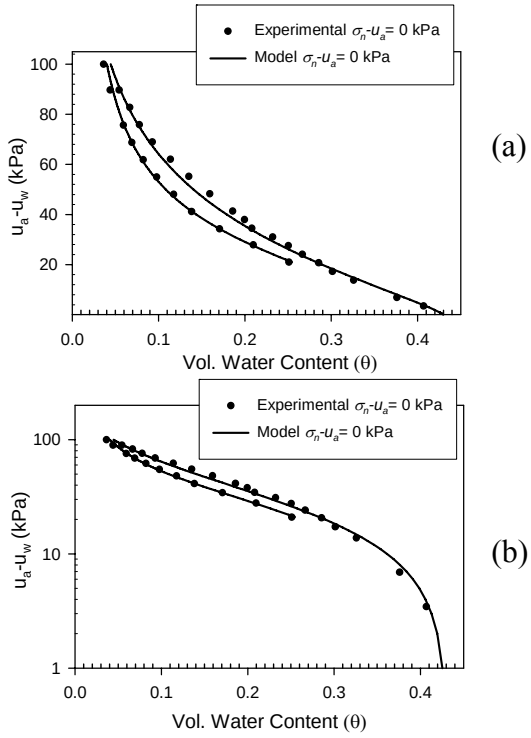

Figure 2.25- Comparison of Model SWCC with Measured Values for Initially Saturated Tests at Net Normal Stress of 0 kPa: a) Linear Plot, b) Semi-log Plot

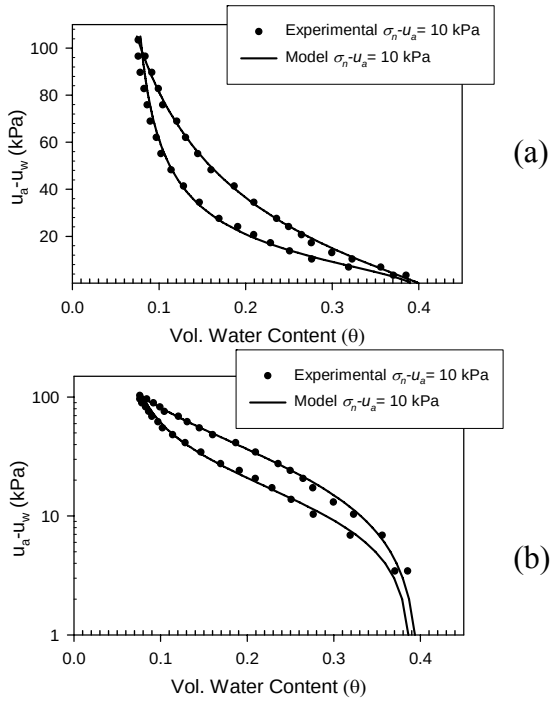

Figure 2.26- Comparison of Model SWCC with Measured Values for Initially Saturated Tests at Net Normal Stress of 10 kPa: a) Linear Plot, b) Semi-log Plot

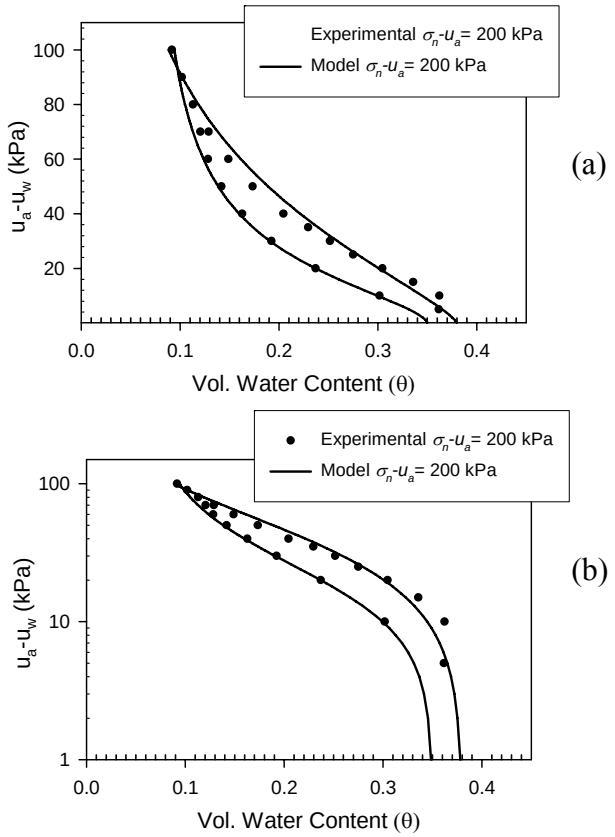

Figure 2.27- Comparison of Model SWCC with Measured Values for Initially Saturated Tests at Net Normal Stress of 200 kPa: a) Linear Plot, b) Semi-log Plot

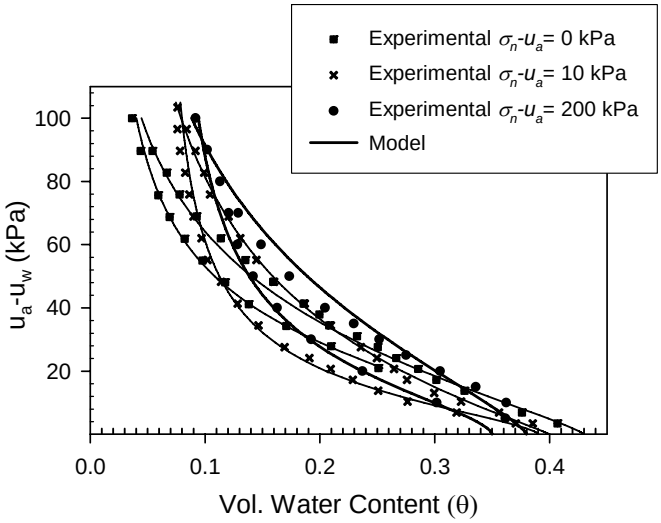

Figure 2.28- Comparison of Model SWCC with Measured Values for Initially Saturated Tests at Net Normal Stresses of 0, 10 and 200 kPa

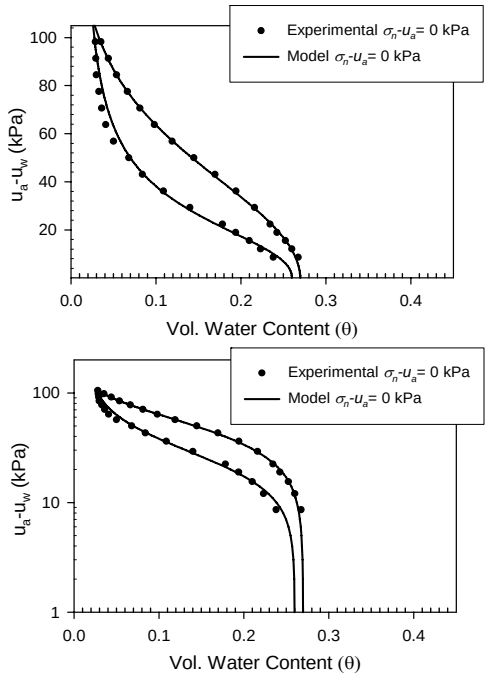

Figure 2.29- Comparison of Model SWCC with Measured Values for As Compacted Tests at Net Normal Stress of 0 kPa: a) Linear Plot, b) Semi-log Plot

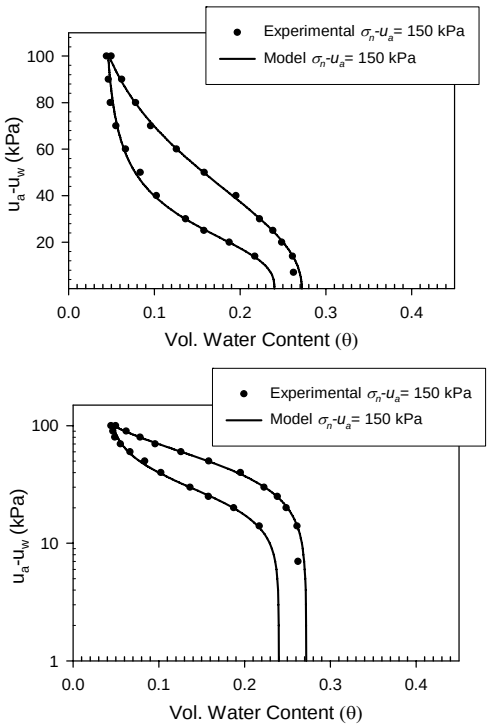

Figure 2.30- Comparison of Model SWCC with Measured Values for As Compacted Tests at Net Normal Stress of 150 kPa: a) Linear Plot, b) Semi-log Plot

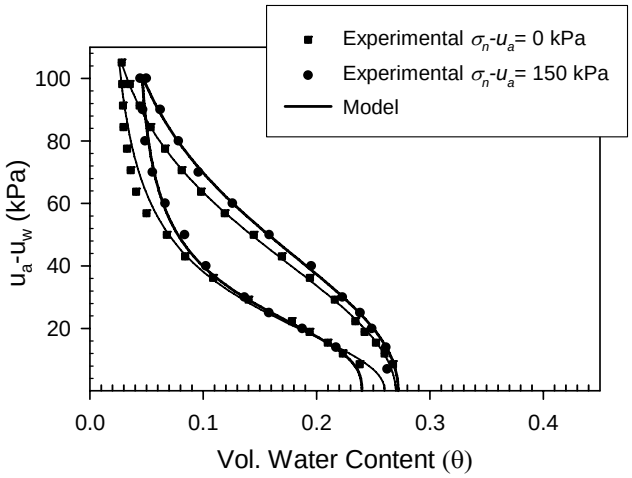

Figure 2.31- Comparison of Model SWCC with Measured for As Compacted Tests at Net Normal Stresses of 0 and 150 kPa

Table 2.1- Fitting Parameters of the Functional Form Models for the Primary Drying and Wetting SWCC Results

Initial Condition	Net Vertical Stress (kPa)	Fredlund and Xing (1994)					Feng and Fredlund (1999)			
		a	m	n	Ψ_r (kPa)	θ_s	a	m	θ_r	θ_s
Saturated	0	110	8.90	1.230	200	0.430	31.64	2.05	0.010	0.360
Saturated	10	65.56	4.18	1.102	300	0.400	17.2	1.56	0.060	0.390
Saturated	200	100	5.30	1.300	1000	0.380	25.96	1.61	0.065	0.350
As Compacted	0	93.4	6.80	2.100	200	0.270	29.08	2.20	0.012	0.260
As Compacted	150	76.06	4.20	2.189	1000	0.272	29.288	2.68	0.039	0.24

2.6.2 Coupled Hydraulic-Mechanical ElastoPlastic Constitutive Model

The hysteretic data (including, primary, secondary and scanning curves) obtained for SWCCs starting from saturation under different stress histories (i.e. under different normal stresses) were modeled as shown below by Miller et al. (2008).

The constitutive model used combines an elastoplastic description of the SWCCs with an elastoplastic description of the stress-strain behavior of the solid skeleton. While the SWCCs are described using a bounding surface elastoplastic model the stress-strain behavior is simulated using the classical plasticity theory. The theoretical descriptions of the model are detailed by Muraleetharan et al. (2008).

Briefly, Muraleetharan et al. (2008) used the intergranular stress and solid skeleton strains to describe the mechanical behavior, and used the matric suction and volumetric water content to describe the hydraulic behavior. The intergranular stress tensor σ^*_{ij} in soil mechanics sign convention (i.e., compressive stresses are positive) is given by:

$$\sigma^*_{ij} = (\sigma_{ij} - u_a \delta_{ij}) + \theta S \delta_{ij} \quad \textbf{(2.6)}$$

where, σ_{ij} = total stress tensor; $S = u_a - u_w$ = matric suction; u_a and u_w are pore air and pore water pressures, respectively; θ = volumetric water content; and δ_{ij} is the Kronecker delta.

Motivated by the observation that all the scanning curves are bounded by the primary wetting curve and the secondary drying curve, Miller et al. (2008) chose the bounding surface plasticity theory originally proposed by Dafalias and Popov (1975, 1976) to describe the SWCCs as described by Muraleetharan et al. (2008). In addition, Equation (2.5) proposed by Feng and Fredlund (1999) is used to describe the bounding curves (the primary wetting curve and the secondary drying curve).

In order to describe the coupled hydraulic-mechanical behavior in one-dimensional problems, the SWCC model is coupled with an isotropic stress-strain model based on the classical plasticity theory in a manner similar to the one proposed by Wheeler et al. (2003). More details of the model are presented by Muraleetharan et al. (2008) and Miller et al. (2008)

For the soil used in this study, the parameters describing the SWCCs were first calibrated using the measured curves for 10 kPa net vertical stress presented in Figure

2.13. The measured SWCCs and predicted curves for calibration are shown in Figure 2.32 and used for all subsequent predictions.

The parameters that describe the coupled hydraulic-mechanical behavior can be obtained from an unloading-reloading portion (here using the initial portion of Figure 2.33) of a constant suction Oedometer test and a wetting induced collapse test as shown in Figure 2.33. Predicted $S-\theta$ curves during wetting and portions of the bounding curves during the wetting process are shown in Figure 2.34.

After obtaining the calibrated model parameters, the SWCC for 200 kPa net vertical stress was predicted following a stress/suction change path that simulated the stress/suction change path for a portion of the experiment. Specifically, starting with as compacted conditions, loading and wetting paths as shown in Figure 2.33 were first simulated. Then the following wetting/drying cycles were simulated: start at zero suction and follow the secondary drying curve to near residual saturation at a suction of 70 kPa, wet back to a point along the primary wetting curve at a suction of 20 kPa, followed by a complete drying and wetting path (suction increase to 60 then decrease back to 20) to establish a scanning curve loop. The measured and predicted portions of the SWCCs for 200 kPa net vertical stress are shown in Figure 2.35. The only parameter that needed adjustment was the residual saturation. A value of $\theta_{res} = 0.06$ was used to predict the behavior at 200 kPa net vertical stress. The comparison in Figure 2.35 demonstrates that the proposed model is well suited to capture the hysteretic nature of the SWCC and a reasonable agreement with experimental results was obtained. To further appreciate the potential of the model to capture the coupled mechanical-hydraulic behavior, the predicted SWCCs for net normal stress of 10 and 200 kPa are plotted with the

experimental data as shown in Figure 2.36a and Figure 2.36b. Results of 10 and 200 kPa are also plotted together for both predicted and experimental as shown in Figure 2.36c. In this figure it is apparent that the model is capturing some of the essential features demonstrated by the experimental data. In particular, the shape and position of the model SWCCs for 10 and 200 kPa normal stress are similar to that exhibited by the experimental curves. That is, the model SWCC for a net normal stress of 200 kPa is slightly steeper and positioned slightly above the model SWCC for a normal stress of 10 kPa. However, the model does not show the slight difference in the air-entry value observed in the experimental results.

The limited experimental data on the hysteretic behavior between suction and water content available in the literature (i.e. SWCC) under different levels of externally applied stress (or at different void ratios) shows the importance of the experimental SWCC results obtained in this study for model validation as presented in this section.

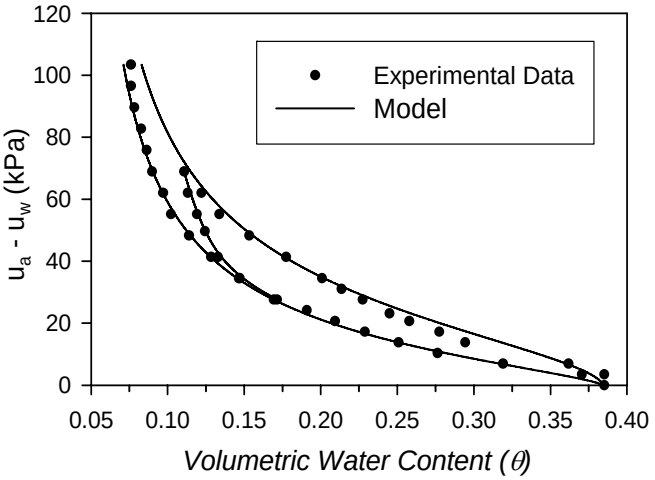

Figure 2.32- Measured SWCCs for a Normal Stress of 10 kPa and Calibrated Predicted Curves Obtained

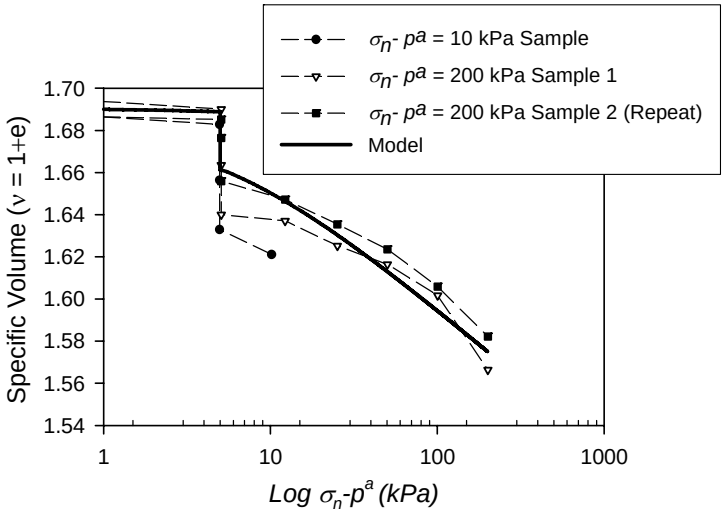

Figure 2.33- Specific Volume versus Normal Stress during Compression for Three Similarly Prepared SWCC Test Specimens Superimposed with the Model Predictions Obtained during Calibration

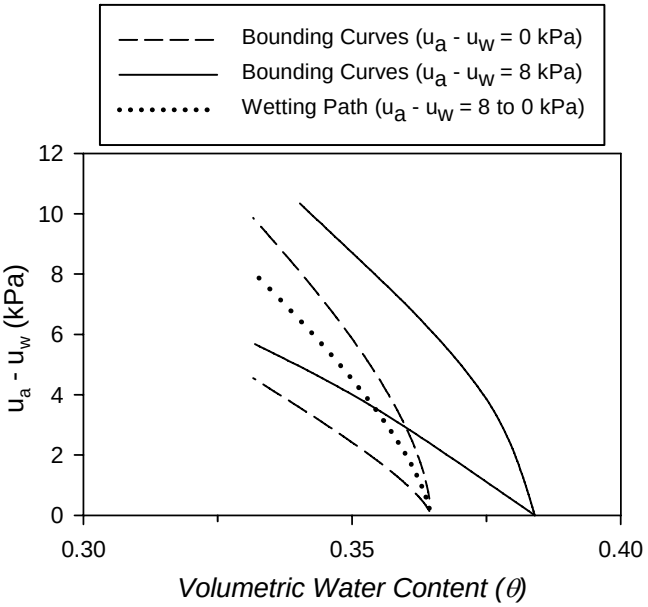

Figure 2.34- Portions of the Wetting Path and the Bounding Curves when Suction Changes from 8 kPa to 0 kPa

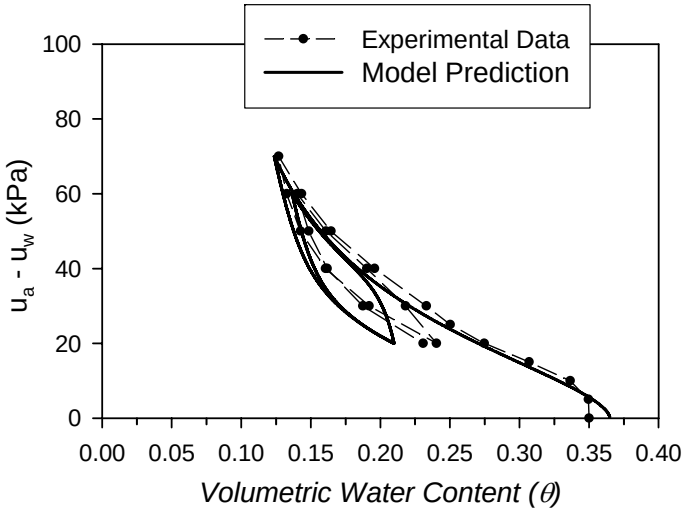

Figure 2.35- Measured and Predicted SWCCs for a Normal Stress of 200 kPa

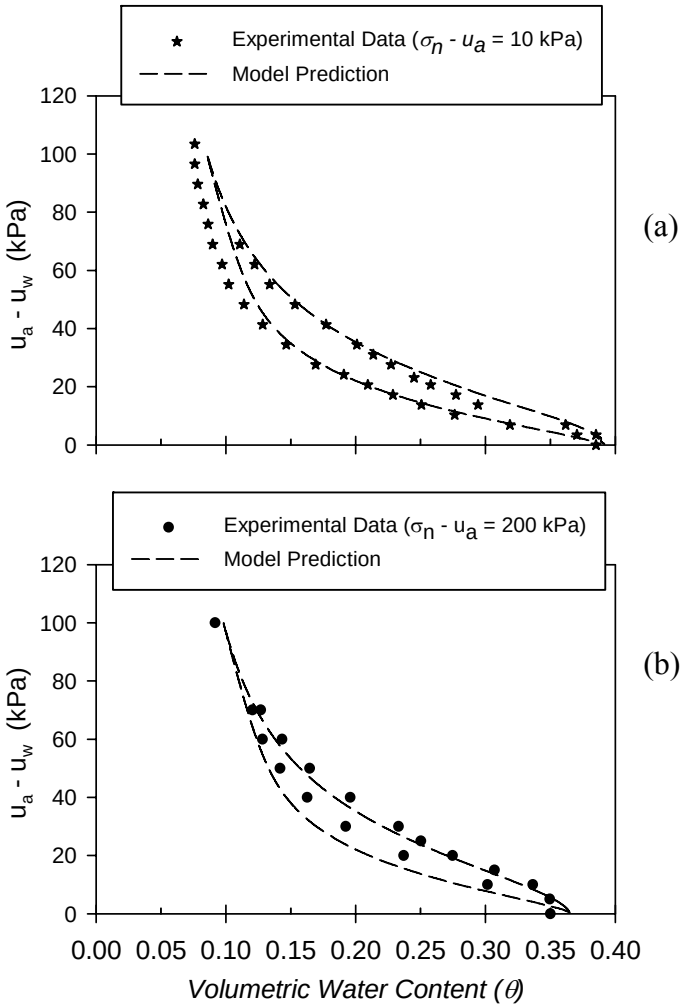

Figure 2.36- Comparison of Measured and Predicted SWCCs for Normal Stresses of 10 and 200 kPa

CHAPTER 3: UNSATURATED SOIL INTERFACES AND HYSTERESIS

3.1 INTRODUCTION

It has been commonly recognized that many structures (e.g. shallow foundations, retaining walls, mechanically stabilized earth (MSE) walls, reinforced soil slopes), are frequently constructed in contact with unsaturated soils, and can be subjected to variations of moisture content due to climate changes. This variation of moisture content influences the stress state (e.g., matric suction), which can significantly influence the mechanical behavior of the soil. The suction-water content relationship (SWCC) is hysteretic as shown in Chapter 2. Thus, the influence of soil suction during drying and wetting on the shearing response of unsaturated soils, rough steel and geotextile interfaces is investigated and presented in this chapter. To this end, suction-controlled direct shear tests along the drying and wetting paths of the SWCC are conducted. The influence of hydraulic hysteresis (i.e. suction hysteresis) on the shear strength is investigated and incorporated into prediction models using the SWCC. In addition, the proposed models are used to predict some results from the literature. Further, investigation and validation of the elastoplastic constitutive model developed by Hamid and Miller (2008) is conducted by comparing the predicted and measured results obtained on rough and geotextile interfaces.

3.2 LITERATURE REVIEW

3.2.1 Unsaturated Soil

3.2.1.1 Soil Suction

Unsaturated soils are generally influenced primarily by the suction present in soil. Soil suction is defined as the free energy state of soil water (Fredlund and Rahardjo 1993). The primary components of soil suction are the matric suction and the osmotic suction, which are related to the total suction as follows (Lu and Likos, 2004):

$$\psi = (u_a - u_w) + \psi_o \qquad \textbf{(3.1)}$$

where, ψ = total suction, (u_a-u_w) = matric suction, ψ_o = osmotic suction.

As described previously in Section 2.2.1, matric suction is associated with air-water menisci, which develops due to capillary action of water in the unsaturated soil pores. Osmotic suction, on the other hand, is the result of dissolved solutes in the pore water. While assuming no change in osmotic suction (i.e. no chemical change in water), the main component of interest would be the matric suction; this is particularly true for cohesionless soils as investigated in this dissertation.

Since this study is most interested in the shear strength of the soil and the effect of hysteresis, it is important to look at the interparticle forces in unsaturated soils. In the absence of externally applied load, the interparticle force (F) is the result of the combined negative pore water pressure (i.e. capillary forces), surface tension, and physicochemical forces of unsaturated soils. For granular soils (e.g silt and sand), the capillary and surface tension are the main forces that tend to pull the soil grains toward one another. An idealized air-water interface in unsaturated soils between two spherical particles with water meniscus is shown in Figure 3.1. When suction (u_a-u_w) increases (or water content

decreases) up to a certain point, interparticle force (F) increases and induces an increase in shear resistance between the soil particles. However there is a limit to which matric suction is beneficial; at some point (very low water content) the liquid-solid interfacial are becomes so small that F reduces. Dry soil represents the extreme case where water content goes to zero and F vanishes.

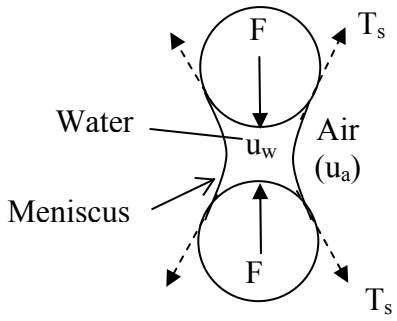

Figure 3.1- Idealized Air-water Interaction for Unsaturated Granular Soils

3.2.1.2 Shear Strength of Unsaturated Soil

Traditional soil mechanics (i.e. saturated/dry soil) is described by the single effective stress state variable known as Terzaghi's effective stress, σ', which is defined as the total stress (σ) minus pore water pressure (u_w). The Mohr-Coulomb (MC) failure criterion is typically used to describe the shear strength of saturated soil as:

$$\tau = c' + (\sigma - u_w)\tan\phi' \qquad \textbf{(3.2)}$$

where, τ = shear stress at failure, c' = effective cohesion, and ϕ' = effective angle of internal friction.

However, for unsaturated soils there exist different approaches for describing the state of stress. Common approaches and theories relevant to this study are described and discussed as follows.

Bishop (1959) presented a modified effective stress approach based on Terzaghi's effective stress. The shear strength is then described by incorporating this stress into the MC failure criterion as follows:

$$\tau = c' + \left[(\sigma - u_a) + \chi(u_a - u_w)\right]\tan\phi' \qquad \textbf{(3.3)}$$

where, u_a = pore air pressure, $(\sigma - u_a)$ = net normal stress, $(u_a - u_w)$ = matric suction, χ = effective stress parameter ($0 < \chi < 1$) that is a function of degree of saturation (S%).

Fredlund and Morgenstern (1978) formulated the shear strength of an unsaturated soil in terms of two independent stress state variables, which are the net normal stress $(\sigma - u_a)$ and the matric suction $(u_a - u_w)$. Using these stress state variables the shear strength of unsaturated soil can be written as:

$$\tau = c' + (\sigma_n - u_a)\tan\phi' + (u_a - u_w)\tan\phi^b \qquad \textbf{(3.4)}$$

where, ϕ' = angle of internal friction associated with the net normal stress variable, and ϕ^b = angle of internal friction associated with the matric suction.

The theory presented and described by Equation (3.4) describes a planar failure envelope. However, according to several studies (e.g. Fredlund and Rahardjo 1993, Oloo and Fredlund 1996, Vanapalli et al. 1996, Xu 2004, and Kayadelen et al. 2007), shear strength test results on unsaturated soil show some nonlinearity in the shear strength versus matric suction failure envelope. The angle ϕ^b at low matric suction seems to be equal to ϕ' but at higher matric suction it decreases to a lower value and varies with suction (Gan et al. 1988, Escario and Juca 1989, Fredlund and Rahardjo 1993). At low matric suction below the air entry value the specimen remains saturated. As long as the soil is saturated an increase in matric suction causes an increase in shear strength in

accordance with the friction angle ϕ′. However, when air enters into the pores at a suction equal to the air entry value of the sample, the soil starts to desaturate. Then the increase in shear strength due to increase in suction will not be as effective as before and will result in a lower value of ϕ^b. For many soils ϕ′ may be nearly constant over a significant range of suction (e.g., Escario and Saez 1986).

Vanapalli et al. (1996) developed models to predict the shear strength of unsaturated soil by relating it to the soil water characteristic curve, as presented in the following equations:

$$\tau_f = c' + (\sigma_n - u_a)_f \tan\phi' + (u_a - u_w)_f \tan\phi' \left(\frac{\theta}{\theta_s}\right)^k \quad \textbf{(3.5a)}$$

$$\tau_f = c' + (\sigma_n - u_a)_f \tan\phi' + (u_a - u_w)_f \tan\phi' \left(\frac{\theta - \theta_r}{\theta_s - \theta_r}\right) \quad \textbf{(3.5b)}$$

where, θ = current volumetric water content, k = fitting parameter, θ_r = residual volumetric water content from a SWCC, and θ_s = volumetric water content from a SWCC at 100 % saturation, as illustrated in Figure 2.2 and Figure 2.13. They used a modified direct shear apparatus to measure the shear strength of compacted glacial till specimens. They first proposed Equation (3.5a), and used experimental results to obtain the best fit value for k. Then, they proposed Equation (3.5b) without the fitting parameter k. From these equations they predicted the unsaturated shear strength and compared the results with the measured shear strength obtained from the modified direct shear apparatus. A good comparison between the experimental results and the predicted values, for the range of 0-500 kPa suction, was observed.

Others, such as Lu and Likos (2006) developed the concept of suction stress characteristic curve (SSCC) for unsaturated soils. They proposed a macroscopic stress called suction stress (σ'_s) which is the resultant of all forces including physicochemical, cementation, surface tension forces and the force from negative pore-water pressure. Suction stress is defined as:

$$\sigma'_s = \left[\sigma_{pc} + \sigma_{cap} + \chi(u_a - u_w)\right] - \sigma_{C0} = \sigma_s - \sigma_{C0} \quad \textbf{(3.6a)}$$

Thus, the effective stress will be,

$$\sigma' = (\sigma - u_a) + \sigma_s \quad \textbf{(3.6b)}$$

where, σ'_s = suction stress, σ_{pc} = physicochemical stresses, σ_{cap} = capillary stress arising from surface tension, χ = Bishop's effective stress parameter, u_a-u_w = matric suction, σ_s = uncorrected suction stress, and σ_{C0} = apparent tensile stress at saturated state.

Recently, Muraleetharan et al. (2008), Wei and Muraleetharan (2002a&b), and Wei (2001) used the theory of mixtures with interfaces (TMI) and the continuum theory of plasticity for modeling the elastoplastic behavior of unsaturated soils. They introduced the theory that resulted in the so called intergranular stress tensor σ^*_{ij}, which is defined by:

$$\sigma^*_{ij} = (\sigma_{ij} - u_a \delta_{ij}) + \theta S \delta_{ij} \quad \textbf{(3.7)}$$

where σ_{ij} = total stress tensor; $S = u_a - u_w$ = matric suction; u_a and u_w are pore air and pore water pressures, respectively; θ = volumetric water content; and δ_{ij} is the Kronecker delta.

Wei and Muraleetharan (2002a&b) and Wei (2001) showed that the intergranular stress is conjugated to plastic solid skeleton strains and the matric suction is conjugated to the irrecoverable (plastic) changes in the volumetric water content to produce mechanical and hydraulic energy dissipations in unsaturated soils.

3.2.1.3 Stiffness of Unsaturated Soils

The stress-strain behavior of unsaturated soil has always been of interest in geotechnical engineering research. Soil stiffness, an important parameter in the analysis and design of geotechnical engineering problems, has been extensively studied. For example, Seed and Chan (1959) studied the behavior of soil samples compacted dry and wet of optimum moisture content (OMC). It was observed that samples compacted wet of OMC resulted in lower stiffness than those compacted dry of OMC. However, failure envelopes were found approximately equal in both tests.

Since soil stiffness is influenced by many factors such as degree of saturation (water content, or matric suction) and strain rate, more research has been recently directed towards the effect of suction on the stiffness of unsaturated soils. Wiebe et al. (1998) conducted unsaturated triaxial compression tests to study the influence of pressure, saturation, and temperature on the behaviour of unsaturated sand-bentonite. Samples were compacted at various moisture contents and then tested. Results showed that strength and stiffness increased with increase in initial (compacted) suction. Others such as Blatz et al. (2002), conducted similar kind of research and compared their results with Wiebe et al. (1998). Blatz et al. (2002), however, performed the triaxial results on samples compacted at same target moisture content and density, and then dried to a series of selected suction values. They concluded that stiffness increased nonlinearly with

increase of suction independent of the confining pressures at all suction levels. They also concluded that increased dry density, associated with shrinkage under increased suction, had a greater impact on the stiffness than the confining pressures. This is especially significant for lower suction values where the rate of shrinkage is the greatest.

Numerous other researchers (Mendoza and Colmenares 2006, Bilotta et al. 2006, Alramahi et al. 2008, and Sharma and Bukkapatnam 2008) conducted investigations on unsaturated soil behavior (mainly stiffness) at very small strains, which is important in assessing the deformation of soils. Most studies conducted small strain tests (using P or S waves through the samples) under controlled suction environment. Results showed that stiffness at very small strains (G_{max}) increased with increase of suction.

Silva et al. (2002) investigated the mechanical response of unsaturated soil under controlled matric suction. They studied the effect of matric suction on stiffness under both low and high strains. Vassallo et al. (2007) studied the effect of net stress and suction history on the small strain stiffness of compacted clayey silt. They reported that the behavior of the soil along loading-reloading cycles of drying-wetting cycles indicated that the initial shear stiffness (G_0) depends significantly not only on the net normal stress (σ-u_a) and suction (u_a-u_w) but also on "the stress history". They emphasized the importance of stress history on G_0 rather than "suction effects" which is still one of the variables affecting the mechanical response. Ng et al. (2009) studied the effect of wetting/drying and stress ratio on anisotropic stiffness of an unsaturated soil at very small strains. Results indicated that the small strain shear modulus (G_0) of soil increased nonlinearly with increase in suction, and a hysteretic behavior was observed for G_0 between drying and wetting curves with matric suction.

Little research has been found on the effect of suction on the stiffness of unsaturated interfaces. Hamid (2005) conducted suction controlled unsaturated direct shear interface tests. Results showed that increasing suction resulted in an increase of maximum shear stress and stiffness.

3.2.1.4 Impact of Hydraulic Hysteresis on Behavior of Unsaturated Soils

3.2.1.4.1 Influence of Hydraulic Hysteresis on Shear Strength

Few researchers studied the effect of suction hysteresis on the shear strength of unsaturated soils. Thu et al. (2006) investigated the effects of hysteresis on shear strength envelopes from constant water content and consolidated drained triaxial tests. Nishimura and Fredlund (2002) studied the hysteresis effects, resulting from drying and wetting under relatively high total suction conditions, on the shear strength (mainly compressive strength) of a compacted silty soil and compacted kaolin. Han et al. (1995) studied the hysteresis effect on the shear strength of residual soils. All the latter studies reported that the drying path showed slightly higher shear strength compared to the wetting path (for silty and clayey soils). They suggested that this difference is related to the contact area of water in the soil (less water during wetting thus less contact area between water and particles) which affects the interparticle forces and results in lower shear strength for wetting. On the other hand, Galage and Uchimura (2006) studied the effects of wetting and drying on the unsaturated shear strength of silty sand under low suctions and reported that the soil at wetting had higher shear strength as compared to the soil at drying under same suction. Shemsu et al. (2005) studied the cyclic suction loading influence on the shear strength of unsaturated soil. It was concluded that specimens that underwent cyclic suction loading showed higher peak shear strength. Other studies such as Nishimura et al.

(1999) investigated the influence of stress history on the strength parameters of an unsaturated statically compacted soil. A total stress ratio (TSR), which is the ratio of compaction pressure to the confining pressure, was used as a measure of stress history. Results showed that the loading history influenced the shear strength parameter (ϕ^b) associated with suction.

3.2.1.4.2 Modeling of Hydraulic Hysteresis and Stress-Strain Behavior

Extensive research has been conducted to study the effect of suction on the mechanical behavior of unsaturated soils. An increasing amount of experimental evidence (e.g. Rampino *et al*., 2000, Geiser *et al.*, 2000, Miller et al. 2008, Muraleetharan et al. 2008) shows that suction history significantly influences the SWCC and in turn the stress-strain behavior of unsaturated soils. A large number of studies have been found in the literature that present models for unsaturated soils (e.g. Alonso *et al*., 1990; Matsuoka *et al*., 2002; Gallipoli et al. 2003, Faris *et al*., 2006); however, these models do not include the effect of SWCC hysteresis. On the other hand, Macari *et al*. (2003), Chiu and Ng (2003) and Thu *et al*. (2007) proposed some new comprehensive models for unsaturated soils that incorporated SWCC hysteresis via suction, which is included in the equation for the yield surface as an independent stress variable. Likos and Lu (2004) presented a model describing the hysteresis of capillary stress in unsaturated soils using a theoretical approach based on the changing geometry of interparticle pore water menisci. Others, such as Wheeler *et al*. (2003) presented a comprehensive constitutive model for unsaturated soils, which captures the coupling effects between hydraulic hysteresis and the mechanical behavior. Sun *et al.* (2007a&b) adopted similar simplified hysteretic SWCCs and yield suction curves to Wheeler *et al.* (2003) in the framework of the Alonso

et al. (1990) model to investigate the unsaturated clay behavior. Sheng *et al.* (2008) have introduced a new modeling approach for unsaturated soils using independent stress variables. In their model, the hysteretic SWCCs are incorporated into stress-strain relationships. Muraleetharan et al. (2008) presented a theoretical framework for modeling the elastoplastic constitutive behavior of unsaturated soils by combining the theory of mixture with interfaces (TMI) and the continuum theory of plasticity. It is important to note that most of these recent models that incorporate SWCC hysteresis are lacking in validation against experimental data. There are extremely limited experimental data available that show the hysteretic behavior of SWCC and its affect on the mechanical behavior of unsaturated soils. This was one of the motivations for the research described in this dissertation, in that the experimental results obtained herein can be used for model validation. For example, parts of the experimental results from this study were published by Miller *et al.* (2008) in which the model by Muraleetharan et al. (2008) was used and validated.

3.2.2 Unsaturated Interface Testing and Modeling

3.2.2.1 Interface Testing (steel/concrete)

Interface behavior has been extensively studied and various devices have been developed for that purpose. Such devices include the direct shear, the annular shear, ring torsion, simple shear, and three dimensional interface testing apparatus among others.

For example, the direct shear testing of interfaces was used by Potyondy (1961) to determine the skin friction between various types of soils and construction materials using both stress and strain control type of shearing. Potyondy (1961) found that four major factors, the moisture content of soil, the roughness of the surface, the composition

of soil, and the magnitude of the normal load determine the skin friction. Acar et al. (1982) also used the direct shear device and concluded that relative density of sand and normal stress both influence the angle of friction between sand and structural materials such as steel, wood, and concrete. In addition, Desai et al. (1985) studied the friction between sand and steel/concrete under cyclic loading. They reported the shear strength is a function of normal stress, relative displacement, number of loading cycles and initial density.

Brumund and Leonards (1973) used the annular shear device for the experimental study of static and dynamic friction between sand and typical construction materials. The device consists of a cylinder of sand encased in a rubber membrane with a rod located along its axis. A normal stress was applied to the sand-rod interface by evacuating air from within the membrane. The rod was then slipped relative to the sand by applying static or dynamic forces in the axial direction. They found that the coefficient of friction increases with the surface roughness and angularity of the sand grains. They also found the dynamic coefficient of friction is about twenty percent greater than the static coefficient, in the case of non-lubricated surfaces.

A ring torsion apparatus to study the behavior of interfaces between sand and steel was used by Yoshimi and Kishida (1981). A static torque was applied to shear the interface under constant normal load applied with weights. The circumferential and vertical displacements of the metal ring were measured during the test. In addition, the deformation of the sand and the slippage at the soil-metal contact were measured in some tests using x-ray radiography.

A simple shear type device that was capable of measuring both sliding displacement between steel and soil as well as shear deformation of the soil mass was developed by Uesugi and Kishida (1986). The container holding the sand was a stack of aluminum plates. The surface of each plate was lubricated to allow the container to follow the shearing deformation of sand with minimum frictional resistance. During shearing a more pronounced peak in shear stress was observed for rough surfaces followed by strain softening until the shear stress leveled off at the residual shear strength.

An apparatus was developed by Fakharian and Evgin (1996) that has the capability of three dimensional monotonic and cyclic loading. It is capable of applying normal stress, and shear stresses in the x and y directions. The apparatus has the capability for direct shear and simple shear testing in 3-D space. Various stress paths were conducted in the x-y plane. Results showed the resultant shear-stress displacement curves did not experience a change with different stress paths. In addition, Evgin and Fakharian (1996) conducted tests on an interface between quartz sand and rough steel plate. Based on the experimental results they concluded that the coefficient of friction corresponding to the resultant peak (τ_p) and residual shear strengths (τ_r) were independent of the stress path.

Generally, the research and analysis of interfaces assumes either dry or fully saturated conditions. To the author's knowledge little research has been conducted on interfaces in unsaturated soil, and more specifically few, if any have focused on the hysteresis effect on unsaturated interfaces. Researchers at the University of Oklahoma (e.g., Hamid 2005, Miller and Hamid 2007) developed a direct shear device for testing of soil-structure interfaces under suction-controlled conditions. A series of soil-steel interface (rough and smooth plates) shear tests was carried out on a low plastic clayey-silt soil at different

moisture contents along a drying path and subjected to different matric suction values (20 kPa, 50 kPa and 100 kPa). Hamid and Miller (2009) found that matric suction clearly influenced the strength of the interface for both rough and smooth counterfaces.

3.2.2.2 Geosynthetic Interface Testing

Although coarse-grained soils are the recommended backfills in MSE walls in North America (Elias et al. 2001, AASHTO 2002), some industry design guides (NCMA 2002) allow for the use of up to 35% fine-grained soils, provided that a properly designed drainage system is present. The British Standard (BS8006 1995) also allows cohesive-frictional soils (i.e., soils with greater than 15% passing 63 μm sieve) to be used for wall backfill materials. Backfills with up to 50% fine grained soils (i.e., passing sieve #200) are allowed in some guidelines for the construction of reinforced embankments and slopes (Elias et al. 2001). In many projects (e.g., Powel et al. 1999, Musser and Denning 2005) low quality backfill soils have been used in slopes and highways due to scarcity and high cost of good backfill soils in local areas. Since fine contents as low as 6-10% can significantly reduce the permeability of soils (BS8006 1995, Elias et al. 2001, Koerner 2005) and since these structures are built in unsaturated soil conditions, one main concern in their stability analysis and design is the reduction of the soil-reinforcement interface shear strength as a result of wetting. Factors such as seasonal precipitation and variation of the ground water table can significantly alter the soil moisture condition and suction, and thus the interface behavior. For example, some case studies of failure or large deformations of MSE walls have been reported (e.g., Mitchell and Zornberg 1995, Christopher et al. 1998, Koerner 2005, Sandri 2005, Lawson 2005, Stulgis 2005) where backfill soils were compacted wet of optimum or where the

structures under construction were subjected to heavy rainfalls resulting in increase of pore water pressure, decrease in matric suction, and thus reduction in shear strength and excessive deformations.

Current laboratory techniques to determine the soil-geosynthetic interface strength include interface shear tests (ASTM 2009; D5321) and pullout tests (ASTM, 2009, D6706) on soil-geosynthetic specimens. Specimens are generally compacted at optimum moisture content and 95% of maximum dry density in order to simulate field conditions during construction. However, no assessments are currently made on the influence of drying and wetting on the soil-geosynthetic interface properties. This constitutes an unsaturated soil problem in which the influence of soil suction on the shearing response of the soil-geosynthetic interface should be investigated.

Numerous studies on direct shear testing of soil-geosynthetic interfaces are found in the literature (e.g., Frost and Han 1999, Goodhue et al. 2001, Gourc et al. 2004, Koerner 2005, and Sia and Dixon 2007 among others). However, very limited studies have been conducted on unsaturated soil-geosynthetic interfaces. Goodhue et al. (2001) carried out direct shear tests on sand and foundry sand samples with geosynthetic (i.e., geogrid, geotextile and textured geomembrane) specimens and found that the drained interface friction angles were in close agreement with the as-compacted friction angles of the foundry sand samples except when a significant amount of bentonite was added to the sand. Fleming et al. (2006) used a modified direct shear device with a miniature pore pressure transducer (PPT) that measured changes in the pore water pressure at smooth geomembrane-soil interfaces. However, they could only measure relatively low suction values (less than 30 kPa) due to limitation of their PPT device. In addition, they were

only able to predict the soil-geomembrane interface shear strength values using unsaturated soil mechanics theory at low normal stress values. At higher normal stress values, the interface behavior appeared to be governed only by the magnitude of total normal stress. They also reported that a near saturated condition at the soil-geomembrane interface resulted in a lower strength. Sharma et al. (2007) used the same device described by Fleming et al. (2006), to measure suction close to the interface of the soil-geomembrane during shearing. They concluded that it is important to evaluate the shear behavior at the interface between geomembrane and unsaturated soil at low matric suction values. Results suggest that soil suction contributes to shearing resistance at low normal stress values but not as much at higher normal stresses.

None of the studies described above carried out interface tests under suction-controlled conditions. The above survey of literature clearly indicates that there is a need to investigate the soil-geotextile interface shearing behavior in unsaturated soil conditions. Part of the current study addressed this need by modifying the direct shear test device (Miller and Hamid 2007) to test soil-geosynthetic interfaces under suction-controlled unsaturated conditions.

3.2.2.3 Interface Constitutive Modeling

In the literature, there are numerous studies on constitutive models of interfaces; starting from the basic Mohr-Coulomb strength models, to the Nonlinear Elastic deformation models, to the Elastoplastic models. Similar to soils, failure criteria have been applied to interfaces. For simplicity, the shear behavior of the interface before failure was originally considered either rigid or elastic. Later, nonlinear elastic models were used for interface modeling. Drumm and Desai (1986) used a modified form of the

Ramberg-Osgood (1943) model, which simulates the interface behavior as piecewise nonlinear elastic, to study sand-concrete interface response to cyclic loading. Clough and Duncan (1971) also introduced a nonlinear elastic model for the analysis of soil structure interaction problems. Interface direct shear tests were used to obtain the hyperbolic relationship of shear strength and relative displacement.

Soon after, the theory of plasticity was used for interface modeling to account for coupling between normal and shear behavior. Desai (1980), Desai and Faruque (1984), and Desai et al. (1986) have introduced the basic formulation of elastoplstic model for frictional materials. Based on the same concept, Desai and Fishman (1991) developed an elastoplastic model for hardening behavior of rock joints with associative and non-associative flow rules. Navayogarajah (1990) and Navayogarajah et al. (1992) modified the latter model for monotonic and cyclic behavior of interfaces between sand-steel and sand-concrete. Another elastoplastic model for interfaces was proposed by Boulon and Nova (1990) for dry sand and rough surfaces. Others such as Fakharian and Evgin (2000) presented an elastoplastic model of stress-path dependent 2-D and 3-D behavior of interfaces based on the model by Navayogarajah et al. (1992). Zeghal and Edil (2002) presented an elastoplastic Mohr-Coulomb isochoric interface model utilizing the work hardening and nonassociative plasticity rules. Hu and Pu (2004) performed sand-steel interface tests to obtain the stress-strain relationship. They developed a damage constitutive model based on the disturbed state concept theory. None of the previous literature, so far, has covered the behavior of interfaces in unsaturated soil except the study by Hamid (2005) and Miller and Hamid (2007). In their study, they have modified the conventional direct shear apparatus for testing unsaturated soil as well as interfaces

between unsaturated soil and steel plates of varying roughness. Miller and Hamid (2007) proposed the following interface shear strength equation, following the same reasoning for Equation (3.4),

$$\tau_f = c'_a + (\sigma_n - u_a)_f \tan\delta' + (u_a - u_w)_f \tan\delta^b \quad \textbf{(3.8)}$$

Where, δ' = the interface friction angle with respect to net normal stress, δ^b = the interface friction angle with respect to matric suction.

Hamid and Miller (2008) developed a constitutive model capable of modeling the behavior of interfaces in dry and saturated soils as well as in unsaturated soils under constant net normal stress. The model was an extension of Navayogarajah et al. (1992) model. The modified model is based on the disturbed state concept, but incorporates two independent stress variables, which are the net normal stress and matric suction.

Part of the current research involved extending the model by Hamid and Miller (2008) to predict the experimental results obtained in this study on a different interface material such as geotextiles.

3.3 INTERFACE DIRECT SHEAR TEST MATERIAL, SAMPLE PREPARATION AND APPARATUS

3.3.1 Interface Materials and Sample Preparation

Two stainless steel plates (counterfaces), designed by Hamid (2005) are used in this study. One steel plate is 25.5 mm thick and 102 mm in diameter with rough surface geometry as shown in Figure 3.2. Another steel plate with polished smooth surface is used with the same dimensions as the rough steel plate. Surface roughness is defined based on the roughness profile. Hamid and Miller (2008) used the normalized surface roughness as proposed by Uesugi and Kishida (1986):

$$R_n = R_{max} / D_{50} \quad \textbf{(3.9)}$$

where, R_{max} is the maximum peak to valley height, and D_{50} is the grain size diameter corresponding to fifty percent finer (for this soil D_{50} is approximately 0.7 mm). The same has been used in this study and based on the grain size analysis of the test soil, R_n= 5.35 and 0.035 for rough and smooth estimated steel plates, respectively.

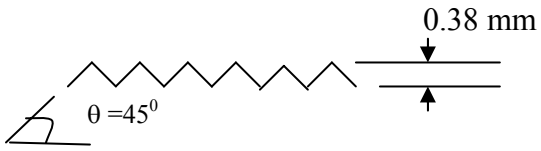

Figure 3.2- Surface Geometry of Rough Steel Plate

The geosynthetic material used in the geosynthetic-soil interface tests was a woven polypropylene (PP) geotextile, with a thickness of approximately 0.9 mm and material properties shown in Table 3.1. R_{max} for geotextile interfaces was approximated by measuring the geotextile peak-valley distance using a caliper, which was approximately equal to 0.3 mm. Figure 3.3 shows an illustration of R_{max} peak-valley measurement.

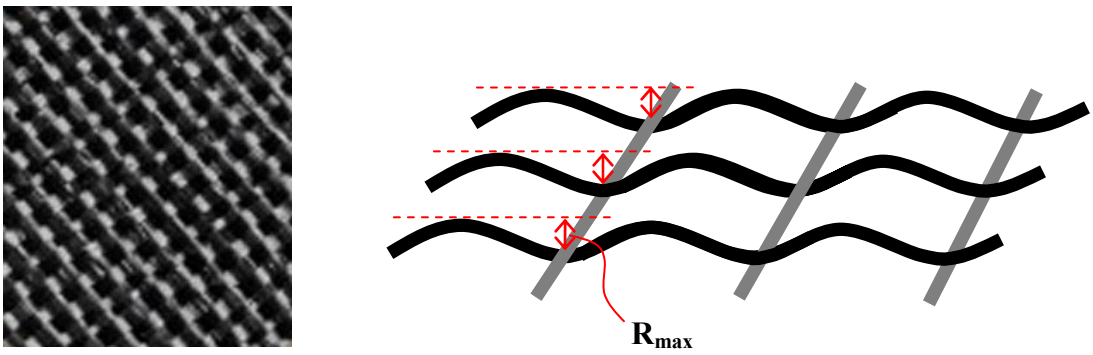

Figure 3.3- Illustration of Geotextile R_{max} measurement

Table 3.1- Properties of the Woven Geotextile Used in the Interface Shear Tests (IFAI, 2009)

Property	Test Protocol	Value/description
Polymer type	-	Polypropylene
Fabric	-	Slit-film, Woven
Mass per unit area (g/m^2)	ASTM D5261	
Percent open area (%)	CWO-22125	
O_{95} (mm), Apparent opening size (U.S. Sieve)	ASTM D4751	0.600 (30)
Permittivity (s^{-1})	ASTM D4491	0.52
Puncture resistance kN (lb)	ASTM D4833	0.8 (179.8)
Trapezoidal tearing strength kN (lb)	ASTM D4533	0.76 (170.8) MD, 0.49 (110.2) XD
Grab tensile strength kN (lb)	ASTM D4632	1.78 (400.1) MD, 1.10 (247.28) XD
Elongation (%)	ASTM D4632	15 (MD), 6 (XD)
Survivability class	AASHTO M288	2,3
Applications	AASHTO M288	Separation, Stabilization, Reinforcement
Wide-width ultimate tensile strength kN/m (lb/ft)	ASTM D4595	47.3 (3241.0) MD, 39.4 (2699.7) XD

Note: MD and XD refer to machine direction and cross-machine direction, respectively.

3.3.2 Soil and Interface Direct Shear Test Apparatus

The modified direct shear test (DST) device (Figure 3.4) for testing of unsaturated soil and soil-structure interfaces under suction-controlled conditions was used in this study and described by Hamid (2005) and Miller and Hamid (2007). Briefly, the modified DST apparatus includes an air pressure chamber, a control system, shear boxes for testing unsaturated soil and interfaces (e.g. steel/geosynthetics, Figure 3.4), a precision stepper-motor pump to control the pore water volume and pressure, drainage lines, high air entry porous disc (HAEPD) and a Diffused Air Volume Indicator (DAVI). The pore water pressure is regulated using a computer-controlled pump capable of maintaining pressure within ±1 kPa and detecting volume changes within ±1 mm^3.

Drainage lines connecting the HAEPD to the water controller consist of 3-mm diameter high-pressure polyvinylidene flouride (PVDF) tubing.

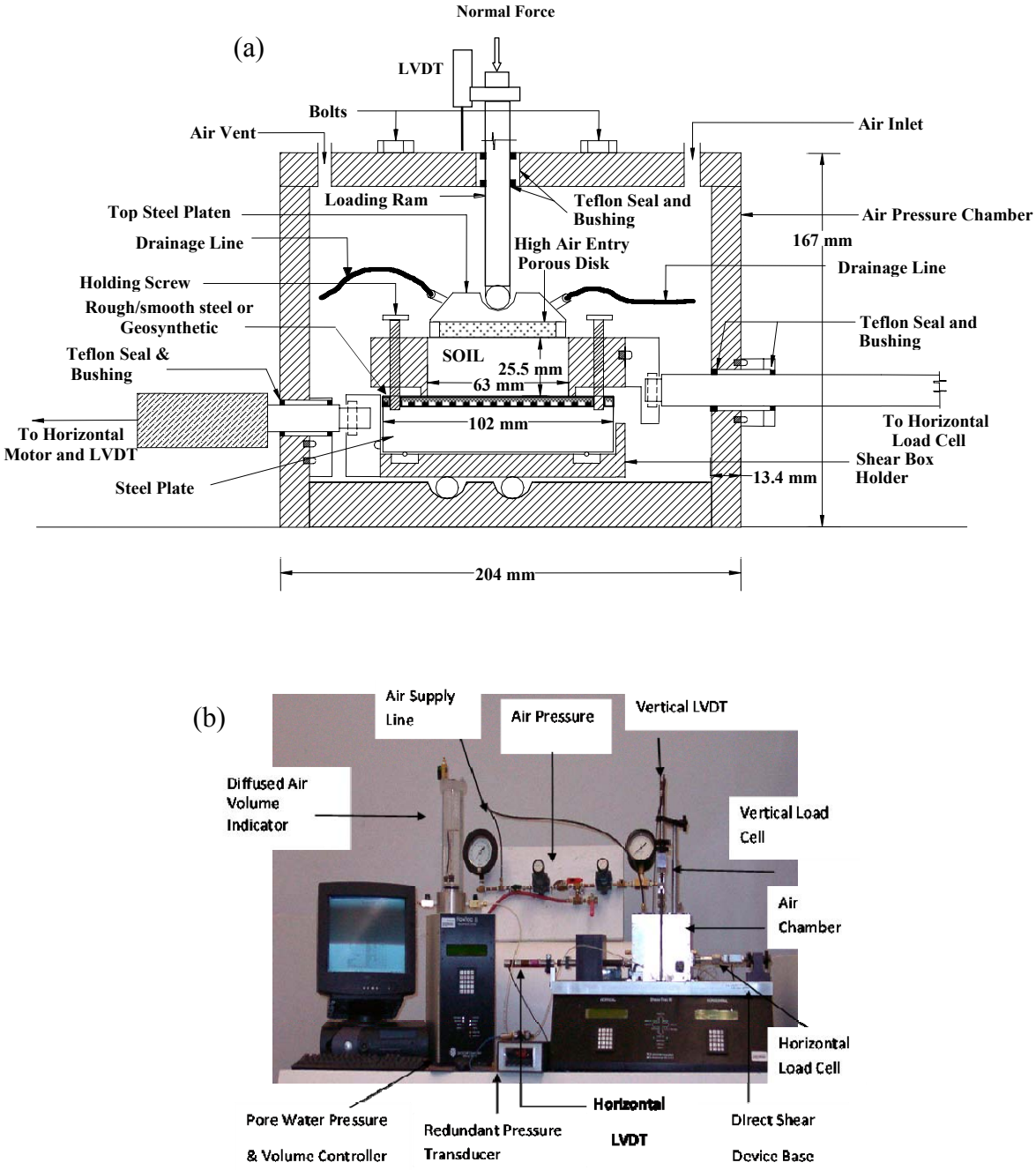

Figure 3.4- a) Schematic View and b) Photo of the Unsaturated DST Apparatus from Hamid (2005)

Air pressure in the chamber is controlled using a regulator and monitored using a pressure gage with a resolution of about 0.7 kPa. The air can access the soil sample through openings in the shear box including the gap (of about 1 mm) created between the two halves of the box and the small space (of about 3 mm) surrounding the top cap. The vertical and horizontal deformations during testing are measured using LVDTs (as shown in Figure 3.4) with an approximate resolution of 3.87 x 10^{-4} mm. The horizontal and vertical loads are measured using load cells with a capacity of 2.23 kN (500 lbf).

3.4 SOIL AND INTERFACE TESTING PROCEDURE

3.4.1 Suction-Controlled Soil and Interface Tests

The procedure to prepare the specimens and to conduct the interface tests is described by Miller and Hamid (2007). As described in Section 2.3.1, the soil sample is first compacted on top of the counterface or geotextile that is mounted on a steel block. After compaction, the shear box cell containing the test specimen is placed in the DST air pressure chamber. The drainage line from the pore-water pressure controller is connected to the top platen inlet port of a high air entry porous disc (HAEPD) placed on the top of the compacted soil (Figure 3.4). It is important to note that the HAEPD is saturated with de-aired water prior to testing. A seating load of 14 to 35 kPa is applied to the test specimen in order to stabilize the position of the upper half of the shear box when it is raised to introduce the gap needed before the shearing process. An illustration of the direct shear test stress loading pattern is shown in Figure 3.5.

Approximately one hour after the initial compression seating load (path OA, Figure 3.5a), the two screws holding the two halves of the shear box together are removed. A gap is created between the two halves of the shear box by turning the four raising screws,

which are then reversed to eliminate any contact between the screws and the box. After creating a gap of about 1 mm (which is slightly greater than the recommended gap of 0.64 mm by ASTM D3080, and also falls in the range of 10-20 times of D_{50} of the soil), the air chamber lid is sealed with bolts (Figure 3.4). The target matric suction value (u_a - u_w) following a drying path (path AB, Figure 3.5) is then applied to the specimen by increasing the air and water pressures simultaneously via the axis translation technique.

The test specimen is allowed to equilibrate under the applied suction value. Equilibrium is completed when negligible change in the water volume is observed. The net normal stress ($\sigma_n - u_a$) is then increased in increments of 35 kPa by applying a vertical load to reach the target net normal stress (path BC, Figure 3.5). After the specimen is consolidated under the target vertical stress, it is subjected to drained shearing (path CD, Figure 3.5) while controlling both suction and net normal stress. Shearing is applied at a displacement rate of 0.005 mm/min up to about 10 mm displacement. For the geotextile interfaces, shearing is applied along the cross machine direction of the woven geotextile specimen. The changes in the specimen height and water volume are measured and recorded during all stages of the test. The specimen height is measured using an LVDT that is attached to the loading ram. During shearing, the horizontal load and the horizontal and vertical displacements are measured and recorded.

3.4.2 Hysteretic Suction-Controlled Interface Tests

Direct Shear Interface Hysteresis Tests are carried out similarl to the procedure described above except that the sample is first dried out by increasing suction on the SWCC drying path to a higher value and wetted again to the previous suction (as shown

in Figure 3.5) where shearing is conducted to investigate the effect of SWCC hysteresis on the shear strength results. Similarly to suction-controlled direct shear tests on the drying path, tests with hysteresis were first consolidated under a seating load (path OA, Figure 3.5) of 14-35 kPa to stabilize the position of the upper half of the shear box. Approximately one hour after the seating load, the two screws holding the two halves of the shear box together are removed and a gap is created between the two halves of the shear. After creating the gap, the target matric suction value is then applied to the specimen following the drying curve (path AB, Figure 3.5). After equilibrium of the target suction, the target net normal stress is then applied (path BC, Figure 3.5). After consolidation under the target vertical stress, the specimen is then subjected to more drying by increasing suction (i.e. increasing u_a while keeping a constant u_w). Suction is increased up to about 100 kPa (path CE, Figure 3.5), after which it is decreased back to the previous target suction and allowed to reach equilibrium (path EF, Figure 3.5). Following equilibrium at point F, shearing (path FG, Figure 3.5) is then applied at the same displacement rate (0.005 mm/min up to about 10 mm displacement) used for tests without hysteresis.

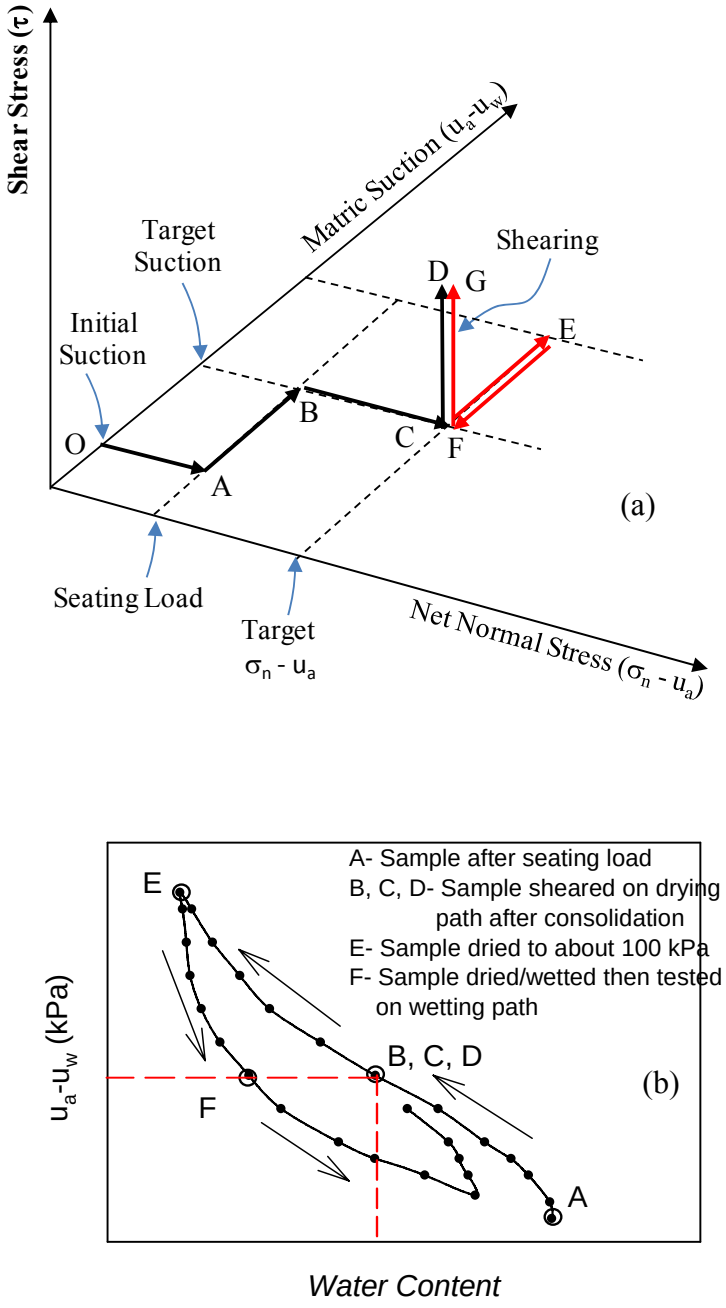

Figure 3.5- Illustration of the DST Interface Suction Hysteresis Test Sequence

3.5 Results and Discussion for Unsaturated Soil Direct Shear Tests

Suction-controlled direct shear tests on unsaturated soils were performed under a range of constant suction and net normal stress of 0-100 kPa and 50-300 kPa, respectively. Test results and the effect of net normal stress and suction (with and without

hysteresis) on the stress-displacement and volumetric behavior of unsaturated soil and interfaces are discussed in this section.

3.5.1 Suction-Controlled Direct Shear Test DRYING Path Results

3.5.1.1 Equalization Phases (Suction and Net Normal Stress)

Figure 3.6-Figure 3.9 show comparisons of the consolidation responses of the soil under different applied suction values (25, 50 and 100 kPa) at all net normal stresses (50 kPa, 100 kPa, 150 kPa and 300 kPa) in order to study the effect of suction on the soil behavior. Figure 3.6 presents the consolidation results for net normal stress of 50 kPa, on which letters A, B and C mark the end of each consolidation stage i.e., seating, suction and net normal stress, respectively, corresponding to the loading points shown in Figure 3.5. Figure 3.6a-Figure 3.9a show plots of change in vertical deformation, normalized to the specimen height (v/H_0), versus time during the equalization phase. In general, for a given net normal stress, the volume changes of the soil specimens due to suction application seemed relatively small (e.g. A-B, Figure 3.6a). In addition, the magnitude of compression due to net normal stress application (e.g. B-C, Figure 3.6a) seems not greatly influenced by soil suction for the range of suction values examined. However, note that soil sample with net normal stress of 100 kPa and suction of 50 kPa (Figure 3.7a) had a seating load of 14 kPa compared to 34 kPa for the other test samples. Thus, the load needed to achieve the target net normal stress value of 100 kPa was higher for this specific test (with 50 kPa suction test) as compared to tests with other suction values. The result is more compression during application of net normal stress for this test as clearly seen in Figure 3.7 and Figure 3.11.

On the other hand, Figure 3.6b-Figure 3.9b show the influence of soil suction on the change in water content (Δw %) in the soil specimens during equalization periods. During the application of suction, water continuously flowed out of each specimen (drying path) to reach the target suction value (e.g. A-B, Figure 3.6b). As expected, it was observed that the water drained (Δw) from the specimen increased with increase in suction. Samples under all net normal stresses seemed to undergo similar change in water content, Δw of about 3.9 %, 8.9 % and 13.6 % for the suction values of 25 kPa, 50 kPa and 100 kPa, respectively. However, the effect of the net normal stress on the change in moisture content (e.g. B-C, Figure 3.6b) was found to be small (i.e., about 0.1 %) for all suction values examined.

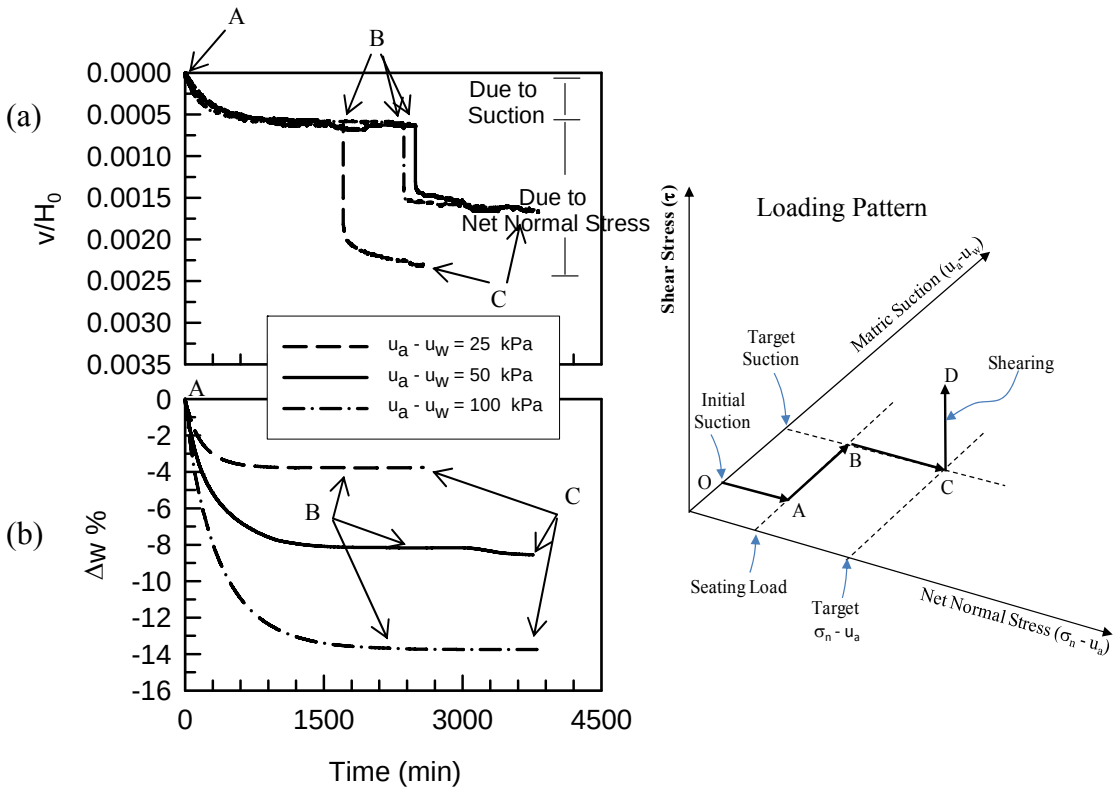

Figure 3.6- Effect of Suction (u_a-u_w) on (a) v/H_0 and (b) Δw % during Equalization of Unsaturated Soil Tests under Net Normal Stress (σ_n-u_a) of 50 kPa

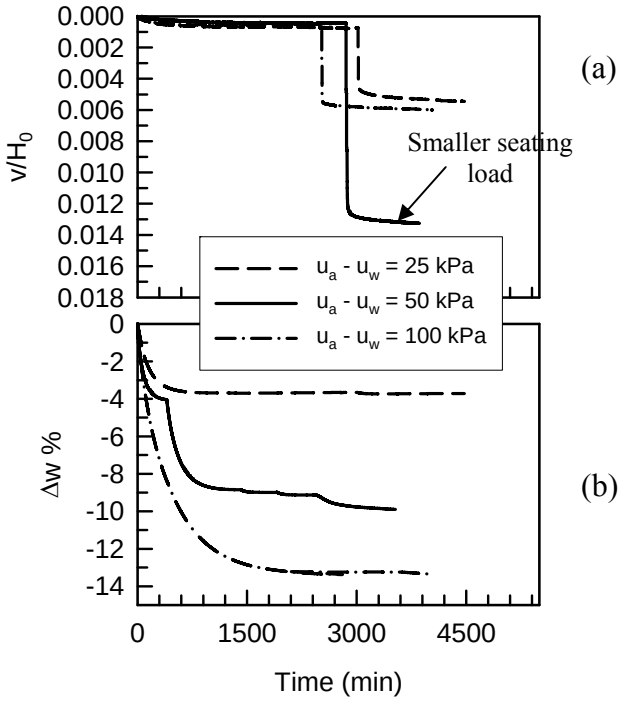

Figure 3.7- Effect of Suction (u_a-u_w) on (a) v/H_0 and (b) Δw % during Equalization of Unsaturated Soil Tests under Net Normal Stress (σ_n-u_a) of 100 kPa

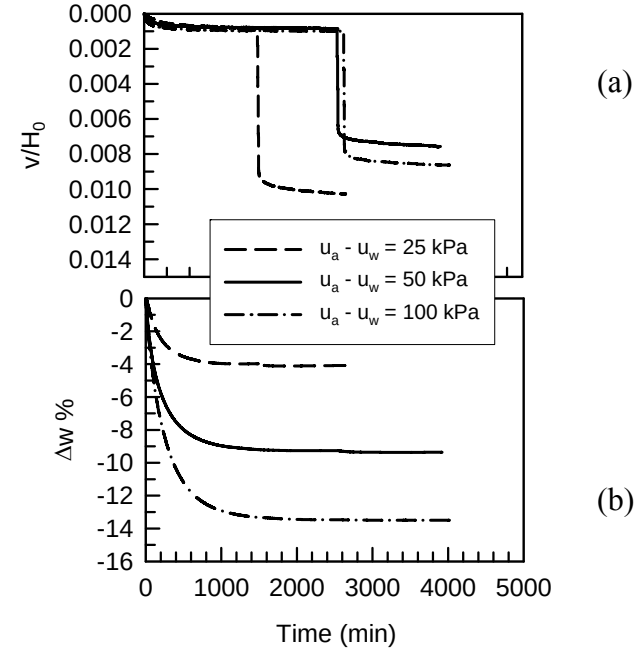

Figure 3.8- Effect of Suction (u_a-u_w) on (a) v/H_0 and (b) Δw % during Equalization of Unsaturated Soil Tests under Net Normal Stress (σ_n-u_a) of 150 kPa

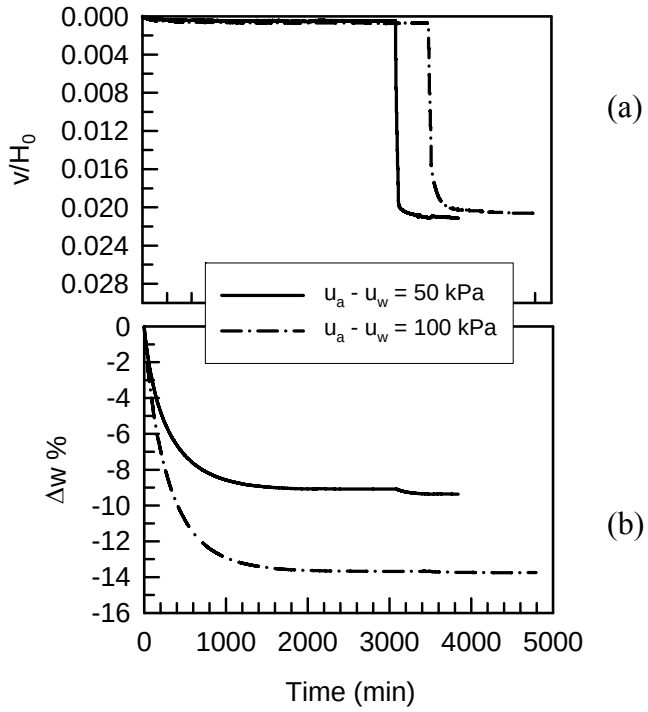

Figure 3.9- Effect of Suction (u_a-u_w) on (a) v/H_0 and (b) Δw % during Equalization of Unsaturated Soil Tests under Net Normal Stress (σ_n-u_a) of 300 kPa

On the other hand, Figure 3.10-Figure 3.12 show the effect of net normal stresses (50, 100 and 150 kPa, and 300 kPa) on the consolidation results at given suction values. Figure 3.10a, Figure 3.11a, and Figure 3.12a show plots of change in vertical deformation, normalized to the specimen height (v/H_0), versus time during the equalization phase. As expected, for a given suction the magnitude of compression increased with increase in net normal stress. Variation in water content for soil samples during equalization are shown in Figure 3.10b, Figure 3.11b, and Figure 3.12b at given suction values and for all net normal stresses. Results indicate that the change in water content (Δw %) is essentially the same at a given suction value; in other words, the water controller pulled approximately the same amount of water from all samples to maintain the required suction.

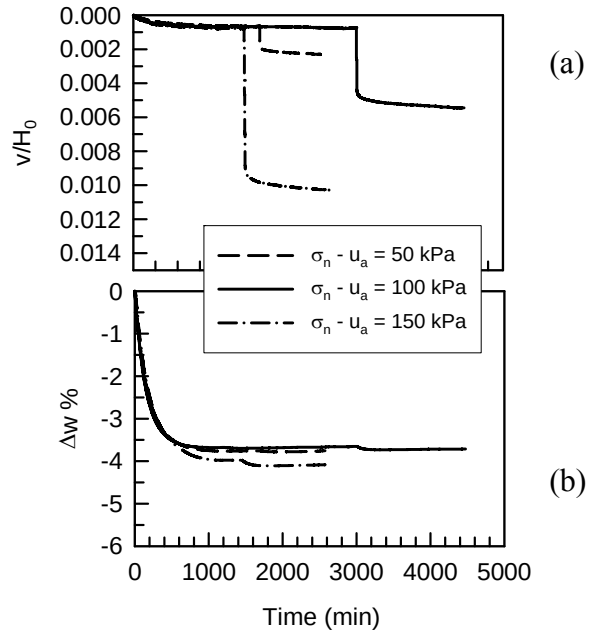

Figure 3.10- Effect of Net Normal Stress (σ_n-u_a) on (a) v/H_0 and (b) Δw % during Equalization of Unsaturated Soil Tests under Suction (u_a-u_w) of 25 kPa

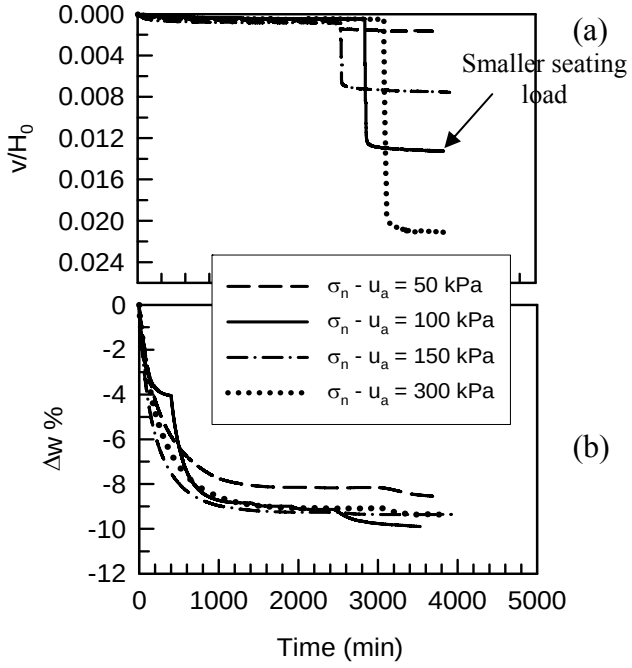

Figure 3.11- Effect of Net Normal Stress (σ_n-u_a) on (a) v/H_0 and (b) Δw % during Equalization of Unsaturated Soil Tests under Suction (u_a-u_w) of 50 kPa

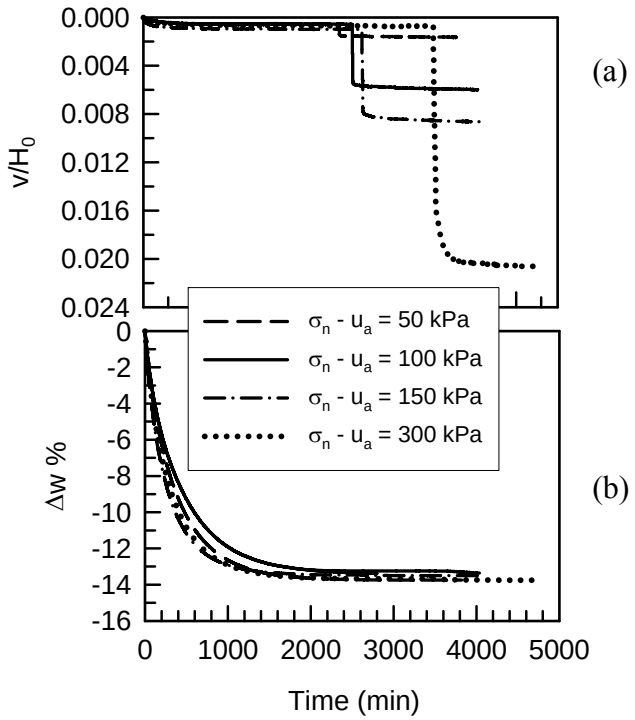

Figure 3.12- Effect of Net Normal Stress (σ_n-u_a) on (a) v/H_0 and (b) Δw % during Equalization of Unsaturated Soil Tests under Suction (u_a-u_w) of 100 kPa

Summary plots of results at end of consolidation under all matric suction and net normal stresses are shown in Figure 3.13 and Figure 3.14. Results in these figures summarize the observed behavior discussed previously where, in general: a) Δw % increased with increase of suction, b) the magnitude of compression increased with increase of net normal stress, and c) suction did not have great influence on the compression magnitude of soil. Note, Δw is the decrease in water content from initial conditions and higher Δw indicates lower water content. Figure 3.13 and Figure 3.14 indicate that the water content of soil samples under suction of 25, 50 and 100 kPa decreased by about 3.9 %, 8.9 % and 13.6 %, respectively. In addition, soil samples under net normal stresses of 50 kPa, 100 kPa, 150 kPa and 300 kPa, exhibited an average vertical compression (v/h_0) of about 0.19 %, 0.57 %, 0.9 % and 2.1 %, respectively.

Note, that the vertical compression magnitude of the sample at net normal stress of 100 kPa and suction of 50 kPa was not comparable with other samples (i.e. samples at same net normal stresses but different suction values), as seen in Figure 3.13 and Figure 3.14, due to the difference in the seating load as explained previously in this section. Water content results at end of drying before shearing corresponding to each target suction value are plotted with SWCC results as shown in Figure 3.15. This plot indicates that the DST suction-controlled tests compared well with the results from independent SWCC testing.

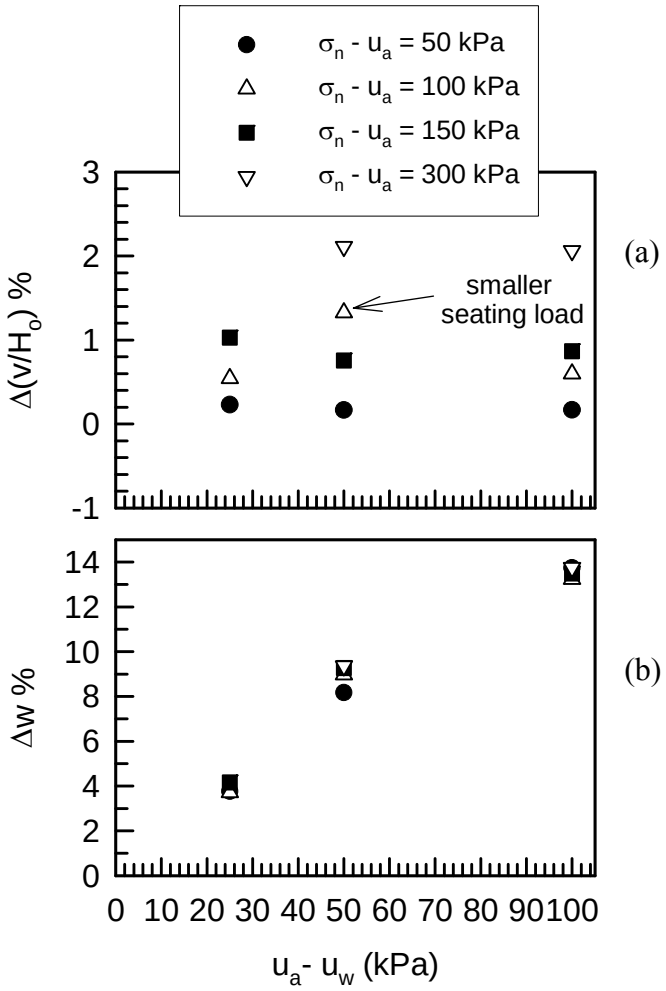

Figure 3.13- Summary of Consolidation Results versus Suction for all Net Normal Stresses

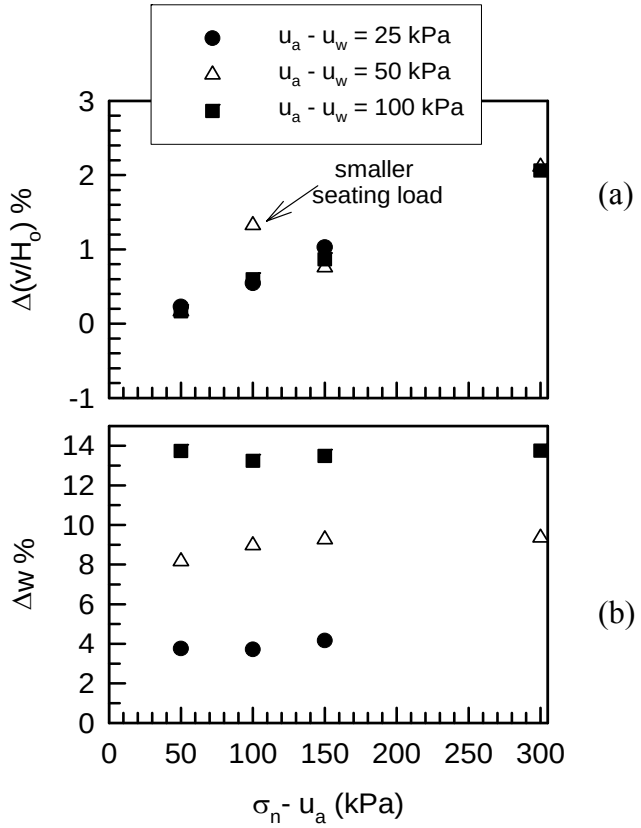

Figure 3.14- Summary of Consolidation Results versus Net Normal Stress for all Suction Values

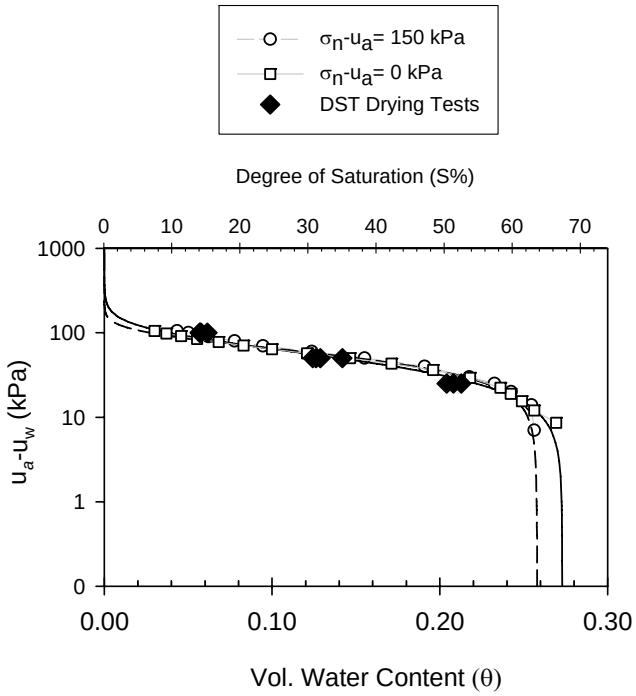

Figure 3.15- Soil Water Characteristic Curves Superimposed with Results from DST Drying (D) Path Soil Tests

3.5.1.2 Shearing Phase

In order to investigate the effect of suction on the soil behavior, shearing results were plotted at a given net normal stress under different applied suction values (25, 50 and 100 kPa) as shown in Figure 3.16-Figure 3.19. Figure 3.16a through Figure 3.19a show the variation of shear stress (τ) with horizontal displacement (u) for the soil specimens at different suction values (i.e., 25 kPa, 50 kPa, and 100 kPa) for net normal stresses of 50 kPa, 100 kPa, 150 kPa and 300 kPa, respectively. In general, results indicated that increasing suction resulted in an increase in the peak shear strength; however, a non consistent behavior for post peak shear strength of the soil specimens was observed with respect to suction. Although, in some cases post peak strength was not greatly influenced by suction. Results also indicate that the magnitude of horizontal displacement corresponding to the peak shear strength decreased slightly with the increase in suction. In addition, Specimens exhibited a slight post-peak drop in shear stress followed by a slight strain hardening.

Volume change results shown in Figure 3.16b-Figure 3.19b indicate a negligible amount of initial contraction followed by dilation in the specimens, during shearing. No consistent effect on dilation was observed due to increase in suction. In each test during shearing, a small amount of water drained out of the test specimen in order to maintain the soil suction at the target value as shown in Figure 3.16c-Figure 3.19c. Water was flowing out of sample even during dilation; this observation is in contrast with the behavior of saturated soil. In saturated soil mechanics, dilation indicates a tendency for generation of negative pore water pressure, which results in water flowing into the sample. For unsaturated soils, changes in pore water pressure are in large part the result

of changes to the air-water interfaces between particles (or menisci); these changes can be independent of total volume changes. Based on the comparison of saturated and unsaturated soil behavior it is postulated that in unsaturated soil during shearing: a) the menisci between soil particles are disrupted, and/or b) due to non-uniformity of pore sizes and water distribution (at high suction above the air entry value), increase in some localized pore water pressures may occur. These caused a tendency for increasing pore water pressure and since these are drained constant suction tests, water is drained during shear to maintain the pore water pressure and suction. Similar observations were made by Hamid and Miller (2009) and Cui and Delage (1996).

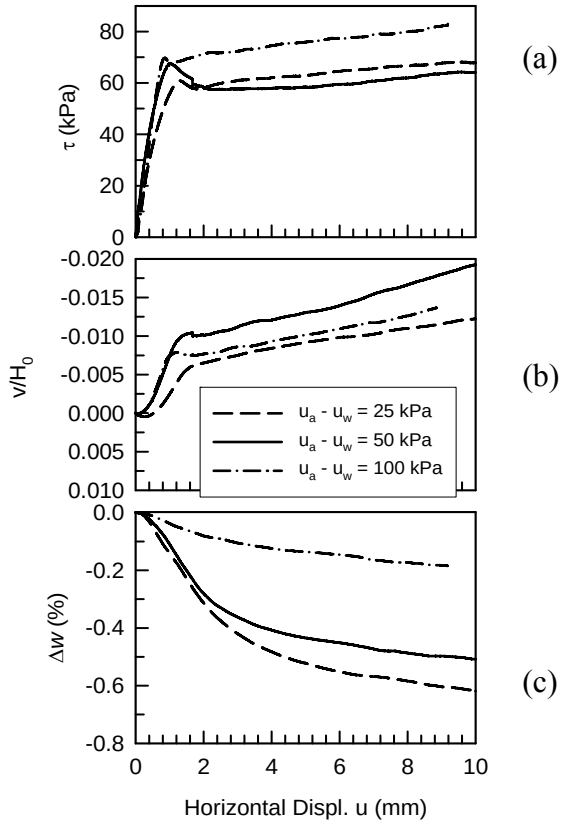

Figure 3.16- Effect of Suction (u_a-u_w) on (a) Shear Stress (τ), (b) v/H_0 and (c) Δw % during Shearing of Unsaturated Soil Tests under Net Normal Stress (σ_n-u_a) of 50 kPa

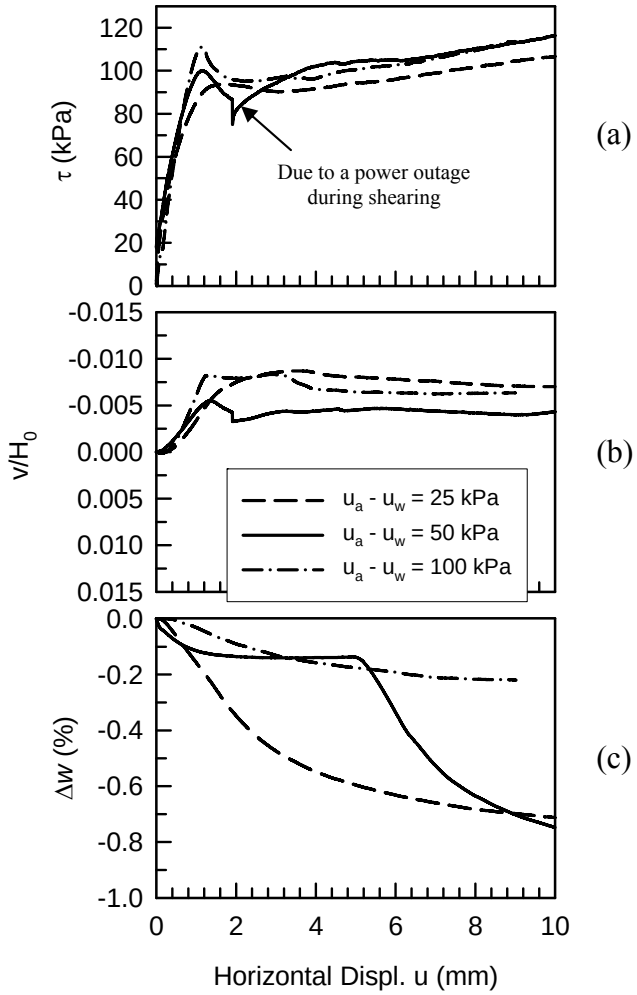

Figure 3.17- Effect of Suction (u_a-u_w) on (a) Shear Stress (τ), (b) v/H_0 and (c) Δw % during Shearing of Unsaturated Soil Tests under Net Normal Stress (σ_n-u_a) of 100 kPa

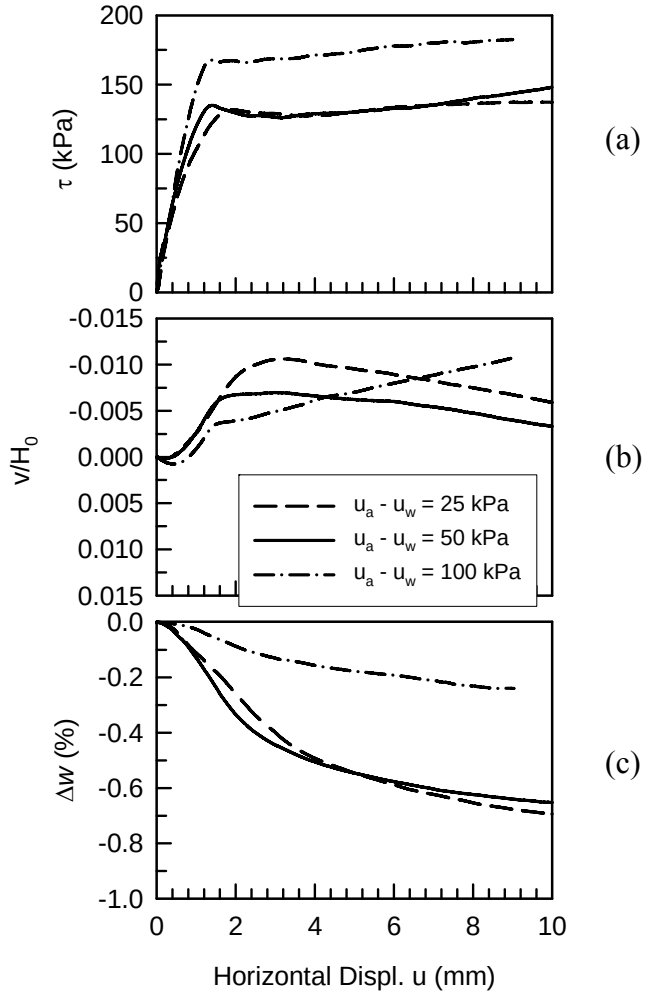

Figure 3.18- Effect of Suction (u_a-u_w) on (a) Shear Stress (τ), (b) v/H_0 and (c) Δw % during Shearing of Unsaturated Soil Tests under Net Normal Stress (σ_n-u_a) of 150 kPa

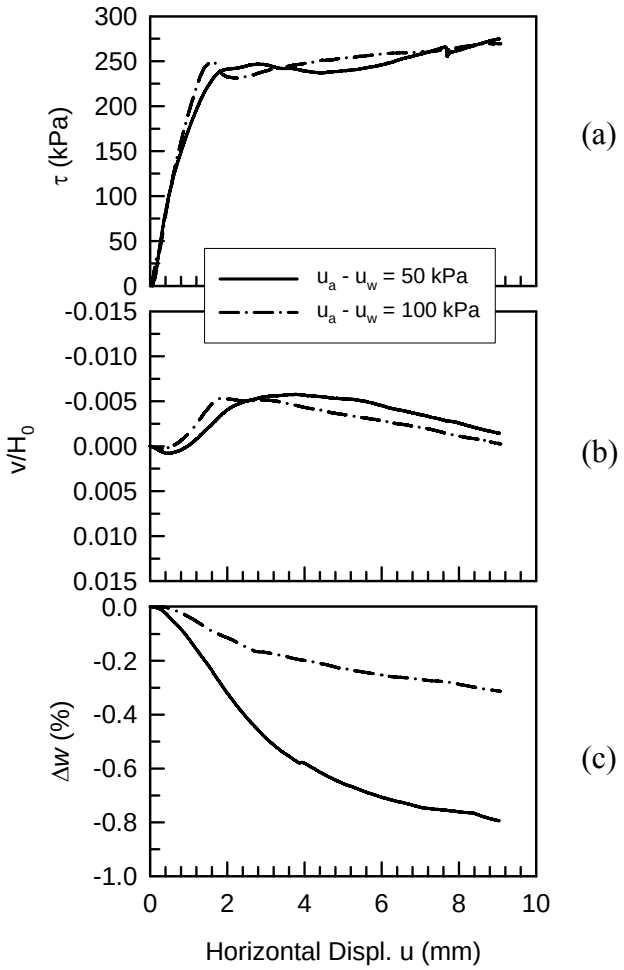

Figure 3.19- Effect of Suction (u_a-u_w) on (a) Shear Stress (τ), (b) v/H_0 and (c) Δw % during Shearing of Unsaturated Soil Tests under Net Normal Stress (σ_n-u_a) of 300 kPa

Figure 3.20 through Figure 3.22 show the shearing results under different net normal stresses (50, 100 and 150 kPa) for suction values of 25, 50 and 100 kPa, respectively. Shear strength of soil increased with increase in net normal stress for a given suction value as shown in Figure 3.20a-Figure 3.22a. Similar strain softening, dilation and change in water content behavior was observed in these figures as compared to previous plots for given net normal stress.

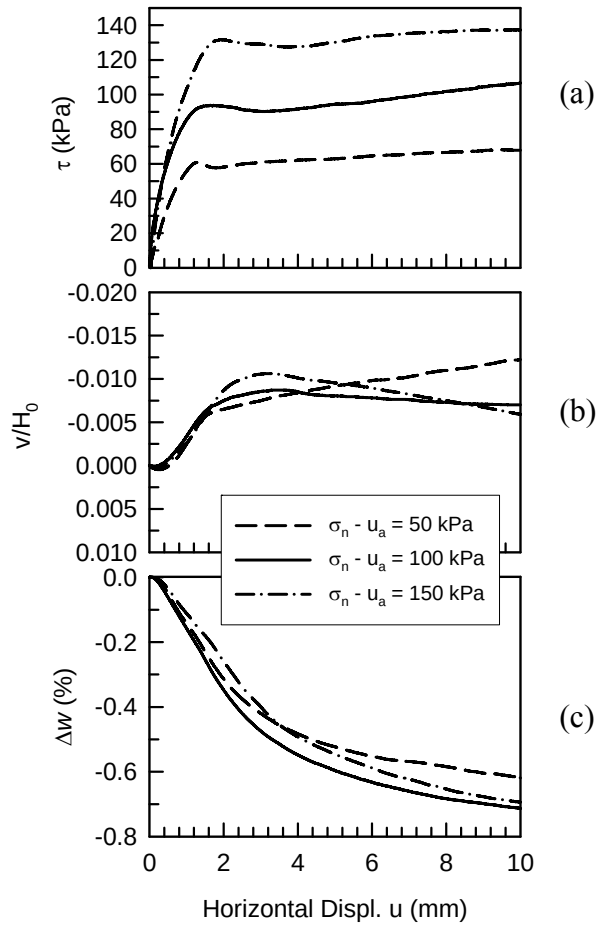

Figure 3.20- Effect of Net Normal Stress (σ_n-u_a) on (a) Shear Stress (τ), (b) v/H_0 and (c) Δw % during Shearing of Unsaturated Soil Tests under Suction (u_a-u_w) of 25 kPa

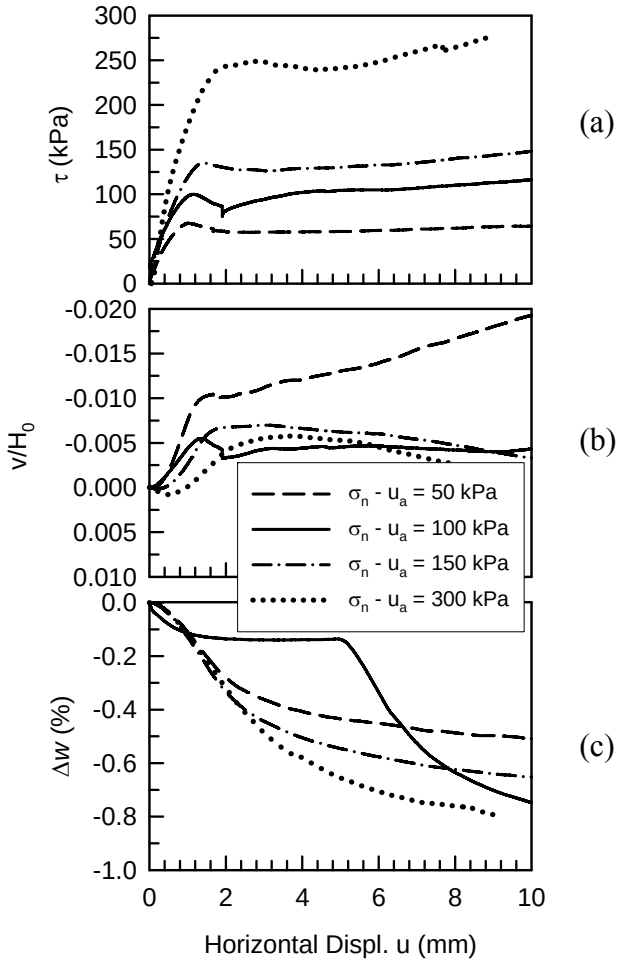

Figure 3.21- Effect of Net Normal Stress (σ_n-u_a) on (a) Shear Stress (τ), (b) v/H_0 and (c) Δw % during Shearing of Unsaturated Soil Tests under Suction (u_a-u_w) of 50 kPa

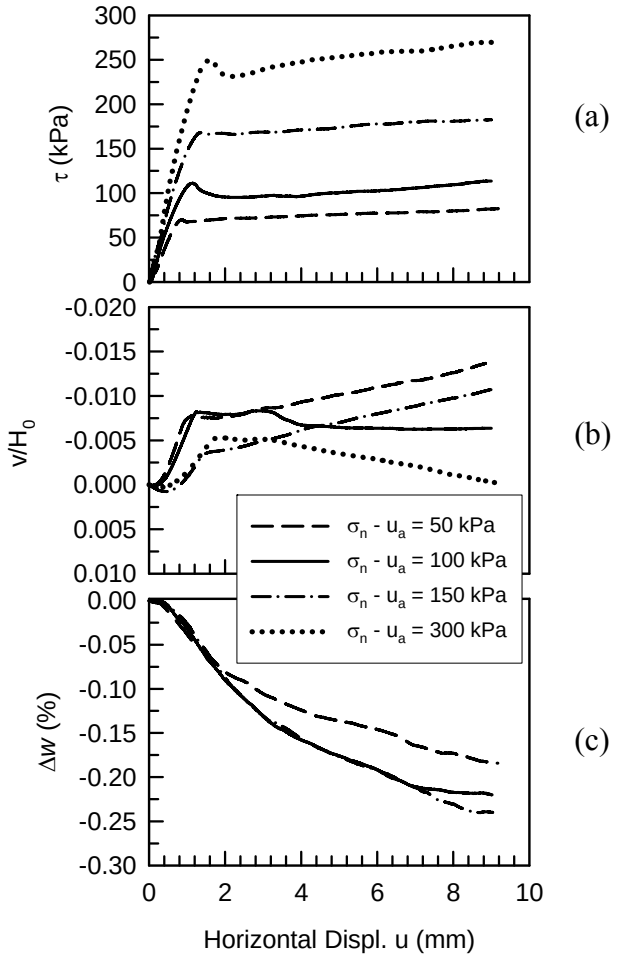

Figure 3.22- Effect of Net Normal Stress (σ_n-u_a) on (a) Shear Stress (τ), (b) v/H_0 and (c) Δw % during Shearing of Unsaturated Soil Tests under Suction (u_a-u_w) of 100 kPa

3.5.2 Suction-Control Direct Shear Test HYSTERESIS (Drying-Wetting Paths) Results

Suction-controlled hysteresis (drying/wetting cycles) tests were performed at target suctions following the drying then wetting path. In other words, after consolidation under the target suctions on the drying path (path AB, Figure 3.5) and the target net normal stresses (path BC, Figure 3.5), specimens were then subjected to more drying by increasing suction up to about 100 kPa (path CE, Figure 3.5). Suction was then decreased back to the previous target value (path EF, Figure 3.5), after which samples were sheared

(path FD, Figure 3.5). Results during consolidation and shearing are presented in the following sections.

3.5.2.1 Equalization Phases (Suction and Net Normal Stress)

In order to study the effect of suction hysteresis on the consolidation results of soil for given net normal stresses (50 kPa, and 150 kPa), results were plotted for different suction values as shown in Figure 3.23 and Figure 3.24. Consolidation results were also plotted for given suction values (8, 25 and 50 kPa) under different net normal stresses as shown in Figure 3.25-Figure 3.27. Figure 3.23 represents the consolidation results for given net normal stress of 50 kPa, on which letters A, B, C, E and F mark the end of each consolidation stages corresponding to the loading patterns from Figure 3.5. Results presented in Figure 3.23a and Figure 3.24a showed slight compression due to application of suction (AB path) that is relatively independent of suction magnitude at a given net normal stress. After application of target net normal stress (BE path) compression magnitude seemed to slightly decrease with increase of suction (for the suction range between 8-50 kPa); this difference is practically negligible (as seen in Figure 3.27a, and Figure 3.28a) and the average change in vertical displacement ($\Delta v/h_0$) was measured as 0.34 % and 1.22 % for net normal stresses of 50 kPa and 150 kPa, respectively. As suction increased up to 100 kPa (CE path) and decreased (wetting) back to prior suction value (EF path) no significant compression was observed.

Figure 3.23b and Figure 3.24b present the change in water content (Δw %) for different suction values (8 kPa, 25 kPa and 50 kPa) at net normal stresses of 50 kPa and 150 kPa, respectively. Results showed that during drying (AB path) water drained out of samples with a decrease in water content (Δw %) of 1.45 %, 3.77 % and 8.95 %, for 8, 25

and 50 kPa suction values, respectively. In addition, at end of 100 kPa suction (BE path), the decrease in water content was on average 13.4 %. Then, as samples were wetted back to prior suction target values (EF path), the net decrease in water content (Δw %) was on average 1.9 %, 6.14 % and 11 % for 8 kPa, 25 kPa and 50 kPa suction, respectively, as shown in Figure 3.28b.

Figure 3.25 through Figure 3.27 show the consolidation test results at given suction values for all net normal stresses. Figure 3.25a-Figure 3.27a indicated that as net normal stress increased compression magnitude increased. On the other hand, Figure 3.25b-Figure 3.27b showed that water changes (Δw %), during all consolidation stages (AB, BE, CE, EF paths), were approximately equal at given suction values for samples under different net normal stresses, which indicates that the system accurately controlled suction.

Results at the end of each consolidation stage were plotted as shown in Figure 3.28 and Figure 3.29. These figures indicate that suction influence on compression magnitude was nearly negligible; a slight decrease was observed as suction increased. In addition, the change in vertical displacement ($\Delta v/H_0$) increased with increase in net normal stress from 50 kPa and 150 kPa with average $\Delta v/H_0$ equal to 0.34 % 1.22 %, respectively. Figure 3.28b and Figure 3.29b show a comparison of Δw % (decrease in water content) results at both end of drying (AB path) and drying/wetting (ABCEF path). Results indicate that end of drying (AB path) resulted in decrease of 1.45 %, 3.77 % and 8.95 % in water content compared to 1.9 %, 6.14 % and 11 % at end of drying/wetting (ABCEF path) for suction values of 8 kPa, 25 kPa and 50 kPa respectively. (Note, higher Δw indicates lower water content)

This hysteresis is similar to the SWCC where for a given suction the water content on the wetting curve is less than that of the drying curve as indicated in Figure 3.30 which presents comparison of water content results from the direct shear tests to the SWCC results.

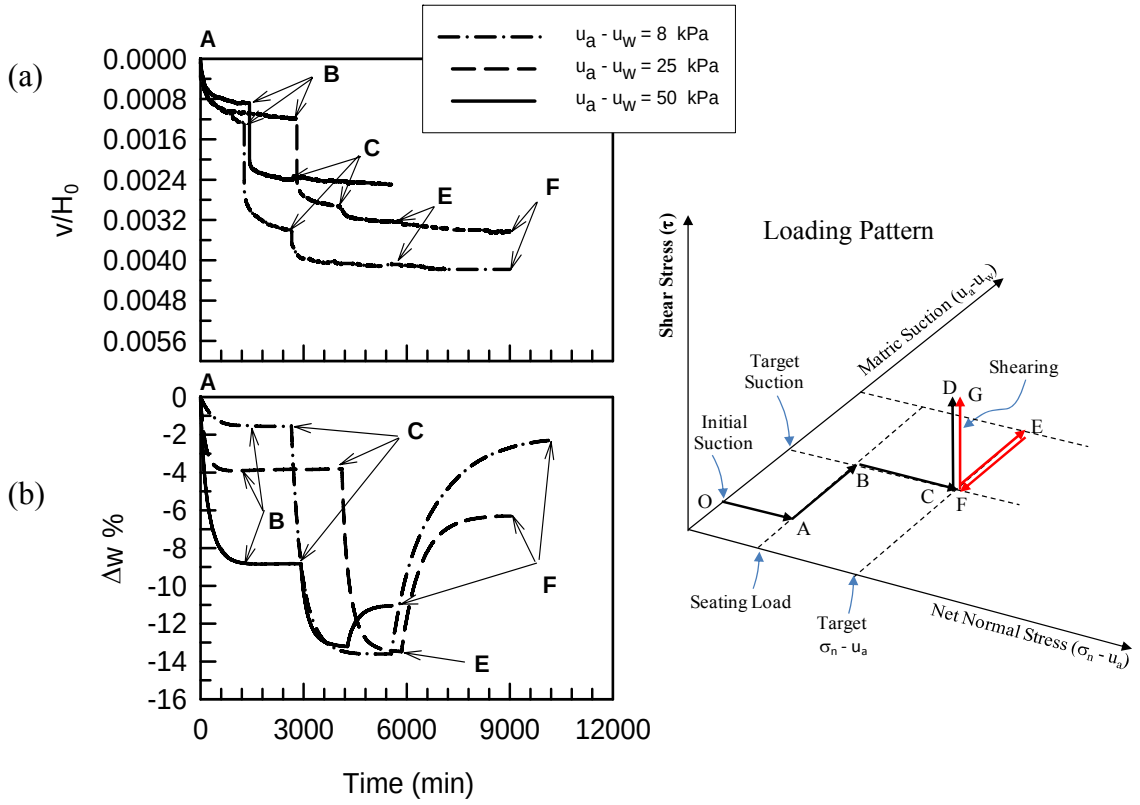

Figure 3.23- Effect of Suction (u_a-u_w) on (a) v/H_0 and (b) Δw % during Equalization of Hysteresis (Drying/Wetting) Unsaturated Soil Tests under Net Normal Stress (σ_n-u_a) of 50 kPa

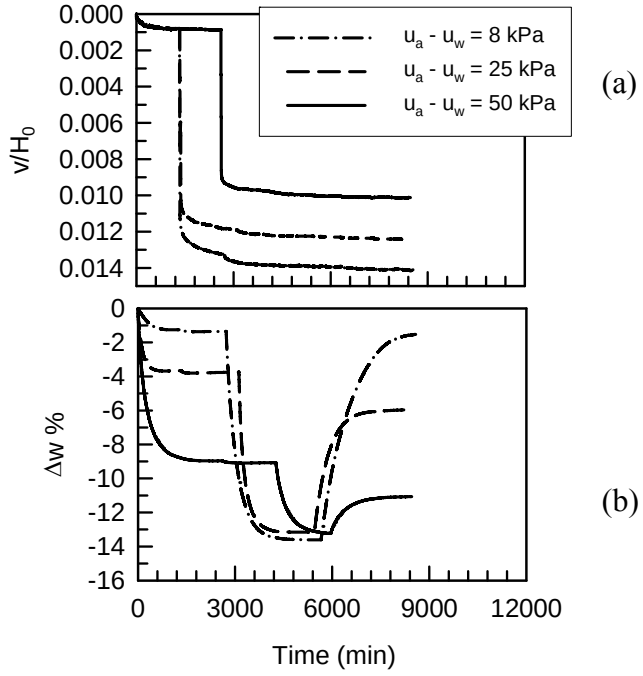

Figure 3.24- Effect of Suction (u_a-u_w) on (a) v/H_0 and (b) Δw % during Equalization of Hysteresis (Drying/Wetting) Unsaturated Soil Tests under Net Normal Stress (σ_n-u_a) of 150 kPa

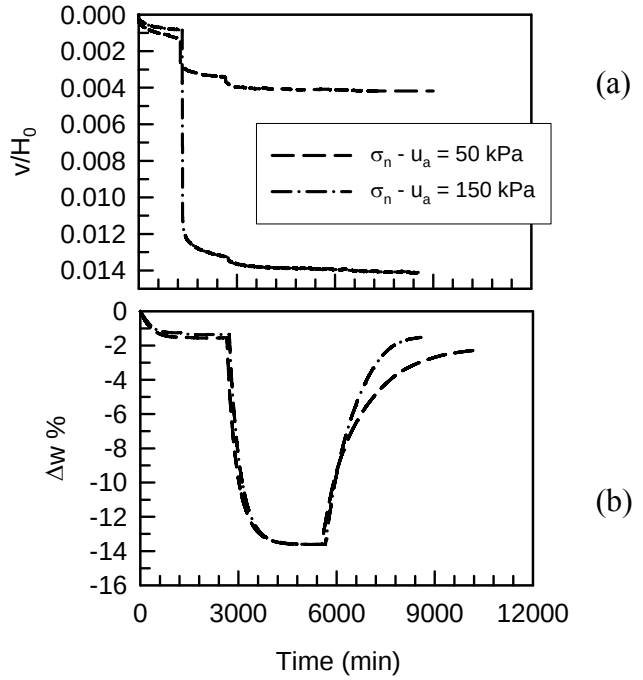

Figure 3.25- Effect of Net Normal Stress (σ_n-u_a) on (a) v/H_0 and (b) Δw % during Equalization of Hysteresis (Drying/Wetting) Unsaturated Soil Tests under Suction (u_a-u_w) of 8 kPa

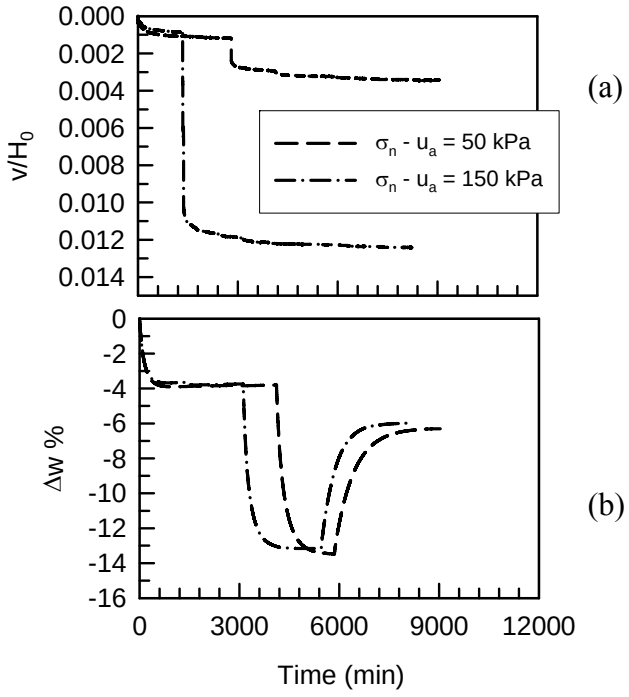

Figure 3.26- Effect of Net Normal Stress (σ_n-u_a) on (a) v/H_0 and (b) Δw % during Equalization of Hysteresis (Drying/Wetting) Unsaturated Soil Tests under Suction (u_a-u_w) of 25 kPa

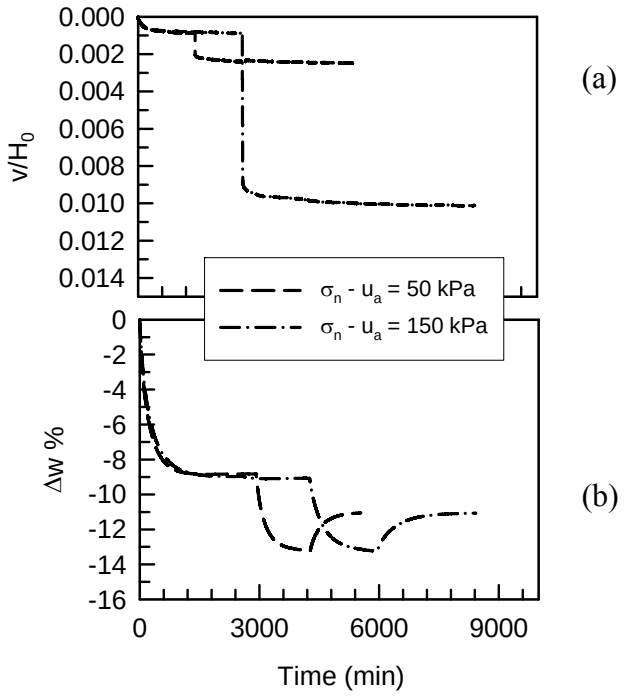

Figure 3.27- Effect of Net Normal Stress (σ_n-u_a) on (a) v/H_0 and (b) Δw % during Equalization of Hysteresis (Drying/Wetting) Unsaturated Soil Tests under Suction (u_a-u_w) of 50 kPa

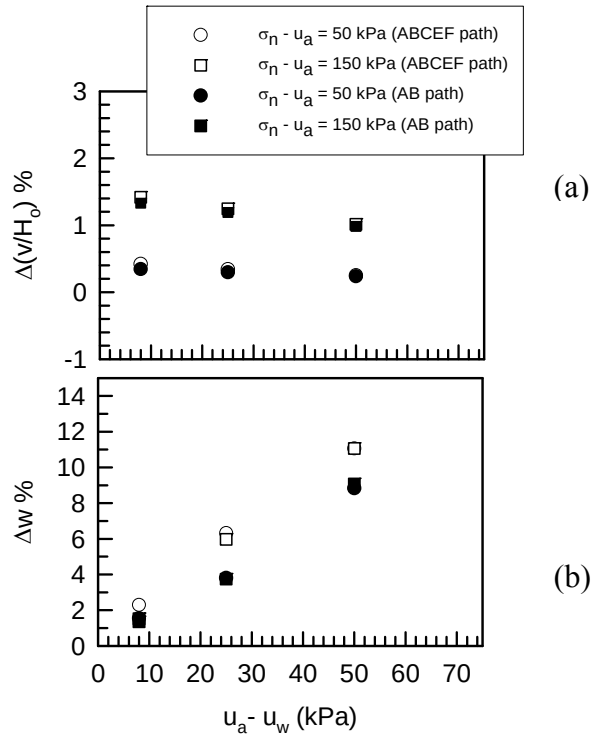

Figure 3.28- Summary of Consolidation Results versus Suction for all Net Normal Stresses

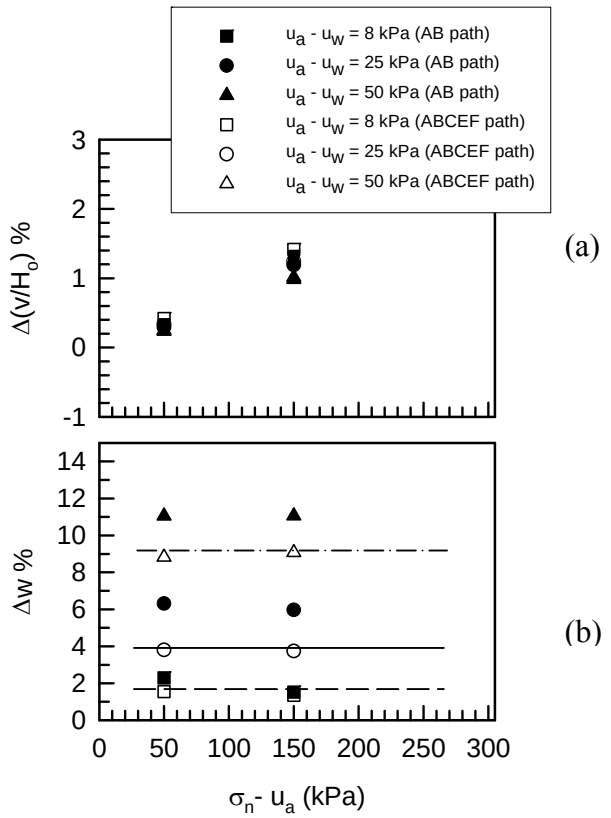

Figure 3.29- Summary of Consolidation Results versus Net Normal Stress for all Suction Values

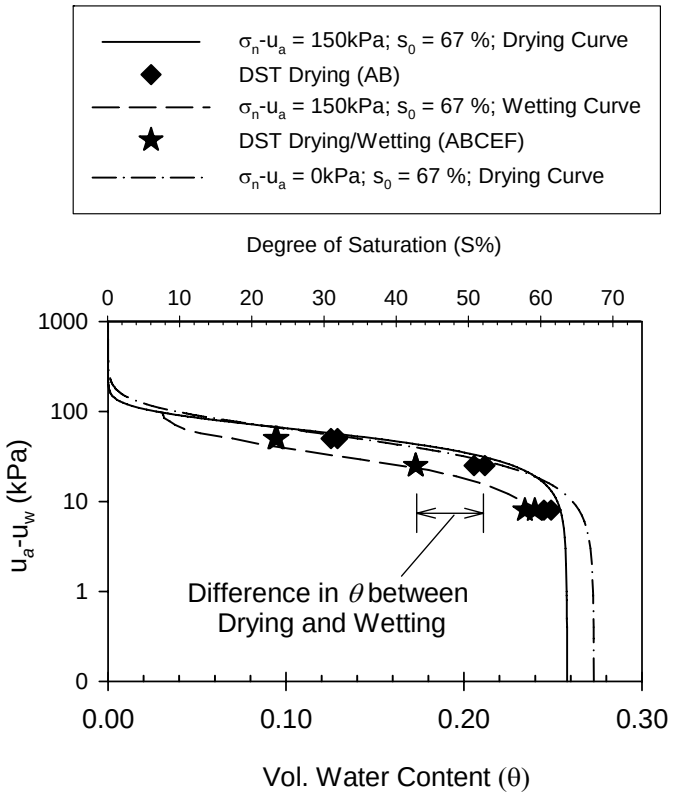

Figure 3.30- Soil Water Characteristic Curves Superimposed with Results from DST of Soils during Drying before Wetting (DBW) and Wetting (DW)

3.5.2.2 Shearing Phase

Figure 3.31-Figure 3.35 show the direct shear test results during shearing after drying/wetting. Figure 3.31 and Figure 3.32 present shearing results at net normal stresses of 50 kPa and 150 kPa, respectively. Results in Figure 3.31a and Figure 3.32a indicate that the shear strength increases with increase of suction. The increase in shear strength seems to be more pronounced when suction increased from 8 kPa to 25 kPa as compared to the increase from 25 to 50 kPa suction. In addition, a slight post-peak drop in shear stress was observed at higher suction value (i.e., 50 kPa) compared to almost none at lower suction values of 8 and 25 kPa. Volume change results during shearing are shown in Figure 3.31b and Figure 3.32b and indicate a slight and negligible compression at the beginning of tests followed by dilation as shear strength was mobilized, that kept

on progressing during the rest of shearing. In general, dilation slightly increased with increasing suction. Figure 3.31c and Figure 3.32c present the change in water content during shearing; interestingly, results indicate that at low suction value of 8 kPa water did flow into the sample contrary to tests at higher suction of 25 and 50 kPa. At suction of 8 kPa that is equal the Air Entry Value (AEV) and of higher degree of saturation than for suction of 25 and 50 kPa, samples behaved more like saturated soil; in other words, dilation in saturated soils indicates a tendency for generation of negative pore water pressure, which results in water flowing into the sample. This observation strengthens the discussion in Section 3.5.1.2 that suggests in unsaturated soil during dilation the menisci between soil particles may be disrupted, and the non-uniform distribution of pore water (at higher suction, above AEV) may result in an increase in localized pore water pressure causing water to drain out of sample during shear to maintain the controlled pore water pressure and suction.

Suction controlled hysteresis direct shear tests are also presented in Figure 3.33-Figure 3.35 at each suction value of 8, 25 and 50 kPa, respectively. Results indicate that shear strength increase with increase in net normal stress (Figure 3.33a-Figure 3.35a). The soil compressed slightly (negligible amount) at the beginning but started to dilate as its shear strength was mobilized (Figure 3.33b-Figure 3.35b). The soil dilation is observed to be more significant when subjected to smaller net normal stress values (e.g., σ_n = 50 kPa). In tests with higher suctions (Figure 3.34c and Figure 3.35c), a small amount of water drained out of the test specimen during shearing in order to maintain the soil suction at the target value. The decrease in the specimen moisture contents during the shearing phase was less than 0.15 %. However, for specimens with suction of 8 kPa the

water content inside the samples increased about 0.4 % due to dilation. This difference in behavior is discussed previously in this section; for low suction values, specimens behave similarly to saturated soils contrary to higher suction tests.

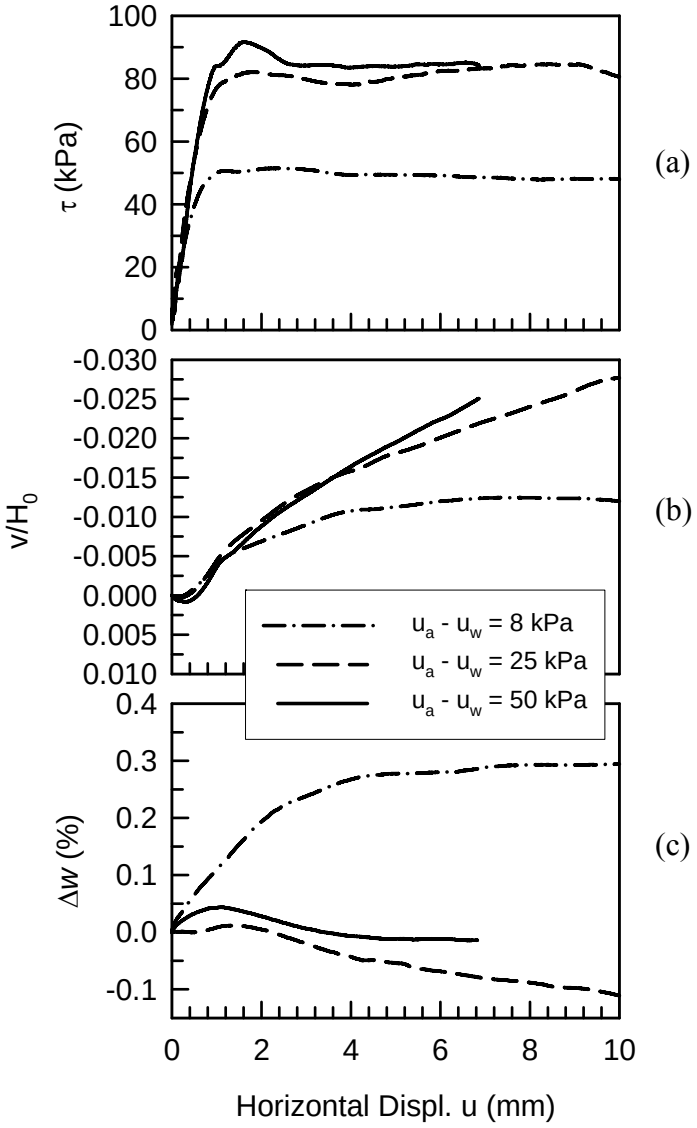

Figure 3.31- Effect of Suction (u_a-u_w) on (a) Shear Stress (τ), (b) v/H_0 and (c) Δw % during Shearing of Unsaturated Soil Hysteresis (Drying/Wetting) Tests under Net Normal Stress (σ_n-u_a) of 50 kPa

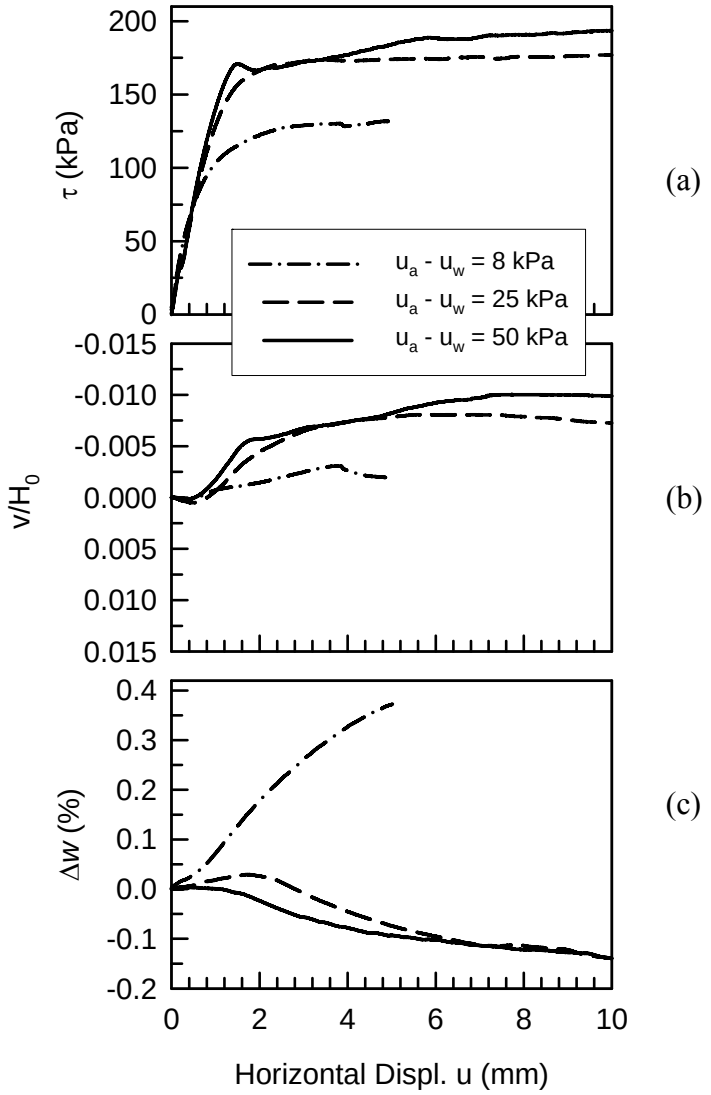

Figure 3.32- Effect of Suction (u_a-u_w) on (a) Shear Stress (τ), (b) v/H_0 and (c) Δw % during Shearing of Unsaturated Soil Hysteresis (Drying/Wetting) Tests under Net Normal Stress (σ_n-u_a) of 150 kPa

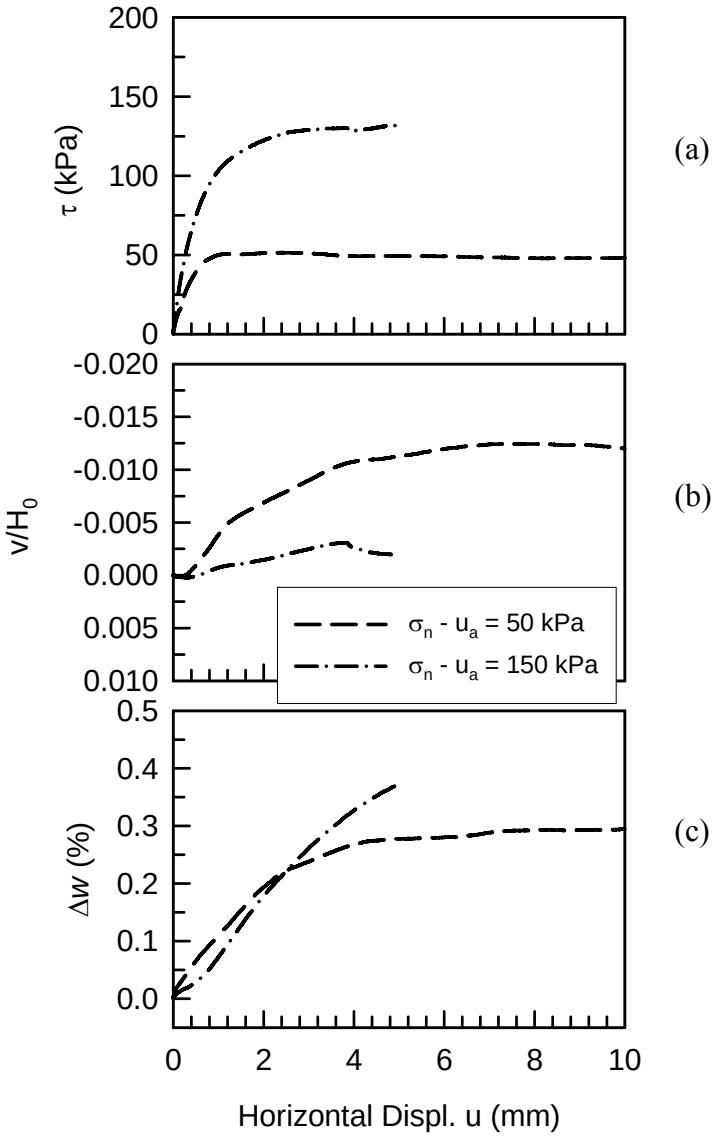

Figure 3.33- Effect of Net Normal Stress (σ_n-u_a) on (a) Shear Stress (τ), (b) v/H_0 and (c) Δw % during Shearing of Unsaturated Soil Hysteresis (Drying/Wetting) Tests under Suction (u_a-u_w) of 8 kPa

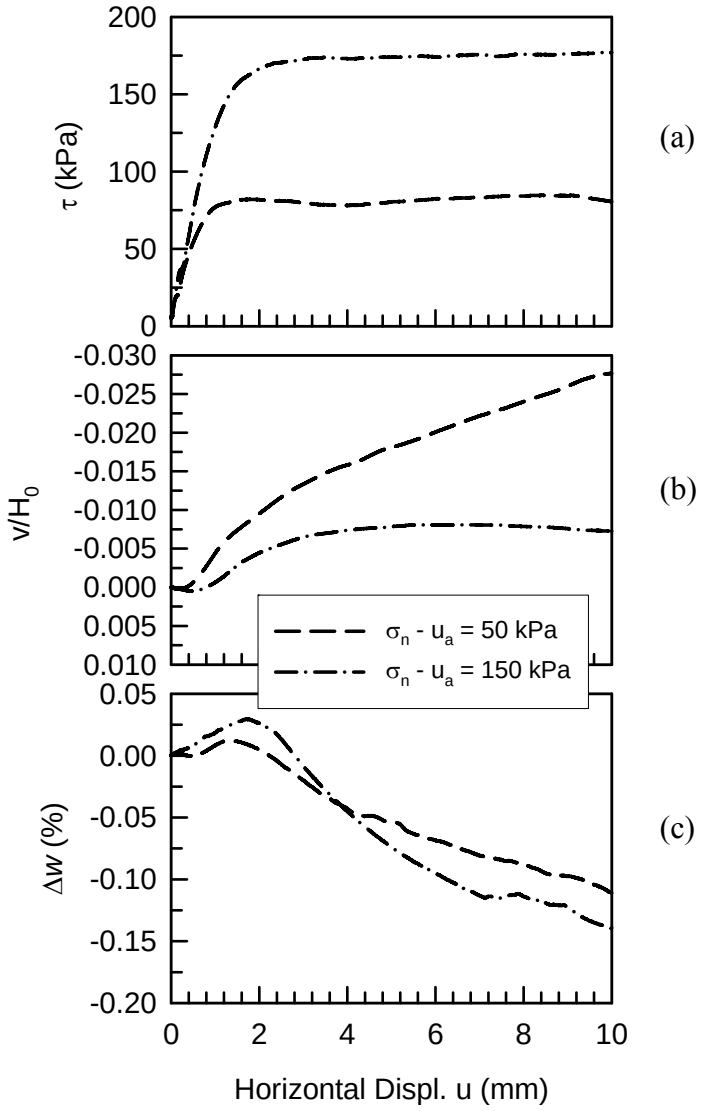

Figure 3.34- Effect of Net Normal Stress (σ_n-u_a) on (a) Shear Stress (τ), (b) v/H_0 and (c) Δw % during Shearing of Unsaturated Soil Hysteresis (Drying/Wetting) Tests under Suction (u_a-u_w) of 25 kPa

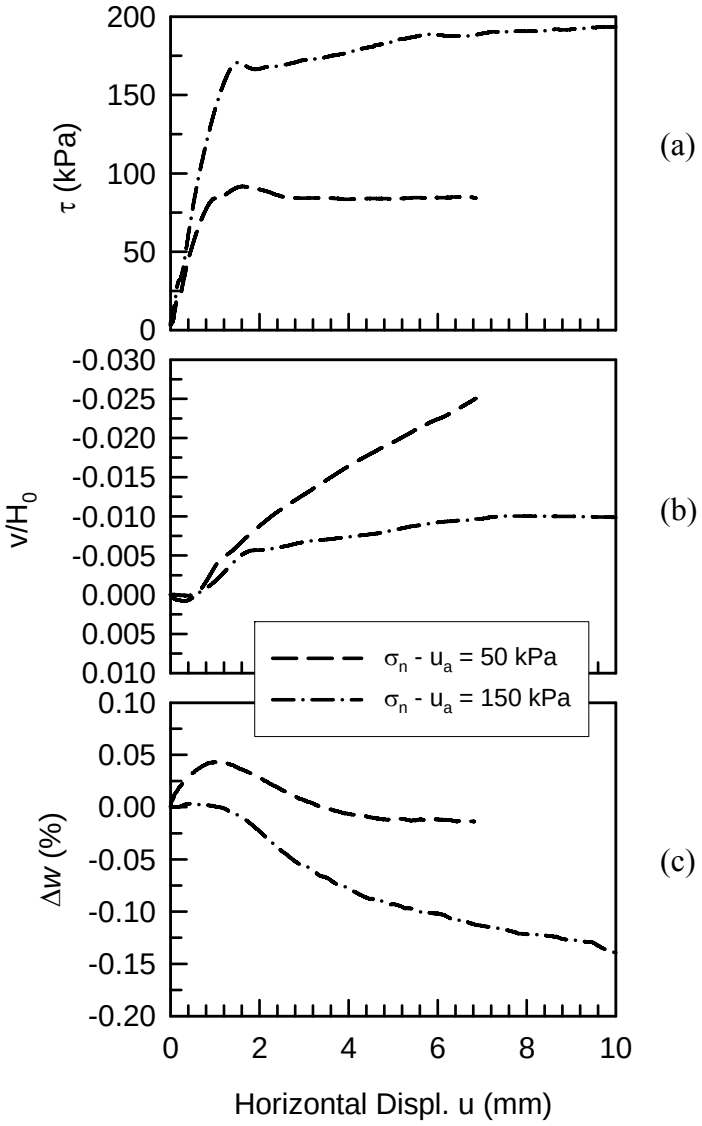

Figure 3.35- Effect of Net Normal Stress (σ_n-u_a) on (a) Shear Stress (τ), (b) v/H_0 and (c) Δw % during Shearing of Unsaturated Soil Hysteresis (Drying/Wetting) Tests under Suction (u_a-u_w) of 50 kPa

3.5.3 Comparison of Results w/o Hysteresis

3.5.3.1 Hysteresis Effect on the Volume Change Behavior

Figure 3.36 and Figure 3.37 show a comparison of consolidation results with and without suction hysteresis. Comparisons at end of consolidation stages between results from drying (D) tests (without hysteresis) with: a) hysteresis test results at end of drying

before wetting (DBW) are shown in Figure 3.38, b) hysteresis test results at end of wetting after drying (DW) are shown in Figure 3.39. Plots of vertical displacement (normalized to the specimen height) with time during the equalization phases for both drying (D) tests and wetting after drying (DW) are presented in Figure 3.36a and Figure 3.37a, for all net normal stresses (50 and 150 kPa) at suction values of 25 and 50 kPa, respectively. It was observed that the magnitude of specimen compression is practically the same at given suction and net normal stress values as also indicated in Figure 3.38a and Figure 3.39a. Comparison of change in water content (Δw %) results during equalization periods in the corresponding drying tests (D) and hysteresis test specimens are shown in Figure 3.36b and Figure 3.37b. In addition, Figure 3.36b, Figure 3.37b and Figure 3.39b indicated that the same amount of water (Δw average ≈ 3.9 %, and 8.9 %) drained from both hysteresis (DBW, end of drying before wetting) and drying (D) test specimens at suction of 25 kPa and 50 kPa, respectively. This indicates that the system is accurately controlling suction in all tests. However, as suction was increased up to 100 kPa and wetted back to prior suction (i.e. DW test specimens), the net decrease in water content obtained was on average about 6.14 % and 11 % for suctions tests of 25, and 50 kPa, respectively. The water content from the drying (D) tests was approximately 2.24 % and 2.1 % higher than that from the (DW) tests at suction, of 25 and 50 kPa, respectively. This difference in the water content is similar to the SWCC hysteresis where for a given suction the water content on the wetting curve is less than that of the drying curve. Water content results at end of Hysteresis (DW) tests and those from Drying (D) tests were plotted together along the SWCC as shown in Figure 3.40.

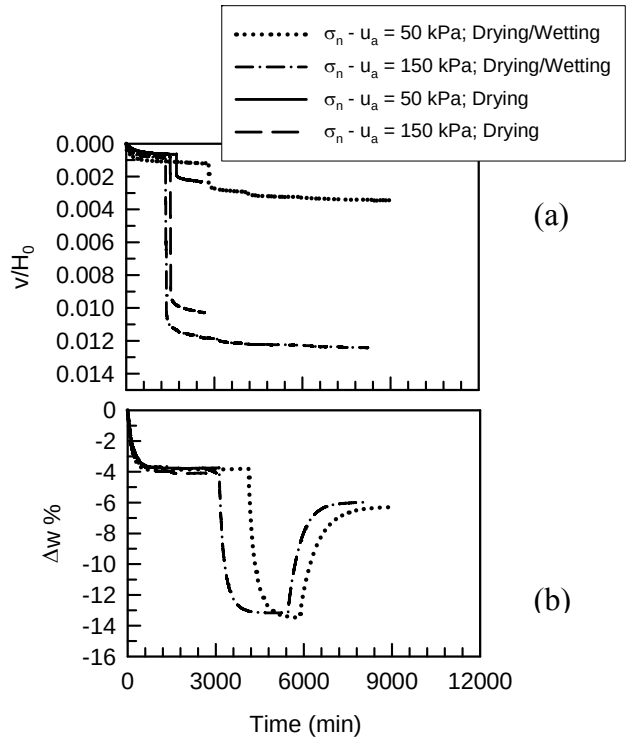

Figure 3.36- Comparison of Consolidation Results between Drying (No Hysteresis) Tests and Unsaturated Soil Hysteresis (Drying/Wetting) Tests under Suction (u_a-u_w) of 25 kPa

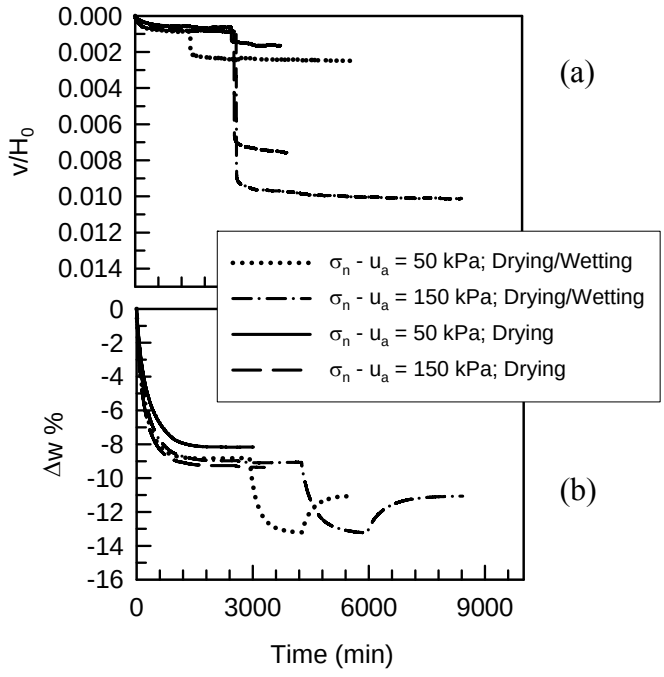

Figure 3.37- Comparison of Consolidation Results between Drying (No Hysteresis) Tests and Unsaturated Soil Hysteresis (Drying/Wetting) Tests under Suction (u_a-u_w) of 50 kPa

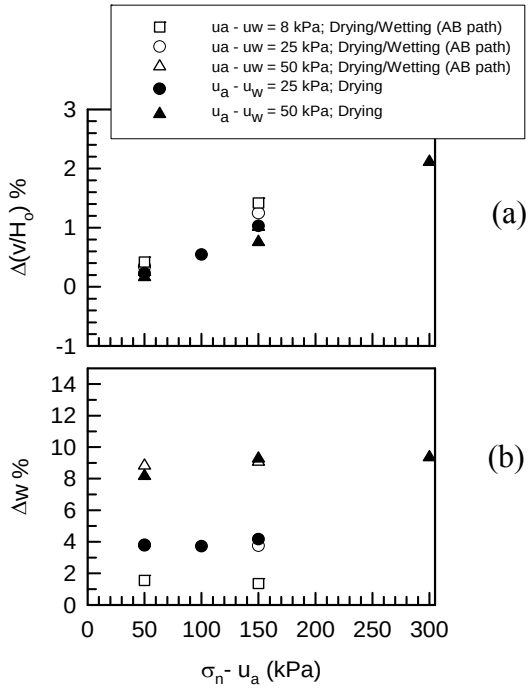

Figure 3.38- Summary Comparison of Consolidation Results between Hysteresis Tests at end of Drying (AB path) and Tests without Hysteresis (Drying)

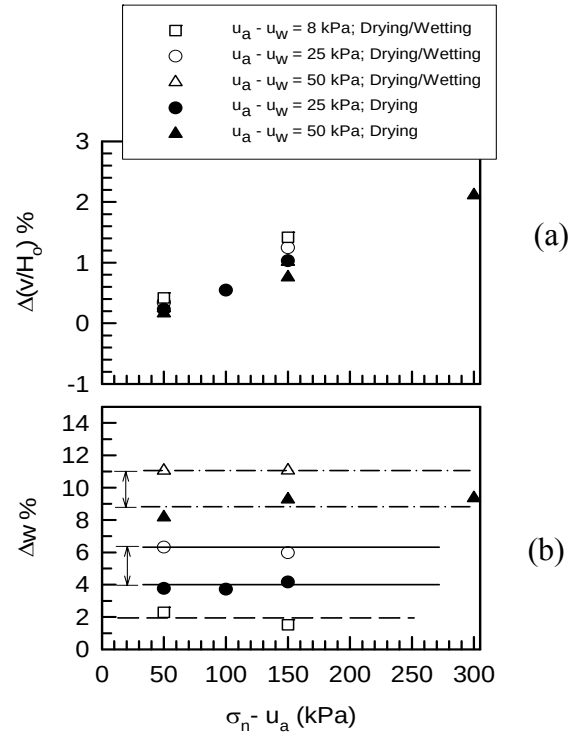

Figure 3.39- Summary Comparison of Consolidation Results between Hysteresis Tests at end of Drying/Wetting (ABCEF path) and Tests without Hysteresis (Drying)

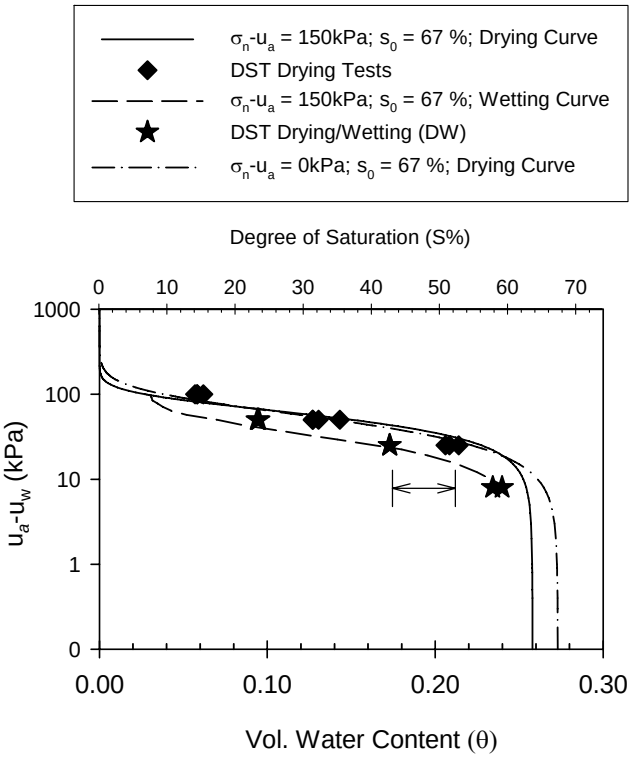

Figure 3.40- Soil Water Characteristic Curves Superimposed with Results from DST of Drying (D) and Wetting (DW) Soil Tests

3.5.3.2 Hysteresis Effect on the Shearing Behavior

Comparison of shear stress (τ) and volume change responses during shearing of unsaturated soil tests subjected to drying (D) and wetting after drying (DW) at same matric suction and net normal stresses are shown in Figure 3.41 and Figure 3.42. Based on these figures, some important observations are summarized as follows:

- During shearing of both (D) and (DW) tests, peak shear strength is achieved followed by a slight drop to a post peak shear stress; a behavior more pronounced at higher suction (e.g. 50 kPa) as shown in Figure 3.42a.
- For a given net normal stress and suction, the peak and post peak shear strength from hysteresis (DW) tests are higher than that of the drying (D) tests.
- In general, the volume changes during shearing (Figure 3.41b and Figure 3.42b) indicate that both test procedures resulted in slight compression initially then

dilation; while negligible, compression was more pronounced for (DW) tests. For both tests, dilation started prior to mobilizing the peak shear strength and then decreased once the shear stress reached the interface post peak shear strength. This was only true for tests with higher net normal stress tests (i.e. 150 kPa). Tests under smaller net normal stress (i.e. 50 kPa) values showed additional increase in dilation but at a lower rate compared to dilation before peak shear strength.

- During shearing, some changes in the specimen water contents (Δw %) were detected in both test types. It was observed that a small amount of water drained out of the sample for (D) tests, even smaller amounts of water drained out the samples for (DW) tests as dilation started. Although both test types showed dilation, water drainage in both cases indicates that there was a tendency for suction to decrease due to increasing pore water pressure. As discussed in previous sections, it seems that the breaking of the air-water menisci during shearing and the non-uniformity of pore water distribution (at high suction) created a tendency for increasing pore water pressure. Since those tests are under drained suction control, water drained during shearing to maintain the pore water pressure and suction. This postulation is strengthened in light of the fact that the amount of water draining out of the drying (D) tests is larger than that for (DW) tests since (D) test samples have higher water contents than that of the (DW) tests at the same suction. In other words, higher water content means additional water distribution in pores and thus tendency for higher increase in pore pressure during shearing at a given suction.

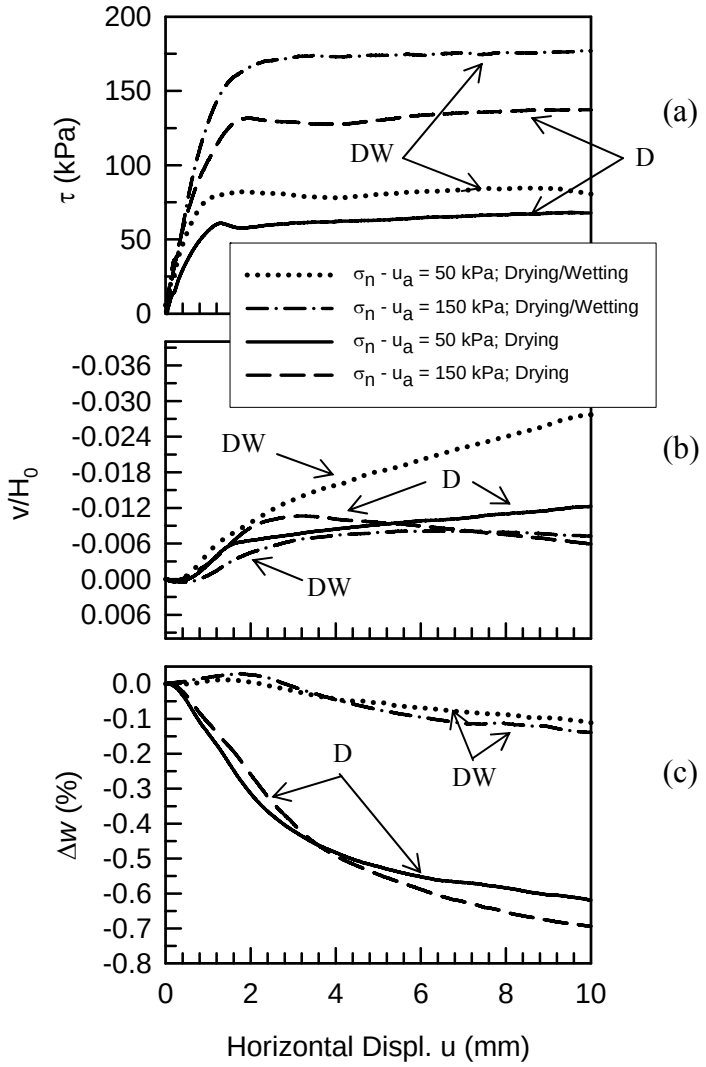

Figure 3.41- Comparison of Results during Shearing between Drying (D) Tests and Hysteresis Drying/Wetting (DW) Tests under Suction of 25 kPa

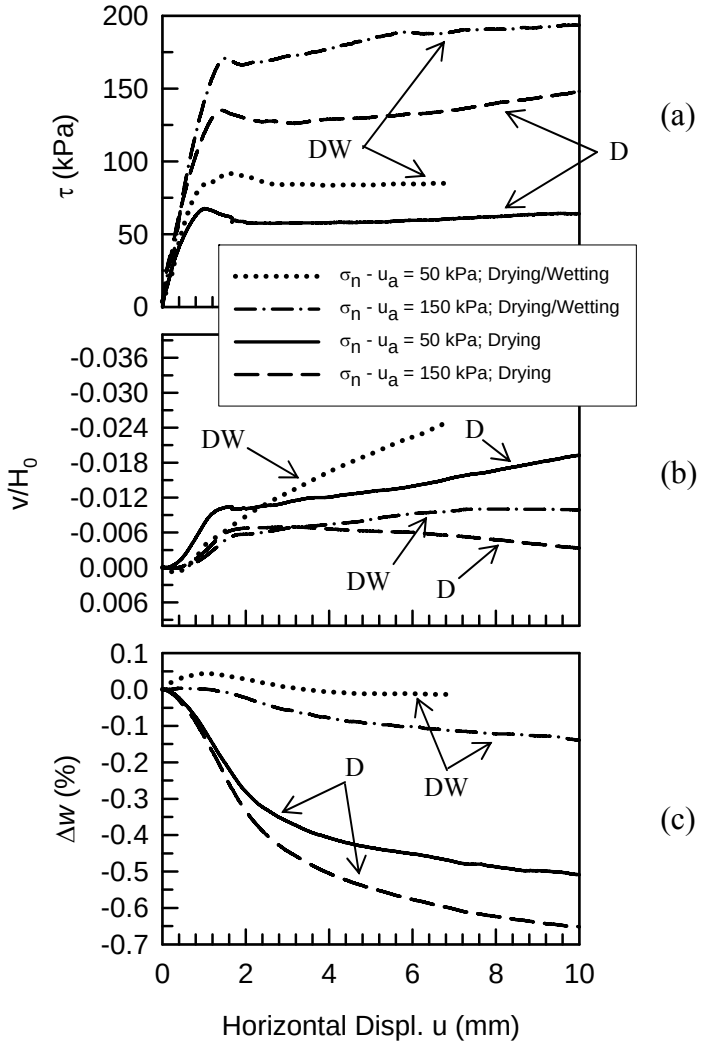

Figure 3.42- Comparison of Results during Shearing between Drying (D) Tests and Hysteresis Drying/Wetting (DW) Tests under Suction of 50 kPa

3.6 RESULTS AND DISCUSSIONS FOR UNSATURATED STEEL INTERFACE TESTS

Suction-controlled interface direct shear tests on unsaturated rough steel interfaces were performed under a range of constant suction and net normal stress of 8-100 kPa and 50-150 kPa, respectively. Test results and the effect of net normal stress and suction on the stress-displacement and volumetric behavior of unsaturated soil and interfaces are discussed in this section for both tests with and without suction hysteresis (wetting after drying).

3.6.1 Suction-Controlled Direct Shear Test DRYING Path Results for Rough Interfaces

3.6.1.1 Equalization Phases (Suction and Net Normal Stress)

Consolidation results during application of suction and net normal stress are presented in Figure 3.43-Figure 3.49. A summary of results at end of each consolidation stage were plotted as shown in Figure 3.50 and Figure 3.51 versus all net normal stresses and suction values. Figure 3.43a-Figure 3.45a show plots of change in vertical deformation, normalized to the specimen height (v/H_0), versus time during the equalization phase. At given net normal stress, results showed that samples compressed slightly during suction application. In addition, the amount of water (Δw%) drained out samples increased with increase of suction; on average water content decreased about 0.9 %, 3.7 %, 8.5 % and 13.7 % inside the specimens under 8, 25, 50 and 100 kPa, respectively, as shown in Figure 3.43b-Figure 3.45b and summarized in Figure 3.50b and Figure 3.51b.

On the other hand, results at given suction (Figure 3.46a-Figure 3.49a and Figure 3.51a) showed that the magnitude of compression increased with increase in net normal stress. As summarized in Figure 3.51a, the change in v/H_0 % was on average approximately 0.52%, 0.56 % and 0.99 % under net normal stresses of 50, 100 and 150 kPa, respectively. Variation in water content for soil samples during equalization are shown in Figure 3.46b-Figure 3.49b and Figure 3.51b at given suction values, and indicate that the change in water content (Δw %) is essentially the same at a given suction value; in other words, the water controller pulled approximately the same amount of water from all three samples to maintain the required suction. As shown in Figure 3.52,

the equilibrium water contents of Rough interface DST tests for a given suction agree well with the soil water characteristic curves obtained independently.

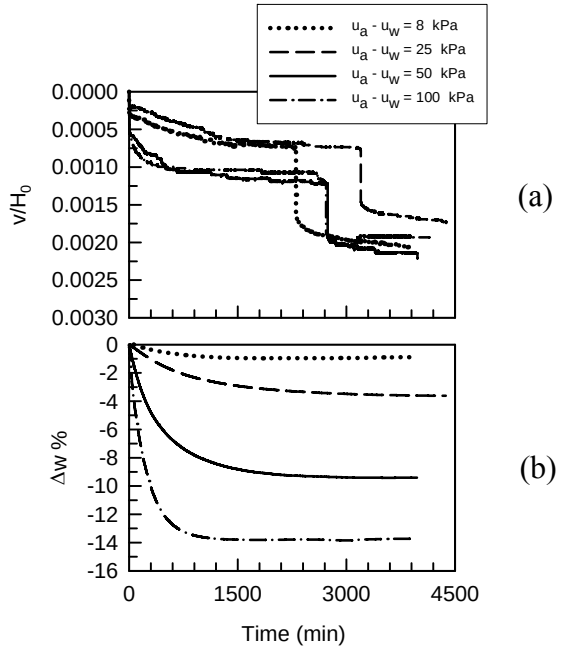

Figure 3.43- Effect of Suction (u_a-u_w) on (a) v/H_0 and (b) Δw % during Equalization of Unsaturated Rough Interface Tests under Net Normal Stress (σ_n-u_a) of 50 kPa

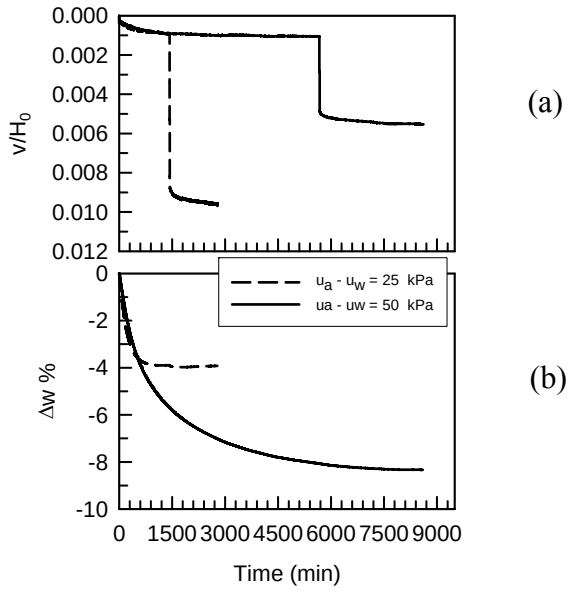

Figure 3.44- Effect of Suction (u_a-u_w) on (a) v/H_0 and (b) Δw % during Equalization of Unsaturated Rough Interface Tests under Net Normal Stress (σ_n-u_a) of 100 kPa

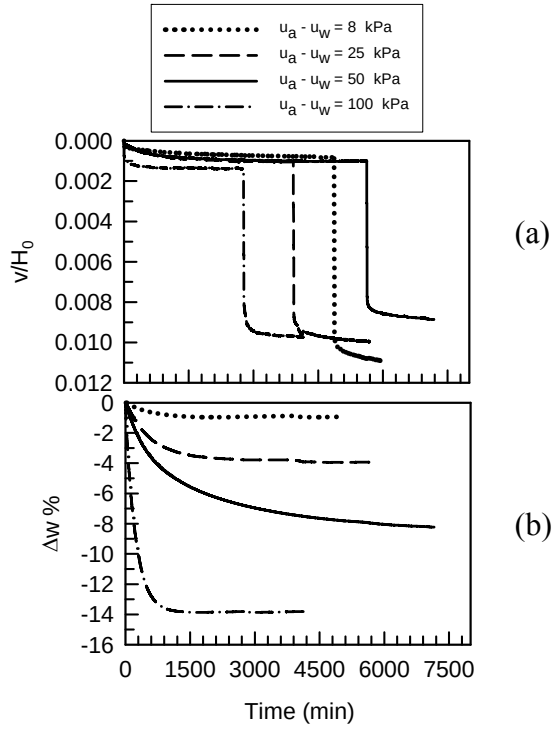

Figure 3.45- Effect of Suction (u_a-u_w) on (a) v/H_0 and (b) Δw % during Equalization of Unsaturated Rough Interface Tests under Net Normal Stress (σ_n-u_a) of 150 kPa

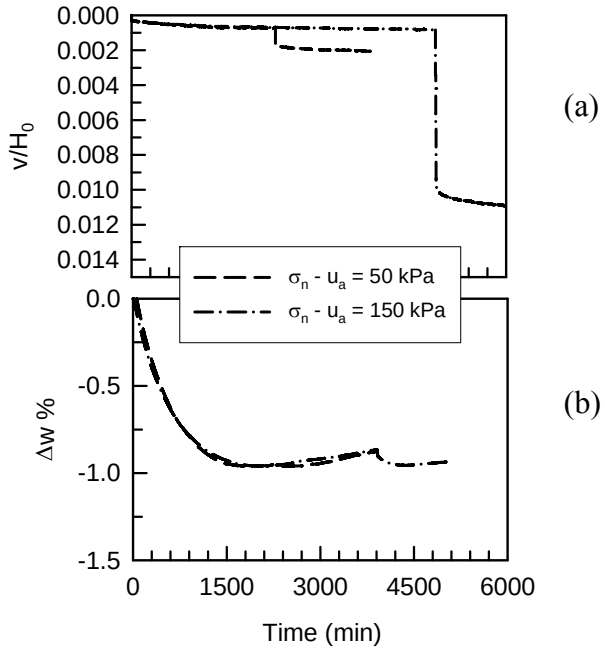

Figure 3.46- Effect of Net Normal Stress (σ_n-u_a) on (a) v/H_0 and (b) Δw % during Equalization of Unsaturated Rough Interface Tests under Suction (u_a-u_w) of 8 kPa

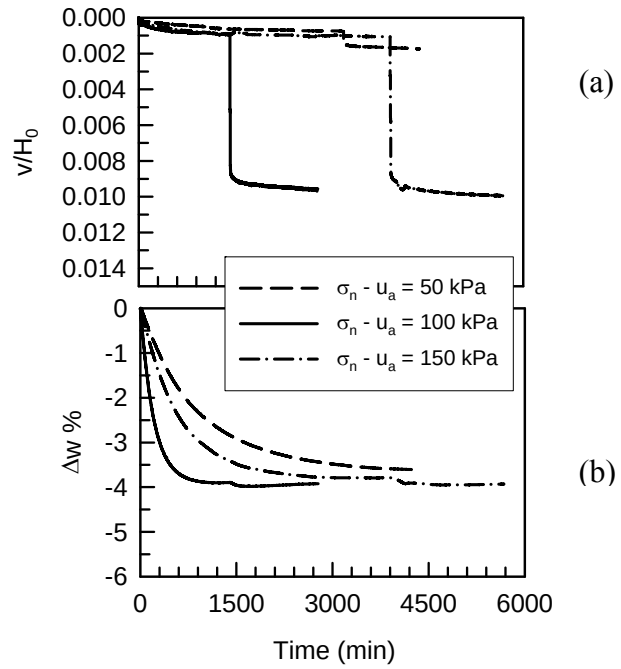

Figure 3.47- Effect of Net Normal Stress (σ_n-u_a) on (a) v/H_0 and (b) Δw % during Equalization of Unsaturated Rough Interface Tests under Suction (u_a-u_w) of 25 kPa

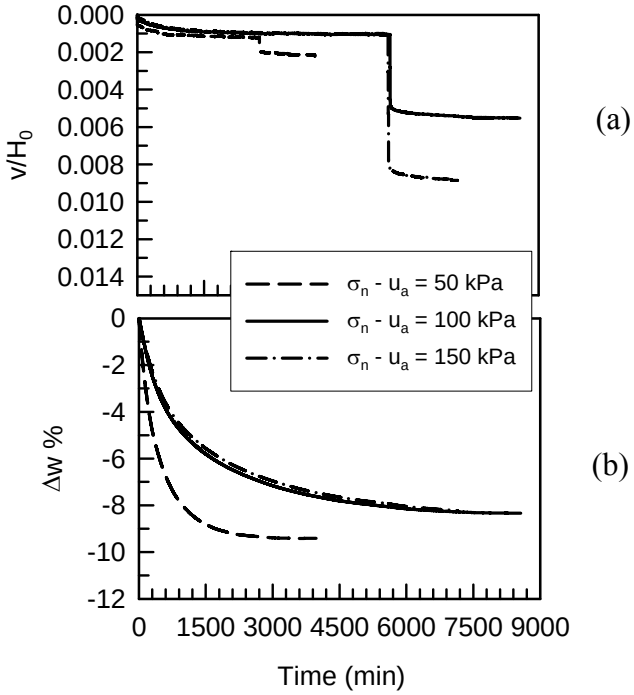

Figure 3.48- Effect of Net Normal Stress (σ_n-u_a) on (a) v/H_0 and (b) Δw % during Equalization of Unsaturated Rough Interface Tests under Suction (u_a-u_w) of 50 kPa

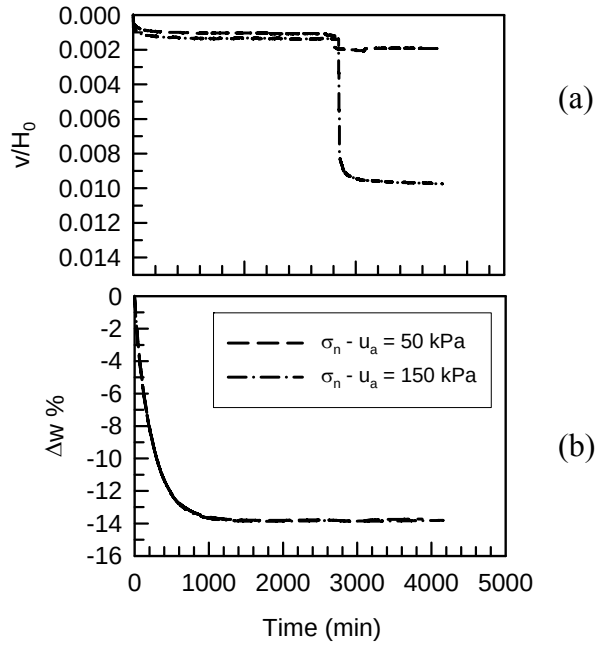

Figure 3.49- Effect of Net Normal Stress (σ_n-u_a) on (a) v/H_0 and (b) Δw % during Equalization of Unsaturated Rough Interface Tests under Suction (u_a-u_w) of 100 kPa

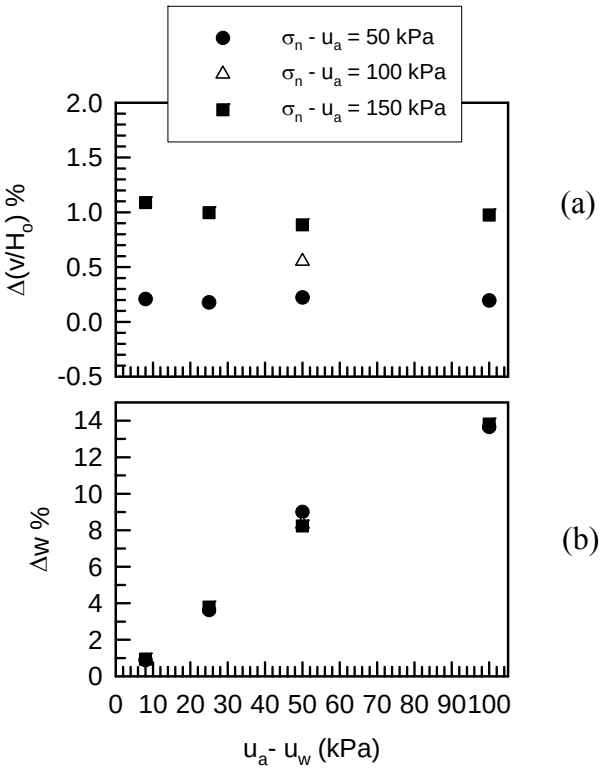

Figure 3.50- Summary of Unsaturated Rough Interface Results at end of Consolidation Stage for all Net Normal Stress Values

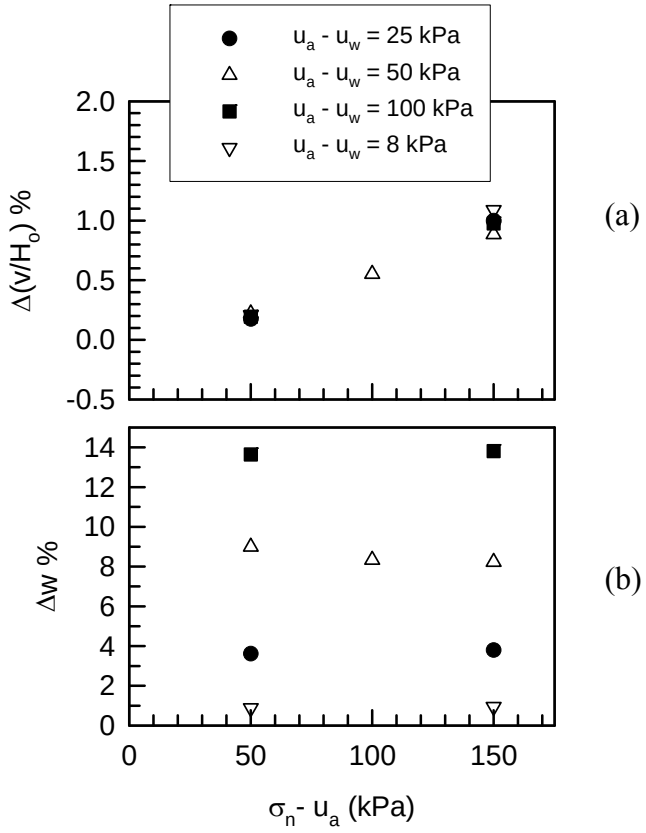

Figure 3.51- Summary of Unsaturated Rough Interface Results at end of Consolidation Stage for all Suction Values

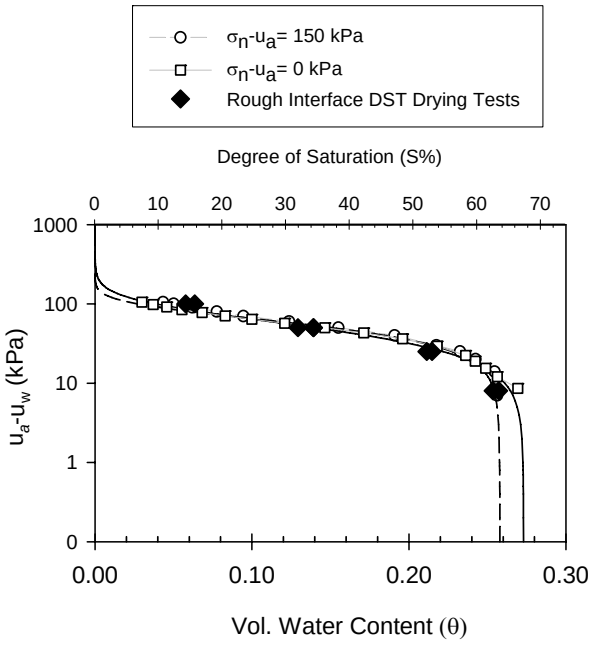

Figure 3.52- Soil Water Characteristic Curves Superimposed with Results from Rough Interface DST Drying (D) Tests

3.6.1.2 Shearing Phase

Figure 3.53a-Figure 3.55a present the shear stress results (τ) versus horizontal displacement (u) for the rough interface at given net normal stresses. Results indicate an increase in peak shear stress with increase in suction for a given net normal stress, similar to the observation for soil. These figures also show that maximum shear stress occurred at slightly lower values of horizontal displacement for increasing suction, illustrating an increasing brittleness of the sample with increasing suction. It can also be observed that strain softening behavior became pronounced with increasing suction. At suction of 8 kPa, rough interfaces didn't show any strain softening; however, as suction increased strain softening magnitude increased.

Unlike soil tests that indicate a non-consistent pattern of post peak shear stress with suction, rough interface values did not seem to change with increase in suction. This observation suggests possibly that water menisci acting in the interface are disturbed during shearing to a similar extent and that the suction has little effect on post peak strength.

Corresponding volume change curves are shown in Figure 3.53b-Figure 3.55b. These curves showed initially negligible contraction followed by dilation that vanished in the region of post peak shear stress. Unlike soil samples that showed a non-consistent effect of dilation due to suction, the rough interface showed increase in dilatancy with increase in suction. This increase was more pronounced when suction increased from 8 to higher suction values (25, 50 and 100 kPa); however, a small to negligible increase was observed above 25 kPa

Similar to soils, and as discussed in the section for unsaturated DST soil tests, the water volume controller pulled water out of the samples (at suction of 25, 50, and 100 kPa) while water flowed into the sample for suction of 8 kPa. At suction of 8 kPa (that is equal to the AEV) behavior was more like that expected for saturated soil. Dilation in saturated soils indicates a tendency for generation of negative pore water pressure, which results in water flowing into the sample. However, in unsaturated soil (at higher suction values) during dilation the menisci between soil particles is postulated to be disrupted, and localized increase of pore water pressure is possibly exhibited due to the non-uniformity of pore water distribution causing a tendency for increasing pore water pressure and thus result in water draining out of sample during shear to maintain the controlled pore water pressure and suction.

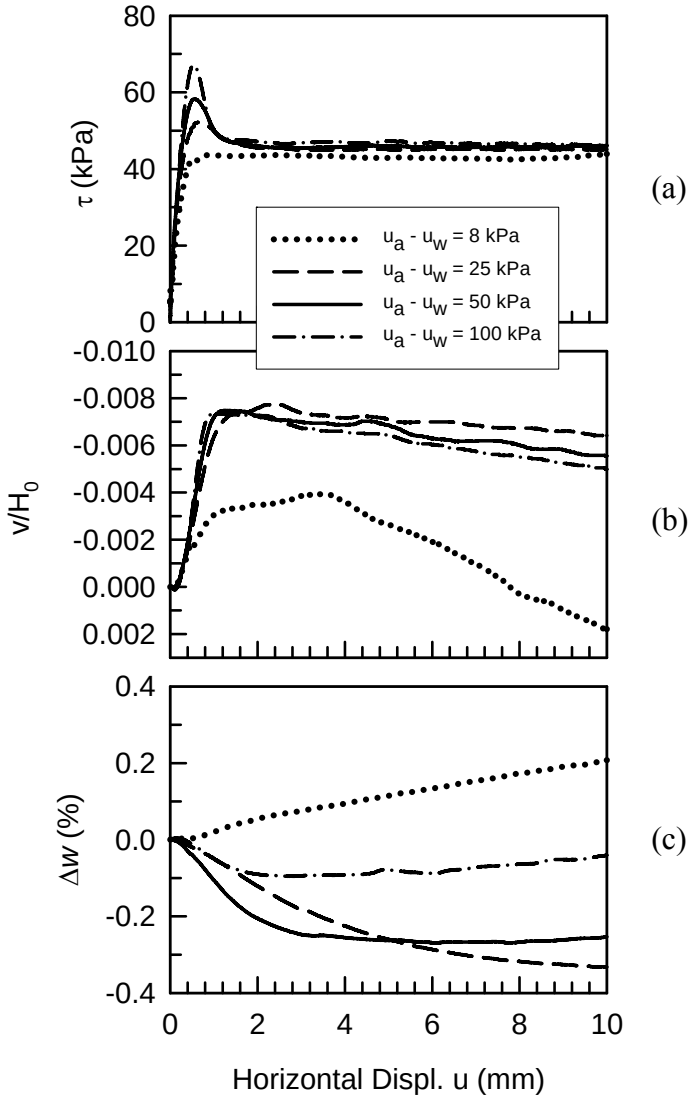

Figure 3.53- Effect of Suction (u_a-u_w) on (a) Shear Stress (τ), (b) v/H_0 and (c) Δw % during Shearing of Unsaturated Rough Interface Tests under Net Normal Stress (σ_n-u_a) of 50 kPa

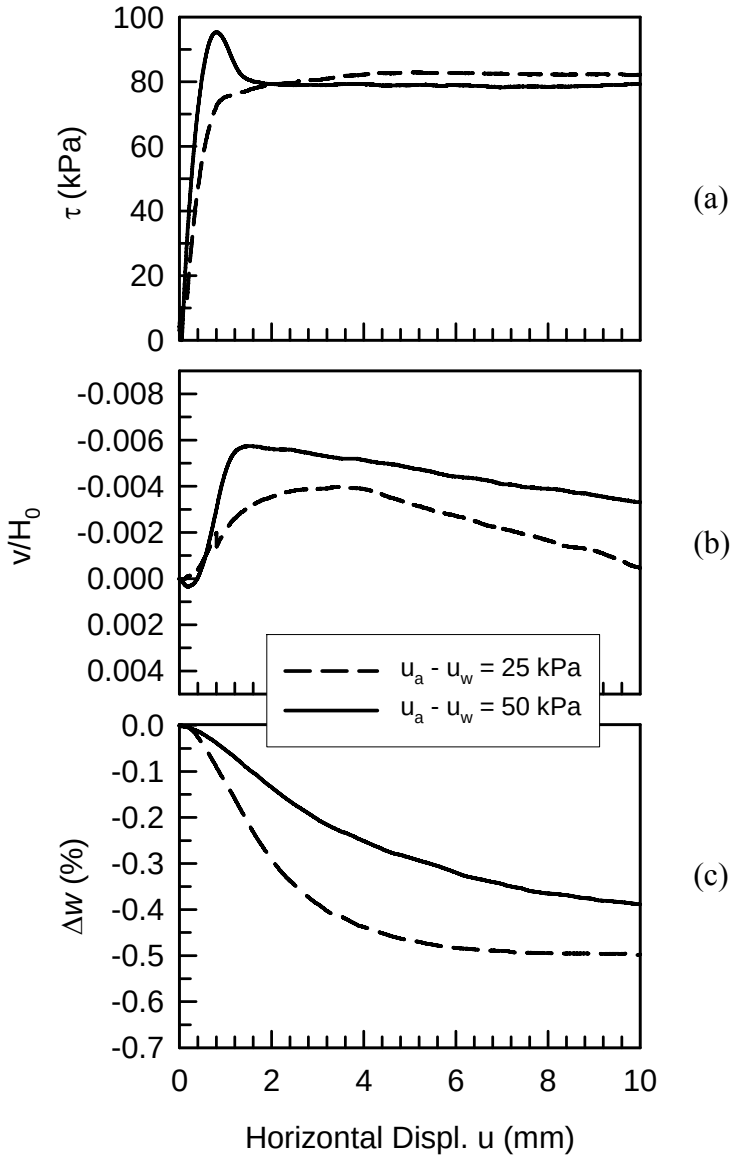

Figure 3.54- Effect of Suction (u_a-u_w) on (a) Shear Stress (τ), (b) v/H_0 and (c) Δw % during Shearing of Unsaturated Rough Interface Tests under Net Normal Stress (σ_n-u_a) of 100 kPa

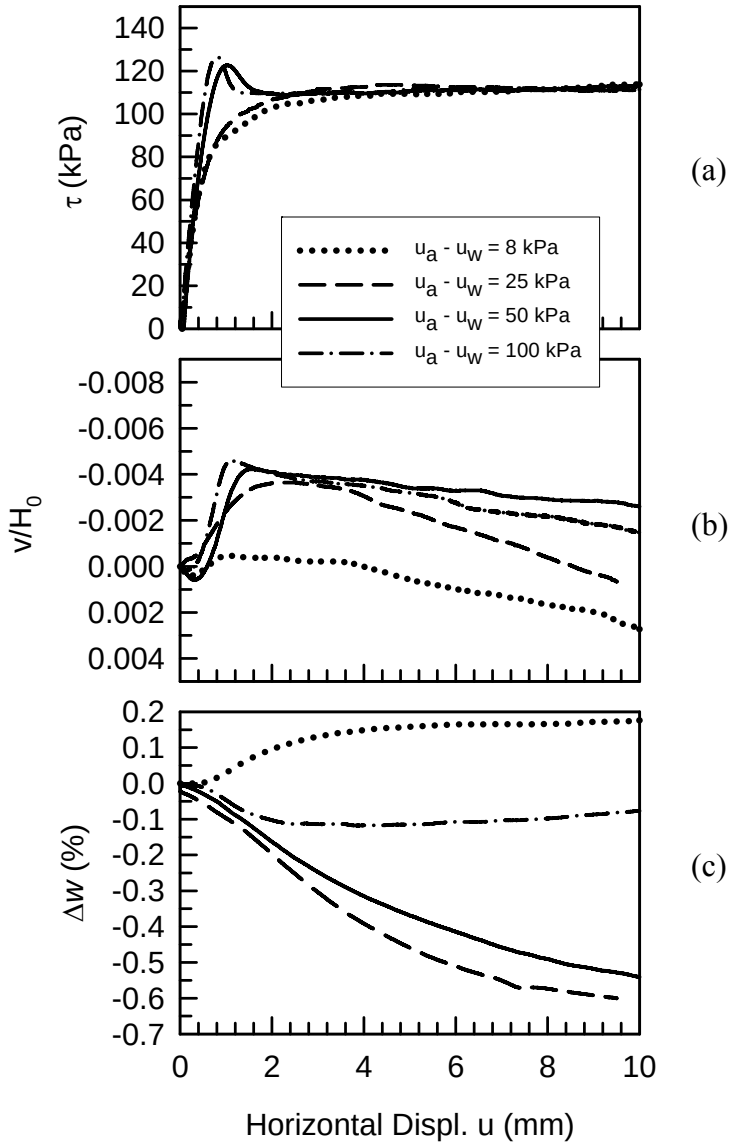

Figure 3.55- Effect of Suction (u_a-u_w) on (a) Shear Stress (τ), (b) v/H_0 and (c) Δw % during Shearing of Unsaturated Rough Interface Tests under Net Normal Stress (σ_n-u_a) of 150 kPa

Results of rough interface tests during shearing are shown in Figure 3.56-Figure 3.59 at given suction values for all net normal stresses. Figure 3.56a through Figure 3.59a show that the peak and post peak shear strength of the rough interface increased with increase in net normal stress. During shearing the rough interface negligibly compressed initially and then started to dilate while approaching the peak shear stress. The rough

interface stopped dilating and then showed a slight compression tendency after the peak shear stress. Dilation was more pronounced in samples that showed stronger strain softening behavior (e.g. Figure 3.58 and Figure 3.59) than those that did not show any significant strain softening behavior (e.g. Figure 3.56 and Figure 3.57). Results also indicated that the amount of dilation decreased as the net normal stress increased (Figure 3.56b-Figure 3.59b). Similarly, and as discussed previously due to the tendency for increasing pore water pressure, the water volume controller pulled water from the sample except at the lowest suction value of 8 kPa (which is expected to behave like saturated soil).

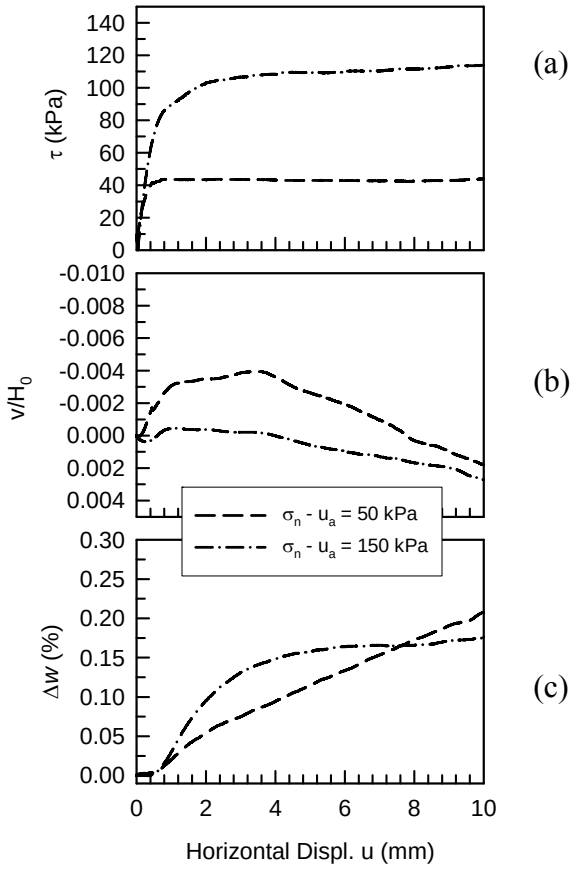

Figure 3.56- Effect of Net Normal Stress (σ_n-u_a) on (a) Shear Stress (τ), (b) v/H_0 and (c) Δw % during Shearing of Unsaturated Rough Interface Tests under Suction (u_a-u_w) of 8 kPa

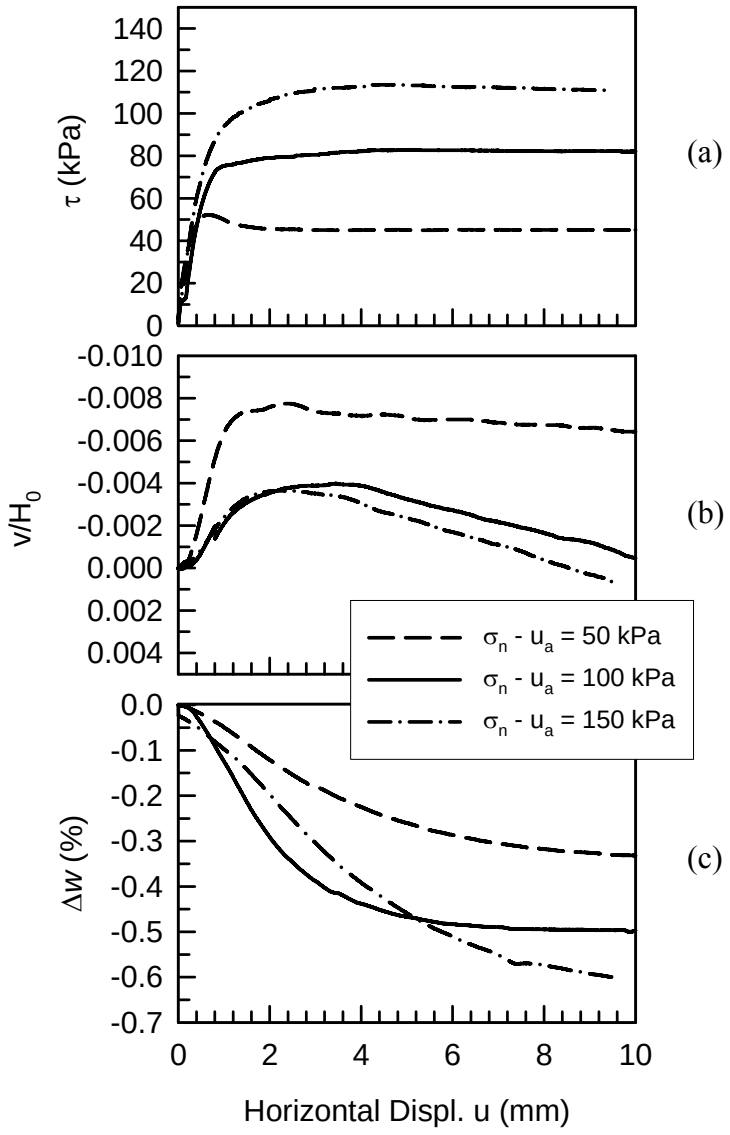

Figure 3.57- Effect of Net Normal Stress (σ_n-u_a) on (a) Shear Stress (τ), (b) v/H_0 and (c) Δw % during Shearing of Unsaturated Rough Interface Tests under Suction (u_a-u_w) of 25 kPa

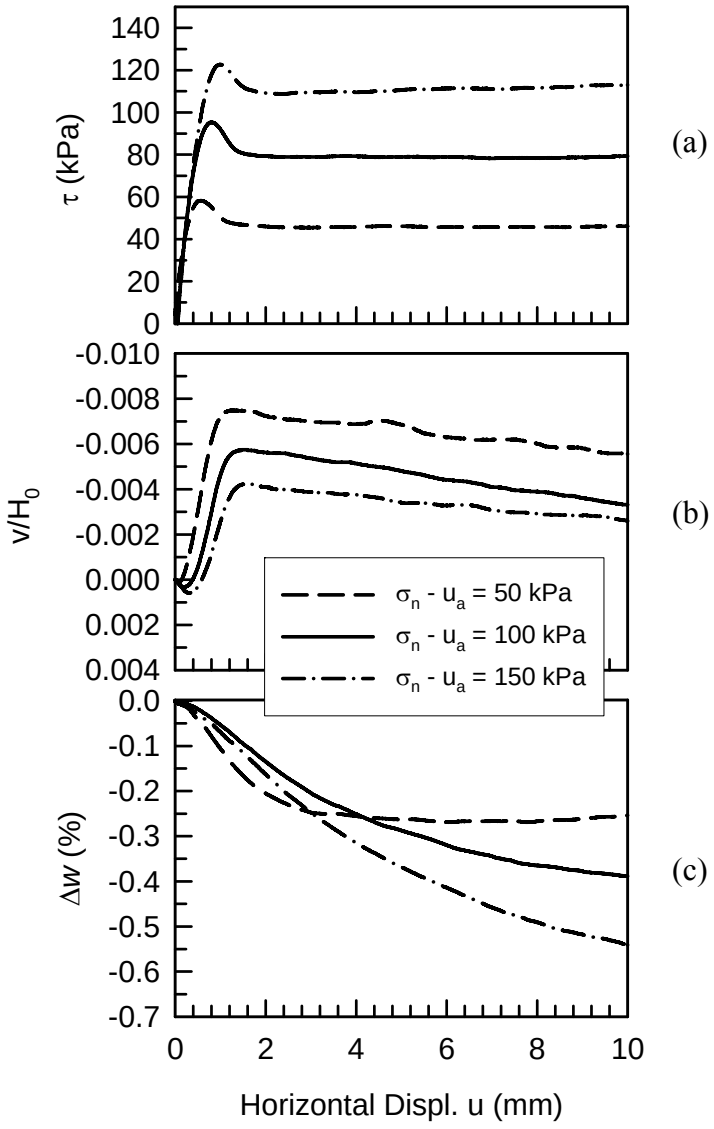

Figure 3.58- Effect of Net Normal Stress (σ_n-u_a) on (a) Shear Stress (τ), (b) v/H_0 and (c) Δw % during Shearing of Unsaturated Rough Interface Tests under Suction (u_a-u_w) of 50 kPa

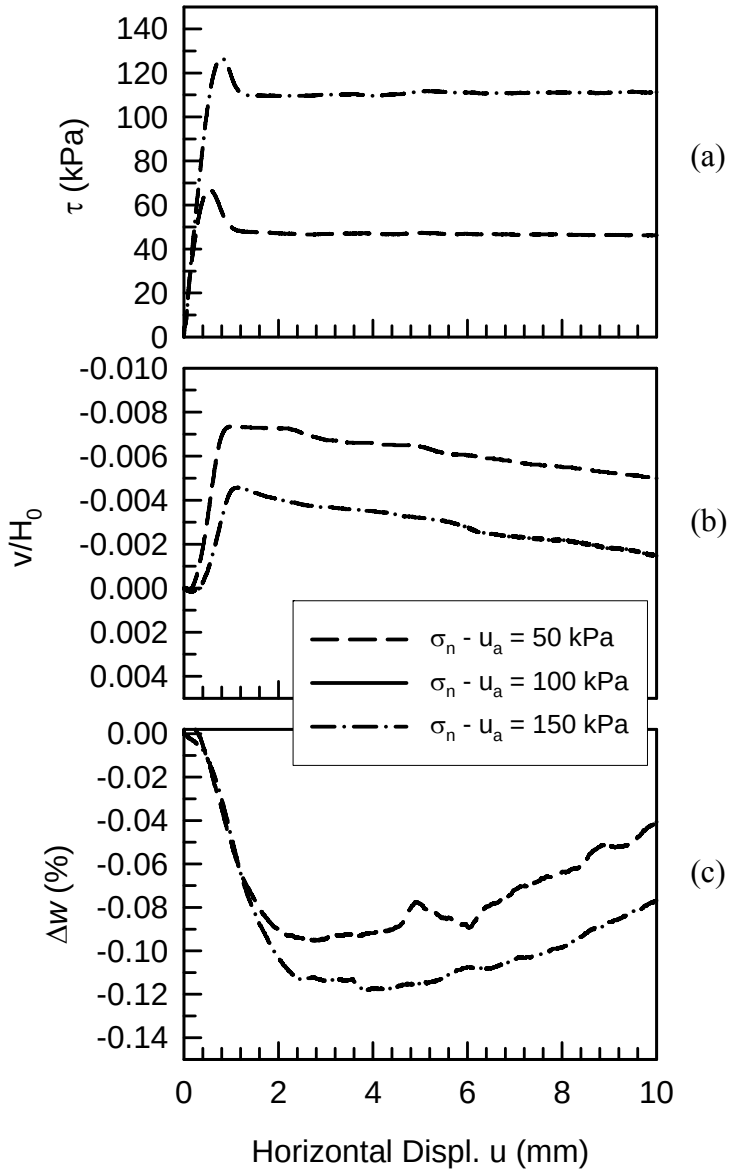

Figure 3.59- Effect of Net Normal Stress (σ_n-u_a) on (a) Shear Stress (τ), (b) v/H_0 and (c) Δw % during Shearing of Unsaturated Rough Interface Tests under Suction (u_a-u_w) of 100 kPa

3.6.2 Suction-Controlled Direct Shear Test HYSTERESIS (Drying-Wetting Paths) Results for Unsaturated Rough Interfaces

Suction-controlled hysteresis (drying/wetting cycles) tests on Rough interfaces were performed at suction following the drying then wetting path. In other words, after consolidation under the target suctions on the drying path (path AB, Figure 3.5) and the

target net normal stresses (path BC, Figure 3.5), specimens were then subjected to more drying by increasing suction up to about 100 kPa (path CE, Figure 3.5). Suction was then decreased back to the previous target value (path EF, Figure 3.5), after which samples were sheared (path FD, Figure 3.5). Results during consolidation and shearing are presented in the following sections.

3.6.2.1 Equalization Phases (Suction and Net Normal Stress)

Consolidation results of Rough interfaces for given net normal stresses (50, 100, 150 and 300 kPa) were plotted under different suction values as shown in Figure 3.60 and Figure 3.61. Results shown in Figure 3.60a and Figure 3.61a showed slight compression due to application of suction (AB path, Figure 3.5) that is relatively independent of suction magnitude at a given net normal stress. After application of target net normal stress (BE path, Figure 3.5) compression magnitude (Figure 3.60a and Figure 3.61a) (under the higher net normal stress, i.e. 150 kPa) seemed to follow a trend exhibiting a slightl decrease with increase of suction; this is more pronounced at higher net normal stress (i.e. 150 kPa) as also seen in Figure 3.65a and Figure 3.66a with average change in vertical displacement ($\Delta v/h_0$) of about 0.25 % for net normal stresses of 50 kPa and a range of 0.81 % to 1.26 % for net normal stress of 150 kPa. As suction increased up to 100 kPa (CE path, Figure 3.5) and decreased (wetting) back to a prior suction value (EF path, Figure 3.5) no significant compression was observed.

Figure 3.60b and Figure 3.61b show the change in water content (Δw %) for different suction values (8 kPa, 25 kPa and 50 kPa) at net normal stresses of 50 kPa and 150 kPa, respectively. Results showed that during drying (AB path, Figure 3.5) water drained out of samples with an average decrease in water content (Δw %) of about 1 %, 3.25 % and

7.4 %, for 8, 25 and 50 kPa suction values, respectively. As samples were dried to 100 kPa and then wetted to prior target suction values (CEF path, Figure 3.5), an average net decrease of 1.22 %, 5.13 % and 9.1 % in Δw was observed for 8, 25 and 50 kPa suction, respectively.

Figure 3.62-Figure 3.64 present the consolidation test results at given suction values for all net normal stresses. Figure 3.62a-Figure 3.64a indicate that as net normal stress increased compression magnitude increased. On the other hand, Figure 3.62b-Figure 3.64b showed that water content changes (Δw %), during all consolidation stages (AB, BE, CE, EF paths), were approximately equal at given suction values for samples under different net normal stresses, which indicates that the system accurately controlled suction.

Results at end of each consolidation stages were plotted as shown in Figure 3.65 and Figure 3.66. These figures indicate that suction influence on compression magnitude was negligible at low net normal stress of 50 kPa; however, at higher net normal stress (i.e. 150 kPa), a slight decrease in vertical compression was observed as suction increased. In addition, the change in vertical displacement ($\Delta v/H_0$) increased with increase in net normal stress from 50 kPa to 150 kPa with average $\Delta v/H_0$ equal to 0.25 % and 1.05 %, respectively. Figure 3.65b and Figure 3.66b show a comparison of Δw % results at both end of drying (AB path) and wetting (ABCEF path). Results indicate that end of drying (AB path) resulted in a decrease of 1 %, 3.25 % and 7.4 % in water content compared to 1.22 %, 5.13 % and 9.1 % at end of wetting (ABCEF path) for suction values of 8, 25 and 50 kPa respectively. This difference in water content for the same suction is similar to the SWCC hysteresis where for a given suction the water content on the wetting curve is less

than that of the drying curve as indicated in Figure 3.67, which presents comparison of water content results from the DST hysteresis tests to the SWCC results.

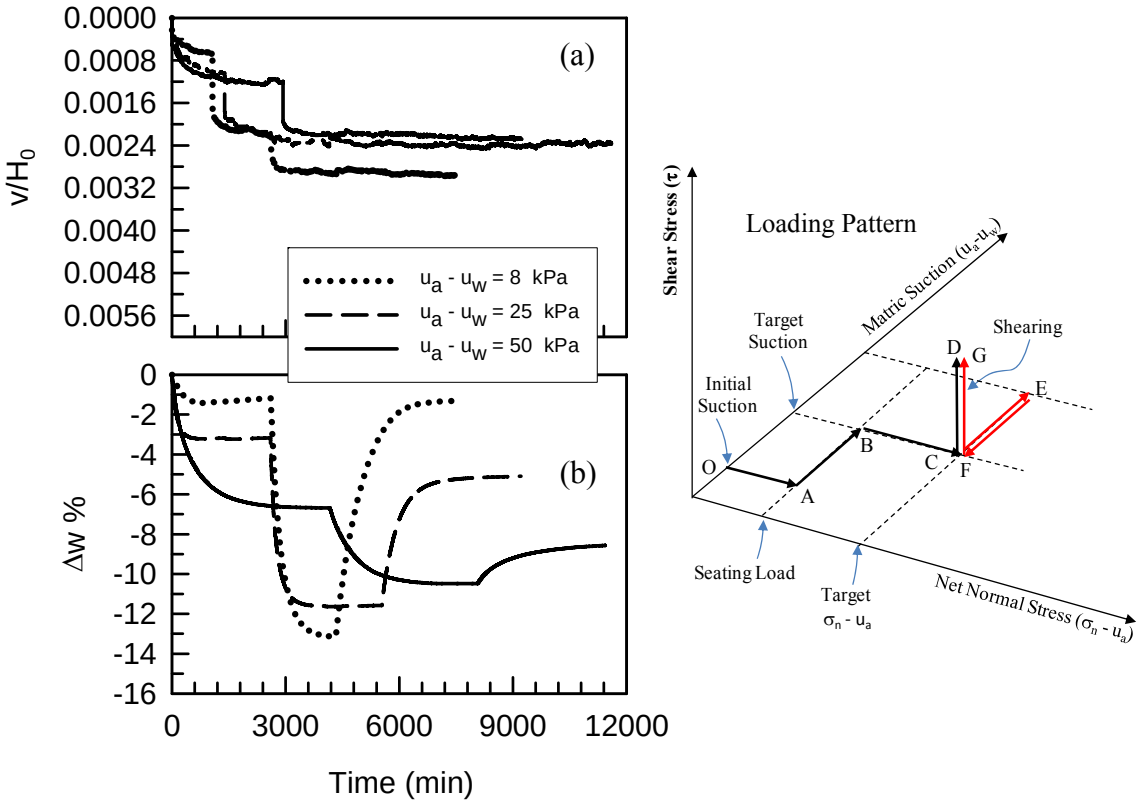

Figure 3.60- Effect of Suction (u_a-u_w) on (a) v/H_0 and (b) Δw % during Equalization of Hysteresis (Drying/Wetting) Unsaturated Rough Interface Tests under Net Normal Stress (σ_n-u_a) of 50 kPa

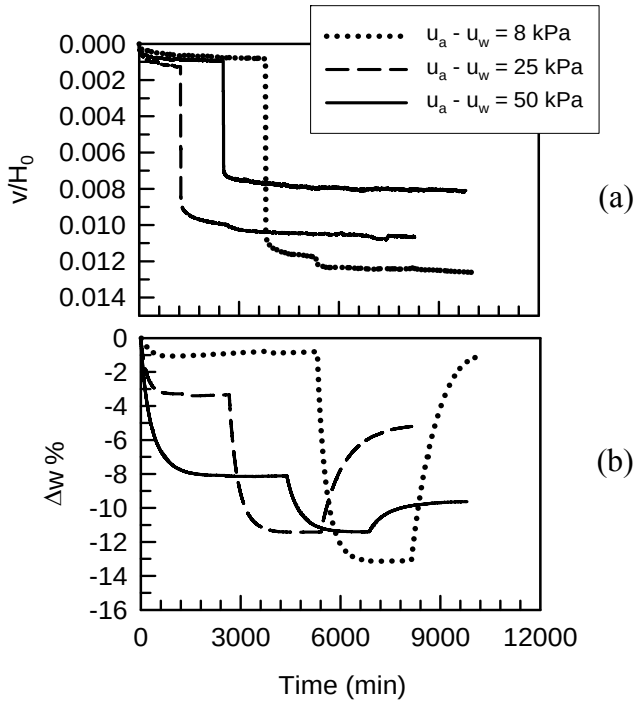

Figure 3.61- Effect of Suction (u_a-u_w) on (a) v/H_0 and (b) Δw % during Equalization of Hysteresis (Drying/Wetting) Unsaturated Rough Interface Tests under Net Normal Stress (σ_n-u_a) of 150 kPa

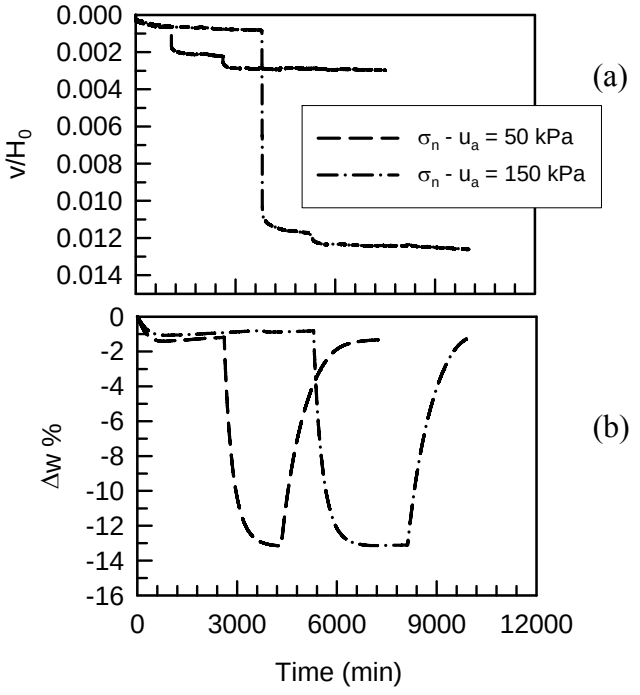

Figure 3.62- Effect of Net Normal Stress (σ_n-u_a) on (a) v/H_0 and (b) Δw % during Equalization of Hysteresis (Drying/Wetting) Unsaturated Rough Interface Tests under Suction (u_a-u_w) of 8 kPa

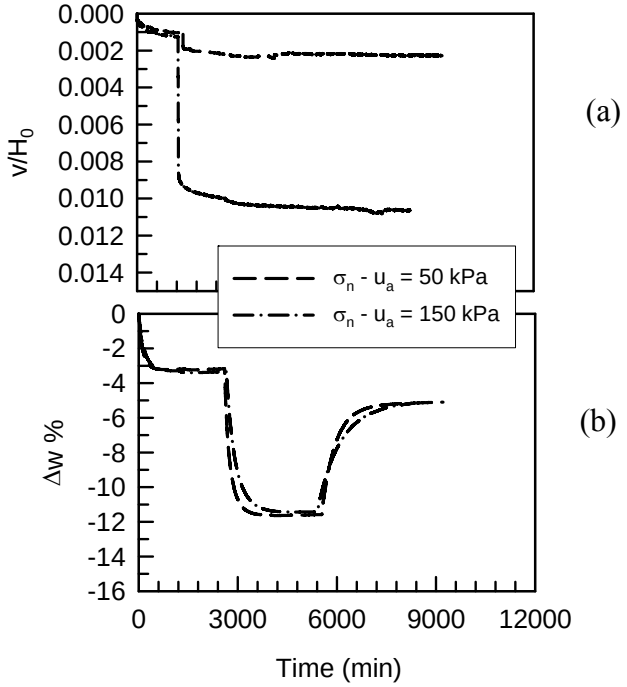

Figure 3.63- Effect of Net Normal Stress (σ_n-u_a) on (a) v/H_0 and (b) Δw % during Equalization of Hysteresis (Drying/Wetting) Unsaturated Rough Interface Tests under Suction (u_a-u_w) of 25 kPa

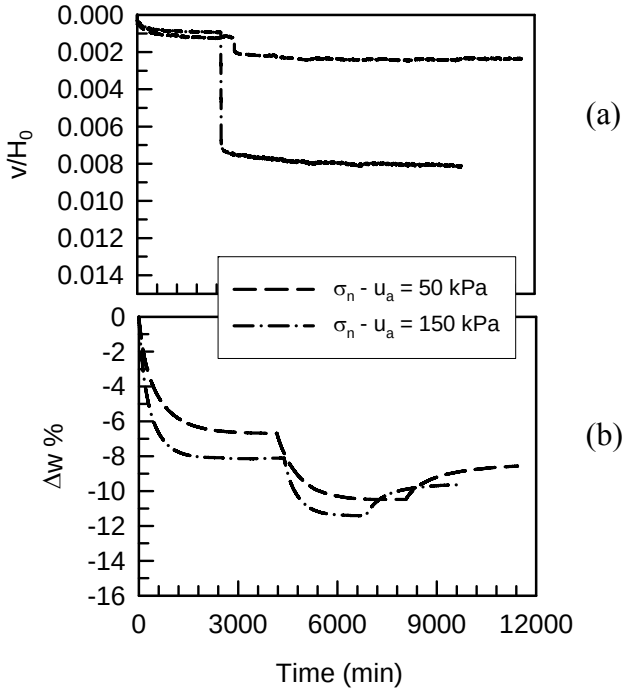

Figure 3.64- Effect of Net Normal Stress (σ_n-u_a) on (a) v/H_0 and (b) Δw % during Equalization of Hysteresis (Drying/Wetting) Unsaturated Rough Interface Tests under Suction (u_a-u_w) of 50 kPa

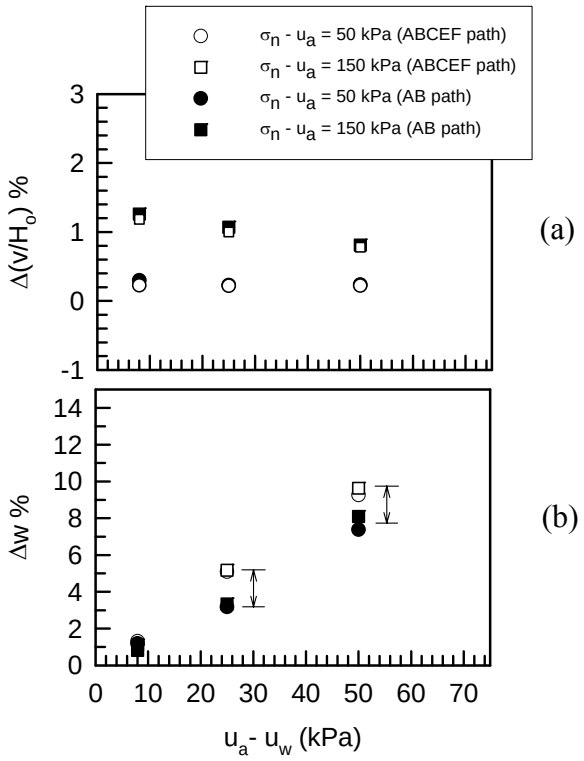

Figure 3.65- Summary of Consolidation Results versus Suction for all Net Normal Stresses

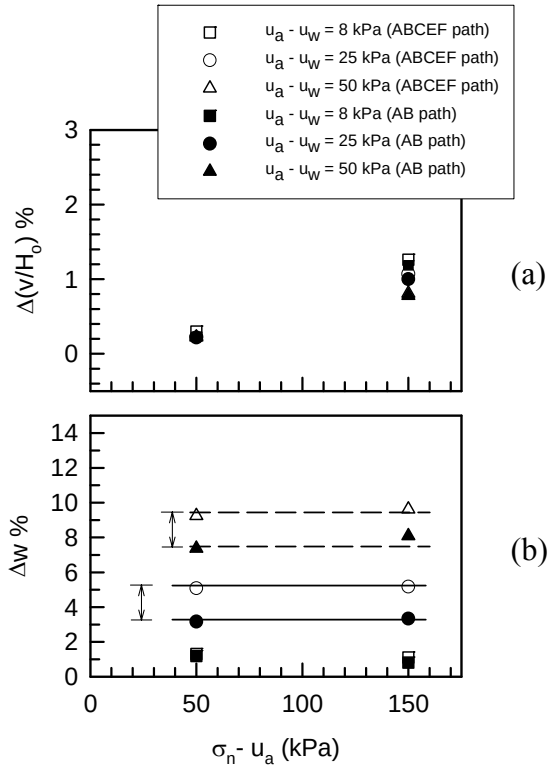

Figure 3.66- Summary of Consolidation Results versus Net Normal Stress Suction for all Suction Values

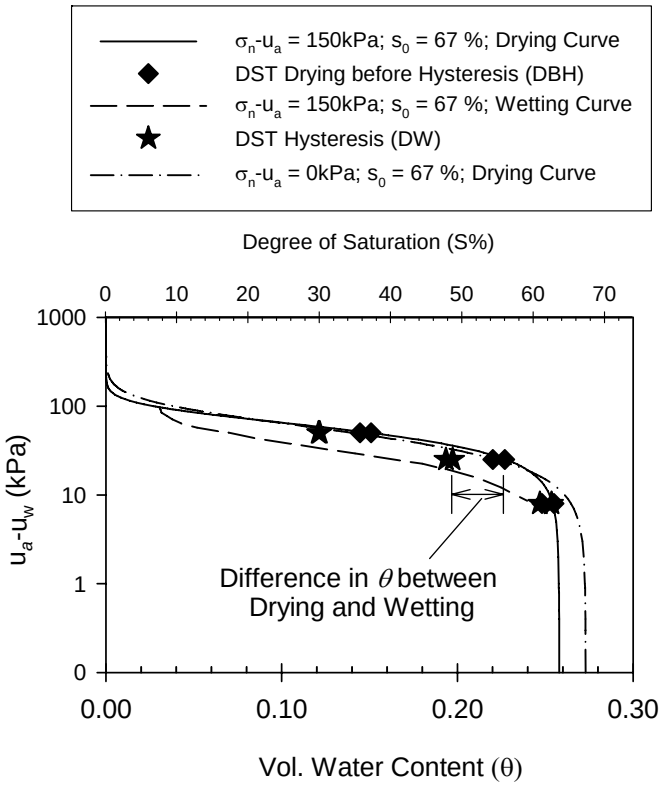

Figure 3.67 - Soil Water Characteristic Curves Superimposed with Results from Rough Interface DST during Drying before Hysteresis (DBH) and Wetting (DW)

3.6.2.2 Shearing Phase

Rough interface direct shear test (DST) results during shearing after suction hysteresis, are shown in Figure 3.68-Figure 3.72. Figure 3.68 and Figure 3.69 present shearing results with suction at net normal stresses of 50 kPa and 150 kPa, respectively. Figure 3.68a and Figure 3.69a indicate that the shear strength increased with increase of suction. The increase in shear strength seems to be more pronounced when suction increased from 8 kPa to 25 kPa as compared to the increase from 25 to 50 kPa suction. In addition, strain softening behavior was observed and more pronounced at higher suction value (i.e., 25 and 50 kPa) compared to negligible strain softening at lower suction values of 8 kPa. Volume change results during shearing are shown in Figure 3.68b and Figure 3.69b and indicate a slight and negligible compression at beginning of a test followed by

dilation as approaching peak shear strength. Then dilation ceased in the region of post peak shear stress although in some cases a slight re-compression was observed toward the end of the post peak process. Unlike rough interface tests without hysteresis (which showed increase in dilatancy with increase in suction), in general, the amount of dilation was not greatly affected by suction; however, the test sample at 50 kPa suction and 50 kPa net normal stress showed lower dilation compared to other suctions tests (Figure 3.68b). Figure 3.68c and Figure 3.69c present the change in water content during shearing. For tests at suction of 25 kPa and 50 kPa the change in water content was practically negligible (<0.07% water content); however, it did show a slight tendency for water inflow during shearing. At low suction (i.e. 8 kPa, which is equal to the AEV) even more water flowed into the sample during shearing similar to rough interface tests without hysteresis, in which it was observed and postulated that during shearing the soil at low suction (near the AEV), behaves like saturated soil.

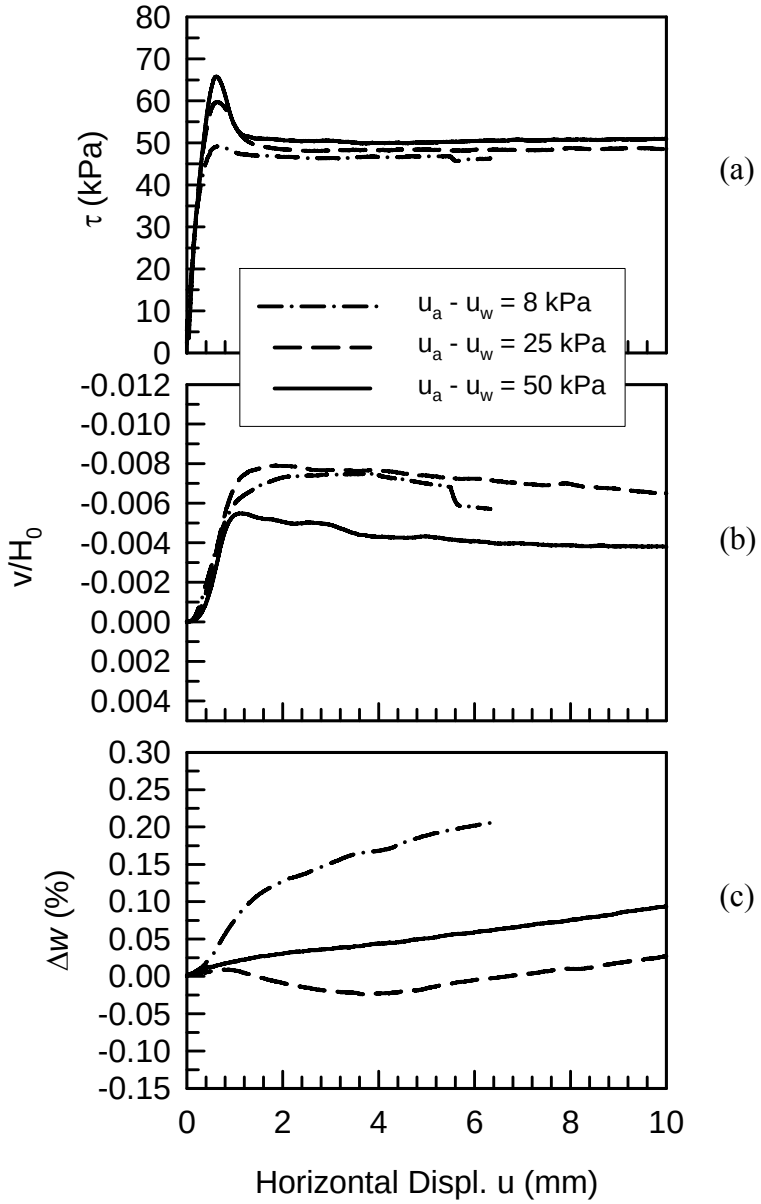

Figure 3.68- Effect of Suction (u_a-u_w) on (a) Shear Stress (τ), (b) v/H_0 and (c) Δw % during Shearing of Unsaturated Rough Interface Hysteresis (Drying/Wetting) Tests under Net Normal Stress (σ_n-u_a) of 50 kPa

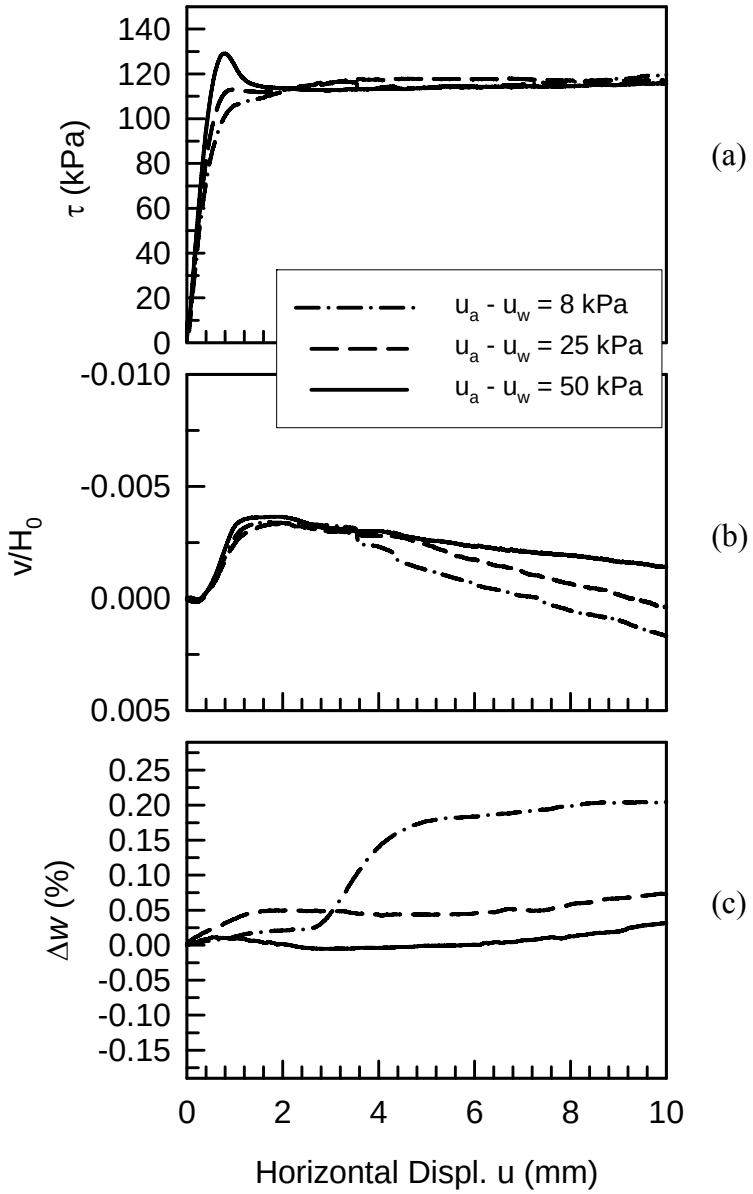

Figure 3.69- Effect of Suction (u_a-u_w) on (a) Shear Stress (τ), (b) v/H_0 and (c) Δw % during Shearing of Unsaturated Rough Interface Hysteresis (Drying/Wetting) Tests under Net Normal Stress (σ_n-u_a) of 150 kPa

Suction-controlled hysteresis of rough interface direct shear tests are also presented in Figure 3.70-Figure 3.72 at given suction value of 8, 25 and 50 kPa, respectively. Results indicate that shear strength increases with increase in net normal stress (Figure 3.70a-Figure 3.72a). The rough interface tests compressed slightly (negligible amount) at the

beginning but started to dilate as approaching the peak shear strength (Figure 3.70b-Figure 3.72b); the amount of dilation decreased with increase in net normal stress. In general dilation ceased during post peak shearing.

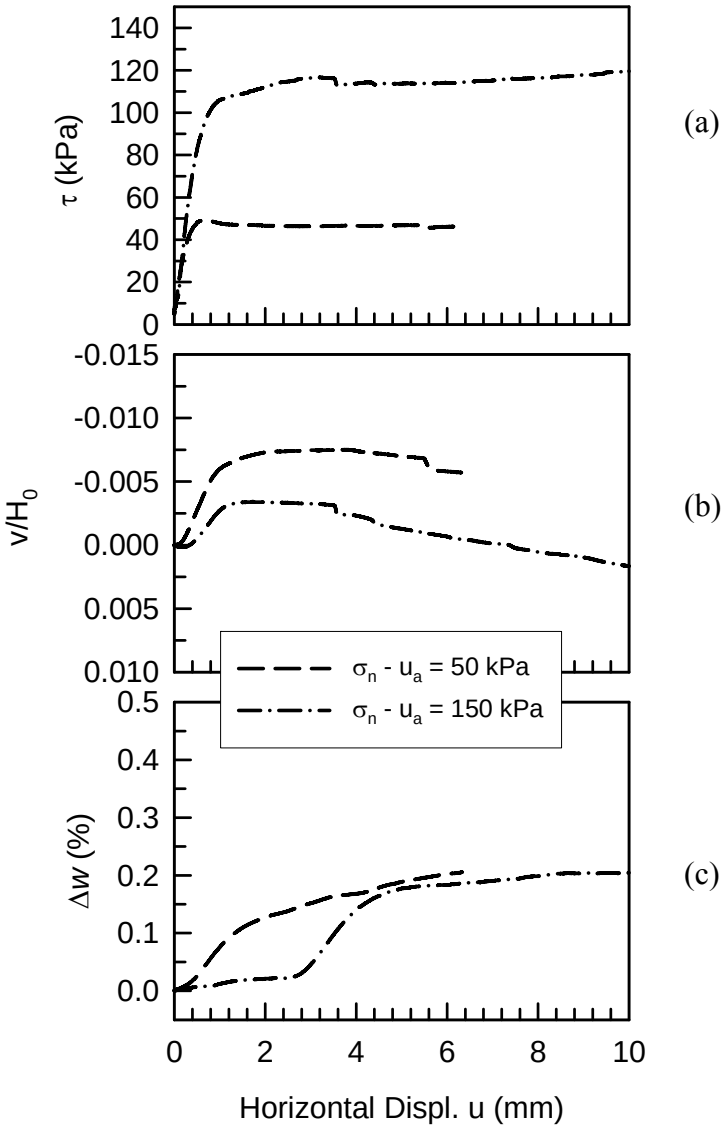

Figure 3.70- Effect of Net Normal Stress (σ_n-u_a) on (a) Shear Stress (τ), (b) v/H_0 and (c) Δw % during Shearing of Unsaturated Rough Interface Hysteresis (Drying/Wetting) Tests under Suction of 8 kPa

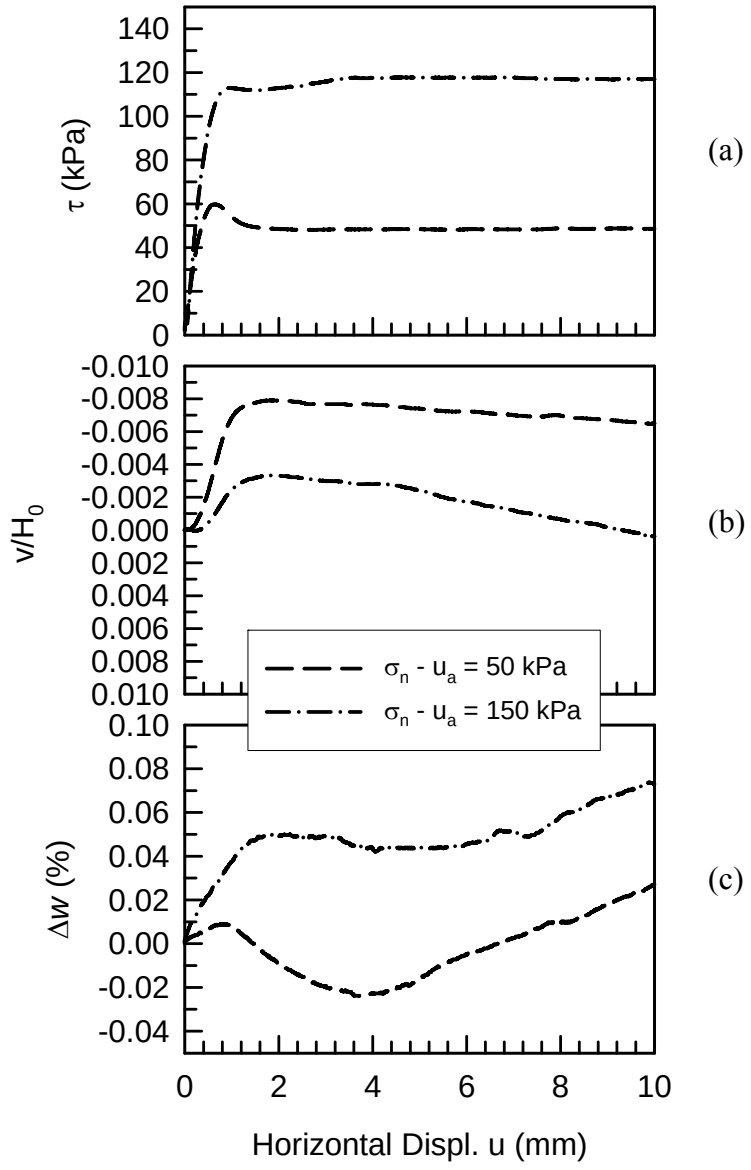

Figure 3.71- Effect of Net Normal Stress (σ_n-u_a) on (a) Shear Stress (τ), (b) v/H_0 and (c) Δw % during Shearing of Unsaturated Rough Interface Hysteresis (Drying/Wetting) Tests under Suction of 25 kPa

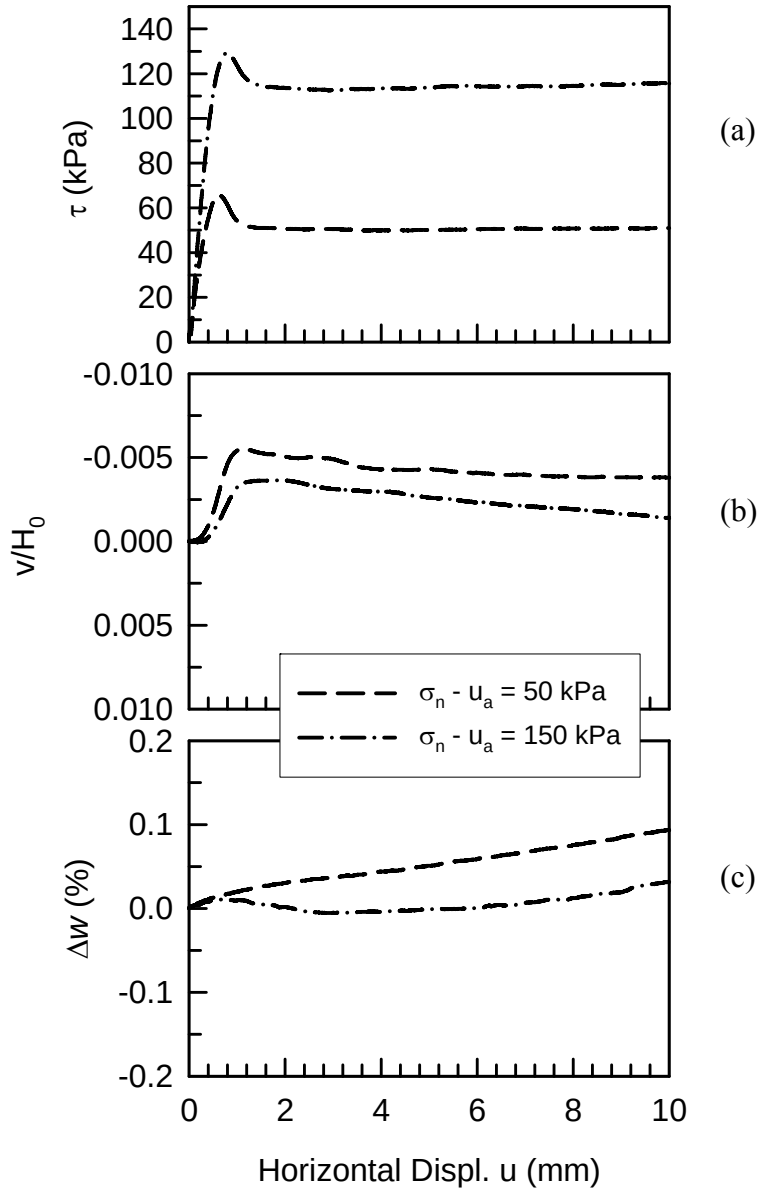

Figure 3.72- Effect of Net Normal Stress (σ_n-u_a) on (a) Shear Stress (τ), (b) v/H_0 and (c) Δw % during Shearing of Unsaturated Rough Interface Hysteresis (Drying/Wetting) Tests under Suction of 50 kPa

3.6.3 Comparison of ROUGH Interface Test Results w/o Hysteresis

3.6.3.1 Hysteresis Effect on the Volume Change Behavior

Comparisons of consolidation results between Rough interface DST with suction hysteresis and Rough interface DST without suction hysteresis (Drying tests) are shown

in Figure 3.73-Figure 3.75. Also comparisons at end of each consolidation stages between results from drying (D) tests (without hysteresis) with: a) hysteresis test results at end of drying before wetting (DBW) are shown in Figure 3.76, b) hysteresis test results at end of wetting (wetting after drying, DW) are shown in Figure 3.77. Plots of vertical displacement (normalized to the specimen height) with time during the equalization phases for both drying (D) tests and wetting after drying (DW) are presented in Figure 3.73a-Figure 3.75a, for all net normal stresses (50 and 150 kPa) at suction values of 8, 25 and 50 kPa, respectively. Results show that the magnitude of specimen compression is practically the same at given suction and net normal stress values as also indicated in Figure 3.76a and Figure 3.77a. Comparison of change in water content (Δw %) results during equalization periods in the corresponding drying tests (D) and hysteresis test specimens are shown in Figure 3.73b-Figure 3.75b. These figures along with Figure 3.76b and Figure 3.77b indicate that in general, the same amount of water (Δw average $\approx$ 1 %, 3.25% and 7.74 %) drained from both hysteresis (DBW, end of drying before hysteresis) and drying (D) test specimens at suction of 8 kPa, 25 kPa and 50 kPa, respectively, except for tests at net normal stress and suction of 50 kPa, which had different initial moisture contents. Although, both had different initial water content and the amount of water change was slightly different, the water content, however, at end of the suction stage was practically the same. This indicates that the system is accurately controlling suction in all tests. As suction was increased up to 100 kPa and wetted back to prior suction (i.e. DW test specimens), the net decrease in water content was on average about 1.2 %, 5.44 % and 9.44 % for suctions tests of 8, 25 and 50 kPa, respectively. The water content from the drying (D) tests was approximately about 0.32 %, 1.74 and 1 %

higher than that from the (DW) tests at suction of 8, 25 and 50 kPa, respectively. This difference in the water content is slightly smaller than the difference in SWCC hysteresis between the wetting curve and the drying curve, as shown in Figure 3.78. This figure shows the water content results at end of Hysteresis (DW) tests and those from Drying (D) tests together along with the SWCCs.

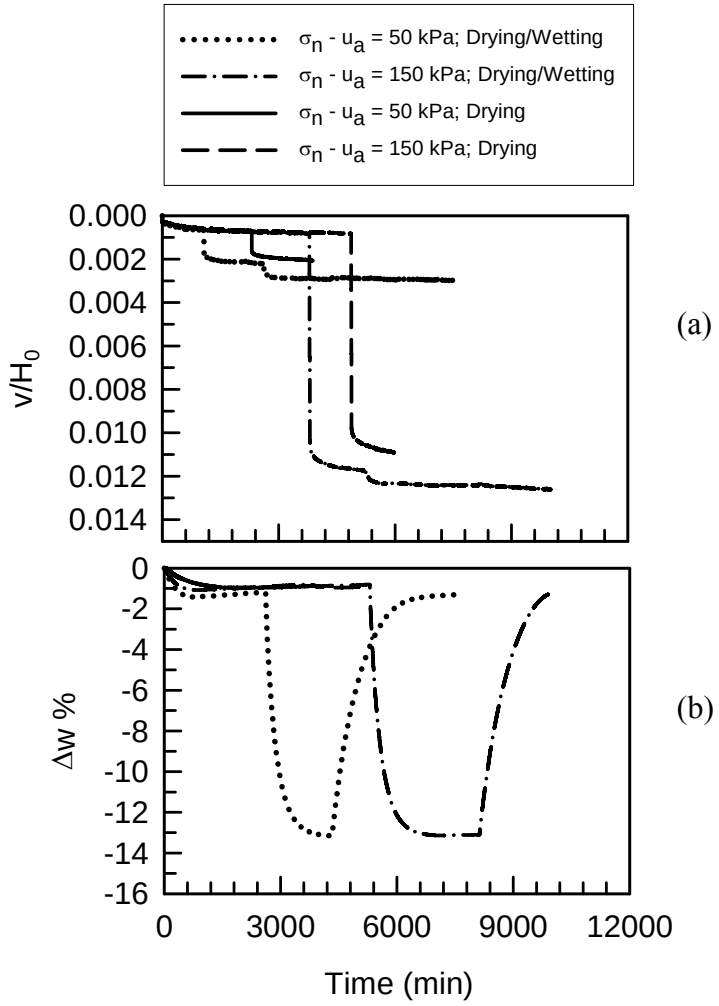

Figure 3.73- Comparison of Consolidation Results between Drying (No Hysteresis) Tests and Hysteresis (Drying/Wetting) Tests of Unsaturated Rough Interfaces under Suction (u_a-u_w) of 8 kPa

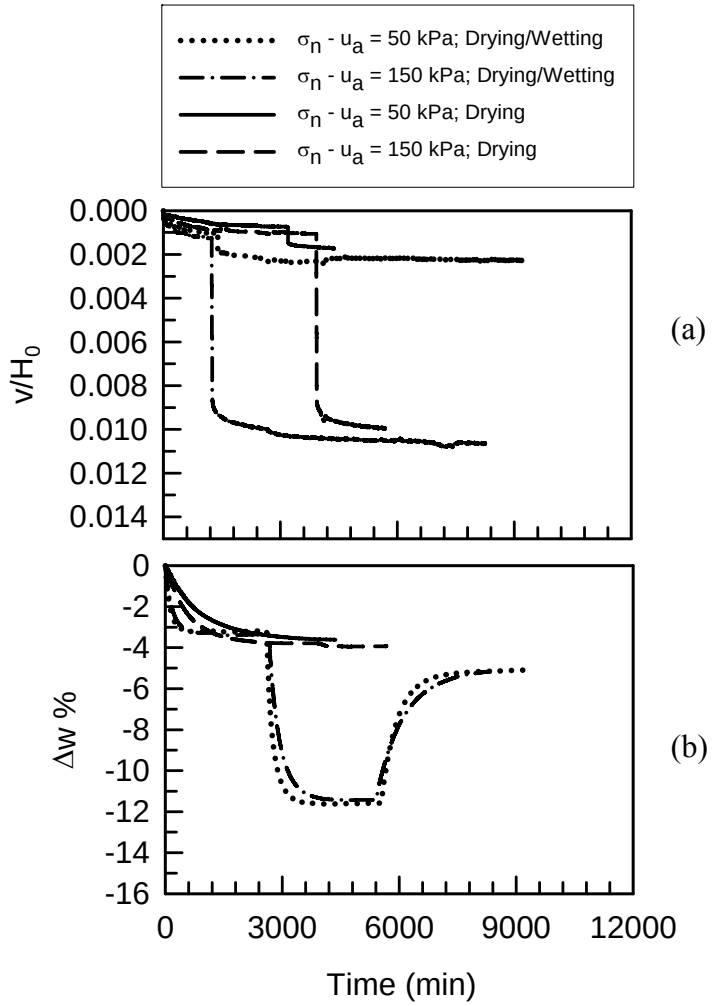

Figure 3.74- Comparison of Consolidation Results between Drying (No Hysteresis) Tests and Hysteresis (Drying/Wetting) Tests of Unsaturated Rough Interfaces under Suction (u_a-u_w) of 25 kPa

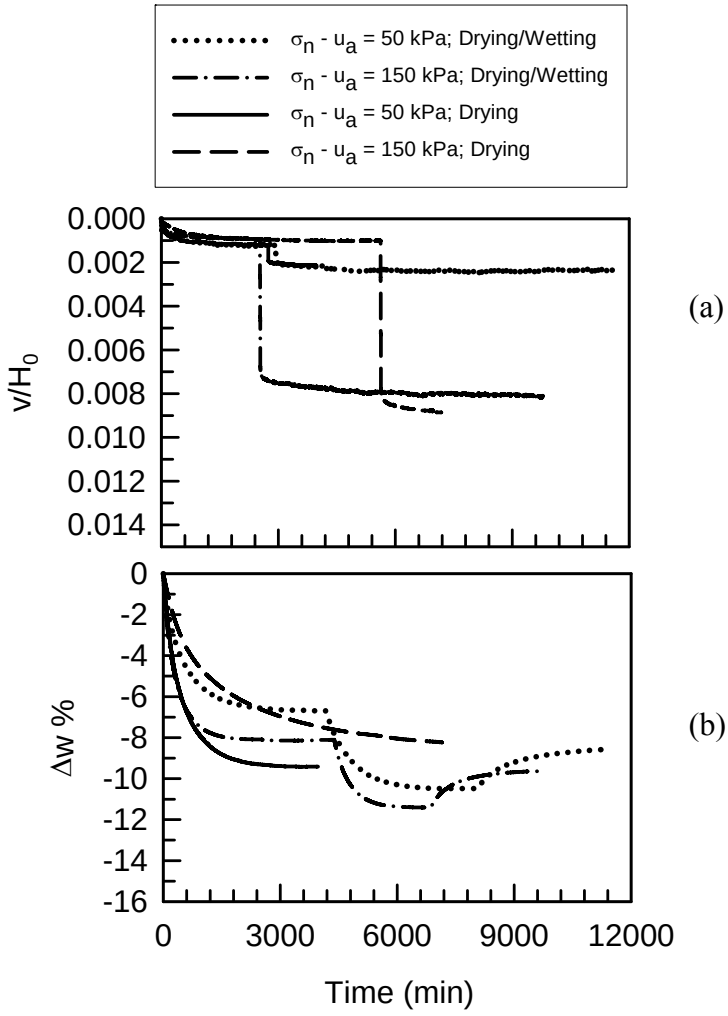

Figure 3.75- Comparison of Consolidation Results between Drying (No Hysteresis) Tests and Hysteresis (Drying/Wetting) Tests of Unsaturated Rough Interfaces under Suction (u_a-u_w) of 50 kPa

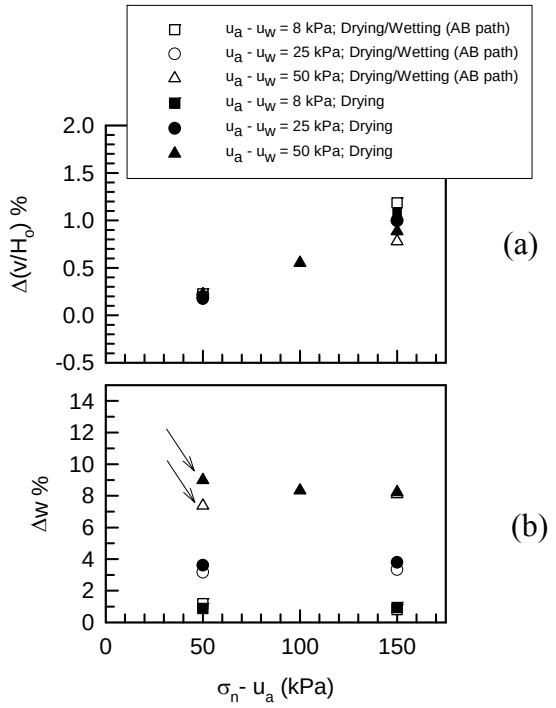

Figure 3.76- Summary Comparison of Rough Interface Consolidation Results between Hysteresis Tests at end of Drying (AB path) and Tests without Hysteresis (Drying)

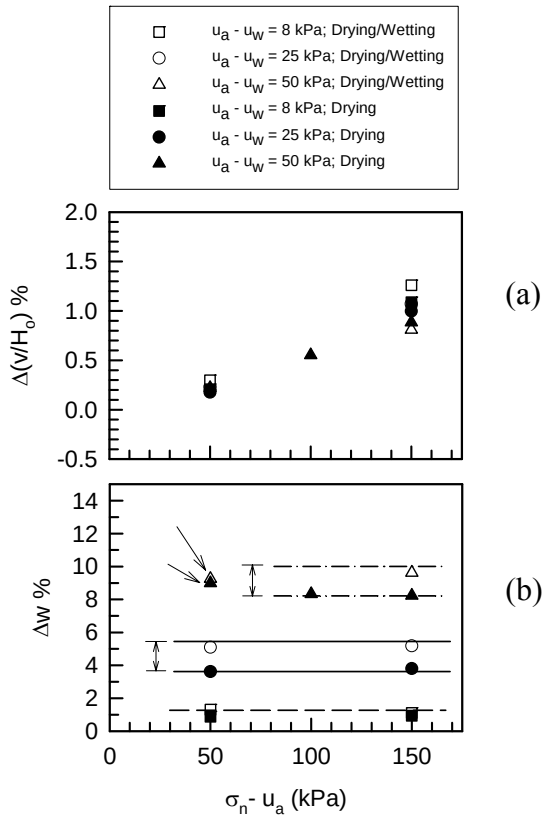

Figure 3.77- Summary Comparison of Rough Interface Consolidation Results between Hysteresis Tests at end of Drying/Wetting (ABCEF path) and Tests without Hysteresis (Drying)

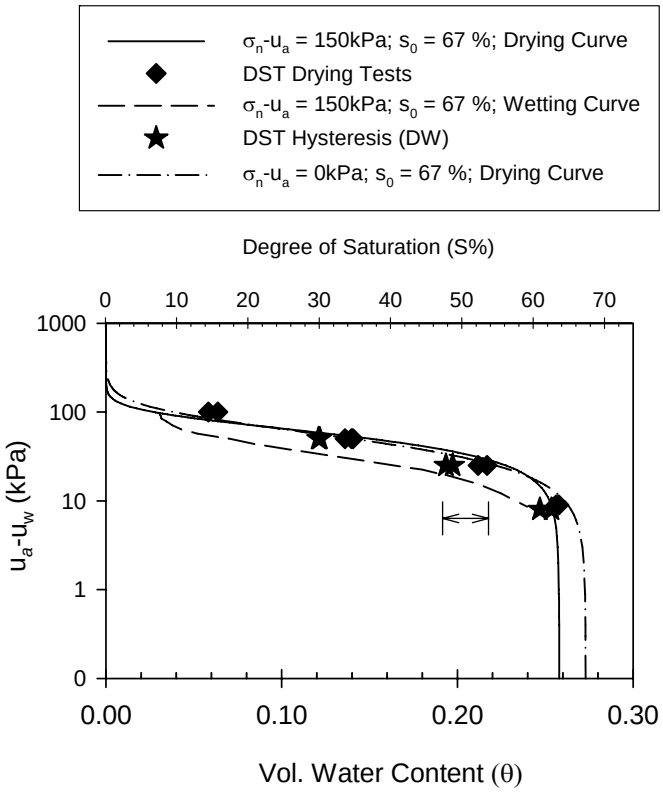

Figure 3.78- Soil Water Characteristic Curves Superimposed with Results from Rough Interface DST of Drying (D) and Drying/Wetting (DW) Tests

3.6.3.2 Hysteresis Effect on the Shearing Behavior

Comparison of shear stress (τ) and volume change responses during shearing of unsaturated rough interface DST tests subjected to drying (D) and wetting after drying (DW) at same matric suction and net normal stresses are shown in Figure 3.79-Figure 3.81. In general, similar trends in the interface shear stress-displacements, volume change behavior were observed for (D) and (DW) tests. Based on these figures, some important observations are summarized as follows:

- During shearing of both (D) and (DW) tests, peak shear strength is achieved followed by strain softening to a post peak shear stress; this strain softening behavior was only observed at higher suctions (e.g. 25 and 50 kPa) as shown in

Figure 3.80a and Figure 3.81a, while no strain softening was observed for 8 kPa suction tests (Figure 3.79a).

- For a given net normal stress and suction, hysteresis (DW) tests exhibited slightly higher interface peak and post peak shear strength compared to drying (D) tests.
- In general, the volume changes during shearing (Figure 3.79b-Figure 3.81b) indicate that both tests slightly compressed initially then started to dilate. For both tests, dilation apparently started as approaching the interface peak shear strength and then ceased, followed by compression once the strain softening process was completed and the shear stress reached the interface post peak shear strength. It was also observed that for both (D) and (DW) tests, amount of dilation decreased with increase in net normal stresses;
- During shearing, some changes in the specimens' water content (Δw %) were detected in both test types. At low suction values (i.e. 8 kPa), water flowed into specimens in both (D) and (DW) tests. At higher suction values (i.e. 25 and 50 kPa), it was observed that water drained out (up to 0.6 % change in water content) of the sample for (D) tests, but a negligible amount (<0.1% Δw) of water did flow mostly into the sample for (DW) tests. Although tests (D) dilate, water drainage at higher suctions indicates a tendency for suction to decrease due to increasing pore water pressure. Whereas, inflow suggests excess pore pressures were tending toward negative values.

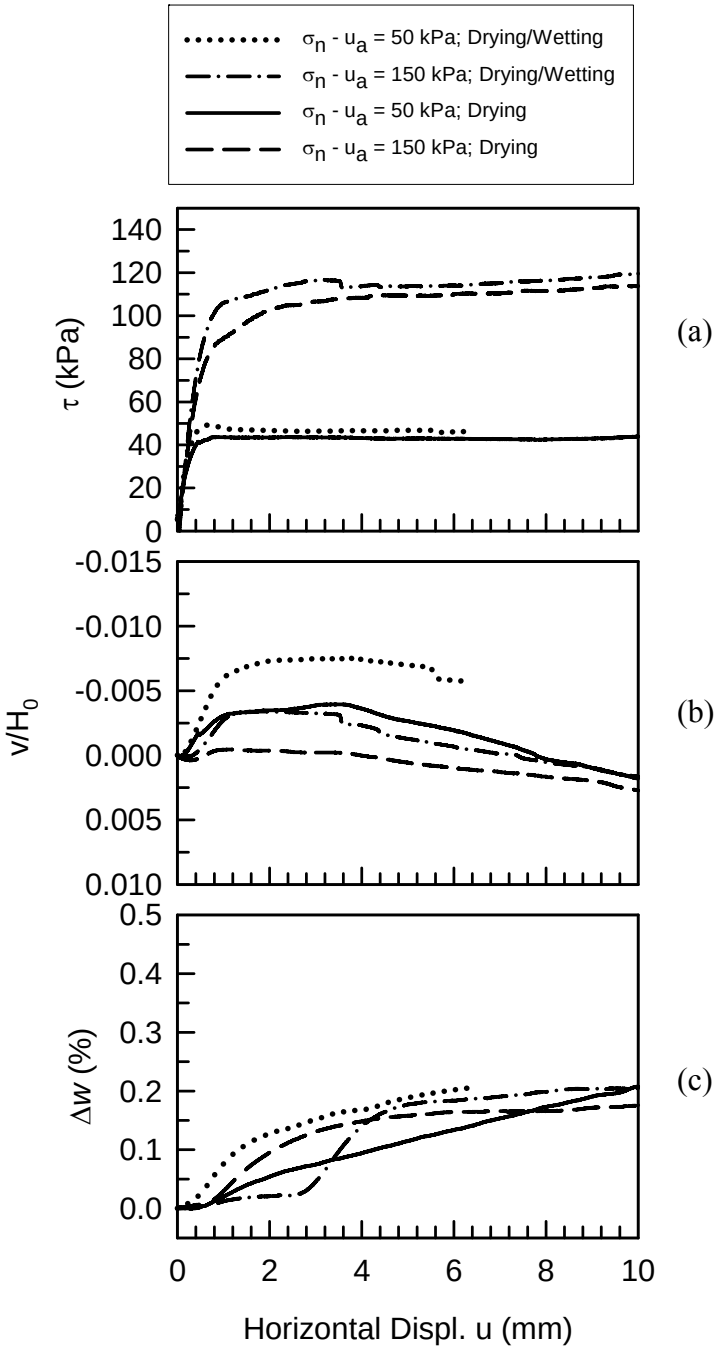

Figure 3.79- Comparison of Results during Shearing between Drying (D) Tests and Hysteresis Drying/Wetting (DW) Tests for Unsaturated Rough Interfaces under Suction of 8 kPa

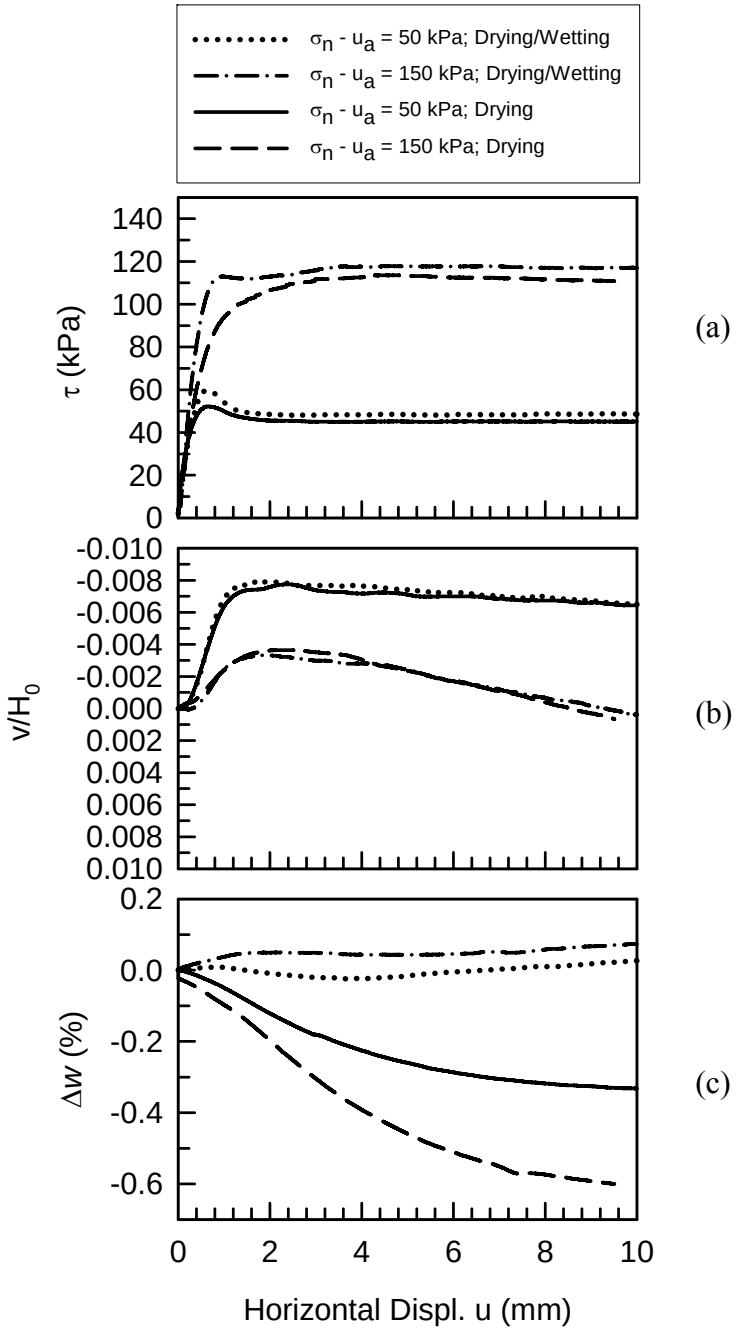

Figure 3.80- Comparison of Results during Shearing between Drying (D) Tests and Hysteresis Drying/Wetting (DW) Tests for Unsaturated Rough Interfaces under Suction of 25 kPa

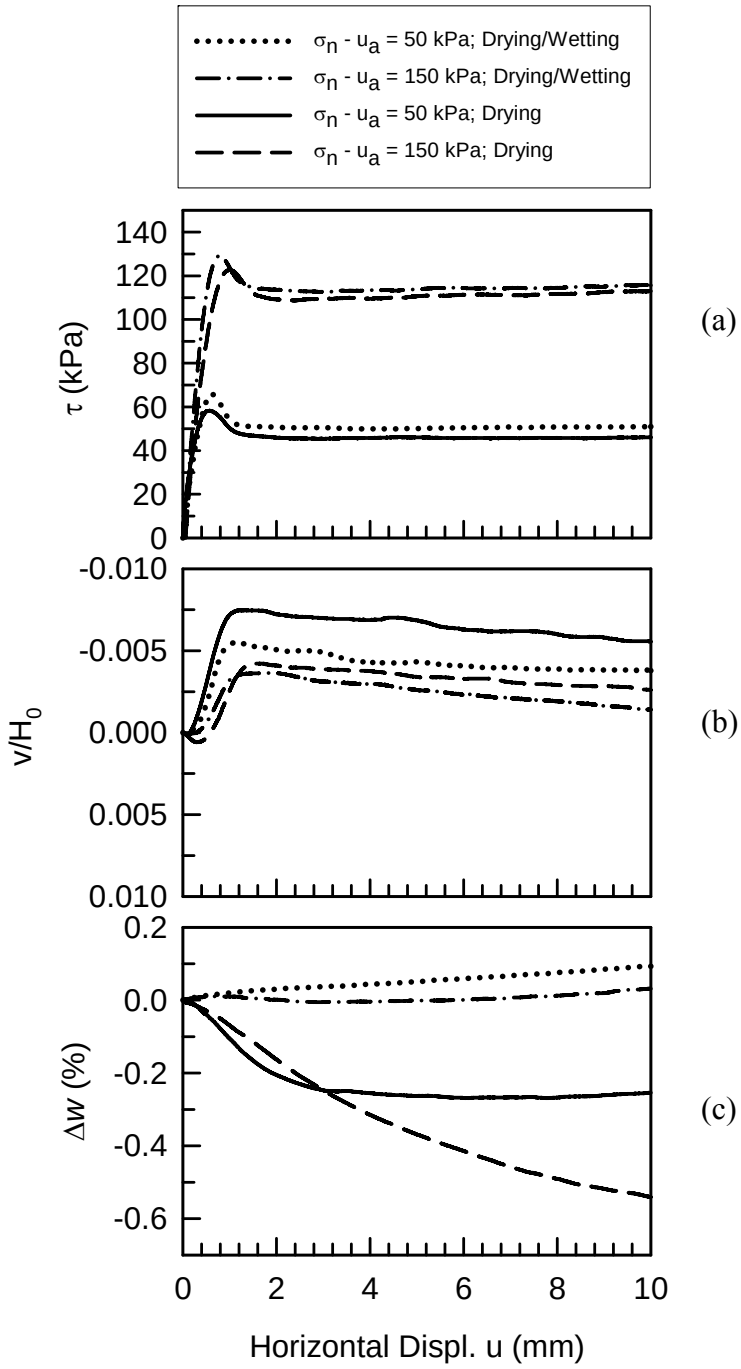

Figure 3.81- Comparison of Results during Shearing between Drying (D) Tests and Hysteresis Drying/Wetting (DW) Tests for Unsaturated Rough Interfaces under Suction of 50 kPa

3.6.4 Suction-Control Direct Shear Test DRYING Path Results for Smooth Interfaces

A limited number of suction-control interface direct shear tests on unsaturated smooth steel interfaces were performed under constant suctions of 50 kPa and net normal stress of 100 and 150 kPa. The effect of net normal stress and suction on the consolidation results, stress-displacement and volumetric behavior of unsaturated smooth interfaces are discussed in this section.

3.6.4.1 Equalization Phases (Suction and Net Normal Stress)

Consolidation results at suction of 50 kPa are shown in Figure 3.82. Figure 3.82a presents the changes in vertical deformation, normalized to the specimen height (v/H_0), versus time during consolidation, which showed that the magnitude of compression increased with increase in net normal stress. The change in v/H_0 % was approximately 0.54 % and 1.10 % under net normal stresses of 100 and 150 kPa, respectively. Variation in water content for smooth interface test samples during equalization are shown in Figure 3.82b at 50 kPa suction, and indicate that the change in water content (Δw %) is essentially the same for both tests (at different net normal stresses); in other words, the water controller pulled approximately the same amount of water ($\Delta w \approx 8.6$ %) from both samples to achieve the required suction.

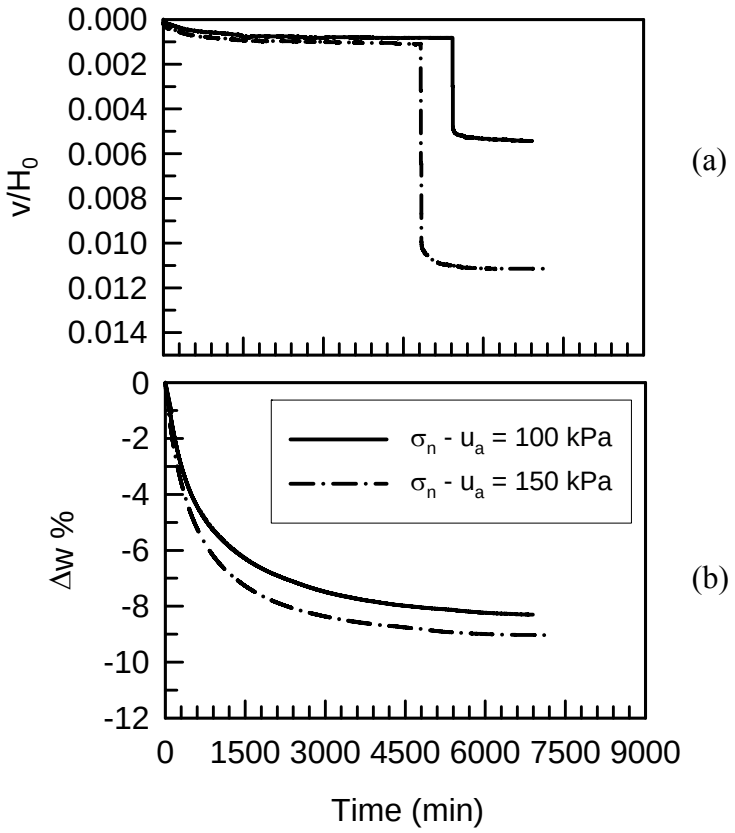

Figure 3.82- Effect of Net Normal Stress (σ_n-u_a) on (a) v/H_0 and (b) Δw % during Equalization of Unsaturated Smooth Interface Tests under Suction (u_a-u_w) of 50kPa

3.6.4.2 Shearing Phase

Plots of the shear stress and volume change behavior for the smooth interface during shearing are shown in Figure 3.83 under suction of 50 kPa and net normal stresses of 100 kpa and 150 kPa. This figure shows that the smooth interface exhibited stick-slip behavior after the maximum shear stress was reached. The stick-slip process continued throughout the test. Shear strength of the smooth interface increased with increase in net normal stress (Figure 3.83a) and little to no strain softening was observed following the peak shear stress.

As opposed to soil and rough interface, the smooth interface (Figure 3.83b) did not show dilatancy behavior as also observed by Hamid and Miller (2009). The smooth

interface tests contracted initially and then the behavior remained steady after reaching the peak shear stress (i.e. did not show significant compression or dilation). Based on this observation it is postulated that for the smooth interface the shearing mechanism is controlled by sliding rather than interlocking between soil particles or soil and smooth steel plate. Similar to rough interface, the water volume controller pulled a small amount of water from the smooth interface during shearing.

The change in the volume of water during shearing was on average approximately 0.29 % (Figure 3.83c).

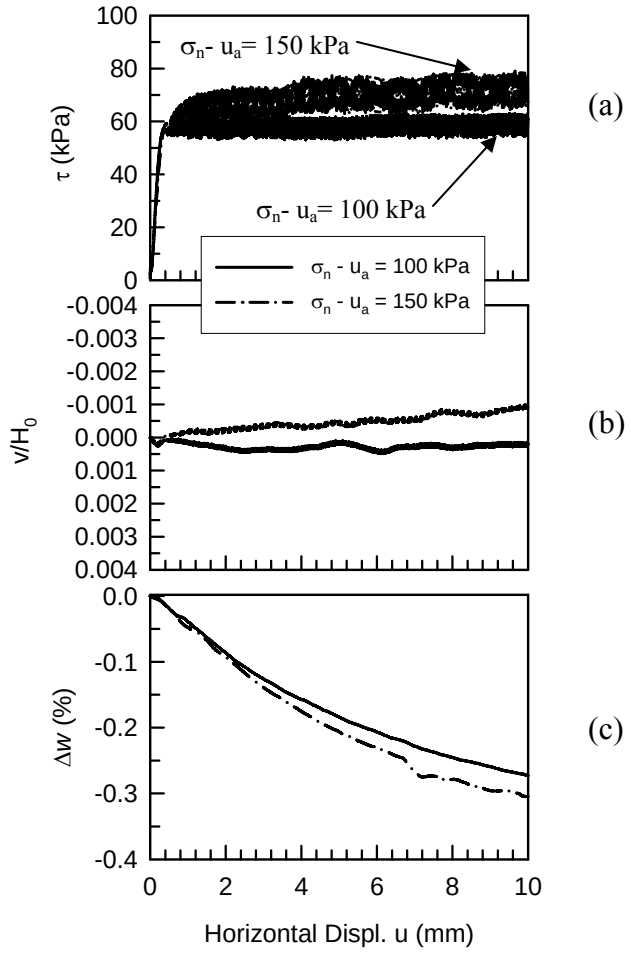

Figure 3.83- Effect of Net Normal Stress (σ_n-u_a) on (a) Shear Stress (τ), (b) v/H_0 and (c) Δw % during Shearing of Unsaturated Smooth Interface Tests under Suction of 50 kPa

Figure 3.84 and Figure 3.85 present comparison of shear strength results between smooth and rough interfaces at suction of 50 kPa and and net normal stresses of 100kPa and 150 kPa. Results indicate that the surface roughness significantly influenced the peak and post-peak shear stress as well as the volumetric behavior of interfaces. The following important observations regarding the effect of surface roughness on the behavior of the interface can be made from these figures:

- A more pronounced peak shear stress was observed for rough than smooth interfaces. Strain softening behavior was observed for the rough interface while the smooth interface showed little to no strain softening following the peak shear stress.
- The peak shear strength for the rough interface was larger and mobilized at larger horizontal deformation than that of the smooth interface.
- The smooth interface initially compressed slightly similar to the rough interface until the peak shear stress was reached and then the behavior remained steady after reaching the peak shear stress (i.e no noticeable change in vertical displacement). However, the rough interface began to dilate after reaching the peak shear stress (τ_p) and dilation continued until the post-peak shear stress was reached.
- A clear stick-slip behavior was observed after the peak shear stress for the smooth surface whereas the rough surface did not show stick-slip behavior.
- A similar amount of water drained out of samples during the shearing process for both smooth and rough interfaces.

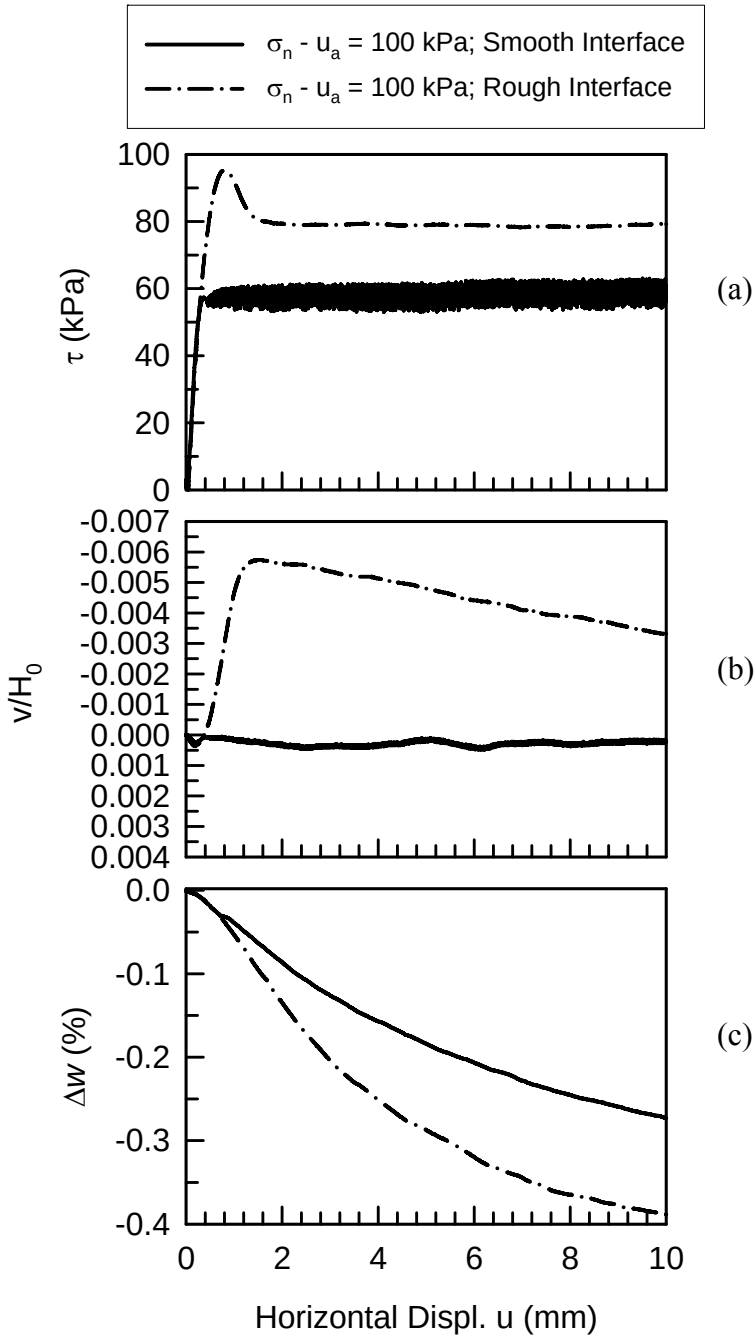

Figure 3.84- Comparison of (a) Shear Stress (τ), (b) v/H_0 and (c) Δw % during Shearing of Unsaturated Smooth and Rough Interface Tests under Suction of 50 kPa and Net Normal Stress of 100 kPa

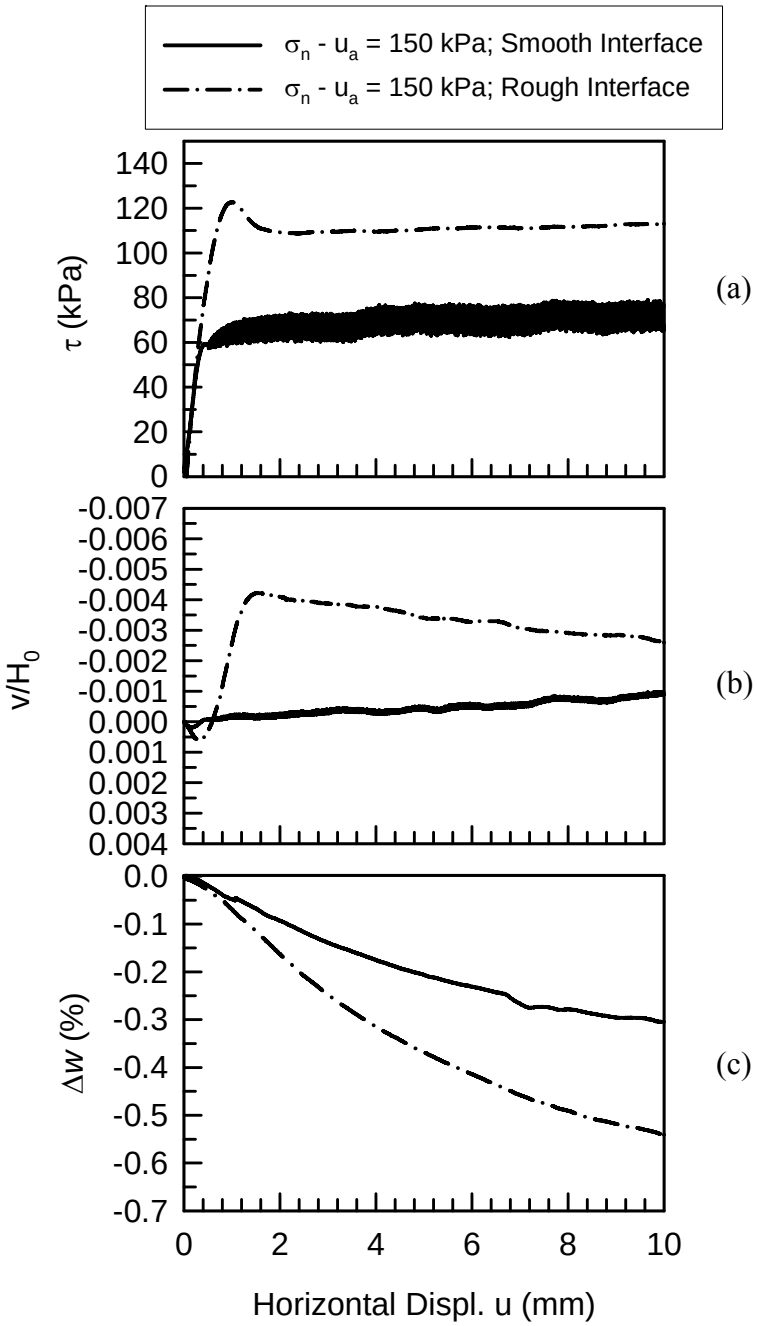

Figure 3.85- Comparison of (a) Shear Stress (τ), (b) v/H_0 and (c) Δw % during Shearing of Unsaturated Smooth and Rough Interface Tests under Suction of 50 kPa and Net Normal Stress of 150 kPa

3.7 RESULTS AND DISCUSSIONS FOR UNSATURATED SOIL-GEOTEXTILE INTERFACE TESTS

3.7.1 Suction-Control Direct Shear Test DRYING Path Results

3.7.1.1 Equalization Phases (Suction and Net Normal Stress)

The tests performed on soil-geotextile interfaces were carried out at different net normal stresses, ranging from 50 kPa to 300 kPa, and suction values ranging from 0 kPa to 100 kPa. Figure 3.86a-Figure 3.88a show plots of v/H_0 versus time during equalization phases for net normal stresses of 50 kPa, 100 kPa and 150 kPa, respectively. In general, the amount of compression under a target net normal stress was approximately equal for all suction values (Figure 3.86a-Figure 3.88a and Figure 3.92a). Note, due to a change in the seating load from 14 to 34 kPa, the change in net normal stress (indicated in the legends of Figure 3.86-Figure 3.88) needed to achieve the target net normal stresses (of 50, 100 and 150 kPa) was lower for all the 100 kPa suction test as compared to tests at lower suction values. The result is less compression during application of net normal stress for the 100 kPa suction tests in Figure 3.86a-Figure 3.88a and Figure 3.92a. For a given change in net normal stress, the magnitude of compression in the specimen was found to be essentially independent of the soil suction for the range of suction values examined. Figure 3.86b-Figure 3.88b present the influence of soil suction on the change in water content (Δw %) for the soil-geotextile interface specimens during equalization periods under suction of 25 kPa, 50 kPa and 100 kPa. During the application of suction, water continuously flowed out of each specimen (drying path) to reach the target suction value. As expected, it was observed that the percent of water change (Δw %) drained

from the specimen increased as suction increased (e.g., $\Delta w \approx 4$ %, 9 % and 13.5 % for the suction of 25 kPa, 50 kPa and 100 kPa, respectively).

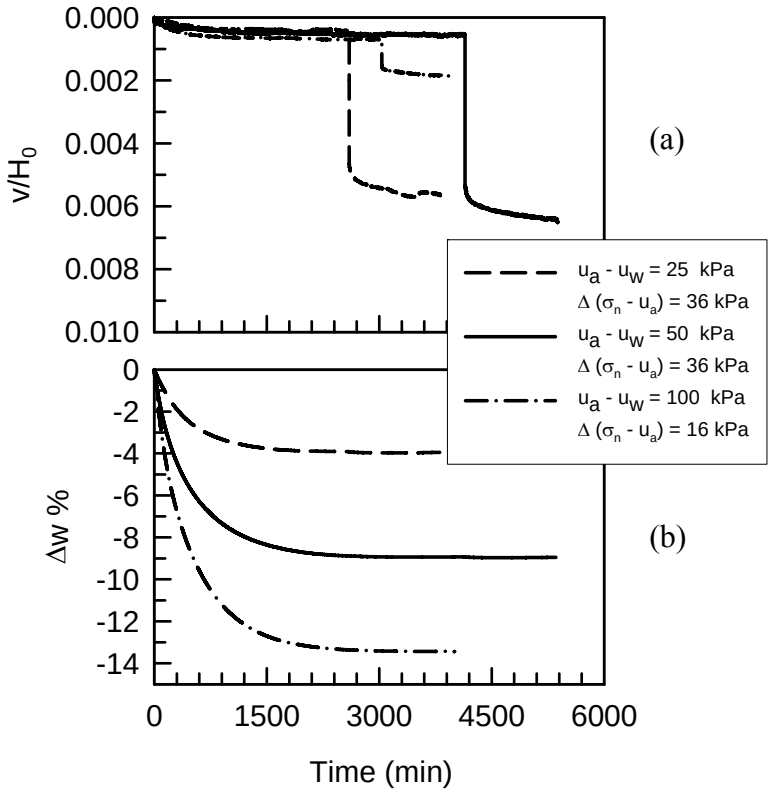

Figure 3.86- Effect of Suction (u_a-u_w) on (a) v/H_0 and (b) Δw % during Equalization of Unsaturated Soil-Geotextile Interface Tests under Net Normal Stress of 50 kPa

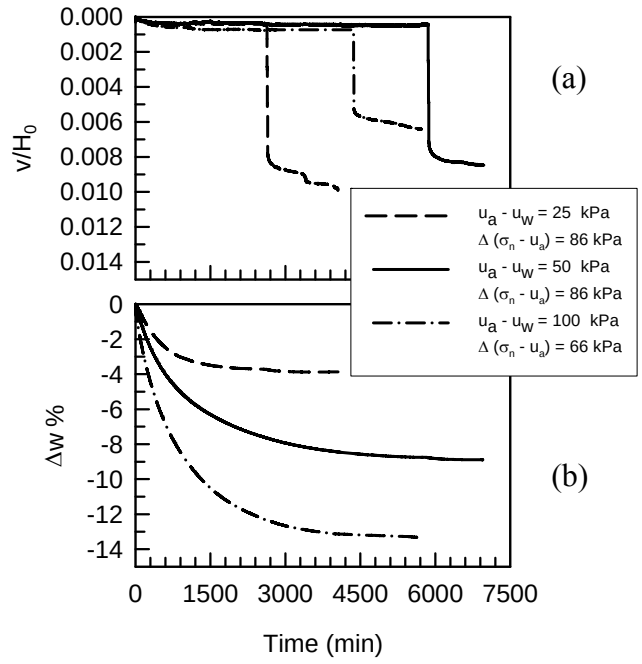

Figure 3.87- Effect of Suction (u_a-u_w) on (a) v/H_0 and (b) Δw % during Equalization of Unsaturated Soil-Geotextile Interface Tests under Net Normal Stress of 100 kPa

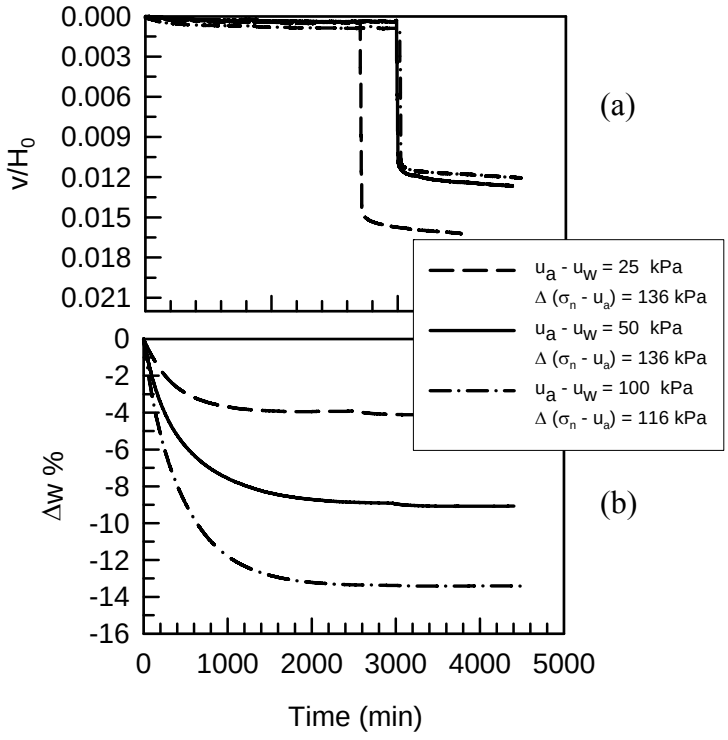

Figure 3.88- Effect of Suction (u_a-u_w) on (a) v/H_0 and (b) Δw % during Equalization of Unsaturated Soil-Geotextile Interface Tests under Net Normal Stress of 150 kPa

On the other hand, results at a given suction (Figure 3.89a-Figure 3.91a and Figure 3.93a) showed that the magnitude of compression increased with increase in net normal stress. As summarized in Figure 3.93a, the change in v/H_0 was on average approximately 0.47%, 0.83 % and 1.37 % under net normal stresses of 50, 100 and 150 kPa, respectively. Variation in water content for soil-geotextile samples during equalization are shown in Figure 3.89b-Figure 3.91b and Figure 3.93b at given suction values, and indicate that the change in water content (Δw %) is essentially the same at a given suction value; in other words, the water controller pulled approximately the same amount of water from all three samples to maintain the required suction. The effect of the net normal stress on the change in moisture content was found to be small (i.e., about 0.1 %) for all suction values examined.

As shown in Figure 3.94, the equilibrium water contents of soil-geotextile DST tests for a given suction agree well with the soil water characteristic curves obtained independently.

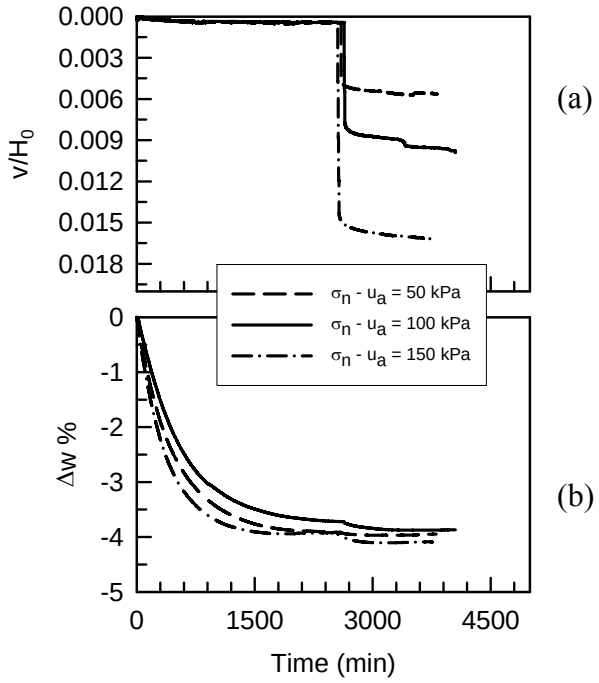

Figure 3.89- Effect of Net Normal Stress (σ_n-u_a) on (a) v/H_0 and (b) Δw % during Equalization of Unsaturated Rough Interface Tests under Suction (u_a-u_w) of 25 kPa

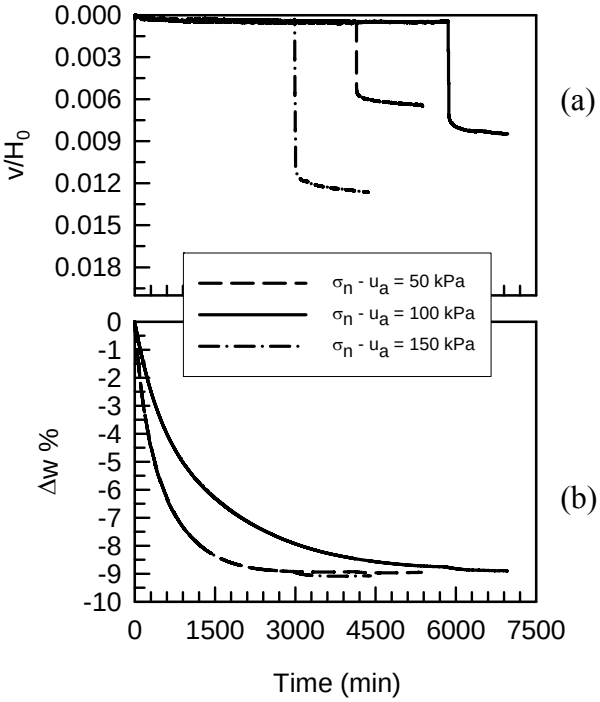

Figure 3.90- Effect of Net Normal Stress (σ_n-u_a) on (a) v/H_0 and (b) Δw % during Equalization of Unsaturated Soil-Geotextile Interface Tests under Suction of 50 kPa

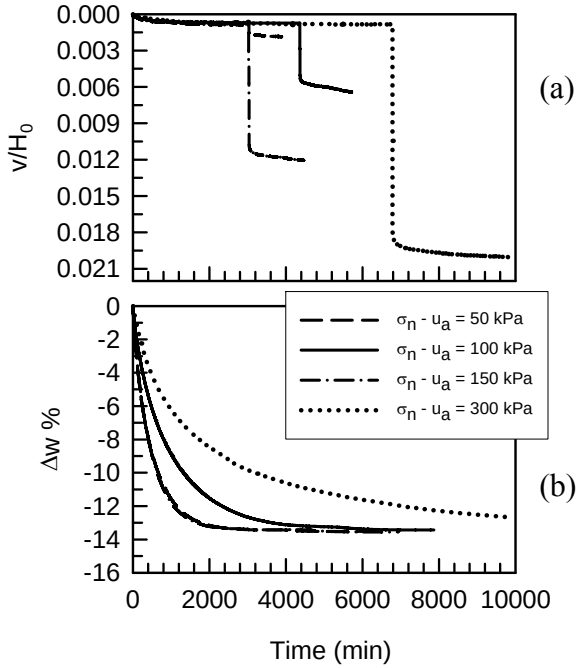

Figure 3.91- Effect of Net Normal Stress (σ_n-u_a) on (a) v/H_0 and (b) Δw % during Equalization of Unsaturated Soil-Geotextile Interface Tests under Suction of 100 kPa

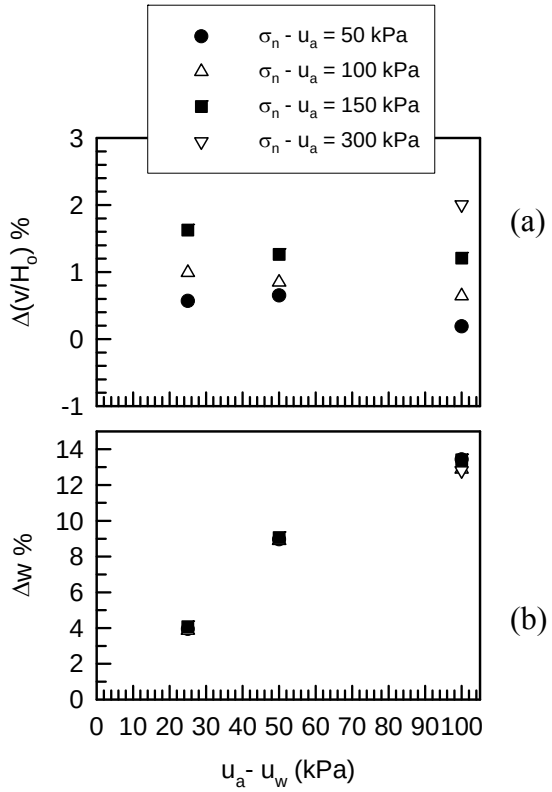

Figure 3.92- Summary of Unsaturated Soil-Geotextile Interface Results at end of Consolidation Stage for all Net Normal Stress Values

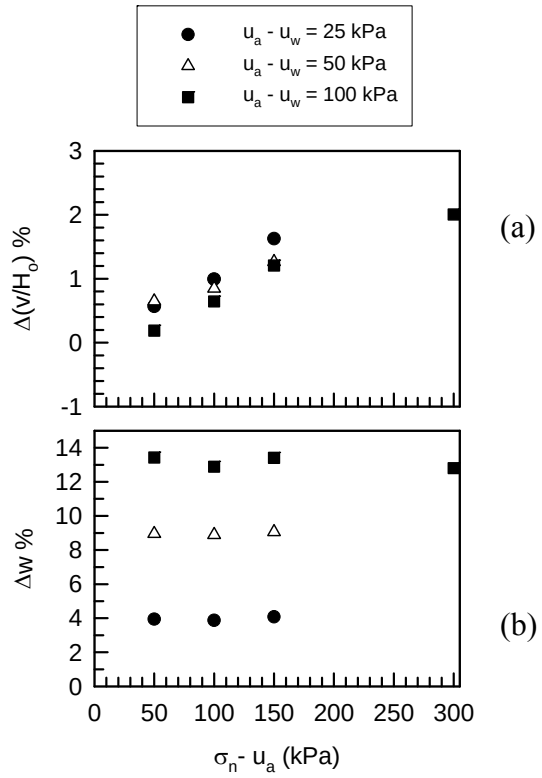

Figure 3.93- Summary of Unsaturated Soil-Geotextile Interface Results at end of Consolidation Stage for all Suction Values

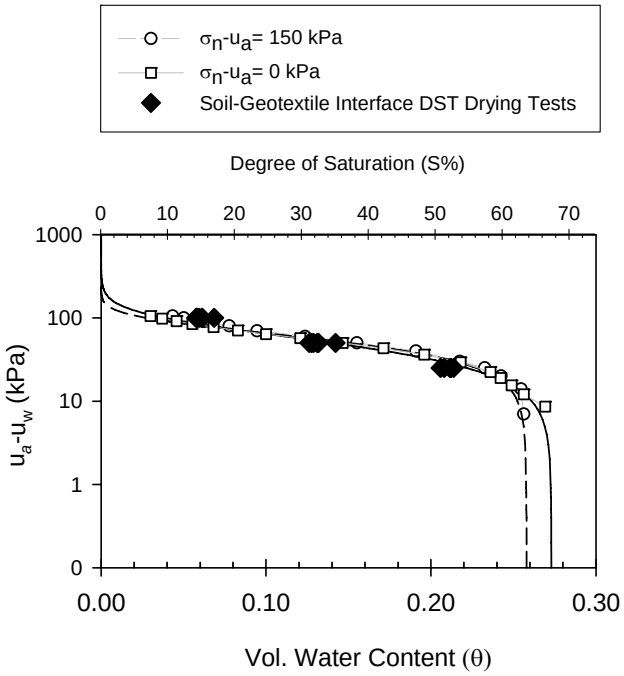

Figure 3.94- Soil Water Characteristic Curves Superimposed with Results from Soil-Geotextile Interface DST of Drying (D) Tests

3.7.1.2 Shearing Phase

The soil-geotextile interface shear test results subjected to net normal stress values of 50, 100 and 150 kPa are shown in Figure 3.95-Figure 3.97. Results presented in these figures show that overall, the unsaturated soil-geotextile interface peak (i.e. maximum) shear strength increased with increase of suction. However, for 100 kPa net normal stress (Figure 3.96) there was a slight drop in peak shear strength from 50 kPa to 100 kPa suction. Also, for 150 kPa net normal stress, there was little difference in the peak strength for 25 kPa and 50 kPa suction. It seems the influence of suction is more pronounced at lower net normal stress. Results also showed that after reaching the interface peak shear strength, soil-geotextiles exhibited a strain softening behavior. In general, the post peak shear strength slightly increased with the increasing normal stress. In general, specimens subjected to a greater suction showed a more pronounced strain softening behavior. It is also observed that the peak shear stress occurred at slightly lower values of horizontal displacement as suction increased. Soil-geotextile interfaces showed a relatively insignificant initial vertical compression before they exhibited dilation during shearing (as shown in Figure 3.95b-Figure 3.97b). Results also indicate that the soil-geotextile specimen stopped dilating following strain softening. The dilation response observed is attributed to the rearrangement of soil grains and sliding of soil particles over each other and over the geotextile surface. Small decreases in water content (i.e. change in Δw %) were detected during shearing of the soil-geotextile interface shear tests, a behavior that was also observed for direct shear test on unsaturated soils and rough steel interfaces and discussed in the previous sections.

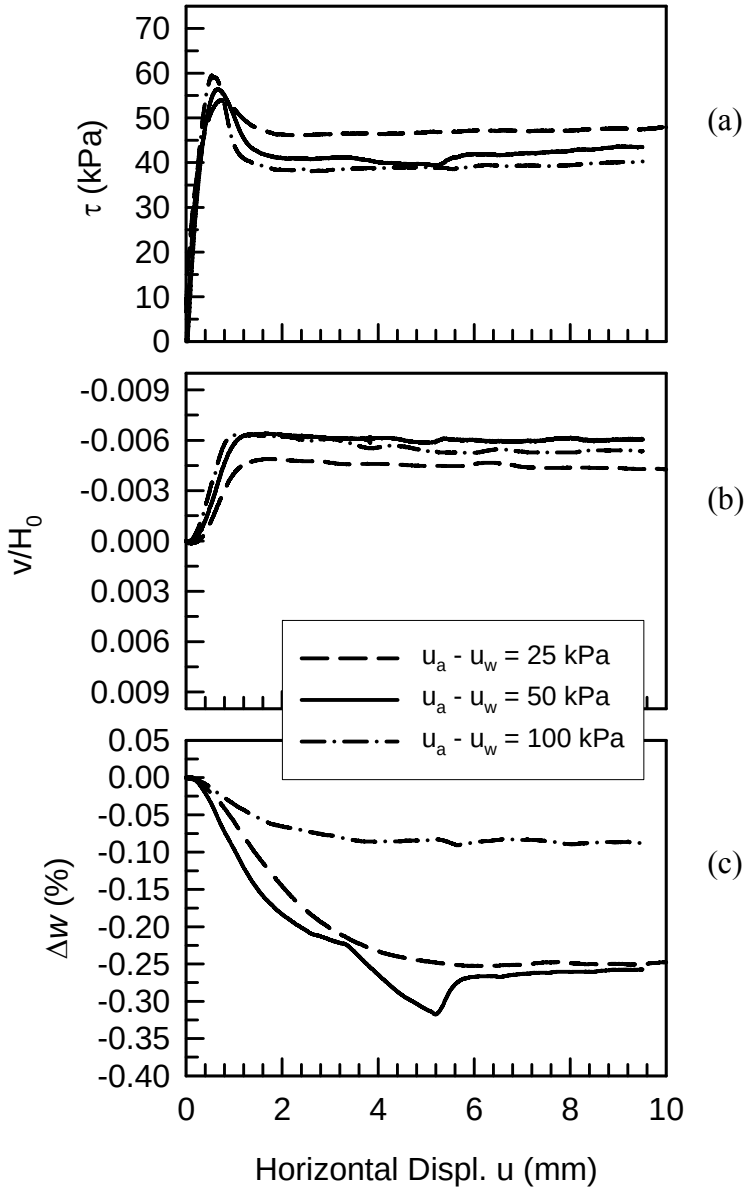

Figure 3.95- Effect of Suction (u_a-u_w) on (a) Shear Stress (τ), (b) v/H_0 and (c) Δw % during Shearing of Unsaturated Soil-Geotextile Interface Tests under Net Normal Stress of 50 kPa

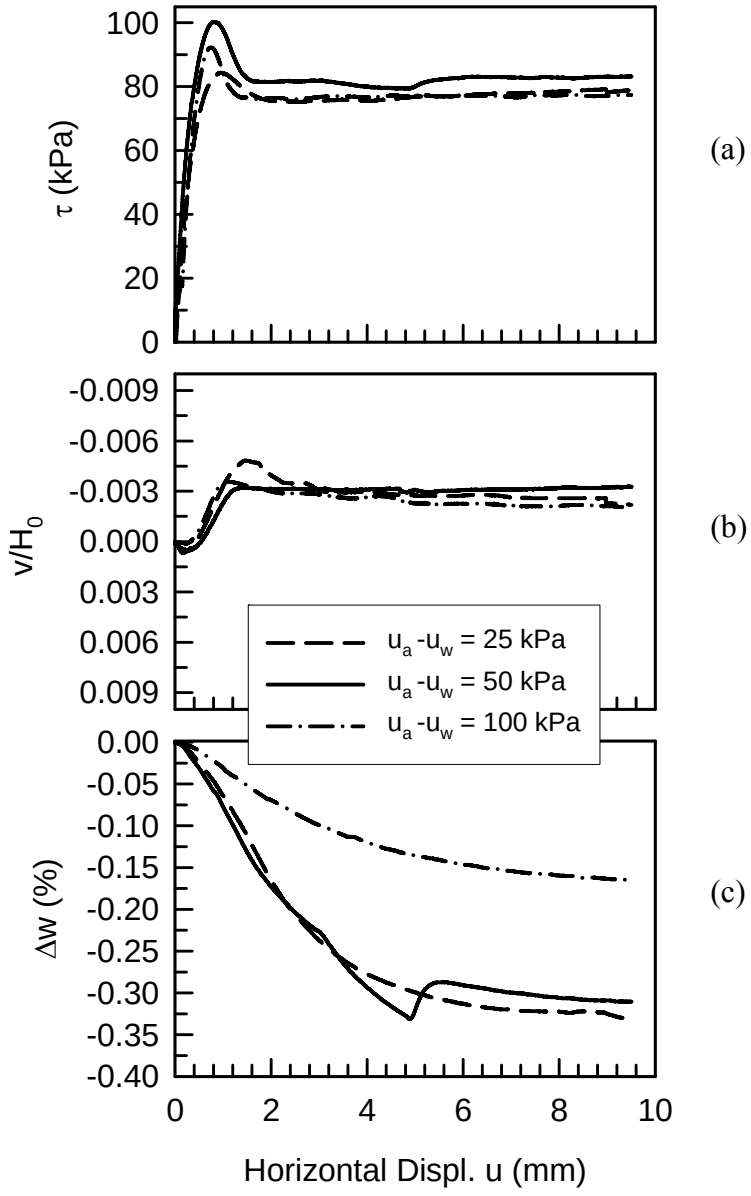

Figure 3.96- Effect of Suction (u_a-u_w) on (a) Shear Stress (τ), (b) v/H_0 and (c) Δw % during Shearing of Unsaturated Soil-Geotextile Interface Tests under Net Normal Stress of 100 kPa

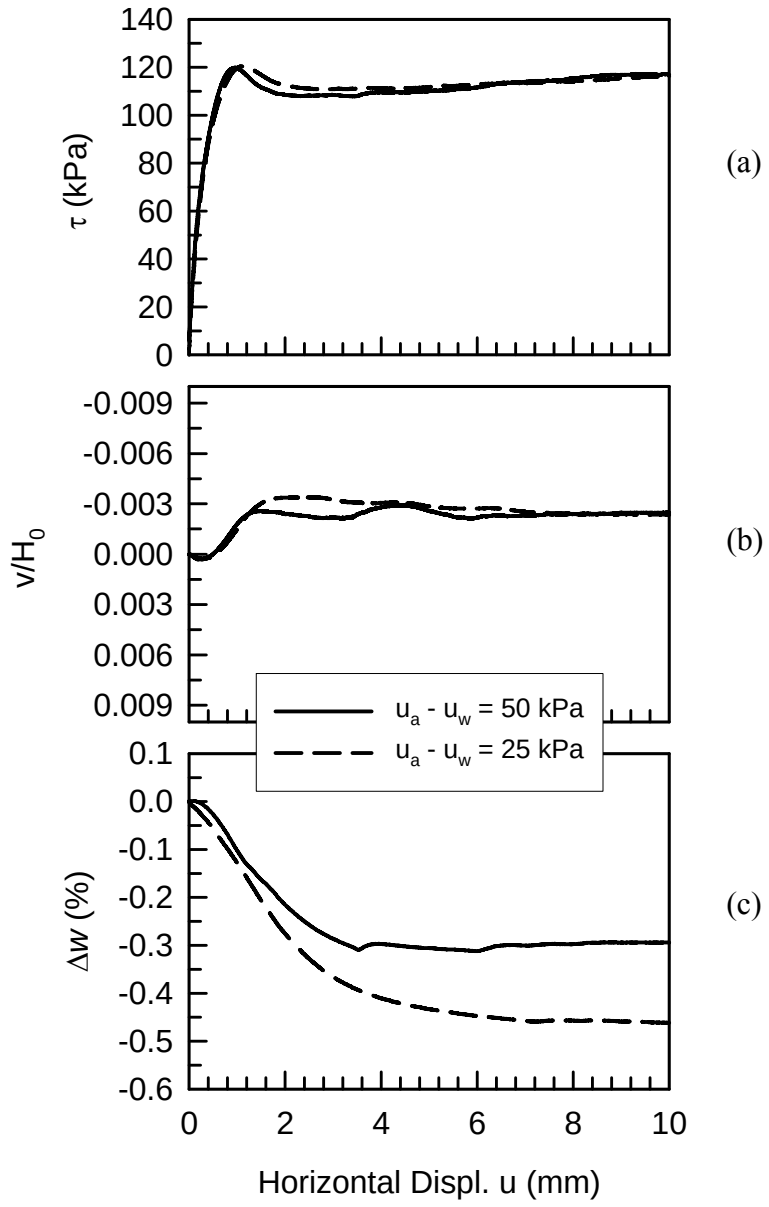

Figure 3.97- Effect of Suction (u_a-u_w) on (a) Shear Stress (τ), (b) v/H_0 and (c) Δw % during Shearing of Unsaturated Soil-Geotextile Interface Tests under Net Normal Stress of 150 kPa

Results of soil-geotextiles interface tests during shearing at given suction values of 25, 50 and 100 kPa are shown in Figure 3.98-Figure 3.100, respectively. These figures show that the peak and post peak shear strength of the soil-geotextile interface increased with increase in net normal stress. During shearing, the soil-geotextile interfaces

compressed initially and then started to dilate as approaching the peak shear stress. The compression magnitude is considered insignificant. The soil-geotextile interfaces ceased to dilate during the post peak shearing. Results also indicate that the amount of dilation decreased as the net normal stress increased (Figure 3.98b-Figure 3.100b). Similarly, and as discussed previously for soils and rough interfaces due to an apparent tendency for increasing pore water pressure, the water volume controller pulled water from the samples to maintain constant suction.

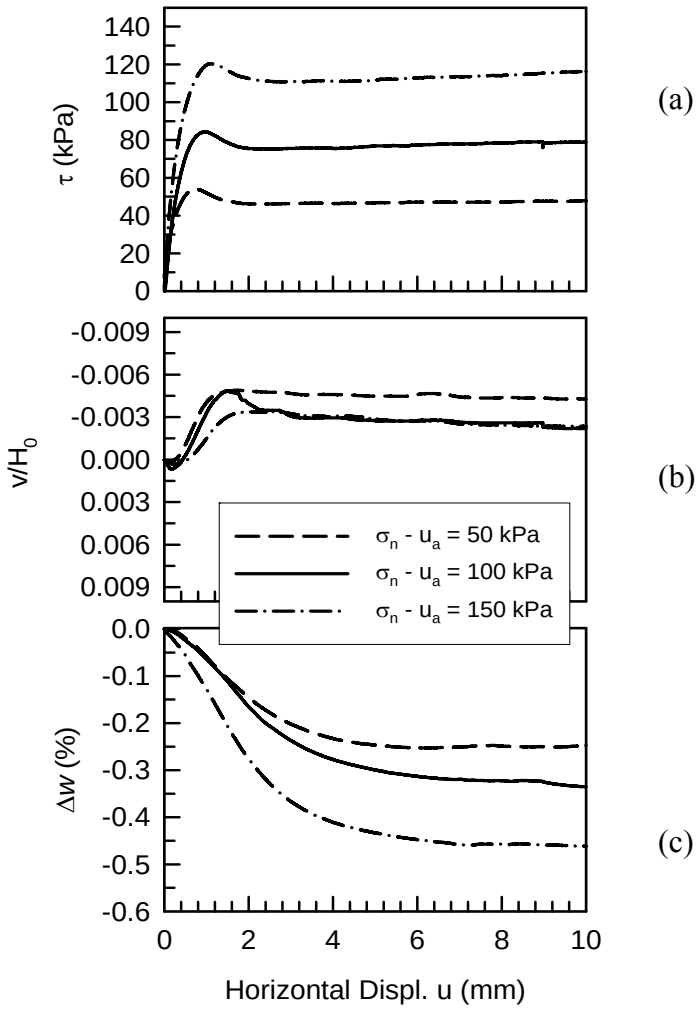

Figure 3.98- Effect of Net Normal Stress (σ_n-u_a) on (a) Shear Stress (τ), (b) v/H_0 and (c) Δw % during Shearing of Unsaturated Soil-Geotextile Interface Tests under Suction of 25 kPa

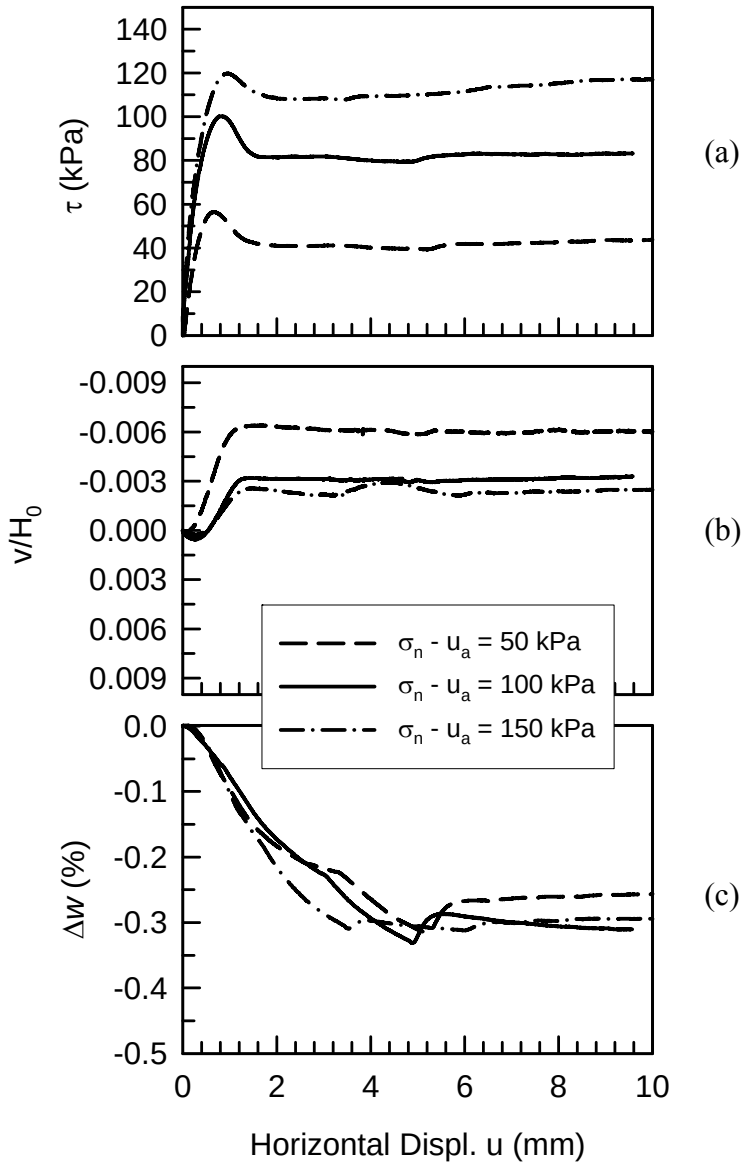

Figure 3.99- Effect of Net Normal Stress (σ_n-u_a) on (a) Shear Stress (τ), (b) v/H_0 and (c) Δw % during Shearing of Unsaturated Soil-Geotextile Interface Tests under Suction of 50 kPa

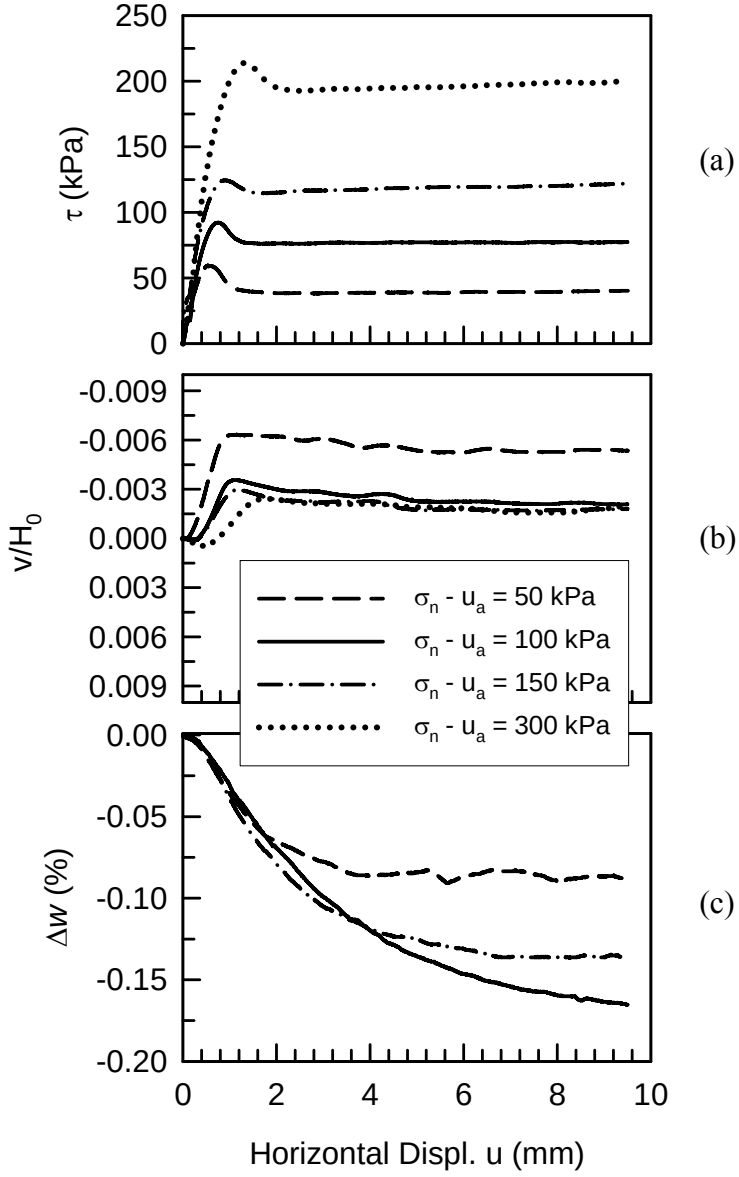

Figure 3.100- Effect of Net Normal Stress (σ_n-u_a) on (a) Shear Stress (τ), (b) v/H_0 and (c) Δw % during Shearing of Unsaturated Soil-Geotextile Interface Tests under Suction of 100 kPa

3.8 MODELING OF UNSATURATED SOILS AND INTERFACES

3.8.1 Modeling due to Drying without Hysteresis

3.8.1.1 Extended Mohr Coulomb Criteria of Unsaturated Soils and Interfaces (Drying)

Numerous models (e.g. Fredlund and Rahardjo 1993, Vanappali et al. 1996), discussed in previous sections (Section 3.2.1.2) have been reported in the literature to predict the shear strength of unsaturated soils. The state of stress for the unsaturated soil can be described by Equation 3.4 ($\tau = c' + (\sigma_n - u_a)\tan\phi' + (u_a - u_w)\tan\phi^b$), using the two stress variables (σ_n-u_a, and u_a-u_w).

Following the same reasoning behind Equation (3.4) Miller and Hamid (2007) proposed Equation 3.8 ($\tau_f = c'_a + (\sigma_n - u_a)_f \tan\delta' + (u_a - u_w)_f \tan\delta^b$) for unsaturated steel interface shear strength, as shown on the extended Mohr-Coulomb failure envelope in Figure 3.101. This equation is used in attempts to model the unsaturated interfaces (rough/smooth steel and geotextiles interfaces); corresponding unsaturated soils and interface shear strength parameters are determined and presented as follows.

Plots of shear stress (τ) versus net normal stress (σ_n-u_a) corresponding to failure, for soil, rough and geotextile interfaces are shown in Figure 3.102a, b, and c, respectively. The peak shear stress was used as the shear stress at failure. The lines plotted through the data points in Figure 3.102 form Mohr-Coulomb failure envelopes for the unsaturated soil and interfaces that represent the frontal plane of extended Mohr-Coulomb failure envelope graph shown in Figure 3.101. Slopes and intercepts of these envelopes are presented in Table 3.2 and Table 3.3 for soil and interfaces, respectively. For soil, slope of the failure envelope is denoted by ϕ' and intercept is denoted by c. For interfaces, the

slope of the failure envelope on τ versus (σ_n-u_a) plane is denoted by δ', whereas, the intercept of this failure envelope yields the values of interface adhesion (c_a).

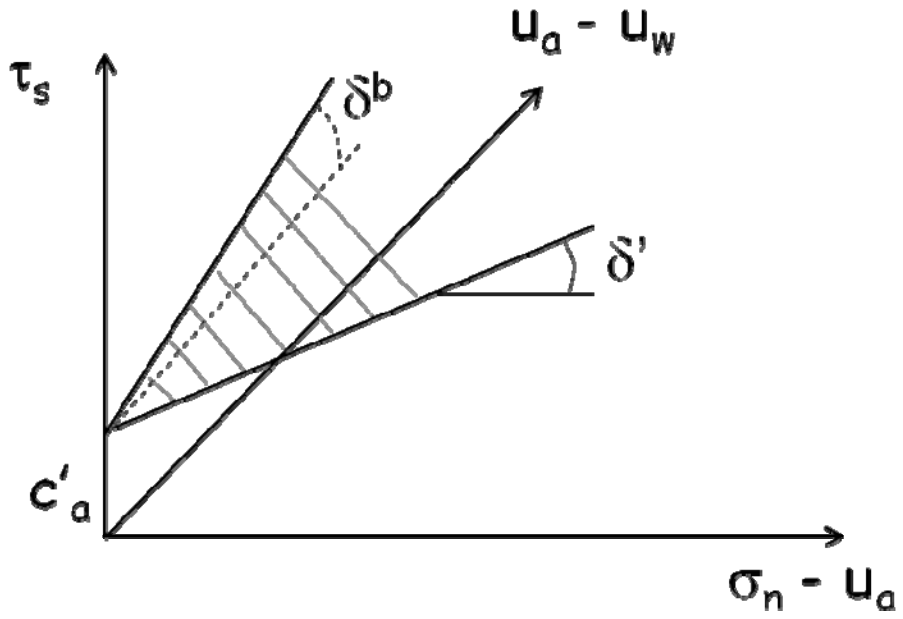

Figure 3.101- Interface Extended Mohr-Coulomb Failure Envelope

In Figure 3.103a, b, c and d results are plotted in the (u_a-u_w)-shear stress plane (i.e. zero net normal stress plane). Each curve in Figure 3.103a, b, and c corresponds to a different value of σ_n-u_a. For soil, the slope of the failure envelope in τ- (u_a-u_w) plane yields angle of internal friction with respect to suction and is denoted by ϕ^b and intercept of the plot indicates cohesion with respect to suction and is denoted by c''. For interfaces the slope of the failure envelope on τ versus (u_a-u_w) plane is denoted by δ^b (i.e. angle of friction between soil and counterface), whereas, the intercept of this failure envelope yields adhesion of interface (c_a''). The values of slopes and intercepts of these plots are summarized in Table 3.4 and Table 3.5.

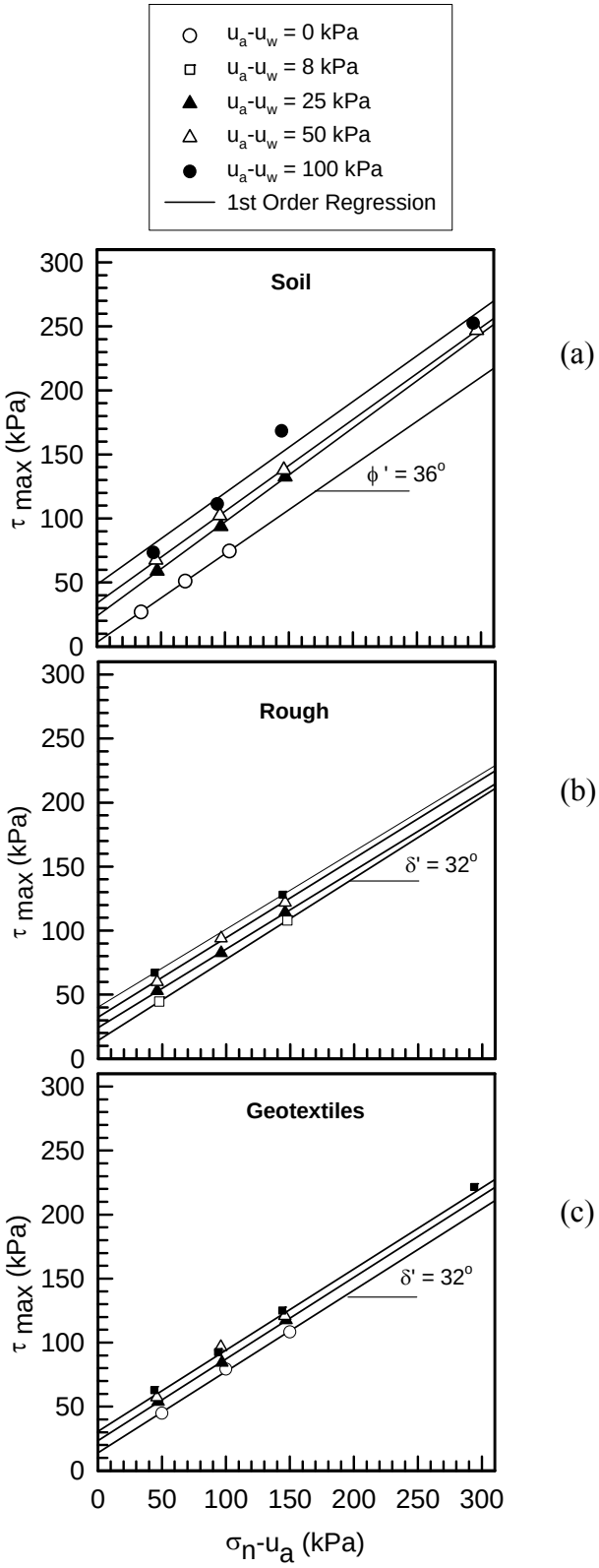

Figure 3.102- Failure Envelope Projections of Unsaturated (a) Soils, (b) Rough, (c) Geotextile Interface Direct Shear Tests on ($\sigma_n - u_a$)-Shear Stress Plane

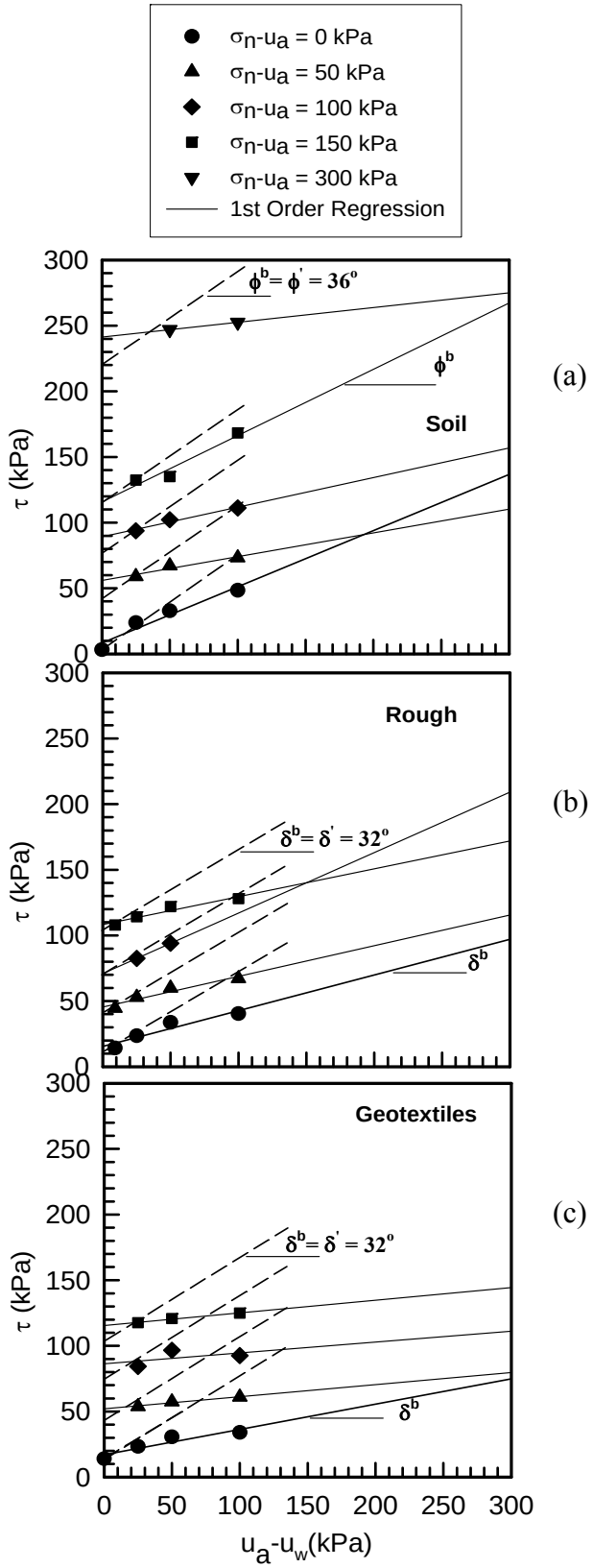

Figure 3.103- Failure Envelope Projections of Unsaturated (a) Soils, (b) Rough, (c) Geotextile Interface Direct Shear Tests on ($u_a - u_w$)-Shear Stress Plane

Table 3.2- Unsaturated Shear Strength Parameters (c, ϕ') for Different Suction Values

Material	Suction (u_a-u_w) kPa	c (kPa)	ϕ' (deg.)	r^2
Soil	0	3.23	35.0	0.999
	25	23.8	36.3	0.999
	50	32.8	35.7	0.999
	100	48.4	35.5	0.979

Table 3.3- Unsaturated Interface Shear Strength Parameters (c_a, δ') for Different Suction Values

Interface Type	Suction (u_a-u_w) kPa	c_a (kPa)	δ' (deg.)	r^2
Rough	9	14.3	32.4	1.000
	25	24.2	31.5	1.000
	50	32.5	31.8	0.997
	100	40.3	31.4	1.000
Geotextiles	0	14.0	32.4	0.999
	25	23.4	32.5	0.999
	50	30.7	32.4	0.981
	100	34.8	32.0	1.000
Smooth	25	--	--	--
	50	32.7	14.4	1.000

Table 3.4- Unsaturated Shear Strength Parameters (c″, ϕ^b) for Different Net Normal Stress Values

Material	Net Normal Stress (σ_n-u_a) kPa	c'' (kPa)	ϕ^b (deg.)	r^2
Soil	50	56.15	10.2	0.911
	100	89.2	12.7	0.972
	150	115.8	26.6	0.929
	300	241.4	6.4	1.000

Table 3.5- Unsaturated Interface Shear Strength Parameters (c''_a, δ') for Different Net Normal Stress Values

Interface Type	Net Normal Stress (σ_n-u_a) kPa	c''_a (kPa)	δ^b (deg.)	r^2
Rough	50	45.4	13.1	0.921
	100	71.0	24.7	1.000
	150	108.3	12.0	0.926
Geotextiles	50	52.3	5.3	0.968
	100	86.4	4.7	0.253
	150	115.5	5.5	0.988

As observed in this study (Figure 3.103), and as reported in numerous studies in the literature (e.g., Gan et al. 1988, Escario and Juca 1989, Fredlund and Rahardjo 1993, and Vanapalli et al. 1996), the shear strength and the angle ϕ^b vary nonlinearly with suction. Therefore, models are proposed to predict the shear strength variation with suction on the drying path and wetting path as shown in Sections 3.8.1.2 and 3.8.2.2, respectively.

3.8.1.2 Model of Shear Strength of Unsaturated Interfaces using the SWCC

Extensive number of research publications have been found to study the shear strength of unsaturated soils, specifically to predict the shear strength either by semi-empirical equations and curve fitting techniques (e.g., Abramento and Carvalho 1989, Rassam and Williams 1999, Rassam and Cook 2002, Lee et al. 2005, Vilar 2006) or by relating to the SWCC (e.g., Vanapalli et al. 1996, Oberg and Sallfours 1997, Bao et al. 1998, Khalili and Khabbaz 1998, Tekinsoy et al. 2004). While these studies were found successful in predicting shear strength of particular types of soils, there is no single prediction that is suitable for all soils (Garven and Vanapalli, 2006). Further studies are needed to provide more reliable techniques and models for prediction of shear strengths of soils. In this study, some existing techniques (i.e. model equations) for prediction and

estimation of unsaturated soil shear strength were explored, used and also applied to unsaturated interface shear strengths, as shown below. In addition, new model equations are proposed for the soil and interfaces used in this study.

Shear strength parameters in Equations 3.4 and 3.5 have been obtained using both direct shear and triaxial shear testing equipment while controlling matric suction. Following the same reasoning, Equation 3.6 (Hamid and Miller 2009) that relates to suction from SWCC is used for modeling unsaturated interfaces as follows:

$$\tau_f = c'_a + (\sigma_n - u_a)_f \tan\delta' + (u_a - u_w)_f \tan\delta' \left(\frac{\theta - \theta_r}{\theta_s - \theta_r} \right) \qquad \textbf{(3.10)}$$

This section explores the use of Equations (2.4) and (3.10) to model the shear strength from a series of unsaturated soil direct shear tests and interface direct shear tests (e.g. steel plates and geotextiles) conducted while controlling matric suction. In addition, the soil water characteristic curve results obtained in this study are used in this formulation to predict the unsaturated interface shear strength. The proposed equation (2.4) by Fredlund and Xing (1994) is used to model the resulting single (primary drying) SWCC behavior.

Equation (3.4) is used in conjunction with Equations (3.5) and (3.10) to model the influence of matric suction on shear strength, where $\tan\delta^b = \tan\delta'[(\theta-\theta_r)/(\theta_s-\theta_r)]$.

Other models have also been based on the formulation by Garven and Vanapalli (2006) and Guan et al. (2010) presented by Equation (3.11) and (3.12), respectively.

$$\tau_f = c'_a + (\sigma_n - u_a)_f \tan\delta' + (u_a - u_w)_f \tan\delta' \left(\frac{\theta}{\theta_s} \right)^k \qquad \textbf{(3.11)}$$

where, $k = -0.0016 I_p^2 + 0.0975 I_p + 1$, I_p = plasticity index of soil.

$$\left.\begin{aligned}
\tau_f &= c'_a + (\sigma_n - u_a)_f \tan\delta' + (u_a - u_w)_f \tan\delta' \left(\frac{\theta - \theta_r}{\theta_s - \theta_r}\right), \\
&\qquad\qquad \text{if } (u_a - u_w) < (u_a - u_w)_b \\
\tau_f &= c'_a + \left[(\sigma_n - u_a) + (u_a - u_w)_b\right]\tan\delta' + \left[(u_a - u_w) - (u_a - u_w)_b\right](b)\left(\frac{\theta}{\theta_s}\right)^k \tan\delta', \\
&\qquad\qquad \text{if } (u_a - u_w) \geq (u_a - u_w)_b
\end{aligned}\right\} \quad \textbf{(3.12)}$$

where, $(u_a - u_w)_b$ = air entry value (AEV), $k = \left[\log(u_a - u_w) - \log(u_a - u_w)_b\right]^y$.

For which, y and b parameters are different for drying and wetting tests defined as follows:

$$y_d = 0.502\ln\left(I_p + 2.7\right) - 0.387,$$

$$b_d = -0.245\left\{\ln\left[n_d\left(I_p + 4.4\right)\right]\right\}^2 + 2.114\left\{\ln\left[n_d\left(I_p + 4.4\right)\right]\right\} - 3.522,$$

$$y_w = 3.55 y_d - 3.00,$$

$$b_w = 0.542 b_d \left(\frac{n_d}{n_w}\right) + 0.389,$$

where, n_d and n_w are the fitting parameters for drying and wetting from SWCC using Fredlund and Xing (1994) fitting equation, respectively.

Equation (3.11) relates the shear strength to SWCC and plasticity index of soil, and is based on fitting regression analysis (through the *k* parameter) from experimental data of twenty soils (Garven and Vanapalli 2006). Equation (3.12) also relates to SWCC but with additional parameters *k*, *y* and *b* that are obtained based on some fitting regression analysis for the soil tested by Guan et al. (2010), and are different for drying and wetting tests.

The models by Guan et al. (2010), Vanapalli et al. (1996) and Garven and Vanappali (2006) (i.e. Equations 3.12, 3.5/3.10 and 3.11 respectively) under predicted the results for soil and rough interface obtained in this study (Figure 3.104). However, the equation (Equation 3.10) based on the model by Vanapalli et al. (1996) (Equation 3.8) predicted fairly well the shear strength results (along the drying curve) with suction for unsaturated geotextiles, as shown in Figure 3.104.

Therefore, a factor (exponent *k*), which is also related to the SWCC, was incorporated into Equation (3.10) as shown in Equation 3.13. Unlike other models, such as Vanapalli et al. 1996, Garven and Vanappalli 2006, and Guan et al. 2010, this model relates to the SWCC without any additional empirically determined parameters. The resulting model equation (Equation 3.13) seems to better represent the shear strength results with suction for the unsaturated soils, rough and geotextile interfaces used in this study, as shown in Figure 3.105.

$$\tau_f = c'_a + (\sigma_n - u_a)_f \tan\delta' + (u_a - u_w)_f \tan\delta' \left(\frac{\theta - \theta_r}{\theta_s - \theta_r} \right)^k \qquad \textbf{(3.13)}$$

where, $k = 1/n$, and "*n*" is the fit parameter from SWCC (Equation 2.4). Noteworthy to mention is that parameter "*n*" is related to the slope of the inflection point (near the AEV value), and generally defines the rate of suction changes due to changes in water content. Parameter "*n*" is influenced by the soil type and the pore size of the sample.

In general, results of the tests shown in Figure 3.105 exhibit a nonlinear relationship between the matric suction and shear strength. The nonlinear representation of the failure envelopes, with respect to suction, proposed by Equation (3.13) seem to better fit the data for the unsaturated soils, rough and geotextile interface tests.

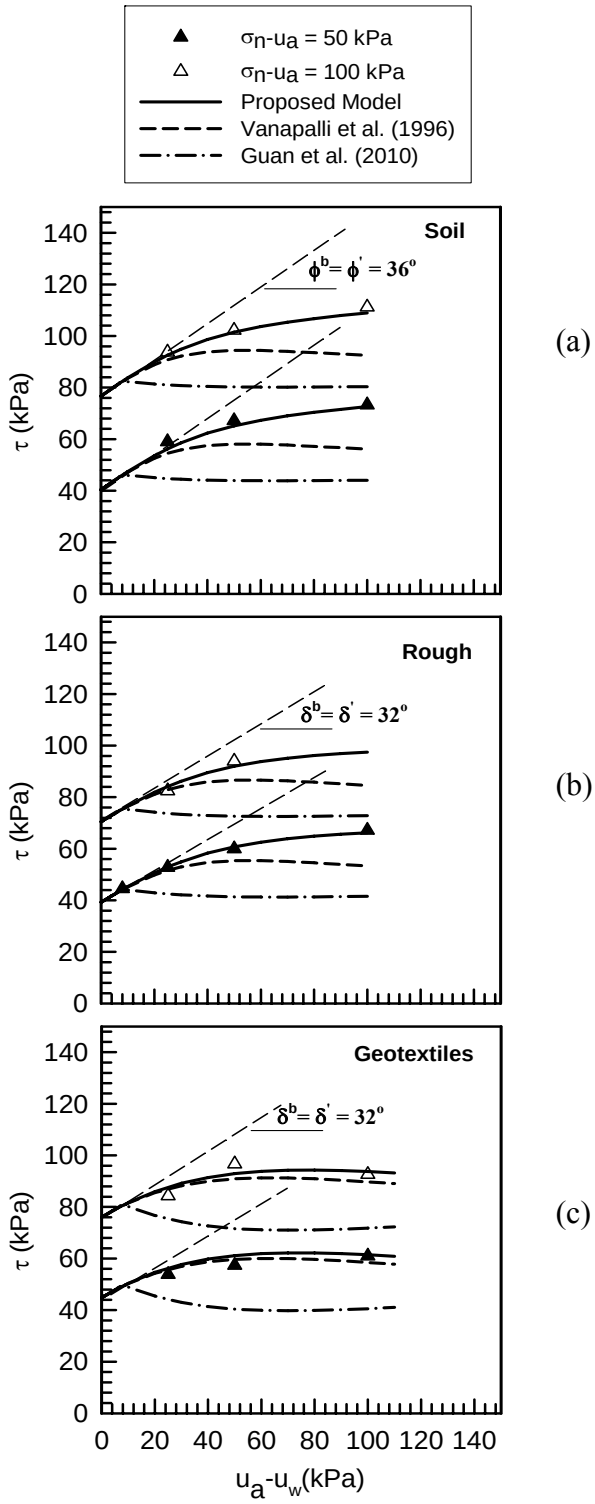

Figure 3.104- Peak Failure Envelope Projected in the Matric Suction Shear-Stress Plane Modeled using Various Equations for Unsaturated (a) Soils, (b) Rough and (c) Geotextiles Interface Direct Shear Tests

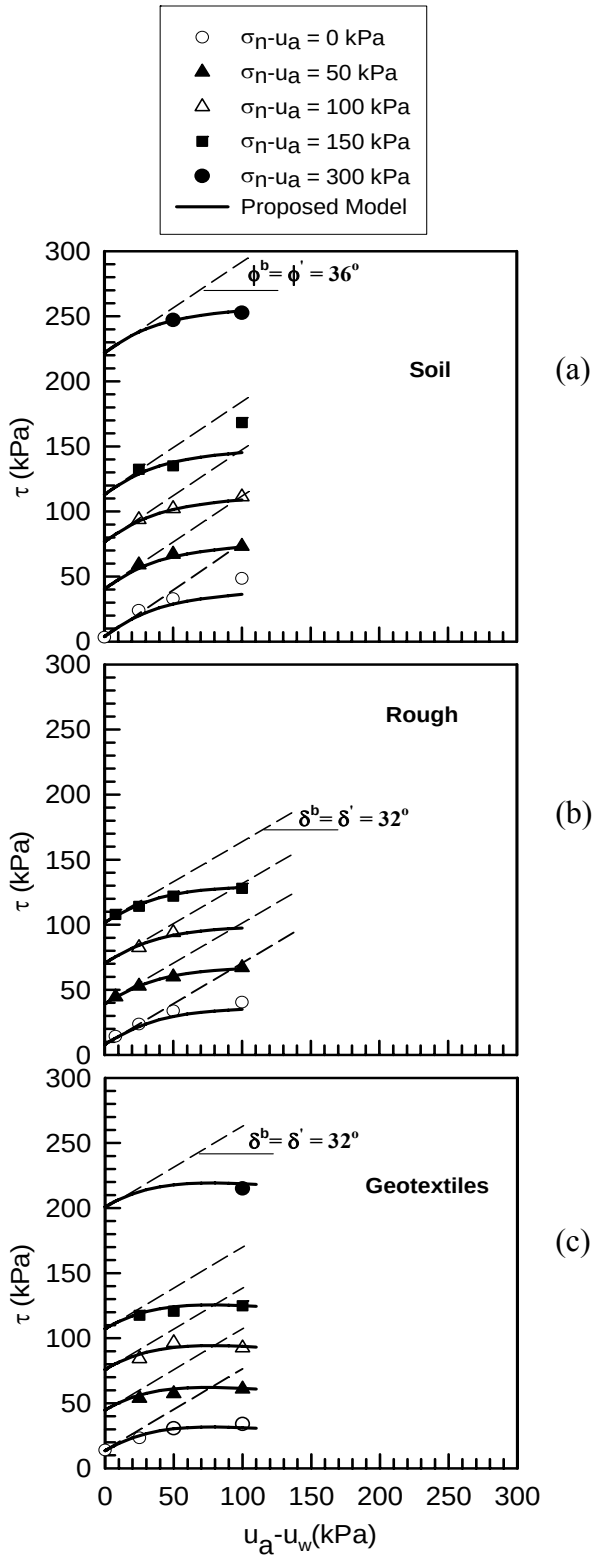

Figure 3.105- Peak Failure Envelope Projected in the Matric Suction Shear-Stress Plane Modeled using SWCC (Proposed Equation 3.13) for Unsaturated (a) Soils, (b) Rough and (c) Geotextiles Interface Direct Shear Tests

The proposed model (Equation 3.13) was also validated by predicting experimental results from the literature such as results of unsaturated soil tests from Escario and Juca (1989) and Vanapalli et al. (1996) as shown in Figure 3.106 and Figure 3.107, respectively; These figures indicate that the model agreed well with the experimental results and seems to better capture the shear strength with suction than the Vanapalli et al. (1996) model (Equation 3.5b). Note, Equation (3.5b) was used for the model by Vanapalli et al. 1996, which does not include the fitting parameter "*k*" (Equation 3.5a) ; a parameter obtained to fit the experimental results.

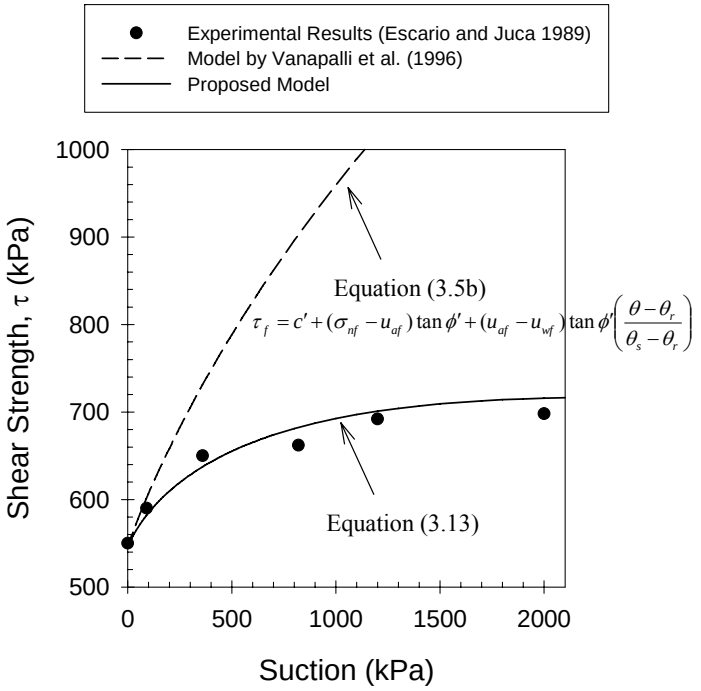

Figure 3.106- Comparison between the Predicted Shear Strength from the Proposed Model and the Model by Vanapalli et al. (1996) using the Experimental Results from Escario and Juca (1989)

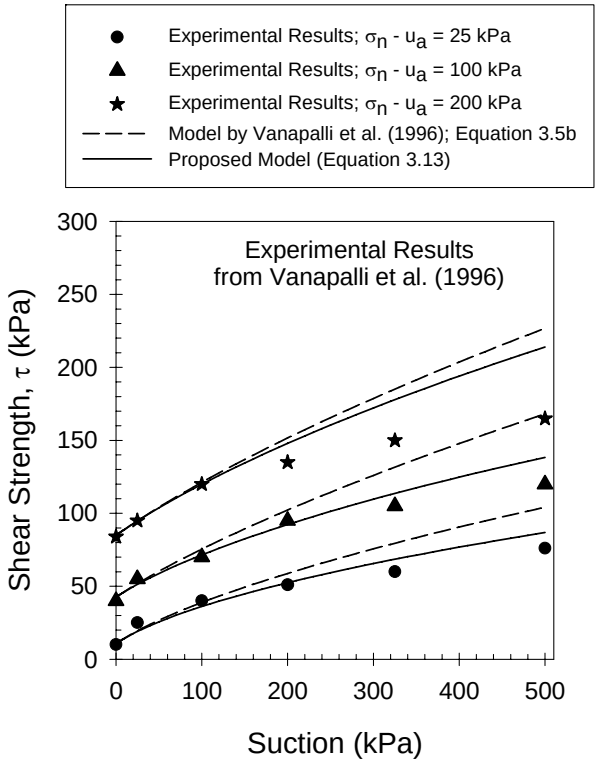

Figure 3.107- Comparison between the Predicted Shear Strength from the Proposed Model and the Model by Vanapalli et al. (1996) using the Experimental Results from Vanapalli et al. (1996)

3.8.2 Modeling of Shear Strength due to Hysteresis (Drying/Wetting)

3.8.2.1 Extended Mohr Coulomb Criteria of Unsaturated Soils and Rough Interfaces (Wetting after Drying)

In this section, failure envelopes for unsaturated soils and rough interfaces from hysteresis (wetting after drying) tests are presented. Figure 3.108 shows the Mohr-Coulomb failure envelopes for unsaturated soil and rough interface test results in the net normal stress (σ_n-u_a) plane that represents the frontal plane of extended Mohr-Coulomb failure envelope graph shown in Figure 3.101. Slopes and intercepts of these envelopes due to wetting after drying are presented in Table 3.6 and Table 3.7 for soil and rough interfaces, respectively. Since, these tests are for wetting, the slope of the failure envelope of soils is denoted by ϕ_w' and intercept is denoted by c_w. Similarly for

interfaces, the slope of the failure envelope on τ versus (σ_n-u_a) plane is denoted by δ_w', whereas, the intercept of this failure envelope yields the values of interface adhesion (c_{aw}).

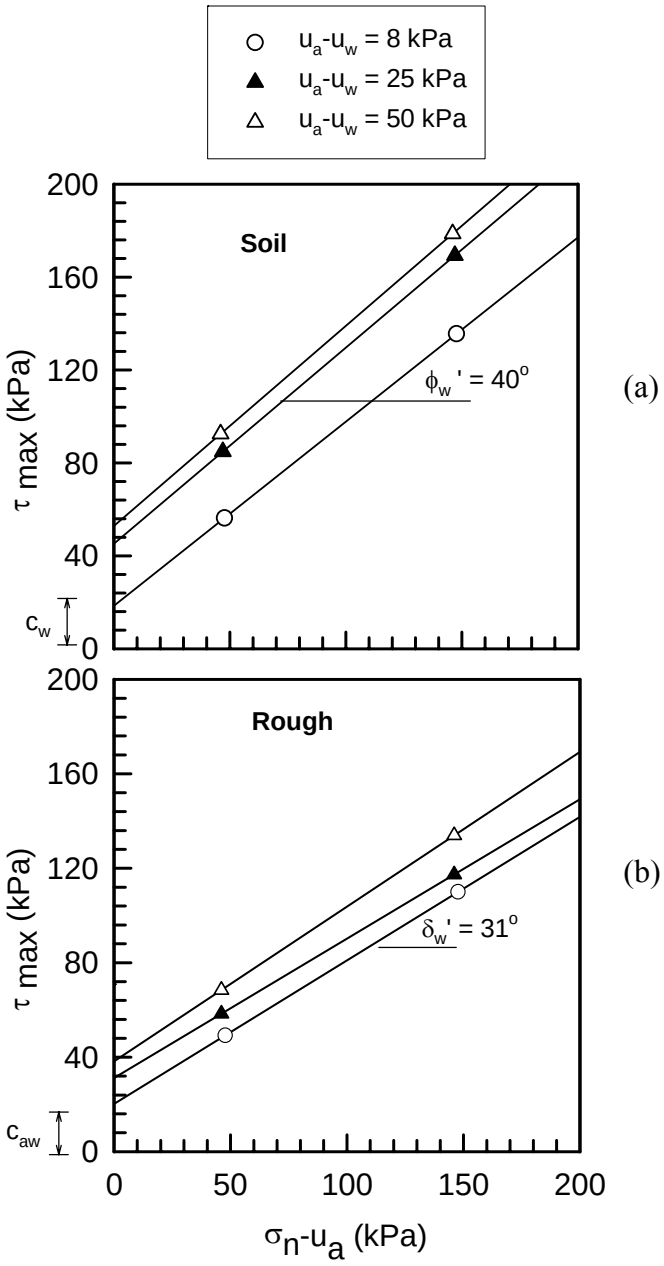

Figure 3.108- Failure Envelope Projections of Unsaturated (a) Soils, and (b) Rough Direct Shear for Hysteresis (Wetting after drying) Tests on ($\sigma_n - u_a$)-Shear Stress Plane

In Figure 3.109 results are plotted in the (u_a-u_w)-shear stress plane (i.e. zero net normal stress plane). Each curve in Figure 3.109 corresponds to a different value of σ_n-u_a. For soil, the slope of the failure envelope in τ- (u_a-u_w) plane yields angle of internal friction with respect to suction and is denoted by ϕ_w^b and intercept of the plot indicates cohesion with respect to suction and is denoted by $c_w^{"}$. For interfaces the slope of the failure envelope on τ versus (u_a-u_w) plane is denoted by δ_w^b (i.e., interface friction angle for wetting tests), whereas, the intercept of this failure envelope yields adhesion of interface ($c_{aw}^{"}$). The values of slopes and intercepts of these plots are summarized in Table 3.8 and Table 3.9.

Table 3.6- Unsaturated Shear Strength Parameters (c_w, ϕ_w') due to Hysteresis for Different Suction Values

Material	Suction (u_a-u_w) kPa	c_w (kPa)	ϕ_w' (deg.)
Soil	8	18.4	39
	25	45.2	40
	50	52.9	40

Table 3.7- Unsaturated Interface Shear Strength Parameters (c_{aw}, δ_w') due to Hysteresis for Different Suction Values

Interface Type	Suction (u_a-u_w) kPa	c_{aw} (kPa)	δ_w' (deg.)
Rough	8	20.2	31.3
	25	30.7	31.2
	50	40.5	31.0

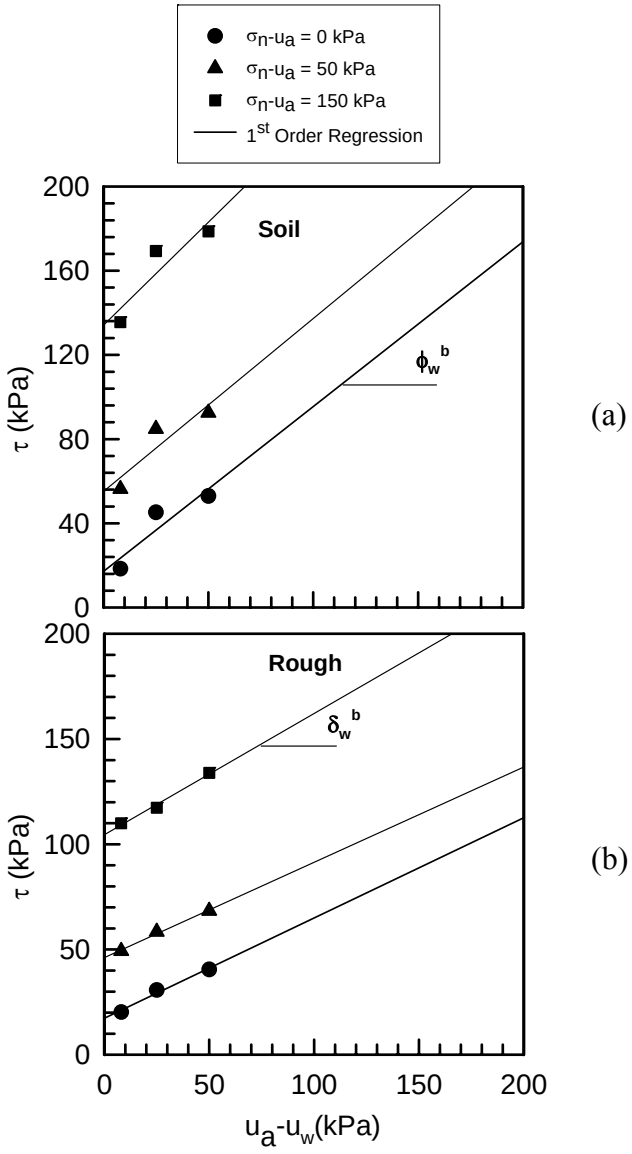

Figure 3.109- Failure Envelope Projections of Unsaturated (a) Soils, and (b) Rough Direct Shear for Hysteresis (Wetting after drying) Tests on ($u_a - u_w$)-Shear Stress Plane

Comparison of failure envelopes between drying and wetting after drying (hysteresis) test results are shown in Figure 3.110. It is observed that for both soils and rough interfaces wetting test results exhibited higher failure envelopes (i.e. higher shear strength) compared to drying test results. In addition, hysteresis influence seems to be more pronounced on unsaturated soils than rough interfaces; the difference between wetting and drying is higher for soils than that of rough interfaces. This higher influence

on soils is believed to be related to the higher difference in water content ($\Delta\theta_{W\text{-}D}$ %) between wetting and drying of soil tests as compared to that for rough interfaces, as shown in Figure 3.112. Results in Figure 3.110 and Figure 3.111 showed that during wetting the friction angle with respect to net normal stress (ϕ_w') of soils was higher than that of drying (ϕ'); however hysteresis did not seem to influence the interface friction angle (δ') of rough interface tests. On the other hand, both the soil friction angles (ϕ_w^b) and the rough interface friction angle (δ_w^b) with respect to suction during wetting seem to be higher than that of the drying tests.

Table 3.8- Unsaturated Shear Strength Parameters (c_w'', $\phi_w{}^b$) due to Hysteresis for Different Net Normal Stress Values

Material	Net Normal Stress (σ_n-u_a) kPa	c_w'' (kPa)	$\phi_w{}^b$ (deg.)	r^2
Soil	50	55.2	39.4	0.825
	150	134.1	44.4	0.830

Table 3.9- Unsaturated Interface Shear Strength Parameters (c''_{aw}, δ_w') due to Hysteresis for Different Net Normal Stress Values

Interface Type	Net Normal Stress (σ_n-u_a) kPa	c''_{aw} (kPa)	$\delta_w{}^b$ (deg.)	r^2
Rough	50	46.1	24.3	0.993
	150	106.7	24.2	0.998

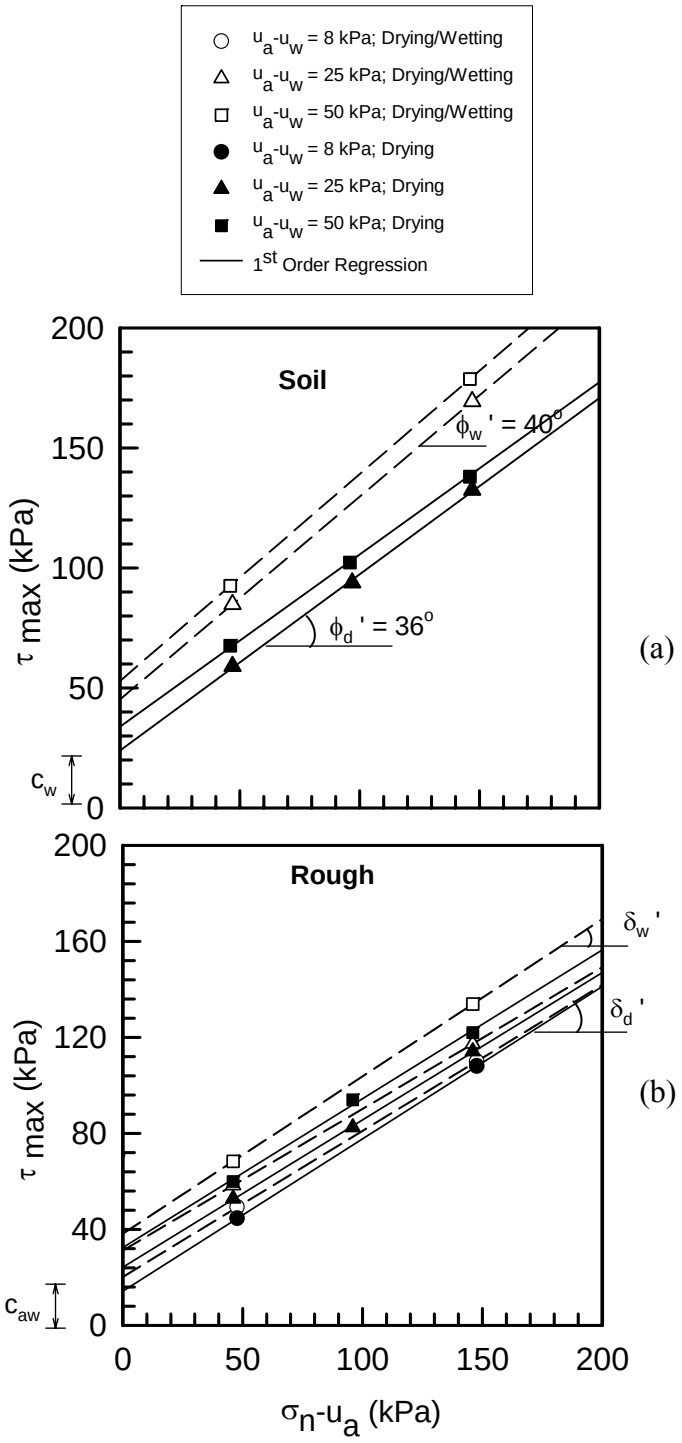

Figure 3.110- Failure Envelope Projections of Unsaturated (a) Soils, and (b) Rough Direct Shear for both Drying and Hysteresis (Wetting after drying) Tests on ($\sigma_n - u_a$)-Shear Stress Plane

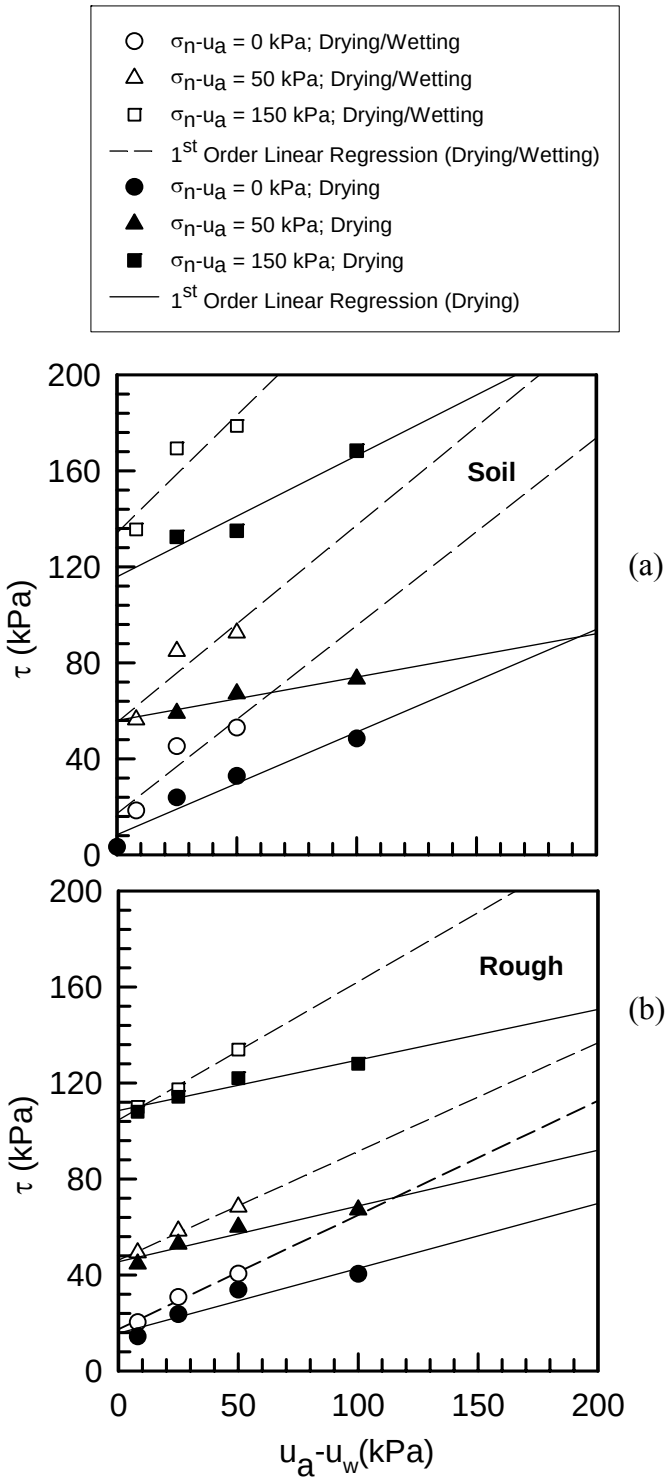

Figure 3.111- Failure Envelope Projections of Unsaturated (a) Soils, and (b) Rough Direct Shear for both Drying and Hysteresis (Wetting after drying) Tests on ($u_a - u_w$)-Shear Stress Plane

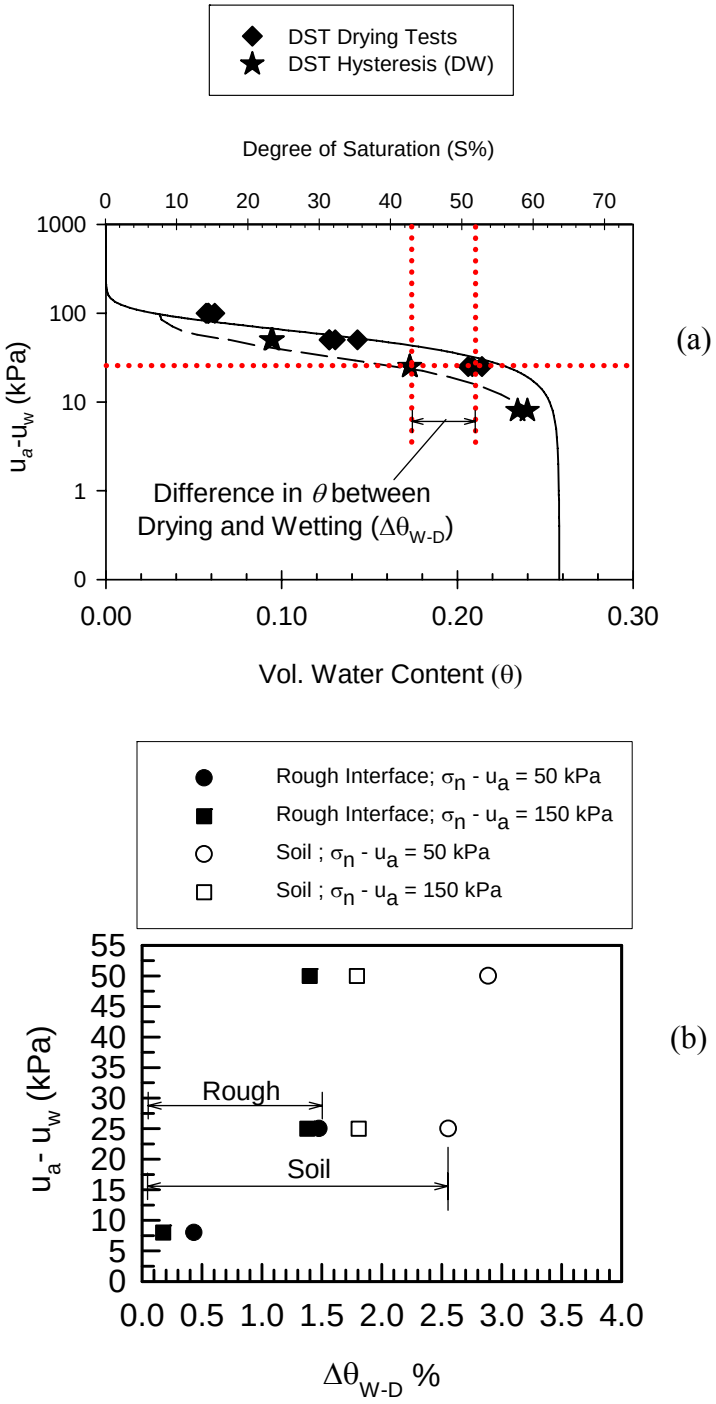

Figure 3.112- (a) Illustration of the Difference in Water Content ($\Delta\theta_{W-D}$) between Wetting and Drying for a Typical SWCC from DST Results, (b) Comparison of the ($\Delta\theta_{W-D}$ %) between Soil and Rough Interface Tests

3.8.2.2 Model to Predict Shear Strength due to Hysteresis (Drying/Wetting)

As discussed in Section 3.8.2.1, most model equations failed to accurately estimate or predict the shear strength of unsaturated soils, rough and geotextiles with changes (mainly increase) in suction on the drying curve. Similarly, these common techniques and model equations (such as Vanapalli et al. 1996, Garven and Vanappalli 2006, Guan et al. 2010) failed to accurately predict the shear strength for soils and interfaces subjected to hydraulic hysteresis (i.e., wetting after drying). For example, Figure 3.113 presents experimental results obtained in this study compared to predicted results of wetting shear strength using Vanapalli et al. (1996) and the wetting SWCC.

In addition, there exist a lack of data illustrating the hysteresis effect on shear strength of unsaturated soils and interfaces. Therefore, this study explores the experimental results presented in previous sections to propose a new technique and model equation to predict shear strength due to hysteresis (i.e. wetting after drying).

The proposed method requires saturated shear strength testing to obtain the saturated shear strength parameters (c', c'_a and ϕ', δ') and SWCC testing with hysteresis to obtain drying and wetting curves. Results from the latter tests are then used with the proposed model to predict shear strength of soils and interfaces along the SWCC drying, and wetting curves as follows.

$$\tau_f = \left[c'_a + (\sigma_n - u_a)_f \tan\delta' + (u_a - u_w)_f \tan\delta' \left(\frac{\theta - \theta_r}{\theta_s - \theta_r} \right)^k \right] \times (F_{DW}) \qquad \textbf{(3.14)}$$

where, the first part $\left[c'_a + (\sigma_n - u_a)_f \tan\delta' + (u_a - u_w)_f \tan\delta' \left(\frac{\theta - \theta_r}{\theta_s - \theta_r} \right)^k \right]$ represents the shear strength during drying (Equation 3.13), and the wetting factor,

$$F_{DW} = \begin{cases} 1, & \text{drying (D) tests only} \\ \theta_d/\theta_w, & \text{wetting (DW) following drying tests for cohesionless soils (i.e. Sand and non-plastic Silt)} \\ \theta_d/\theta_w, & \text{wetting (DW) following drying tests for cohesive soils (i.e. Clay and Silt with high plasticity)} \end{cases}$$

where θ_d and θ_w = the volumetric water content along the drying curve, and wetting curves of the SWCC, respectively.

As presented by Equation (3.14), the shear strength on the wetting curve (due to hysteresis) is basically predicted directly from the drying results by multiplying with the proposed factor (F_{DW}) obtained from the hysteretic SWCC results. With all its simplicity, this proposed formulation seems to capture the hysteretic behavior of shear strength for soils and interfaces tested in this study, as shown in Figure 3.114. This ratio represents the change in water content between drying and wetting at a given suction value, which appears to have a significant influence on the shear strength results on the wetting compared to the drying at same suction. With significant number of SWCC tests performed in this study and some other results from the literature (e.g. Topp 1971 and Pham et al. 2003), an interesting behavior of the ratio (θ_d/θ_w) was observed with suction, as shown in Figure 3.115 through Figure 3.120. A consistent trend (i.e. bell shape type, an increase then decrease) was observed for different soil types and test conditions. Figure 3.115 and Figure 3.116 represent data from SWCC tests obtained in this study (mixed artificial soil) under different initial conditions (i.e. initially saturated, as compacted, and under different net normal stresses). Figure 3.117 and Figure 3.118

present results obtained from DST of soils and rough interfaces in the current study, respectively. Figure 3.119 and Figure 3.120 present results from SWCC tests by Topp (1971) and Pham et al. (2003), respectively. The trend of (θ_d/θ_w) with suction is consistent with the behavior of shear strength due to hysteresis; as suction (on the wetting curve) increases, shear strength increases then gradually decreases (Figure 3.114) to the same value at the intersection between drying and wetting on the SWCC curves (Point A, Figure 3.121), which corresponds to a ratio (θ_d/θ_w) of 1.

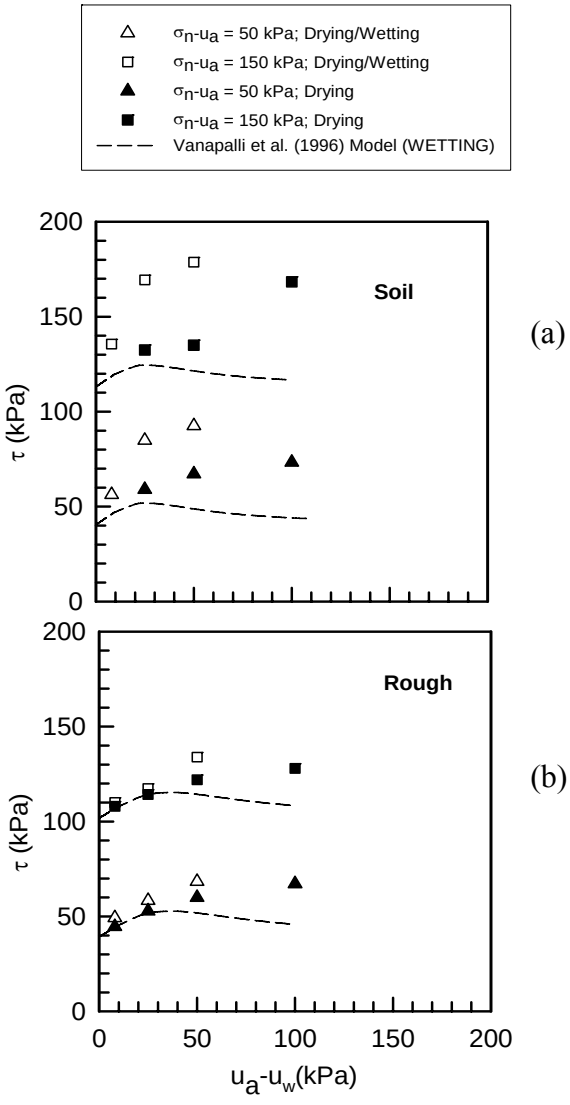

Figure 3.113- Comparison of Wetting Shear Strength using Vanapalli et al. (1996) Model with Experimental Results from the Current Study

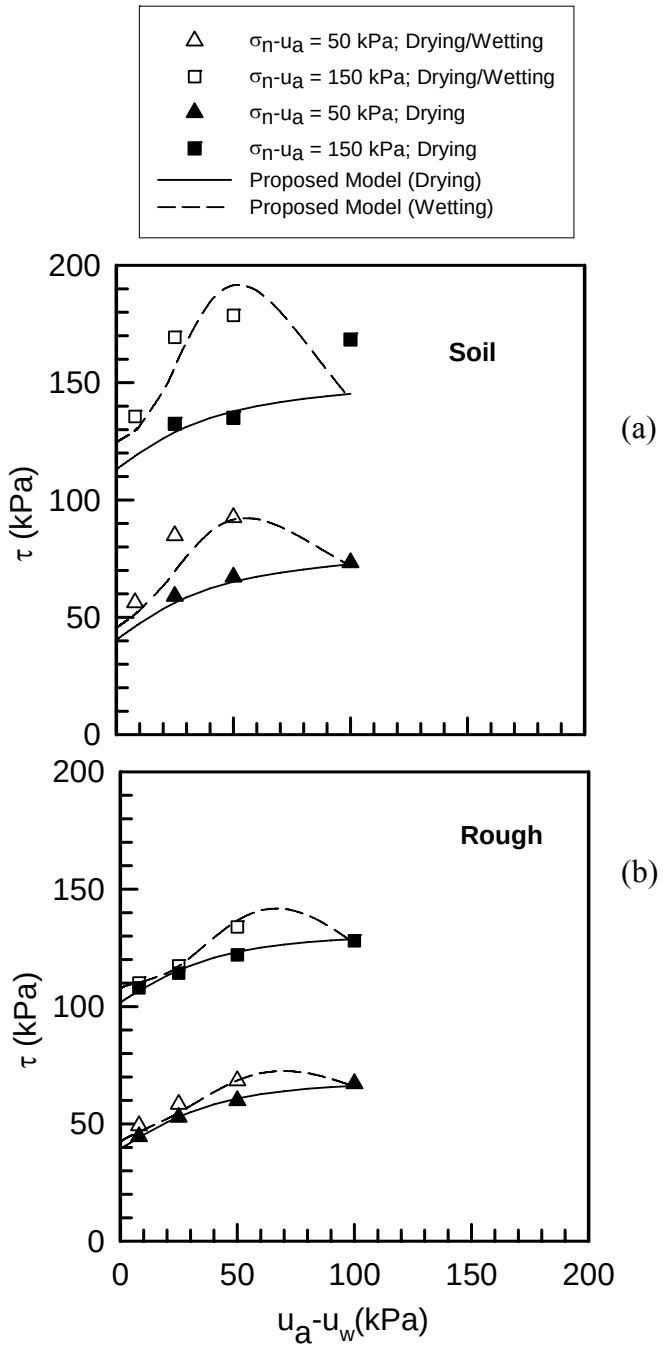

Figure 3.114- Comparison of Predicted Shear Strength Results using the Proposed Model of with Experimental the Results from Unsaturated (a) Soils, and (b) Rough Direct Shear for both Drying and Hysteresis (Wetting after Drying) Tests

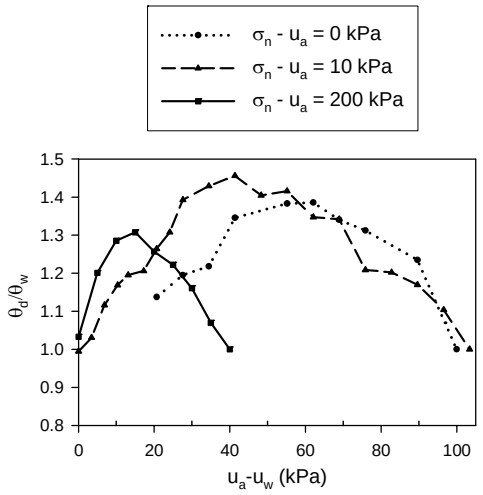

Figure 3.115- Ratio (θ_d/θ_w) versus Suction for Initially Saturated SWCC Tests

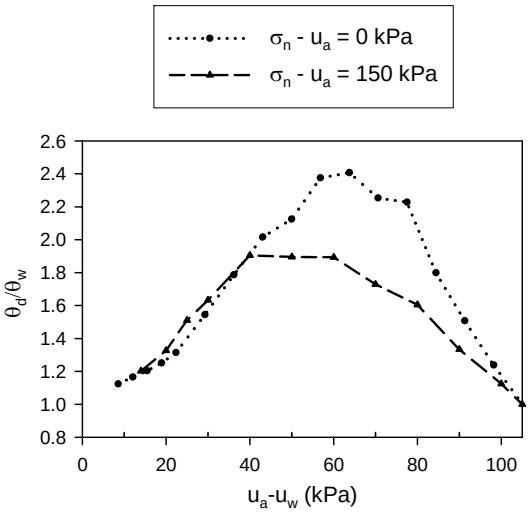

Figure 3.116- Ratio (θ_d/θ_w) versus Suction for As Compacted SWCC Tests

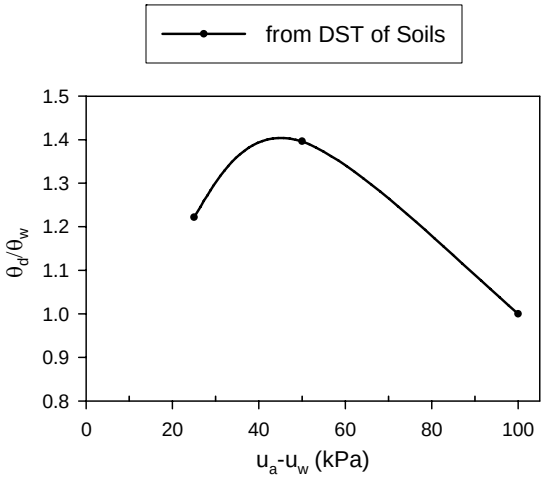

Figure 3.117- Ratio (θ_d/θ_w) versus Suction for DST of Soils

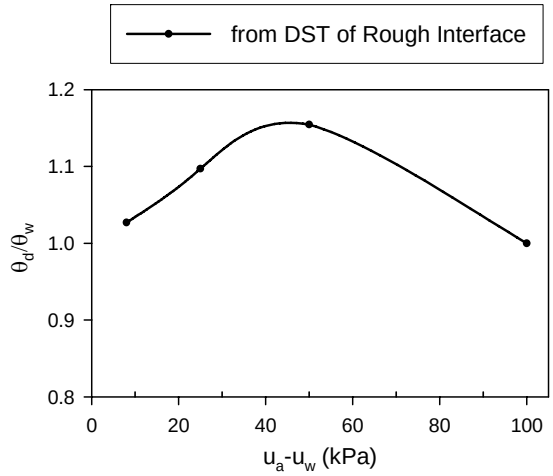

Figure 3.118- Ratio (θ_d/θ_w) versus Suction for DST of Rough Interfaces

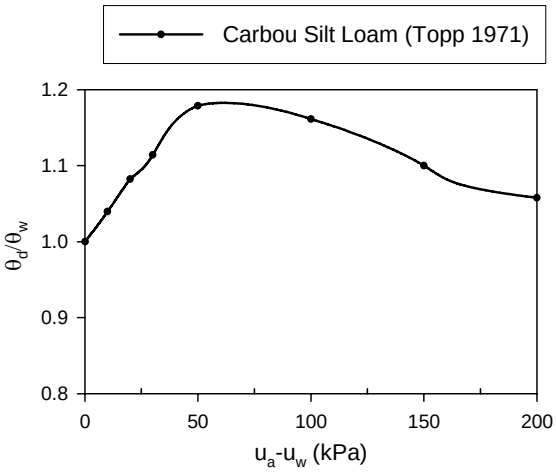

Figure 3.119- Ratio (θ_d/θ_w) versus Suction for SWCC Tests of Caribou Silt Loam (Topp 1971)

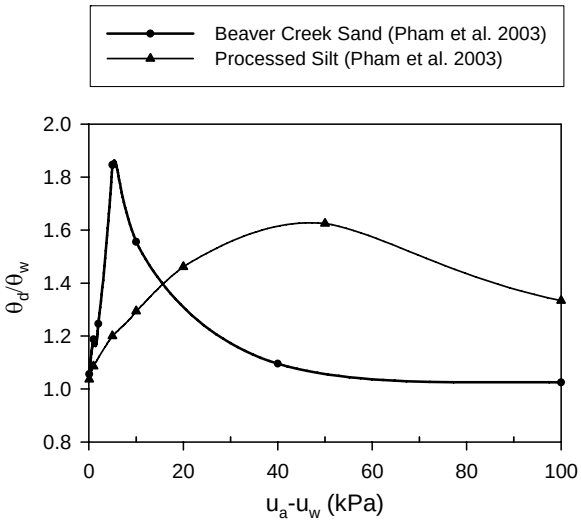

Figure 3.120- Ratio (θ_d/θ_w) versus Suction for SWCC Tests of two Soils (Pham et al. 2003)

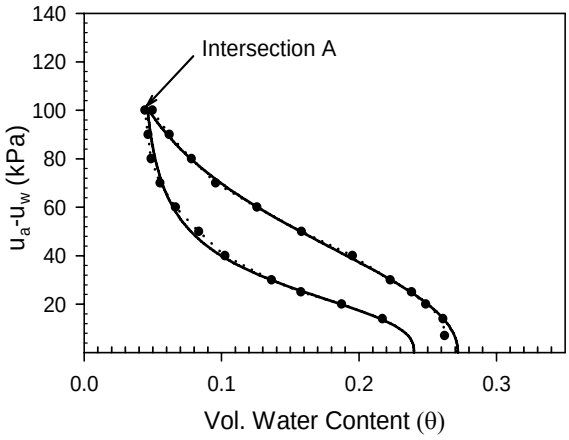

Figure 3.121- Typical SWCC during Primary Drying and Wetting

As presented and discussed previously in this study, hysteresis (wetting after drying, DW) tests exhibited higher shear strength compared to drying (D) tests for a given net normal stress and suction. This behavior is believed to be influenced by many factors, one of which is that for the soil used water, may be acting as lubricant. Thus, more water results in less interparticle friction and lower shear strength. The proposed ratio represents the difference in the amount of water between drying and wetting and since $\theta_w < \theta_d$, multliplying by (θ_d/θ_w) results in lower shear strength at higher water content (drying) compared to wetting with lower water content.

On the other hand, other studies (e.g. Thu et al. 2006, Han et al. 1995, Guan et al. 2010) reported that the drying path showed higher shear strength compared to the wetting path (for clayey soils and silt with high plasticity). They suggested that this difference is related to the contact area of water in the soil (less water during wetting thus less contact area between water and particles), which affects the interparticle forces and results in lower shear strength for wetting.

Therefore, the proposed equation (Equation 3.14), which captures the shear strength of unsaturated soil is validated by predicting the shear strength from other studies (e.g. Guan et al 2010) for clayey soils that exhibited lower strength during wetting than drying (where $F_{DW} = \theta_w/\theta_d$). The ratio ($\theta_w/\theta_d$) used in this equation is related to the amount of water in the soil (between drying and wetting) which influences the solid-liquid interfacial contact area; and thus resulting in lower shear strength for wetting compared to drying.

Limited results are available in the literature that shows the effect of hydraulic hysteresis on the shear strength of unsaturated soils. Guan et al. (2010) presented shear strength results during drying and wetting at two suction values (50 and 200 kPa) at one net normal stress of 100 kPa. The proposed model (Equation 3.15) was applied to the results from Guan et al. (2010) in order to predict the shear strength due to wetting from the drying results. Figure 3.122a presents the experimental results from Guan et al. (2010) compared to the predictions using the proposed model in this study. Figure 3.122b presents the experimental SWCC for the corresponding tests from Guan et al. (2010), along with the SWCC fitting curves using Fredlund and Xing (1994) and Feng and Fredlund (1999). The proposed equation seemed to provide good predictions for both drying and wetting. The existing models (e.g., Garven and Vanapalli 2006, Guan et al 2010) that relates to the SWCC to predict the shear strength with suction are based mainly on sensitivity and regression parameters (e.g. represented by the parameter *k*, as shown in Equations 3.11 and 3.12) related to Plasticity Index (I_p) for selected soil types. However, the proposed model equation relates directly to the SWCC hysteresis based on the parameters (i.e. θ_s, θ_r, n, θ_d and θ_w) described previously, without any parameters

empirically related to type of soil (e.g. plasticity index). The proposed model parameters from SWCC represent the behavior of each soil type.

Findings of this research and related studies from literature, although limited, suggest that the soil type may be a major indication for using either the ratio (θ_d/θ_w) or its inverse for predicting the shear strength (Equations 3.14) due to wetting after drying. Soils that behave similar to sand seem to exhibit higher shear strength upon drying then wetting compared to drying (D) tests for a given net normal stress and suction. On the other hand, some studies from the literature (e.g. Thu et al. 2006, Han et al. 1995, Guan et al. 2010) reported that the drying path showed higher shear strength compared to the wetting path (for clayey soils and silt with high plastticity). While both soil behaviors are believed to be influenced by suction loading history and water-solid contact area, it is postulated that the behavior due to drying/wetting for each soil type (i.e., soil behaving as sand or clay) maybe dominated more by one or the other. For soils behaving as sand, cyclic suction stress (resulting in hardening effect) and the amount of water that may be acting as a lubricant may be the predominant influence resulting in higher shear strength for wetting compared to drying (since $\theta_w < \theta_d$). As shown in Equation 3.14, the ratio (θ_d/θ_w) is proposed for this type of soil which predicts lower shear strength at higher water content for drying compared to wetting with lower water content. For clayey soils, whose shear strength due to drying/wetting appears lower than drying tests, the interfacical contact area with solid particles is believed to be the predominant influence on the results. Thus, the ratio (θ_w/θ_d) was used for clayey soils, resulting in lower shear strength for wetting compared to drying.

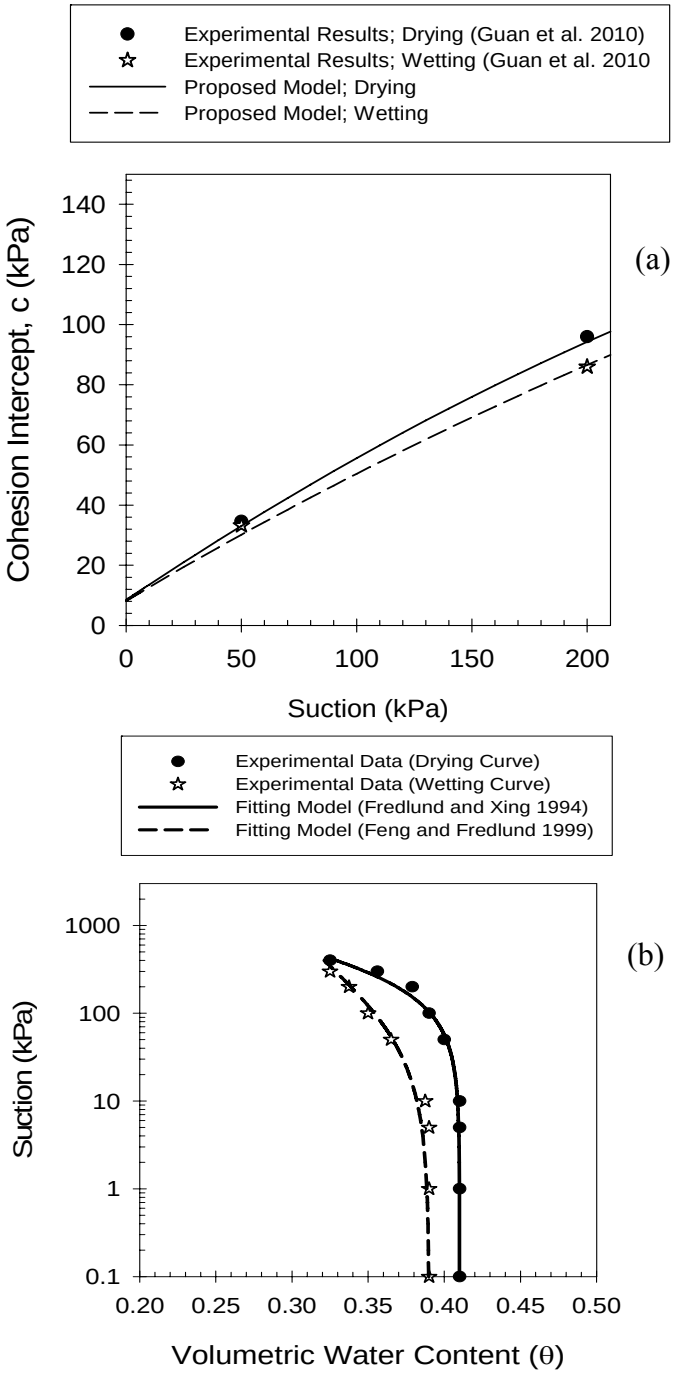

Figure 3.122- a) Comparison of Predicted Shear Strength with the Experimental Results for Drying and Wetting from Guan et al. (2010), b) SWCC Corresponding to Test Results from Guan et al. (2010)

3.8.3 General Elastoplastic Constitutive Model

In this study, the Hamid and Miller (2008) elastoplastic constitutive model is used and validated on rough steel and geotextile interfaces. Briefly, the Hamid and Miller (2008) model is an expansion of the model by Navayogarajah et al. (1992) to simulate the suction-controlled interface direct shear test results of rough and smooth steel plate interfaces. The Navayogarajah et al. (1992) model was originally developed for simulating the behavior of frictional materials by Desai (1980), Desai and Faruque (1984), and Desai et al. (1986). The latter hierarchical approach has the capability of modeling non-associativeness, strain softening, and cyclic loading. It was specialized by Desai and Fishman (1991) for modeling the behavior of rock joints. Navayogarajah et al. (1992) employed the same model for idealization of sand-steel and sand-concrete interfaces.

The original model is modified within the framework of the disturbed state concept. Disturbed state concept has also been employed to predict the behavior of joints in rocks and interfaces between different materials. However, beside Hamid and Miller (2008) no interface models available in the literature have incorporated the effect of suction on the behavior of interfaces. Hamid and Miller (2008) model was capable of capturing the important features of unsaturated soil-interfaces and describes the behavior in terms of two stress state variables, suction, u_a-u_w and net normal stress, σ_n-u_a. Using these stress state variables, yield, potential, and hardening functions were proposed (by Hamid and Miller 2008) for unsaturated soil-steel interface as follows:

$$F = \tau^2 + \alpha(s)\left[\sigma_{net} + R(s)\right]^n - \gamma(s)\left[\sigma_{net} + R(s)\right]^2 \qquad \textbf{(3. 15)}$$

where: F = yield function, τ = shear strength, $\sigma_{net} = \sigma_n - u_a$ = net normal stress, $R(s)$ = bonding stress, which is the increase in the strength of the unsaturated interface with the increase in suction defined as $R(s) = \lambda(s)(u_a - u_w) + \lambda^*$; the plot of R(s) versus (u_a-u_w) gives the slope λ(s) and intercept λ^*. However, in this study and due to the observation that interface shear strength increased nonlinearly with suction, R(s) was defined as a nonlinear function of suction as $R(s) = \lambda_1(s)(u_a - u_w)^2 + \lambda_2(s)(u_a - u_w) + \lambda^*$; For each interface, λ^* is plotted versus R_n (defined in Equation 3.9) which provides parameters λ_1 (slope) and λ_2 (intercept), such as $\lambda^* = \lambda_1 R_n + \lambda_2$. $\gamma(s)$ = material parameter that defines the limiting state of stress, as follows:

$$\gamma(s)^{1/2} = \frac{\tau_p}{\sigma_{net} + R(s)} = \mu_{p1} + \mu_{p2} R_n \qquad \textbf{(3.16)}$$

where, τ_p = peak shear strength.

The intercept and slope of $\gamma(s)^{1/2}$ versus R_n yield the material constants μ_{p1} and μ_{p2}, respectively. Parameter $\alpha(s)$ is a hardening parameter that defines the evolution of the yield surface during deformation (Equation 3.18); (s) indicates dependence of the parameters on matric suction, and n is a phase change parameter related to a state of stress at which the material passes through a state of zero volume change.

$$\left.\begin{array}{ll} \alpha(s) = \gamma(s)\exp(-a\xi_v)\left(\frac{\xi_D^* - \xi_D}{\xi_D^*}\right)^b, & \xi_D < \xi_D^* \\ \text{and,} & \\ \alpha(s) = 0, & \xi_D \geq \xi_D^* \end{array}\right\} \qquad \textbf{(3.17)}$$

Parameters *a*, *b*, and ξ_D^* are functions of *R(s)* and roughness ratio R_n. $\xi_v = \int \left| dv^p \right|$, $\xi_D = \int \left| du^p \right|$; dv^p and du^p are the plastic displacements normal and tangential to the shearing surface, respectively, and ξ_D^* is the value of ξ_D when shear stress reaches its peak value.

A non-associative flow rule was adopted in the model to correlate the volume change behavior and loading. By modifying the growth function, $\alpha(s)$ in the yield surface, a potential function (*Q)* was proposed as follows:

$$Q = \tau^2 + \alpha_Q(s)\left[\sigma_{net} + R(s)\right]^n - \gamma(s)\left[\sigma_{net} + R(s)\right]^2 \quad \textbf{(3.18)}$$

where, $\alpha_Q(s)$ was defined as

$$\alpha_Q(s) = \alpha(s) + \alpha_{ph}(s)\left(1 - \frac{\alpha(s)}{\alpha_i}\right)\left[1 - \kappa\left(1 - \frac{D}{D_u}\right)\right] \quad \textbf{(3.19)}$$

where, *Q* the potential function, *k* a material parameter (non-associative parameter) related to the normalized roughness, net normal stress, and suction. *D* = damage function, α_{ph} is the value of $\alpha(s)$ at the phase change point and α_i the value of $\alpha(s)$ at the initiation of the non-associativeness, defined as $\alpha_i = \gamma(s)(\sigma_{net} + R(s))^{2-n}$, and $D_u = \frac{\tau_p - \tau_r}{\tau_p}$; τ_p and τ_r are the peak and residual shear stresses, respectively. The residual shear stress τ_r is related to R_n through the model parameter μ_0 as follows: $\tau_r = \sigma_{net} \times \mu_0 = \sigma_{net} \times \left[\mu_{01} + \mu_{02} R_n\right]$, where μ_{01} and μ_{02} are the intercept and slope of the plot μ_0 versus R_n. The determination and meaning of the model parameters are presented in Appendix A. The constitutive model expressed by Equations 3.16 through 3.20 was

applied to the results of the unsaturated rough and soil-geotextile interface tests carried out in this study; comparison between experimental and model results is shown below.

3.8.3.1.1 Application of the Constitutive Model to the Unsaturated Rough Interface Test Results

The model parameters for the rough interface tests in this study were obtained similarly as described by Hamid and Miller (2008) and as shown in Appendix A. The normalized surface roughness (R_n) value for the rough interface was estimated to be 5.4 in this study as described in Section 3.3.1. The constitutive model parameters determined from the experimental data for $\sigma_n - u_a$ of 50, 100 and 150 kPa and u_a - u_w of 8, 25, 50 and 100 kPa are summarized in Table 3.10.

Table 3.10- Model Parameters for the Unsaturated Rough Interface

Parameters			Value
	$\xi_D^*(mm)$	$\xi_{D1}^*(mm)$	0.2043
		$\xi_{D2}^*(mm)$	0.06
	γ (s)	μ_{p1}	0.409
		μ_{p2}	0.0573
	n		2.1
	κ	κ_1	-0.095
		κ_2	-0.0299
	μ_0	μ_{01}	0.4625
		μ_{02}	0.0665
	R (s), (kPa)	λ_1 (s)	-0.0033
		λ_2 (s)	0.63
		λ_1	-4
		λ_2	30.8
	a		35
	b		4.5
	K_n (kPa)		1050
	K_s (kPa)		282
Notes: R(s) is a nonlinear function of suction			
All parameters are dimensionless unless indicated otherwise			

Comparison of predicted and measured results during shearing of rough interfaces for all suction under given net normal stresses of 50, 100 and 150 kPa are shown in Figure 3.123-Figure 3.127. Results are also plotted for all net normal stresses at given suction values of 8, 25, 50 and 100 kPa as shown in Figure 3.128, Figure 3.129, Figure 3.130 and Figure 3.131, respectively. Figure 3.123(a) through Figure 3.131(a) compare the predicted and measured results of shear stress (τ) versus horizontal shear displacement (u) subjected to different suction and net normal stress values. The comparison between the experimental and predicted results reveals that the model is capable of capturing the behavior of the unsaturated rough interfaces with reasonable accuracy. The following observations can be made:

1. The peak shear strength of rough interface increased with increase in suction.
2. The post peak shear strength did not seem to be influenced with increase in suction.
3. The peak and post peak shear strength increased with the net normal stress.
4. Strain softening increased with increase in suction.

Noteworthy to mention is that the model does not seem to capture the shear strength behavior of rough interfaces at low suction values (i.e. 8 and 25 kPa). In other words, the model showed a peak interface shear strength followed by strain softening, a behavior not observed for experimental data at low suctions. This difference can be related to the model parameter (i.e. μ_0) that influence the residual shear strength and suggests peak strength followed by softening behavior.

Figure 3.123(b) through Figure 3.131(b) compare the predicted and measured results of vertical strain (v/H_0) versus horizontal shear displacement (u) for different suction and net normal stresses. Important volume change behavior of unsaturated rough interfaces was captured using this model:

1. Unsaturated rough interface predictions generally followed the overall trend (mostly dilation) of volume change behavior. However, in most cases experimental results showed compression following dilation that was not captured by the model. This can be related to model parameters (e.g. n, μ_{p1}, μ_{p1}, γ, ξ_D^*) obtained and used for prediction which are not able to capture such behavior of compression after dilation.
2. Specimens did not show any dilation after the softening behavior was completed.
3. While small and negligible, the model seems to capture fairly well the decrease in dilation under greater net normal stress values and the increase in dilation with suction.

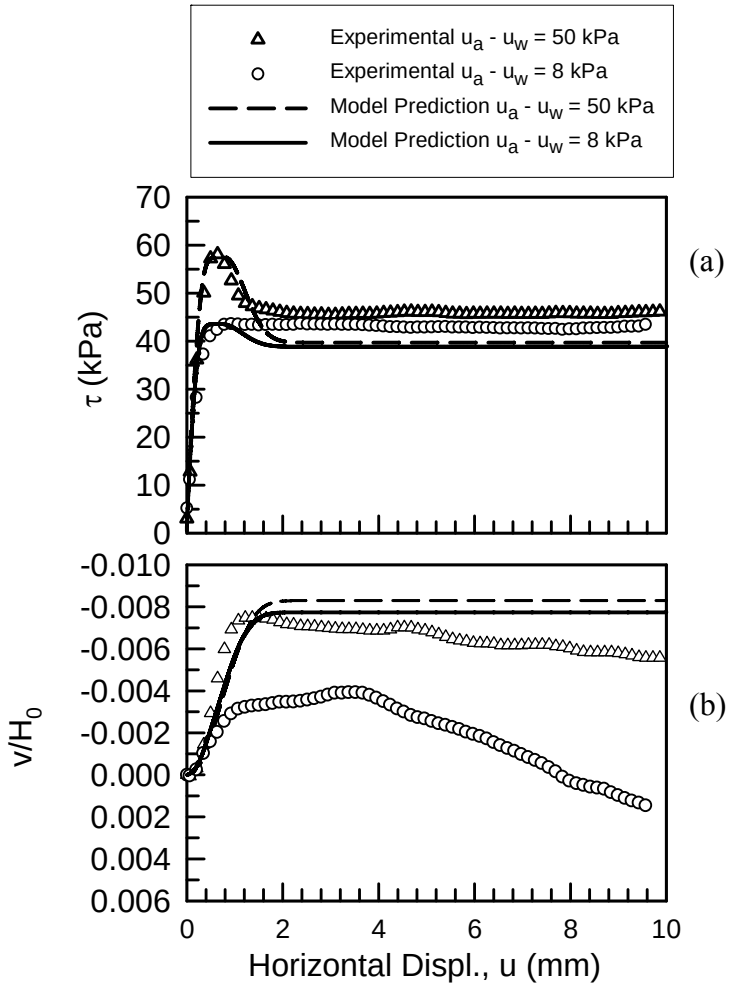

Figure 3.123- A Comparison of Experimental Shear Response Results with Model Predictions for Rough Interface at a Net Normal Stress of 50 kPa for Suction of 8 and 50 kPa

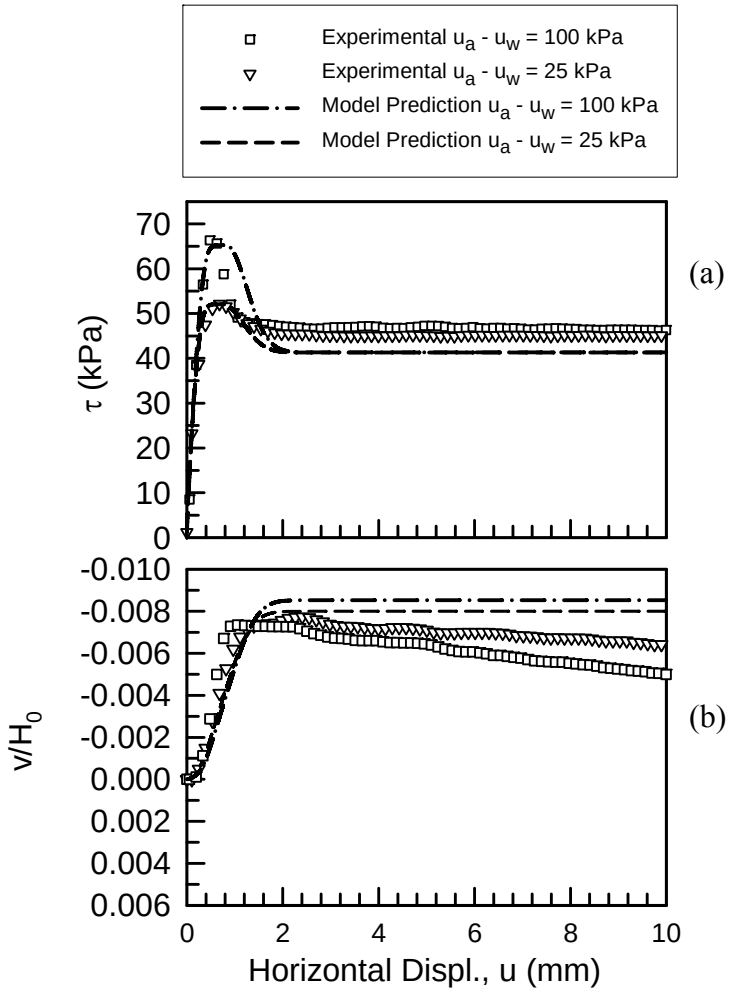

Figure 3.124- A Comparison of Experimental Shear Response Results with Model Predictions for Rough Interface at a Net Normal Stress of 50 kPa for Suction of 25 and 100 kPa

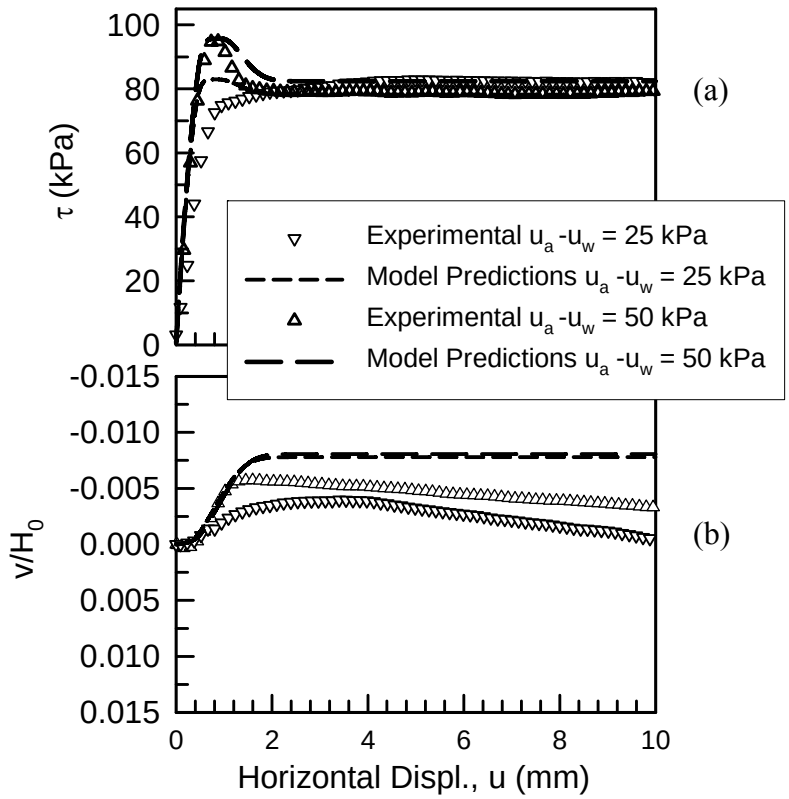

Figure 3.125- A Comparison of Experimental Shear Response Results with Model Predictions for Rough Interface at a Net Normal Stress of 100 kPa for Suction of 25 and 50 kPa

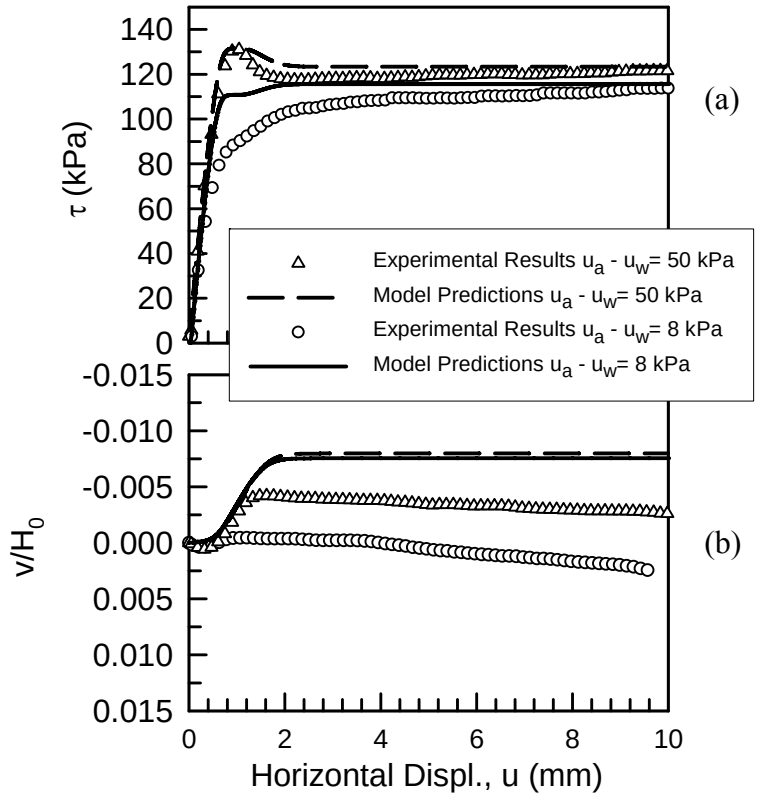

Figure 3.126- A Comparison of Experimental Shear Response Results with Model Predictions for Rough Interface at a Net Normal Stress of 150 kPa for Suction of 8 and 50 kPa

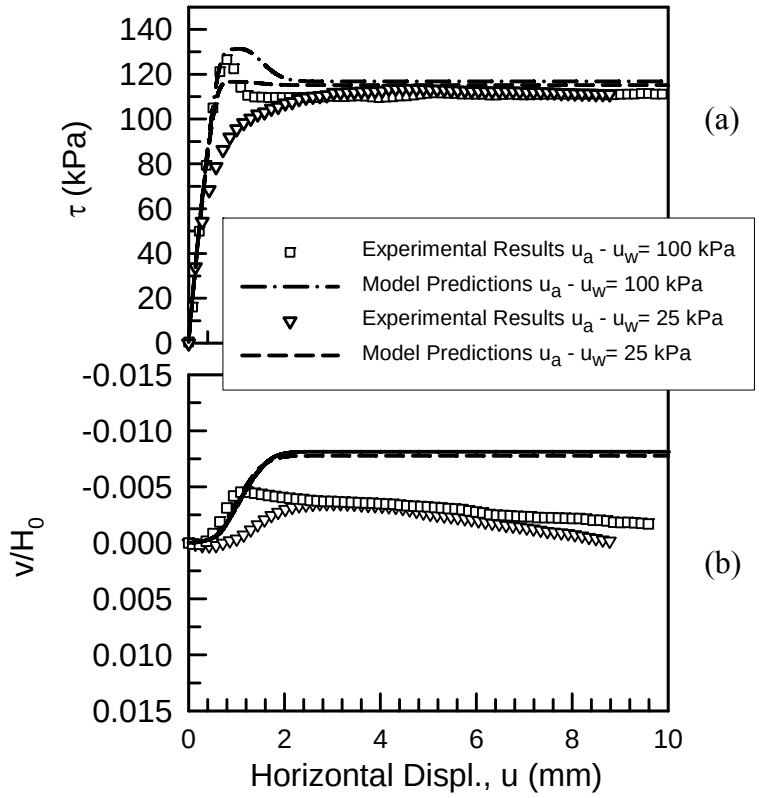

Figure 3.127- A Comparison of Experimental Shear Response Results with Model Predictions for Rough Interface at a Net Normal Stress of 150 kPa for Suction of 25 and 100 kPa

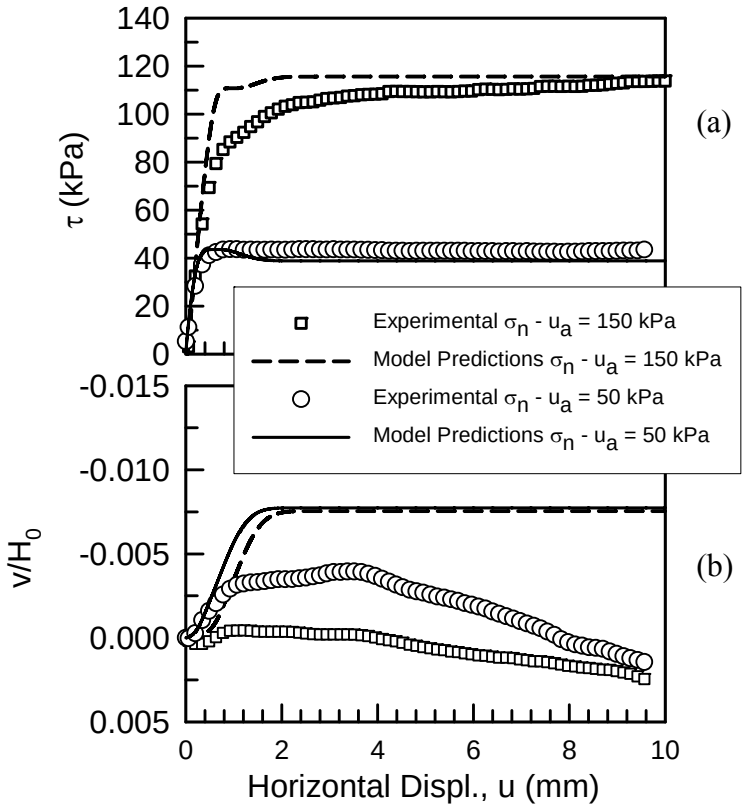

Figure 3.128- A Comparison of Experimental Shear Response Results with Model Predictions for Rough Interface at Suction of 8 kPa

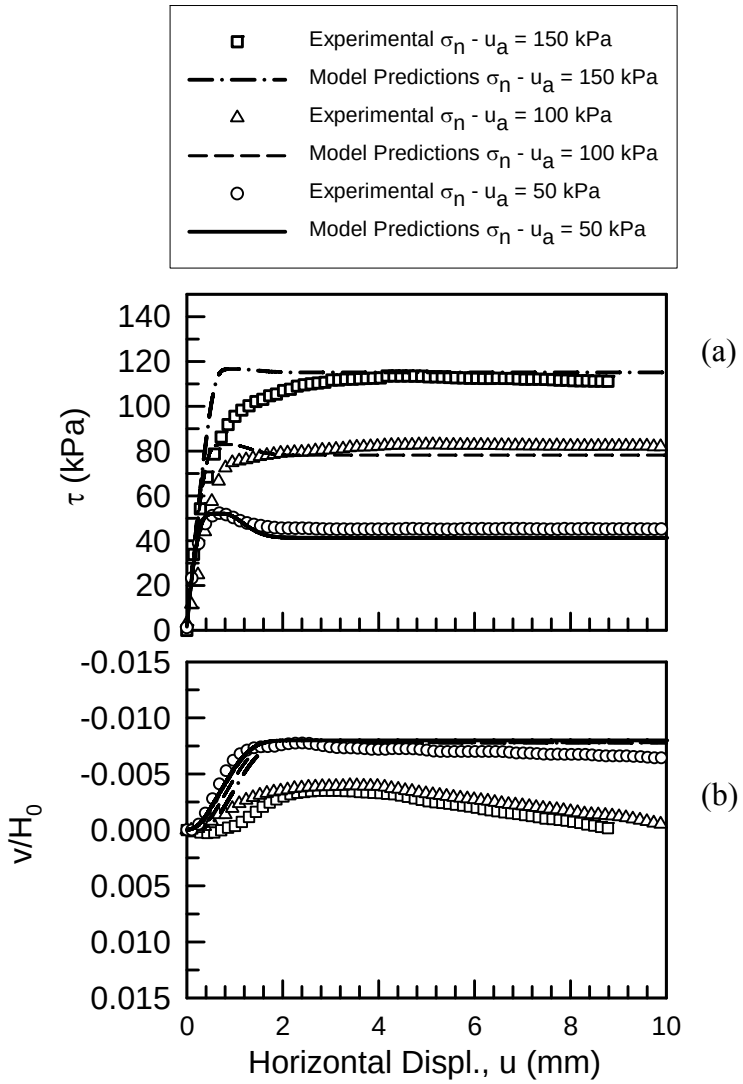

Figure 3.129- A Comparison of Experimental Shear Response Results with Model Predictions for Rough Interface at Suction of 25 kPa

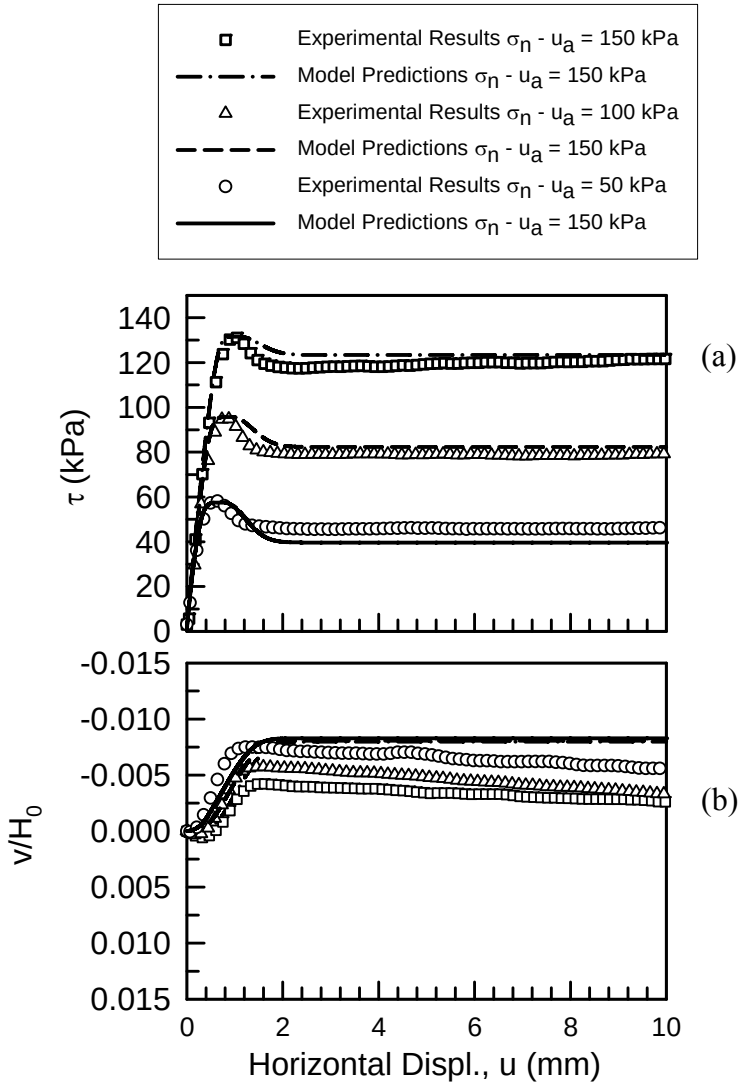

Figure 3.130- A Comparison of Experimental Shear Response Results with Model Predictions for Rough Interface at Suction of 50 kPa

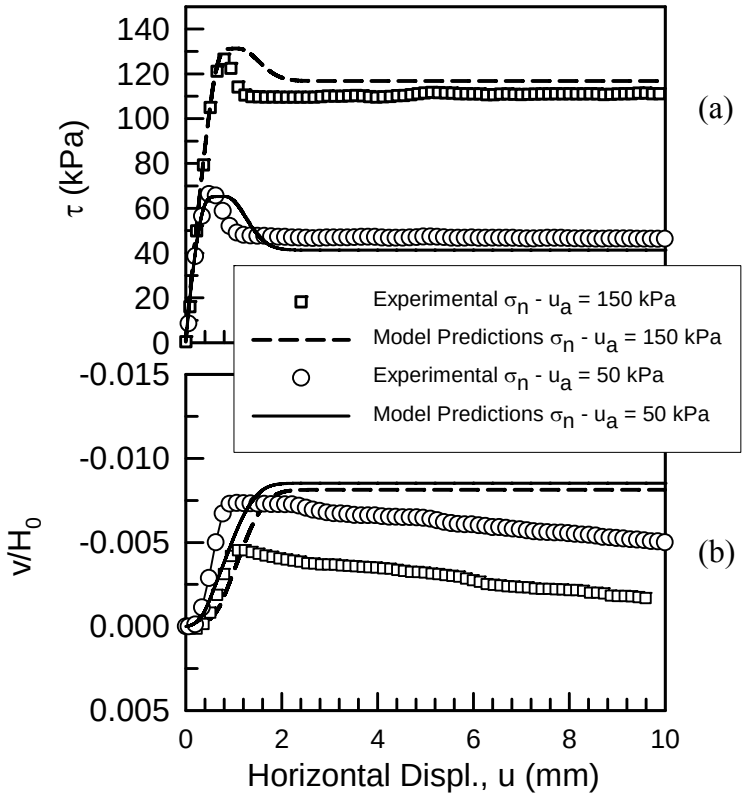

Figure 3.131- A Comparison of Experimental Shear Response Results with Model Predictions for Rough Interface at Suction of 100 kPa

3.8.3.1.2 Application of the Constitutive Model to the Unsaturated Soil-Geotextile Interface Test Results

The model parameters for the soil-geotextile interface tests in this study were obtained using the same procedure as described by Khoury et al. (2010). The normalized surface roughness (R_n) value for the soil-geotextile interface was estimated to be 4.2 in this study. The roughness of the geotextile surface is somewhere in between rough and smooth surfaces as defined by Hamid and Miller (2008). For this study, R_{max} was found to be approximately equal to 0.3 mm by crudely measuring the geotextile peak-valley distance (as shown in Section 3.3.1 and Figure 3.3). The constitutive model parameters

determined from the experimental data for $\sigma_n - u_a$ of 50, 100 and 150 kPa and u_a - u_w of 25, 50 and 100 kPa are summarized in Table 3.11.

Table 3.11- Model Parameters for the Unsaturated Soil-Geotextile Interface

Parameters			Value
$\xi_D^*(mm)$	$\xi_{D1}^*(mm)$		0.1714
	$\xi_{D2}^*(mm)$		0.0715
γ (s)	μ_{p1}		0.3995
	μ_{p2}		0.0639
n			2.3
κ	κ_1		-0.0962
	κ_2		-0.0323
μ_0	μ_{01}		0.4682
	μ_{02}		0.0755
R *(s),* (kPa)	λ *(s)*		0.1454
	λ_1		-13.268
	λ_2		77
a			34
b			4.1
K_n (kPa)			1050
K_s (kPa)			282
Notes: All parameters are dimensionless unless indicated otherwise			

Figure 3.132(a) through Figure 3.141(a) compare predicted and measured results of shear stress (τ) versus horizontal shear displacement (u) for the soil-geotextile interface examined in this study subjected to different suction and net normal stress values. The comparison between the experimental and predicted results reveals that the model is capable of capturing the behavior of the unsaturated soil-geotextile interface with reasonable accuracy. For instance, the predicted peak shear strengths and corresponding

displacements were within ± 5% and ± 12% of experimental results, respectively. The following observations can be made:

1. The peak shear strength of soil-geotextile interface increased with suction. However, the model was not able to capture the slight drop in peak shear strength from 50 kPa to 100 kPa suction at net normal stress of 100kPa.
2. Influence of suction was more pronounced at lower net normal stress (i.e. 50 kPa).
3. The post peak shear strength did not increase notably with suction for most cases.
4. The peak and post peak shear strength increased with the net normal stress.
5. Strain softening was more pronounced at higher suction and higher net normal stress values.

Figure 3.132(b) through Figure 3.141 (b) compare the predicted and measured results of vertical strain (v/H_0) versus horizontal shear displacement (u) for different suction and net normal stresses. Important volume change behavior of unsaturated soil-geotextile interfaces was captured using this model:

1. Unsaturated soil-geotextile interface predictions generally followed the overall trend (mostly dilation) of volume change behavior. However, in most cases experimental results showed a slight amount of compression following dilation that the model did not capture.
2. Specimens did not show any dilation after the softening behavior was completed.

3. The magnitude of dilation decreased under greater net normal stress values. However, while negligible, change in dilation magnitude from the experimental data did not show a consistent trend with increase in suction, but the model seems to show generally any increase or decrease of dilation with suction.

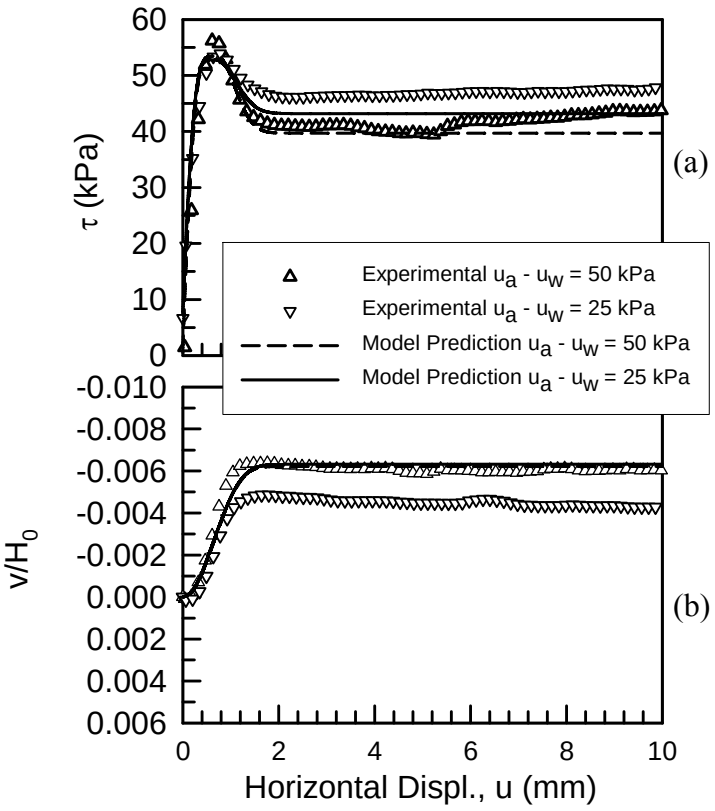

Figure 3.132- A Comparison of Experimental Shear Response Results with Model Predictions for Soil-Geotextile Interface at a Net Normal Stress of 50 kPa for Suction of 25 and 50 kPa

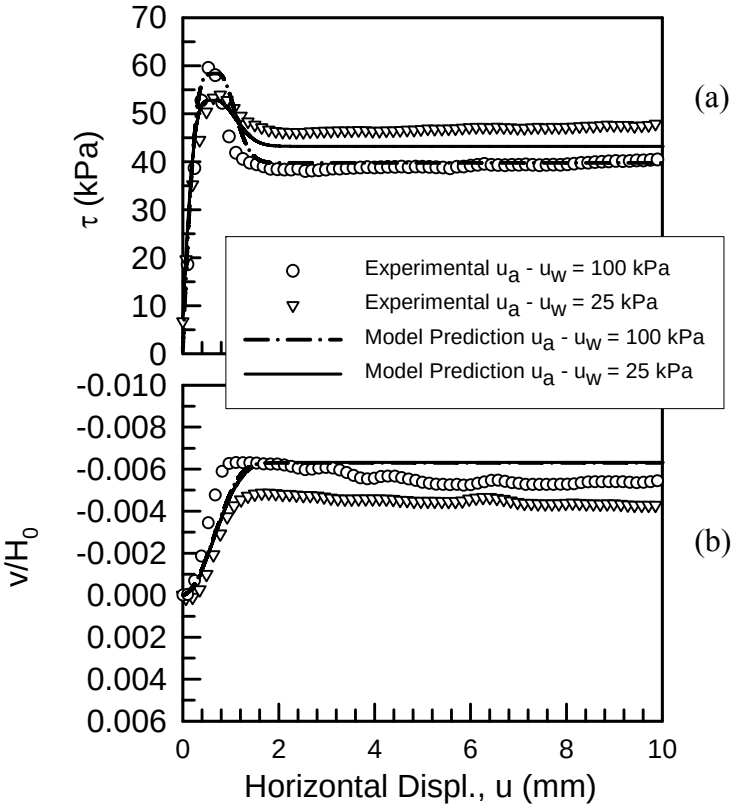

Figure 3.133- A Comparison of Experimental Shear Response Results with Model Predictions for Soil-Geotextile Interface at a Net Normal Stress of 50 kPa for Suction of 25 and 100 kPa

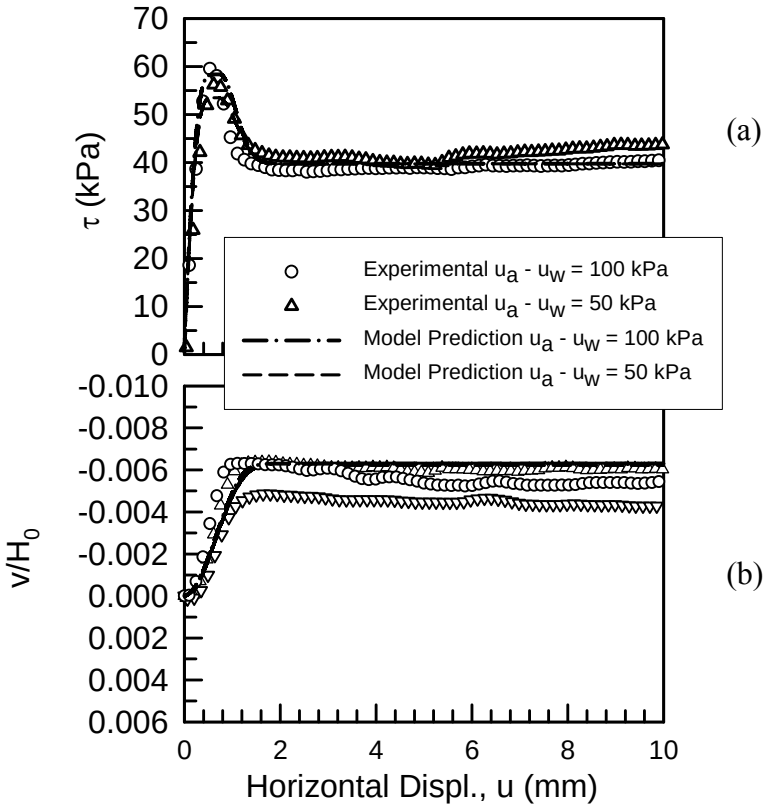

Figure 3.134- A Comparison of Experimental Shear Response Results with Model Predictions for Soil-Geotextile Interface at a Net Normal Stress of 50 kPa for Suction of 50 and 100 kPa

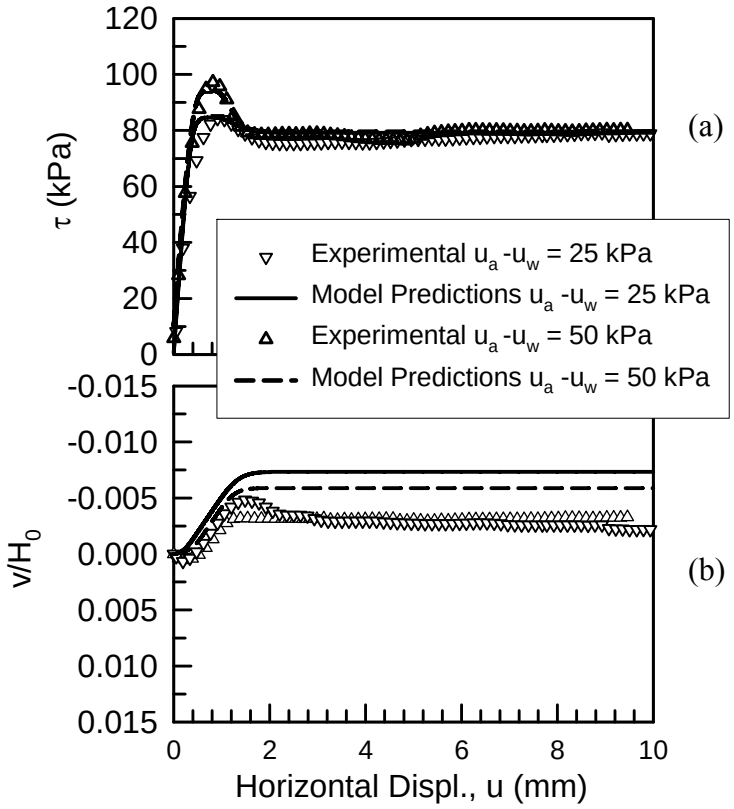

Figure 3.135- A Comparison of Experimental Shear Response Results with Model Predictions for Soil-Geotextile Interface at a Net Normal Stress of 100 kPa for Suction of 25 and 50 kPa

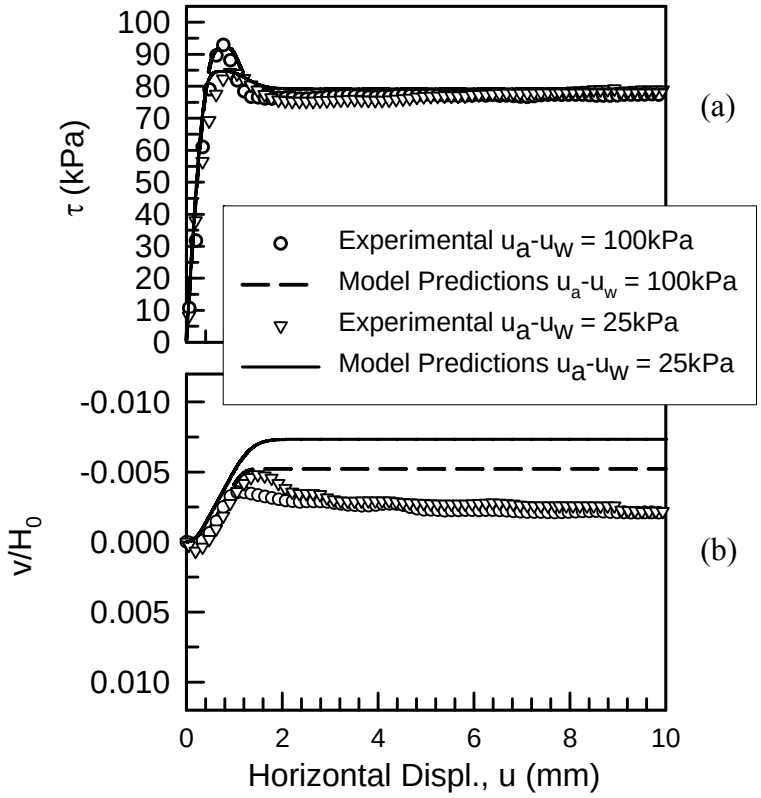

Figure 3.136- A Comparison of Experimental Shear Response Results with Model Predictions for Soil-Geotextile Interface at a Net Normal Stress of 100 kPa for Suction of 25 and 100 kPa

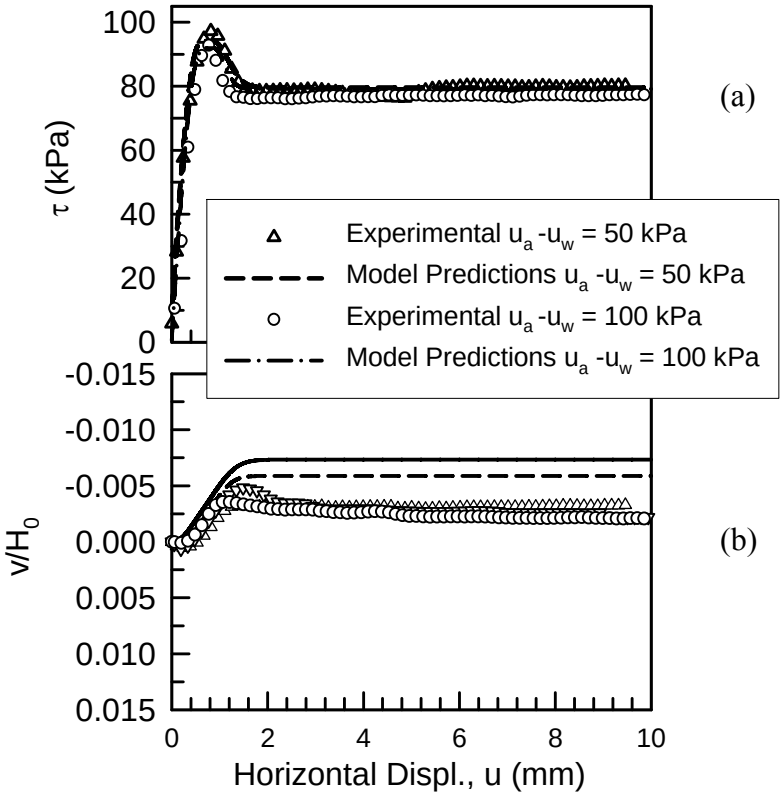

Figure 3.137- A Comparison of Experimental Shear Response Results with Model Predictions for Soil-Geotextile Interface at a Net Normal Stress of 100 kPa for Suction of 50 and 100 kPa

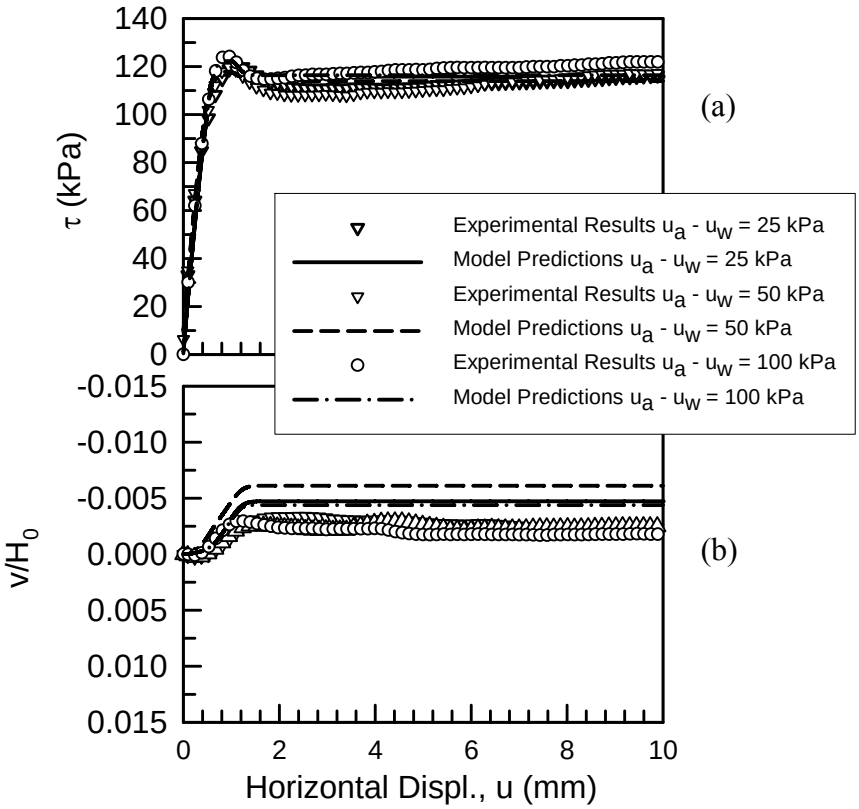

Figure 3.138- A Comparison of Experimental Shear Response Results with Model Predictions for Soil-Geotextile Interface at a Net Normal Stress of 150 kPa for Suction of 25 and 50 kPa

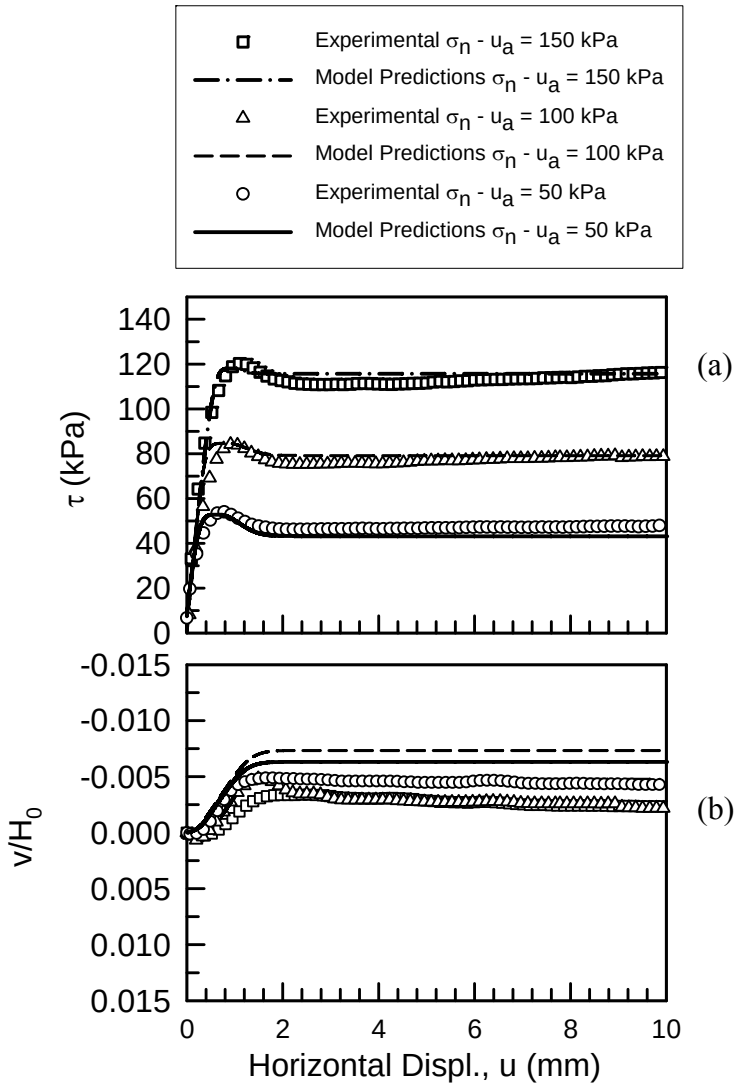

Figure 3.139- A Comparison of Experimental Shear Response Results with Model Predictions for Soil-Geotextile Interface at Suction of 25 kPa

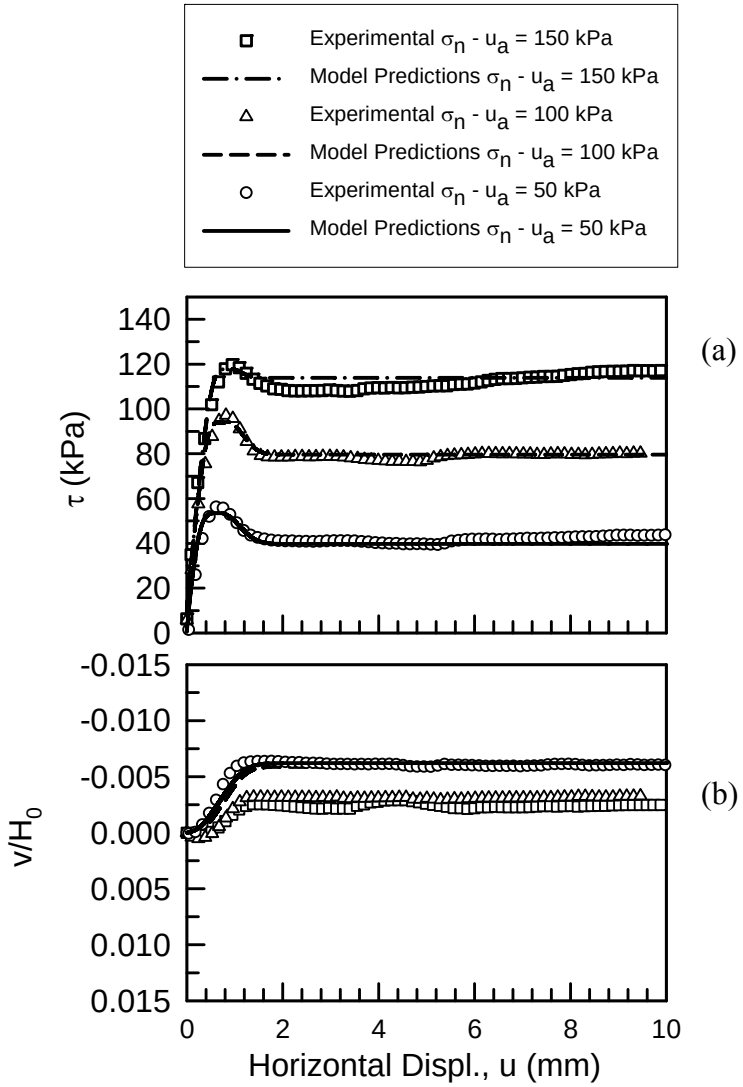

Figure 3.140- A Comparison of Experimental Shear Response Results with Model Predictions for Soil-Geotextile Interface at Suction of 50 kPa

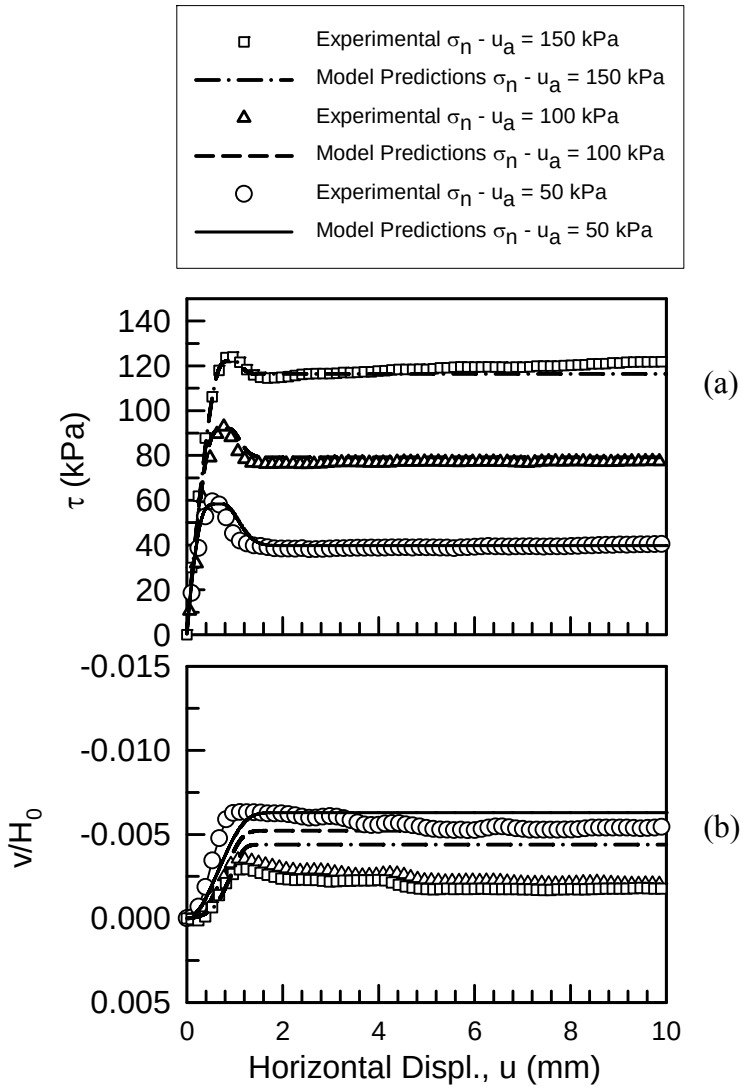

Figure 3.141- A Comparison of Experimental Shear Response Results with Model Predictions for Soil-Geotextile Interface at Suction of 100 kPa

3.9 REPEATABILITY

Two additional tests were conducted on the soil specimens to check for repeatability of the results. One test at 50 kPa suction and 50 kPa net normal stress and another at 50 kPa suction and 150 kPa net normal stress were repeated. As shown in Figure 3.142, similar behavior was exhibited during equalization and shearing. While some slight difference is observed in post peak response, shearing behavior is quite similar up to the point of yielding. To be more precise, the difference in the interpreted shear strength was

within 3 kPa (i.e. 2.5 %) for a given net normal stress and suction value. Although, repeatability data is limited, these duplicated suction-controlled direct shear tests on soil specimens in addition to the consistent patterns observed in the Mohr-Coulomb failure envelopes (presented in Sections 3.8.1.1 and 3.8.2.1) for soil, rough and soil-geotextiles suggest that the data are valid and repeatable.

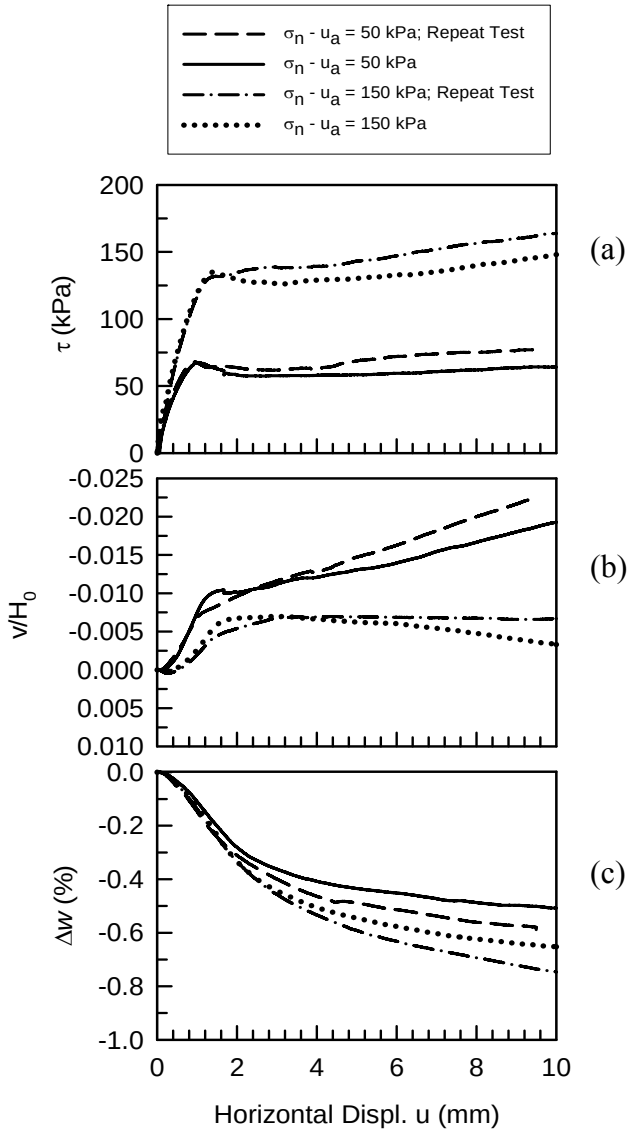

Figure 3.142- Comparison of Direct Shear Test Results on Soils with Repeated Tests at Suction of 50 kPa and Net Normal Stresses of 50 and 150 kPa

3.10 SUMMARY DISCUSSION OF HYSTERESIS EFFECT AND VOLUME CHANGE BEHAVIOR

Some major findings related to the behavior of unsaturated soils and interfaces were observed in this chapter and summarized as follows:

- It was observed that during shearing water drained out of samples tested at suction higher than 8 kPa (i.e. 25, 50 and 100 kPa) while the opposite (i.e. water flowed into the sample) was observed at 8 kPa suction. At suction of 8 kPa behavior was more like that expected for saturated soil. Dilation in saturated soils indicates a tendency for generation of negative pore water pressure, which results in water flowing into the sample. However, for unsaturated soils (i.e. above the air entry value, AEV) changes in pore water pressure are in large part the result of changes to the air-water interfaces between particles (or menisci); these changes can be independent of total volume changes. Based on the comparison of saturated and unsaturated soil behavior it is postulated that in unsaturated soil at suction greater than the air entry value (AEV) during dilation: a) the menisci between soil particles is disrupted, and/or b) due to non-uniformity of pore sizes and water distribution, increase in pore water pressures can occurr. Since these are drained constant suction tests, water drained during shear to maintain the pore water pressure and suction. Figure 3.143 shows the postulated mechanism of pore water pressure increase during shearing. Figure 3.143a presents the postulated disruption of menisci between the soil particles; as shown, during shearing dilation particles are believed to slide on top of each others, resulting in possible breaking or disruption of water menisci (decrease in suction), represented by the

dashed lines, which may reduce the capillary pressure (suction) between the soil particles. Figure 3.143b shows the variation and non-uniformity of pore sizes, and therefore it is believed that above the AEV pore water distribution is not uniform. This was described by Kohgo et al. (1993) who presented three saturation conditions (insular air saturation, fuzzy saturation and pendular saturation) according to pore size variation. This non-uniformity of pore water inside the sample may result in some localized positive pore water pressure where some voids are saturated as shown in Figure 3.143b, and since this is a drained controlled suction test, water will drain out during shearing to maintain the pore water pressure and suction.

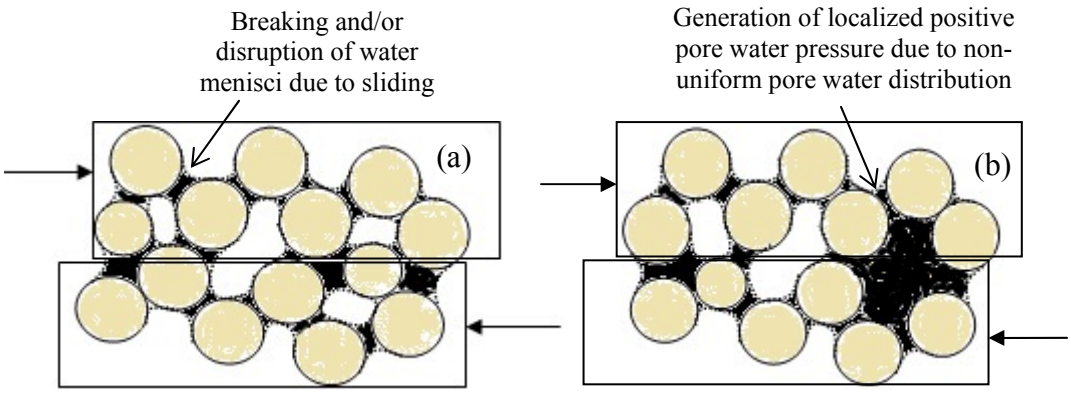

Figure 3.143- Illustration of Postulated Mechanism of Water Pressure Change during Shearing, a) due to menisci disruption, b) due to non-uniformity of pore water distribution

- A most interesting and somewhat unexpected behavior observed in this study, is the higher shear strength for wetting after drying (DW) tests compared to drying (D) tests. Possible reasons for this behavior are discussed in the following paragraph. But before presenting these factors, a brief summary of some related studies shown previously in the literature (Section 3.2.1.4.1) are restated here again for giving a better insight into this problem. Thu et al. (2006), Nishimura

and Fredlund (2002), Han et al. (1995), and Guan et al. (2010) reported that the drying path showed higher shear strength compared to the wetting path (for silty and clayey soils). They suggested that this difference is related to the liquid-water interfacial contact area in the soil (less water during wetting thus less contact area between water and particles), which affects the interparticle forces and results in lower shear strength for wetting. In another related study, Galage and Uchimura (2006) reported that the soil at wetting had higher shear strength as compared to the soil at drying under same suction, for sandy-silt soil. Shemsu et al. (2005) concluded that unsaturated soil specimens that underwent cyclic suction loading showed higher peak shear strength. Noteworthy is that these studies showing higher shear strength for wetting than drying have been conducted on cohesionless soil (e.g. sandy-silt), similar to the soil used in this study; however, other studies that showed higher drying than wetting results were conducted on more fine grained soils (e.g. silt with high plasticity and clayey soils). Also, Nishimura et al. (1999) investigated the influence of stress history on the strength parameters of an unsaturated statically compacted non-plastic silty soil. A total stress ratio (TSR), which is the ratio of compaction pressure to the confining pressure, was used as a measure of stress history. Results showed that the loading history influenced the shear strength parameter (ϕ^b) associated with suction. In addition, Vassallo et al. (2007) studied the effect net stress and suction history on the small strain stiffness of a compacted clayey silt, and found that cyclic suction, in particular increasing of suction beyond the past maximum value, induced significant accumulation of irreversible strains and resulted in a higher stiffness.

Based on the literature and the findings from this study, this behavior of higher strength on wetting than drying may be affected by the following factors: (1) suction loading history, (2) water-particle contact area and (3) soil type. These factors raise a question as to the dominate reason behind the higher strength on the wetting than on the drying curves. First, by considering the water-particle contact area (less water during wetting thus less contact area between water and particles over which suction acts) the interparticle forces are affected and believed to result in lower shear strength for wetting, which is not the case in this study. One possible explanation is that water for the artificial soil used in this study may be playing the role of lubricant between the solid particles, and thus resulting in lower strength for drying with higher water content as compared to wetting with lower water content.

The other factor is the loading stress history, which plays a major role into the behavior of unsaturated soils, especially if hysteresis (cyclic suction) is involved. As described previously in this study, hysteresis was induced by drying the soil samples up to 100 kPa and then wetting back to target suction, at which shearing results were compared to that at similar suction on the drying path. The soil used in this study is sandy silt and the residual suction obtained from the SWCC is approximately 100 kPa (which is in the typical range 0-200 kPa for sandy and silty soil, Vanapalli et al. 1996) using the corresponding SWCC plot on an arithmetic scale (e.g., Figure 2.29 and Figure 2.30). This raises the question whether cyclic suction, where past maximum value is exceeded, may have a significant influence on the shearing behavior observed. To this end, it is worth recalling the loading collapse (LC) and suction increase (SI) yield loci (Figure 3.144) that were introduced by Alonso et al. (1990), which will be used to interpret the data. Alonso

et al. (1990) proposed that preconsolidation pressure (P_c) increases with suction, and that irreversible strains are developed once the soil reaches a maximum previously attained suction (S_o). In this study, only one saturated oedometer test was performed while no consolidation results are available at different suction. From the saturated consolidation test the preconsolidation stress (Po*) was approximately 210 kPa. Based on the results from this study, is it estimated that S_o maximum is close to the residual saturation of about 100 kPa, and most likely less than 100 kPa. Further, since the net normal stresses for hysteresis tests performed (i.e. the maximum net normal stresses applied is 150 kPa) are less than 210 kPa (Po*) and since P_c increases with suction the yield locus LC is assumed and plotted as shown in Figure 3.145. In other words, the tests performed in the range of net normal stresses will not reach the LC curves; however, since suction hysteresis tests reached the S_o value of 100 kPa at constant net normal stress, irreversible strains may develop resulting in a stiffer sample condition.

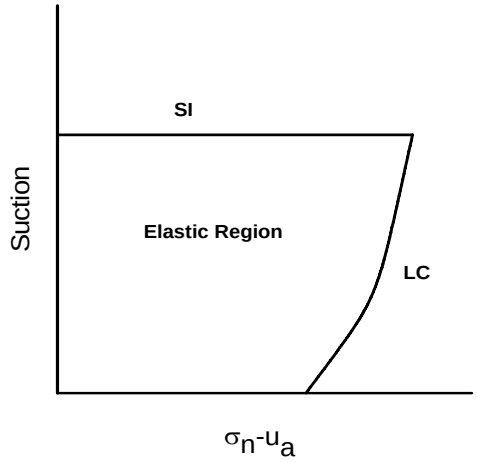

Figure 3.144- Typical Suction Increase (SI) and Loading Collapse (LC) Yield Loci

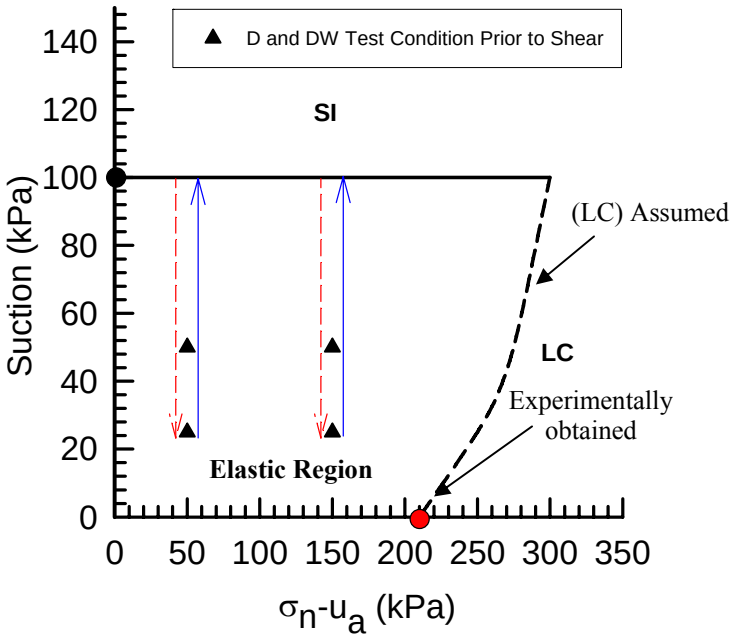

Figure 3.145- Suction Increase (SI) and Loading Collapse (LC) Yield Loci for the Soil used in this Study

Figure 3.146 presents a plot of specific volume (v) versus suction that further confirms the irreversibility of strains after equalization of suction. This behavior which results in an increase of the soil stiffness (in particular sandy and silty soil) is believed to be another major factor for higher strength due to suction hysteresis (wetting after drying) compared to drying tests. Noteworthy, as previously mentioned, this behavior of higher strength due to suction loading was also observed by Shemsu et al. (2005) on cohesionless soil (e.g. sandy-silt). All these factors and behavior needs to be further explored by conducting hysteresis tests on natural clayey soil.

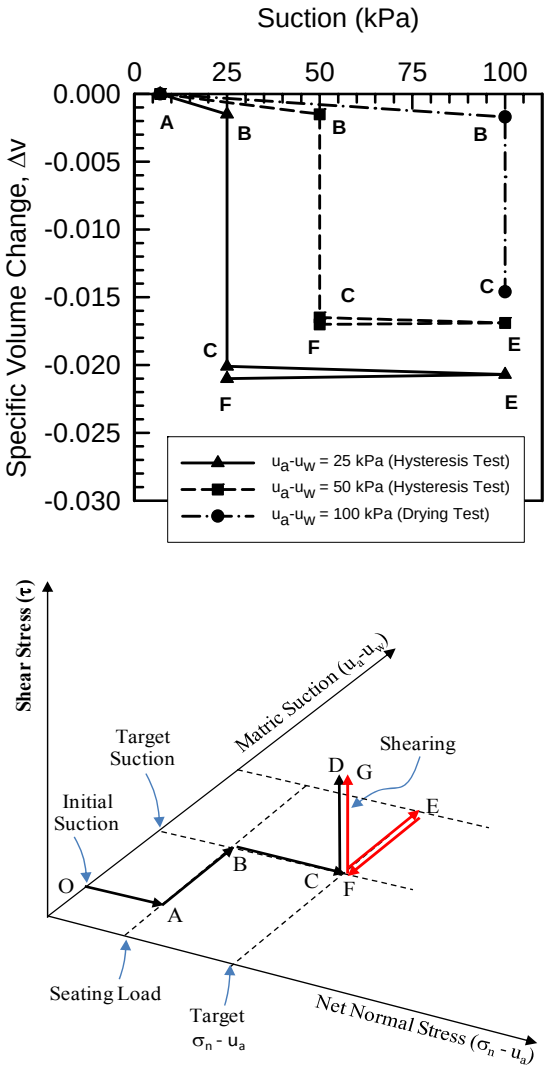

Figure 3.146- a) Specific Volume Changes (Δv) during Cyclic Suction, b) Loading Stress Sequence

CHAPTER 4: UNSATURATED RESILIENT MODULUS

4.1 INTRODUCTION

Resilient Modulus (M_r), a key parameter for the design of pavements, is influenced by different variables such as the dry density, moisture content, and stress states among others. Numerous research projects have been conducted to study the effect of those factors on M_r, but there is still much research needed to fully understand the role of moisture content changes (e.g. suction hysteresis) in subgrade behavior and pavement performance. Therefore, this study aimed at assessing the effect of soil suction hysteresis on the resilient modulus (M_r) of a subgrade soil. To this end, suction-controlled M_r tests along the drying and wetting (hysteresis) curves of the SWCC were performed on the same test soil used to study the SWCC, as described in the previous chapters. A relationship between resilient modulus and matric suction herein called the resilient modulus characteristic curve (MRCC) is presented. In addition, a new model related to the SWCC is proposed to predict the M_r results during drying and wetting (due to suction hysteresis).

4.2 LITERATURE REVIEW

4.2.1 Background and Relevant Work on Resilient Modulus

Resilient modulus (M_r) of subgrade soil was introduced as an important parameter in the 1986 AASHTO Guide for Design of Pavements, and is treated as such in the revised 1993 and 2002 AASHTO Guides. Although AASHTO and DOTs have made major investments in resilient modulus studies over the past years, little research has been

conducted to address the effect of suction hysteresis on resilient modulus of subgrade soils.

A number of studies have been undertaken previously to evaluate changes in moisture condition and soil suction with resilient modulus. For example, Khoury and Khoury (2009) and Khoury et al. (2009) studied the variation of moisture content on the behavior of M_r; results showed that M_r-moisture content relationship exhibits a hysteretic behavior due to the wetting and drying process. Liang et al. (2007) proposed a new predictive equation for the resilient modulus of cohesive soils using the concept of soil suction. Yang et al. (2008) conducted suction controlled M_r tests using the axis translation technique on clayey soils. Their study indicates that M_r increases with an increase in suction. Kung et al. (2006) studied the variations of M_r and plastic strains with the post-construction moisture content and soil suction for cohesive subgrade soils. Results indicated that M_r increased with increasing suction and decreased with increasing deviator stress, while plastic strains decreased with increase in suction. Yang et al. (2004b) also used the filter paper technique to study the effect of matric and total suction on M_r. In their study, matric suction was the key parameter for predicting the mechanical behavior of subgrade soil. Yuan and Nazarian (2003) investigated the effect of wetting and drying on the seismic modulus of compacted base and subgrade specimens. Ceratti et al. (2004) conducted both in-situ and laboratory tests to determine the effect of seasonal variation on subgrade resilient modulus of soils from southern Brazil. They reported that wetting after drying can lower the resilient modulus up to four times compared to drying only. Khoury and Zaman (2004) used the filter paper technique to evaluate the variation of resilient modulus with post-compaction moisture content and suction for a selected

clayey subgrade soil in Oklahoma and found that M_r-moisture content relationships exhibit a hysteretic behavior due to wetting and drying and that M_r and suction were influenced by the compacted moisture content. Drumm et al. (1997) examined the effect of post-compaction moisture variation on the resilient modulus of subgrade soils in Tennessee. Resilient modulus for all subgrade soils exhibited a decrease with increase in degree of saturation. The authors are not aware of any other significant studies that address the effect of suction hysteresis on the M_r of subgrade soil, especially with regard to primary drying and wetting, secondary drying and states on the scanning curves. The aforementioned studies have used the filter paper method to study the effect of suction on M_r, except Yang et al. (2008). In their study Yang et al. (2008) controlled the pore air (u_a) and pore water (u_w) pressures during testing. However, the limitations associated with the low hydraulic conductivity (e.g. unsaturated fine-grained soils) leads to very long equilibrium times associated with suction changes during testing.

4.2.2 Relevant Resilient Modulus Models

The generalized universal model adopted by the mechanistic-empirical pavement design guide (MEPDG) M_r-Stress Model is presented below:

$$M_r = k_1 p_a \times \frac{\theta}{p_a}^{k_2} \times \left(\frac{\tau}{p_a} + 1\right)^{k_3} \qquad \textbf{(4.1)}$$

In this model, the resilient modulus (M_r) is expressed as a function of, θ = bulk stress = $\sigma_1+\sigma_2+\sigma_3$; σ_1, σ_2, and σ_3 are the three principal stresses, and τ = octahedral stress = $(\sqrt{2}/3)$ $(\sigma_1-\sigma_3)$. The coefficients k_1, k_2, and k_3 are model regression parameters. This model does not take into consideration the variation of moisture content effect. In an attempt to study the effect of seasonal variation in moisture content in pavement design,

AASHTO (2007) presented a new MEPDG model. The MEPDG incorporates the enhanced integrated climatic model using the resilient modulus for the optimum moisture content (Larson and Dempsey 1997). The current model predicts the change of modulus due to a change in degree of saturation of the soils as follows:

$$Log\left(\frac{M_r}{M_{ropt}}\right) = a + \left(\frac{b-a}{1+\exp\left(\ln\frac{-b}{a} + k_m \times \left(S - S_{opt}\right)\right)}\right) \qquad \textbf{(4.2)}$$

where, M_r/M_{ropt} = resilient modulus ratio, M_r = resilient modulus at a given degree of saturation, M_{ropt} = resilient modulus at a reference condition, a = minimum of $\log(M_r/M_{ropt})$, b = maximum of $\log(M_r/M_{ropt})$, k_m = regression parameter, and $(S-S_{opt})$ = variation in degree of saturation.

However, the MEPDG equation does not combine the effects of state of stress and water content (Liang et al. 2007). Various relationships between soil suction and resilient modulus (M_r) were presented by Edris and Lytton (1976), Khoury et al. (2003), and Khoury and Zaman (2004) among others. Yang et al. (2004b), presented a model based on the effective stress concept; their study reflects the effects of seasonal variation of moisture content on the resilient modulus of subgrade soils in a deviator stress-matric suction model. Kung et al. (2006) also presented a model including the effect of moisture content variations on M_r; the model is the same as presented by Yang et al. (2004b), which is based on the effective stress concept of unsaturated soil. The latter model explicitly includes the effect of stress and suction. In this model, the regression parameters must be calibrated at each water content in order to predict resilient modulus.

Yang et al. (2004b) used the effective stress approach (Bishop 1959) and explicitly incorporated the effect of external applied stress and matric suction in a prediction model for M_r, as shown below:

$$M_r = k_1\left(\sigma_d + \chi_m \psi_m\right)^{K_2} \quad \textbf{(4.3)}$$

where, χ_m = Bishop's parameter, k_1 and k_2 are model regression parameters

Liang et al. (2007), proposed the following model for predicting the effect of moisture variations on M_r, using the effective stress (Bishop 1959) concept and assuming the pore air pressure equal to zero (u_a=0):

$$M_r = K_1 \times P_a \times \left(\frac{\theta + \chi_w \cdot \psi_m}{P_a}\right)^{K_2} \left(\frac{\tau_{oct}}{P_a} + 1\right)^{K_3} \quad \textbf{(4.4)}$$

where, θ = bulk stress = $\sigma_1+\sigma_2+\sigma_3$; σ_1, σ_2, and σ_3 are the three principal stresses, τ_{oct} = octahedral shear stress; $\tau_{oct} = (\sqrt{2}/3)\ (\sigma_1-\sigma_3)$, Ψ_m = matric suction; X_w = Bishop's parameter, P_a= atmospheric pressure, and k_1, k_2, k_3 = regression constants.

Recently Gupta et al. (2007) proposed a new analytical model presented in the following equation:

$$M_r = k_1 p_a \times \left(\frac{\theta - 3k_6}{P_a}\right)^{k_2} \times \left(\frac{\tau}{P_a} + k_7\right)^{k_3} + \alpha_1 \times (u_a - u_w)^{\beta_1} \quad \textbf{(4.5)}$$

where, k_1, k_2, k_3, k_6, k_7, α_1, β_1 are regression parameters and u_a-u_w is the soil matric suction. Gupta et al. (2007) reported that such a model is simple and does not require measurements of both water content and suction to estimate the resilient modulus.

Cary and Zapata (2010) proposed a regression model by incorporating suction as a fundamental variable within the stress state for unsaturated soils, as follows:

$$M_r = k_1^{'} p_a \times \left(\frac{\theta_{net} - 3\Delta u_{w-sat}}{P_a} \right)^{k_2^{'}} \left(\frac{\tau_{oct}}{P_a} + 1 \right)^{k_3^{'}} \left(\frac{\left(\psi_{m_0} - \Delta \psi_m \right)}{P_a} + 1 \right)^{k_4^{'}} \quad \textbf{(4.6)}$$

where, $\theta_{net} = \theta - 3u_a$ = net bulk stress, Δu_{w-sat} = build up of pore water pressure under saturated conditions, in this case $\Delta \psi_m = 0$, τ_{oct} = octahedral shear stress, ψ_{m_o} = initial matric suction, $\Delta \psi_m$ = relative change of matric suction with respect to ψ_{m_o} due to build up of pore water pressure under saturated conditions, in this case $\Delta u_{w-sat} = 0$. Coefficients k'_1, k'_2, k'_3 and k'_4 are regression parameters.

While the Liang et al. (2007) model may be able to predict M_r due to moisture variations, it doesn't include the effect of suction hysteresis (drying/wetting) on M_r. Gupta et al. (2007) model predicts M_r values only at a specific suction (as compacted). Also, Cary and Zapata (2010) model predicts M_r based on regression analysis due to changes in matric suction (drying only) without hysteresis. The work described herein provides information to better understand the influence of the suction hysteresis on M_r, and proposes a new model to predict the M_r due to hysteresis for a cohesionless fine-grained soil.

4.3 SUCTION-CONTROLLED RESILIENT MODULUS TESTS

Figure 4.1 shows an illustration of the suction control M_r test setup. In this study, M_r tests were performed in accordance with the AASHTO T 307-99 test method. M_r tests consisted of applying a cyclic haversine-shaped load with a duration of 0.1 seconds and rest period of 0.9 seconds. For each sequence, the applied load and the vertical displacement for the last five cycles were measured and used to determine M_r. The load was measured by using an internally mounted load cell with a capacity of 2.23 kN (500

lbf). The resilient displacements were measured using two linear variable differential transformers (LVDT's) fixed to opposite sides and equidistant from the piston rod outside the test chamber, refer to Figure 4.1. The LVDT's had a maximum stroke length of 5.0 mm (0.2 in). In this study, with a 16-bit data acquisition card, the LVDT resolution used for M_r tests was estimated at approximately $5.0/2^{16} = 7.63 \times 10^{-5}$ mm. The expected M_r displacement for unsaturated soil, in the range of suction (or moisture content) used in this study is generally between 1.4×10^{-2} mm to 3.5 mm. Therefore, the deviation or maximum relative error was approximately in the range of 0.002 %-0.6 %.

M_r tests were conducted on remolded specimens; while the effect of soil suction was evaluated using controlled suction via an automated system to control air pressure and water pressure in the sample using the axis translation technique (Fredlund and Rahardjo 1993). The pore water pressure (u_w) was digitally controlled using a commercially available, high precision, motorized piston pump and transmitted to the bottom of the soil sample via a high air entry porous disc (HAEPD). A similar pump, having a larger piston volume, was used to control the air pressure (u_a) on top of the sample in order to apply matric suction (u_a-u_w). These pumps can accurately resolve pressure and volume changes on the order of 1 kPa and $1mm^3$, respectively. Air pressure in the chamber (σ_3) above the confining fluid (water) was controlled using a regulator and monitored using a pressure gage with a resolution of about 0.7 kPa.

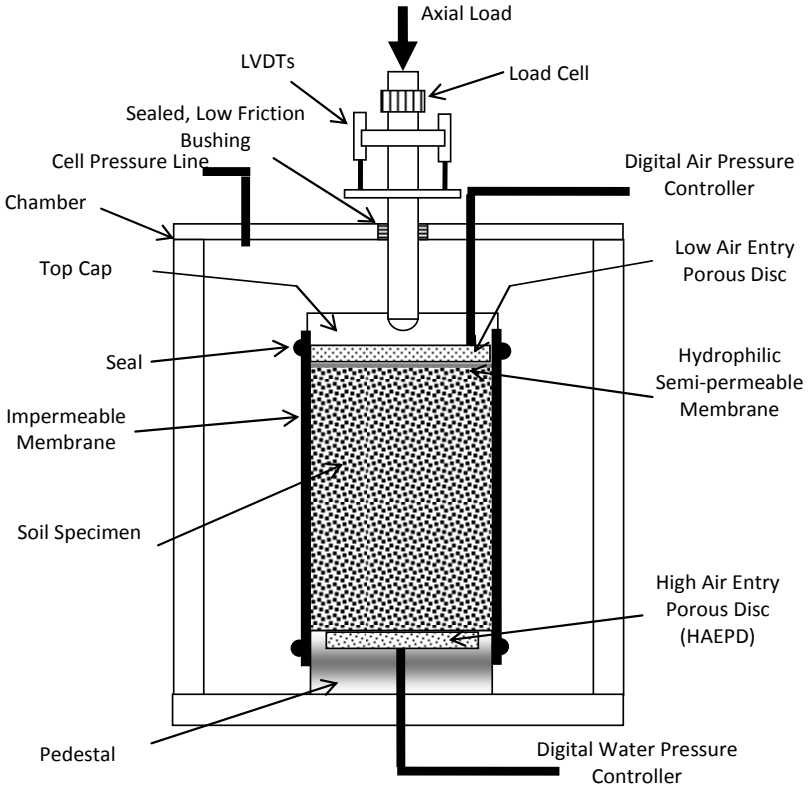

Figure 4.1- Schematic Plot of the Triaxial/Resilient Modulus Testing Cell for Unsaturated Soils (not to scale)

The procedure and loading patterns used to study the influence of suction hysteresis (i.e. drying, wetting and scanning curves) on M_r are illustrated schematically in Figure 4.2, and summarized as follows:

1. Water was first conditioned in the tubes and pumps. The HAEPD was then saturated by applying water pressure of about 14 kPa (2 psi) underneath the disk. The water pressure was applied for about 48 hours during which de-aired water was flowing out of the HAEPD.

2. After HAEPD saturation, the compacted soil sample was mounted on top of the HAEPD; the sample was sealed by a membrane and the chamber filled with water. A minimal cell pressure of 14 kPa (2 psi) was applied to hold the sample together while the valves connecting to the pore water pressure were open.
3. The desired net confining stresses and matric suction were applied using the axis translation technique. For this study, pore water pressure (u_w) was held constant at a pressure of 15 kPa, while increasing the air pressure (u_a) and cell pressure to reach the desired target suction values (25 kPa, 50 kPa, 75 kPa and 100 kPa) and net confining stresses (41 kPa, 28 kPa, and 14 kPa). Basically, the soil sample was dried out by increasing the suction on the drying path (i.e. primary drying) starting from a compacted suction value of approximately 8 kPa.
4. After reaching equilibrium of suction (e.g. 25 kPa), an M_r test was conducted at the three net confining stresses (41 kPa, 28 kPa, and 14 kPa). Equilibrium of suction was assumed when changes in water content became negligible.
5. After the M_r test, suction was increased following the drying path (e.g. suction of 50 kPa, 75 kPa and 100 kPa). At the end of the drying curve, the soil sample was wetted (primary wetting) by decreasing u_a to reach target suctions similar to that of the drying paths. Sample was tested for M_r at each suction value (e.g. 25, 50, 75, and 100 kPa) on the way up (drying) or down (wetting) the SWCC path.
6. Step 5 was repeated again so that the secondary drying/wetting and scanning curves were developed, resulting in a relationship between resilient modulus and matric suction called herein the resilient modulus characteristic curve (MRCC).

In this study, M_r tests were conducted at different suction values along the drying, the wetting path and the secondary drying and wetting curves. Table 4.1 summarizes the cell pressure (σ_3), pore air pressure (u_a), and pore water pressure (u_w) for each target suction (u_a-u_w) and net confining stress (σ_3-u_a). It is noteworthy to mention that M_r in this aforementioned procedure was performed on the same sample at each target suction value along the drying and wetting paths. However, in order to check influence of previous M_r loading history on the results, selected samples are tested at different points on the SWCC without previous M_r testing. For example, samples were tested for M_r at suction along the drying curve without previous M_r testing at lower suction values. Similar samples were also prepared and subjected to drying then wetting and tested on the wetting curve with similar suction of that on the drying curve.

Table 4.1- Summary of the Suction Control Test Conditions

Target Suction u_a-u_w (kPa)	Target Net Confining Stress σ_3-u_a (kPa)	Cell Pressure (σ_c)	Pore Water Pressure (u_w)	Pore Air Pressure (u_a)
25	41	81	15	40
	28	68	15	40
	14	54	15	40
50	41	106	15	65
	28	93	15	65
	14	79	15	65
75	41	131	15	90
	28	118	15	90
	14	104	15	90
100	41	156	15	115
	28	143	15	115
	14	129	15	115

(a)

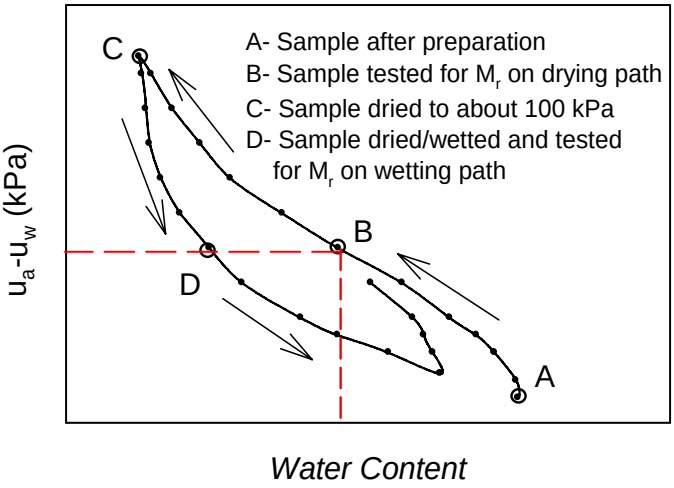

(b)

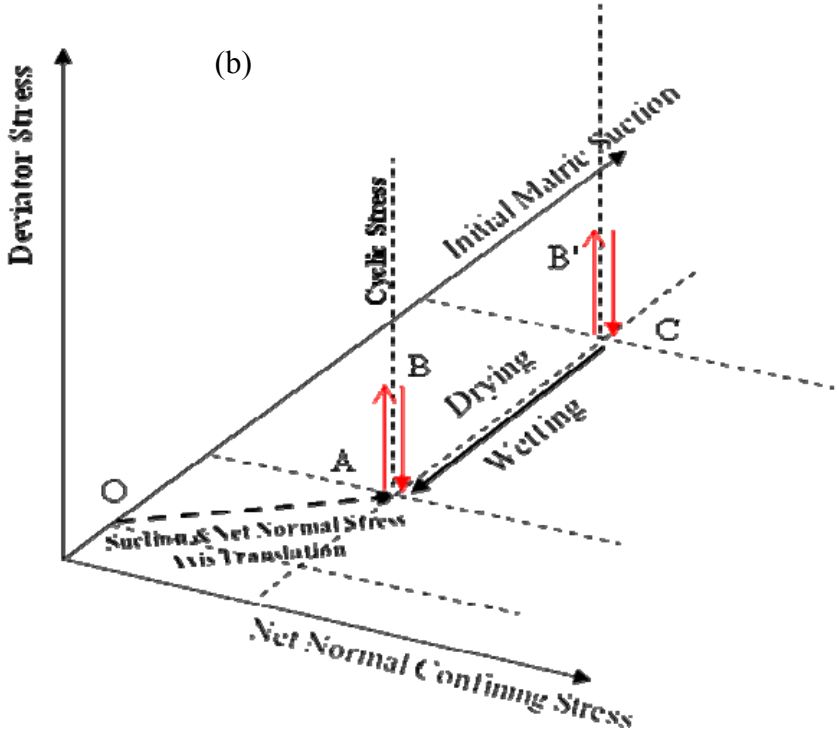

Figure 4.2- Illustration of (a) Suction Hysteresis and M_r Tests, (b) Suction-Stress Path Loading History

4.4 RESILIENT MODULUS TEST RESULTS AND DISCUSSIONS

4.4.1 Samples Continuously Tested for M_r along the Drying and Wetting Curves

4.4.1.1 Equilibrium of Matric Suction and Net Confining Stress

During the suction-controlled M_r tests, the change in moisture content for each desired suction value was recorded and plotted versus time, as shown in Figure 4.3. As can be seen in Figure 4.3, water flowed out of the sample during drying and then back into the sample during wetting. Suction was assumed to reach equilibrium when negligible change of water content was observed. Figure 4.3 indicates that more than 3 months was needed to generate M_r tests for primary drying, primary wetting, and secondary drying for the manufactured soil used in this study.

The relationship between suction and gravimetric water content (at the end of suction equilibrium) was obtained during the M_r test as shown in Figure 4.4. A comparison of this relationship with the SWCC's at different net confining stresses is shown in Figure 4.5. The relationship between suction and water content during the suctioncontrolled resilient modulus tests in this study seems reasonably consistent with the SWCC results. That the SWCC from M_r testing is rotated slightly clockwise relative to the other curves may be due to the complex stress history of the test, which affect the void ratio of the soil specimen during testing. Also, M_r SWCC represents isotropic net normal stress while other SWCCs represent 1-D net normal stress states in oedometer.

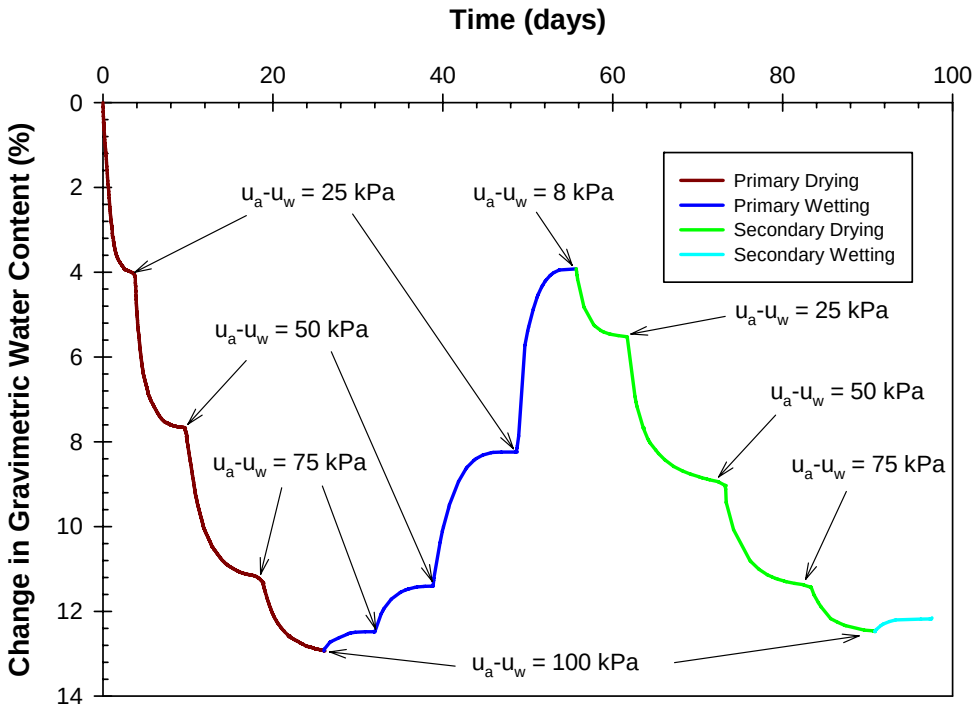

Figure 4.3- Water Content Change for Primary Drying, Wetting, Secondary Drying and Wetting

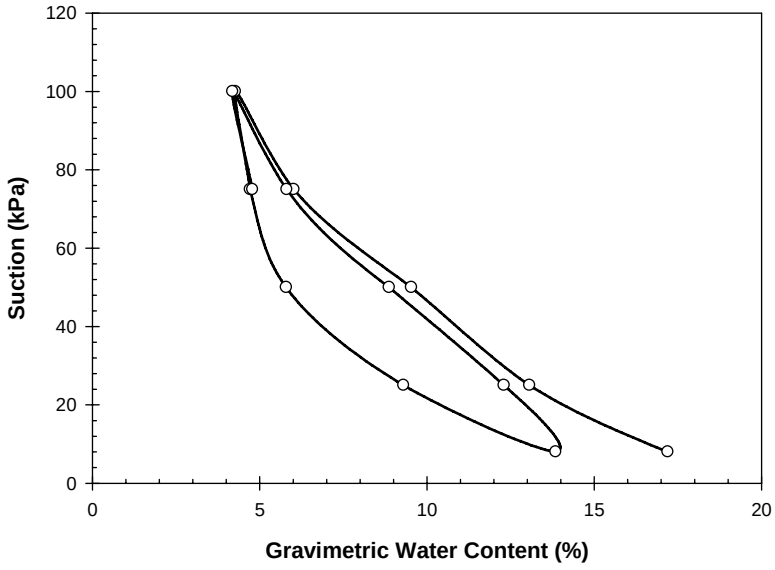

Figure 4.4- Suction versus Gravimetric Water Content Obtained During M_r Suction Control Tests

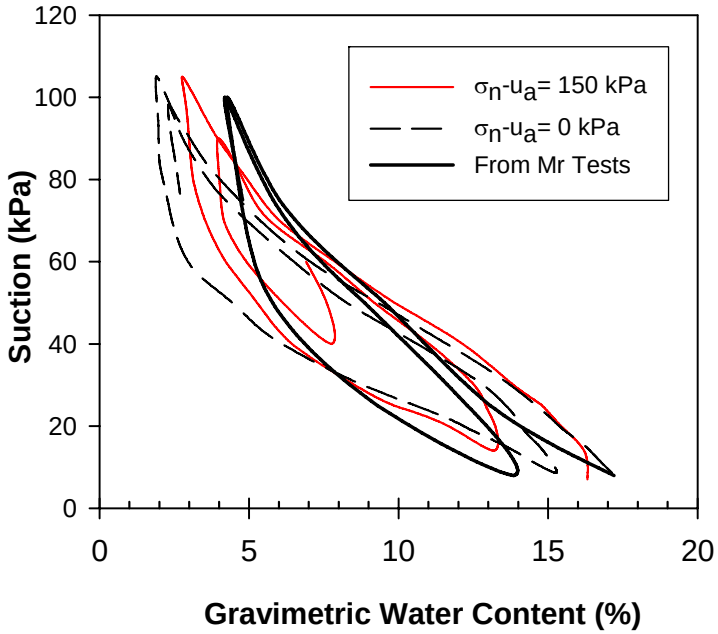

Figure 4.5- Comparison of Soil-Water Characteristic Curves from M_r Suction Control Tests with SWCC at Net Normal Stresses of 0 kPa and 150 kPa

4.4.1.2 Effect of Suction Hysteresis on Resilient Modulus (M_r Characteristic Curve MRCC)

Figure 4.6 shows resilient modulus (M_r) versus deviator stress (σ_d), for various net confining stress of 41 kPa (6 psi), 28 kPa (4 psi) and 14 kPa (2 psi) under different matric suction values (25, 50, 75 and 100 kPa) on the primary drying curve of the SWCC. In general, results (Figure 4.6) indicate that M_r increases slightly with increasing deviator stress. This increase seems more pronounced at higher suction values (e.g. 100 kPa); this behavior was also observed by Yang et al. (2008) for a residual lateritic and pulverized mudstone soils both classified as lean clayey (CL) soil.

In this study, the effect of suction hysteresis variations was evaluated on the M_r values determined at a bulk stress (θ) of approximately 154.6 kPa (22.5 psi) and at an octahedral stress (τ) of 14 kPa (2 psi) as suggested by SHRP Protocol P-46). The generalized universal model (Equation 4.1) adopted by the MEPDG was used for this

purpose. In this model, the resilient modulus (M_r) is expressed as a function of bulk stress (θ) and octahedral stress (τ). Model parameters (k_1, k_2 and k_3) and M_r values at the aforementioned stresses, for primary drying (PD), primary wetting (PW), and secondary drying (SD) and secondary wetting, (SW) are summarized in Table 4.2.

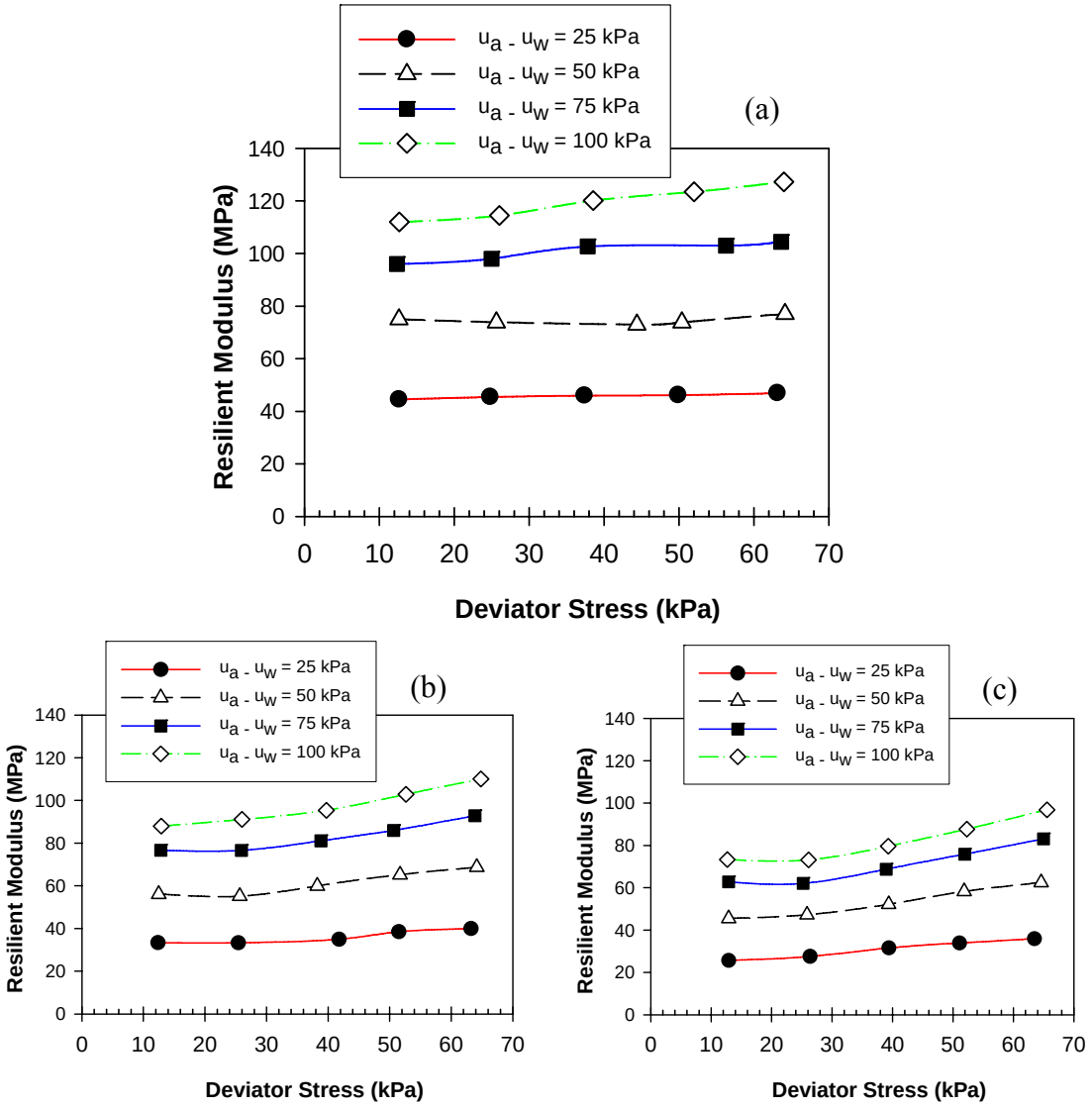

Figure 4.6- Resilient Modulus versus Deviator Stress for Different Suction Values during Primary Drying at (a) Net Confining Stress of 41 kPa (6psi), (b) Net Confining Stress of 28 kPa (4psi) and (c) Net Confining Stress of 14 kPa (2psi)

Table 4.2- A Summary of Model Parameters and M_r Values a Net Confining Stress of 41 kPa and Deviator Stress of 28 kPa

Condition	Suction (kPa)	w(%)	k_1	k_2	k_3	R^2	M_r (MPa)
Primary Drying	8	17.2	235.5	0.4339	-0.1609	0.900	28.1
	25	13.1	356.5	0.5640	-0.3733	0.943	43.8
	50	9.6	590.9	0.4901	-0.2385	0.925	71.6
	75	6.1	797.9	0.5053	-0.2746	0.950	96.9
	100	4.3	927.4	0.5253	-0.2347	0.956	114.1
Primary Wetting	75	4.8	861.6	0.6194	-0.2373	0.963	110.3
	50	5.9	758.9	0.6659	-0.1984	0.943	99.5
	25	9.0	630.6	0.7197	-0.3777	0.955	82.8
Secondary Drying	25	11.0	535.3	0.6187	0.0828	0.955	71.2
	50	7.9	696.9	0.5729	0.1490	0.952	91.6
	75	5.7	887.5	0.4886	-0.0243	0.966	110.3
	100	4.4	1026.4	0.5523	-0.4020	0.952	125.2
Secondary Wetting	75	4.7	910.9	0.6125	-0.1831	0.942	117.0
	50	5.7	783.9	0.6316	-0.0431	0.9412	100.7
	25	7.6	629.3	0.6332	0.3092	0.9631	84.5

Figure 4.7 shows the M_r-(u_a-u_w) relationship, known as MRCC, at the aforementioned stress levels. Some important observations were made based on Figure 4.7 and Figure 4.8, which are typical of the suction-controlled M_r test results at all stress levels:

1. Resilient Modulus increased with increased matric suction (drying), and decreased as suction decreased (wetting). The increase in resilient modulus was attributed to the fact that higher soil suction results in stiffening of the specimens, and thus higher resilient modulus. It seems that higher suction increases the integrity of soil structure (i.e., increasing rigidity of soil skeleton). This behavior is consistent with the work of Yang et al. (2008), Gupta et al. (2007), Khoury and Zaman (2004), and Motan and Edil (1982).
2. At a given suction value, M_r values along PD and SD curves were lower than the corresponding values on the PW curve. For example, the average M_r value on PD at a suction of 50 kPa was 74 MPa (10.73 ksi) compared to

approximately 101 MPa (14.65 psi) on *PW*. It is an indication that the MRCC relationship of compacted subgrade, due to wetting and drying, is hysteretic.

The fact that the M_r tests were performed on the same sample at each target suction along the drying and the wetting, raises a question as to the reason behind the higher M_r on the wetting than on the drying curves. Would that difference be attributed to suction hysteresis only, to cyclic stress loading history, or to a combination of both? To this end, selected tests were performed at target suction without previous M_r tests as discussed in the next section (Section 4.4.2).

The M_r-(u_a-u_w) relationship, at a different stress level (i.e., for net confining stress of 14 kPa and deviator stress of 69 kPa, which is the worse condition with highest deviator stress and lowest confining stress) is also shown in Figure 4.8 superimposed with the MRCC at the previously mentioned stress level. Similar behavior of MRCC, discussed above, was observed at both stress levels. However, at given suction as deviator stress increased and net confining stress decreased, M_r decreased resulting in a downward shift in MRCC (Figure 4.8).

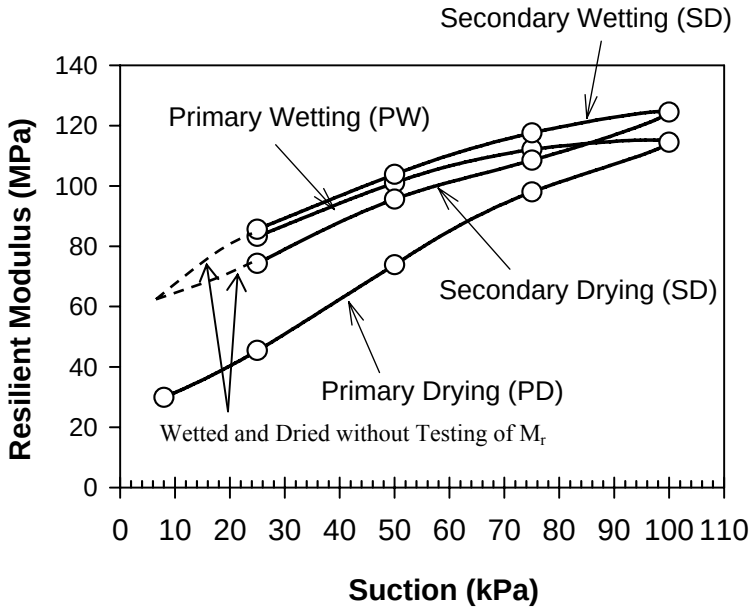

Figure 4.7- Resilient Modulus Characteristic Curve (MRCC) at Net Confining Stress of 41 kPa (6psi) and Deviator Stress of 28 kPa (4psi)

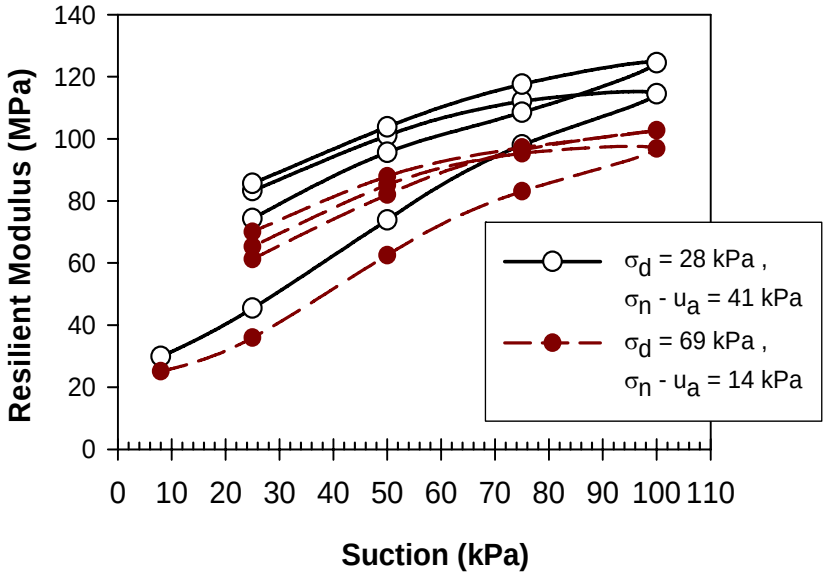

Figure 4.8- Resilient Modulus Characteristic Curve (MRCC) for Two Different Stress Levels

One repeated M_r test was conducted following the same suction path to investigate experimental variability. Figure 4.9 shows the comparison of results from the two nominally identical tests. For the repeat test, only the primary drying and a portion of the

primary wetting curve were obtained because the system developed a leak that could not be repaired during testing. Nevertheless, the comparison of the MRCC curves was favorable. While the number of repeat tests was limited, the results for a duplicate test (of the primary drying and wetting paths) demonstrate that the MRCC was reproducible to reasonable accuracy.

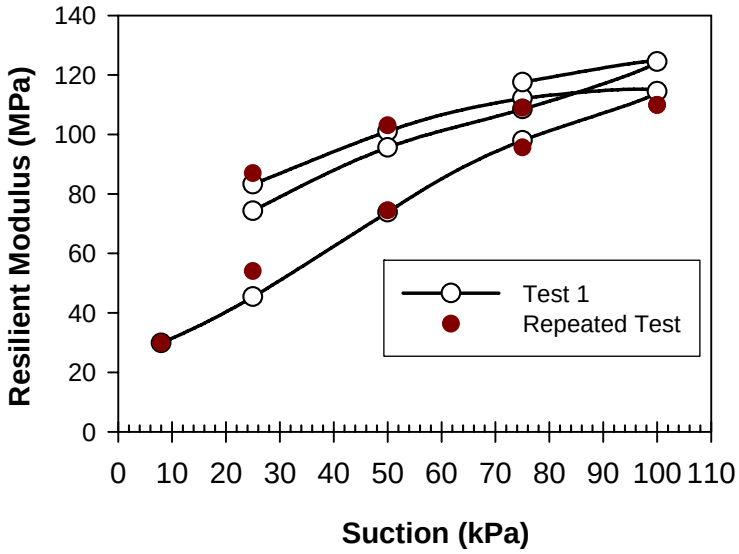

Figure 4.9- Comparison of MRCC Results from Two Nominally Identical Tests at net confining stress of 41 kPa and deviator stress of 28 kPa

4.4.2 Test Results for Samples without Previous M_r Testing

Selected samples were tested at different points on the SWCC without previous M_r testing. One sample was tested for M_r at suction of 50 kPa along the drying curve without previous M_r testing at lower suction values. A similar sample was also prepared and subjected to drying then wetting (DW) and tested on the wetting curve at suction of 50 kPa which is similar suction to that on the drying. Also similar samples were tested at 25 kPa on the drying (D) and on the wetting (DW) curves without any previous M_r tests. Suction and net confining stress equilibrium and M_r results are presented below.

4.4.2.1 Equilibrium of Matric Suction and Net Confining Stress

The change in moisture content at the desired suction values was recorded and plotted versus time as shown in Figure 4.10 and Figure 4.11 for each test. Comparison of results between tests at 50 kPa suction on the drying (D) and wetting (DW) are shown in Figure 4.10 while the results for (D) and (DW) tests at suction of 25 kPa are shown in Figure 4.11. From these figures it is observed that water flowed out of the sample during drying and then back into the sample during wetting. Suction was assumed to reach equilibrium when negligible change of water content was observed. Results indicate that approximately the same amount of water was drained out of sample in all tests at a specific suction (e.g., at suction of 50 kPa on the drying curve of Figure 4.10 and suction of 25 kPa on drying curve of Figure 4.11).

The relationship between suction and gravimetric water content (at the end of suction equilibrium) was obtained during the M_r test and shown together in Figure 4.12 along with results for samples previously tested for M_r. Figure 4.12 indicates that water content changes due to suction applications for all tests are significantly comparable.

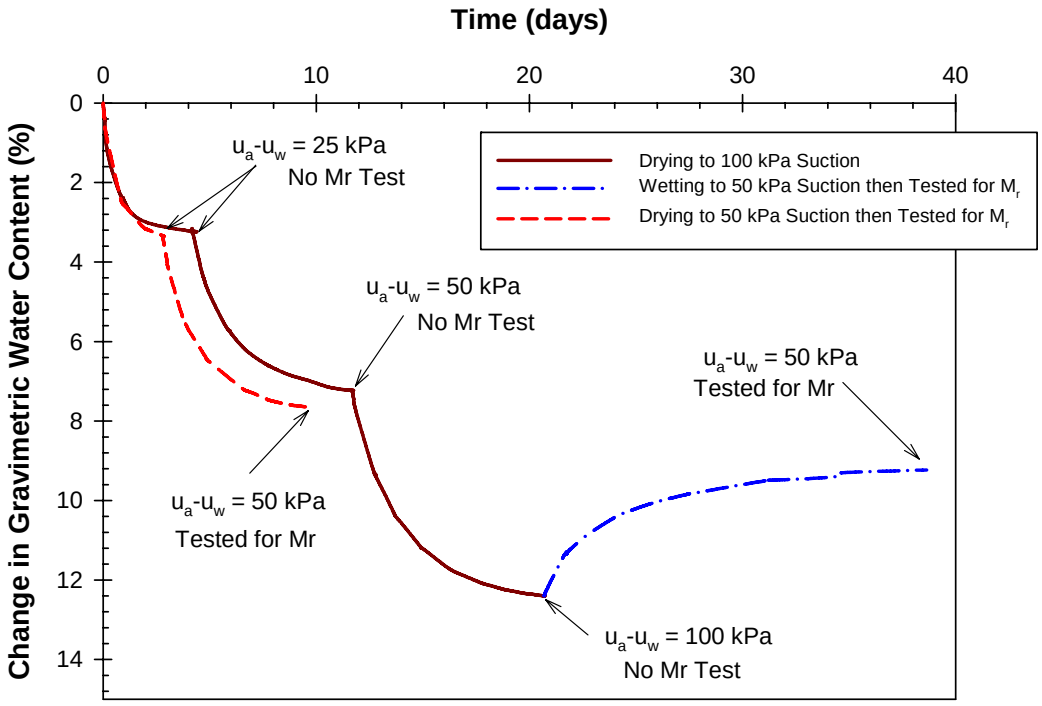

Figure 4.10- Comparison of Water Content Change for both Samples on Drying Curve and Wetting after Drying at target Suction of 50 kPa

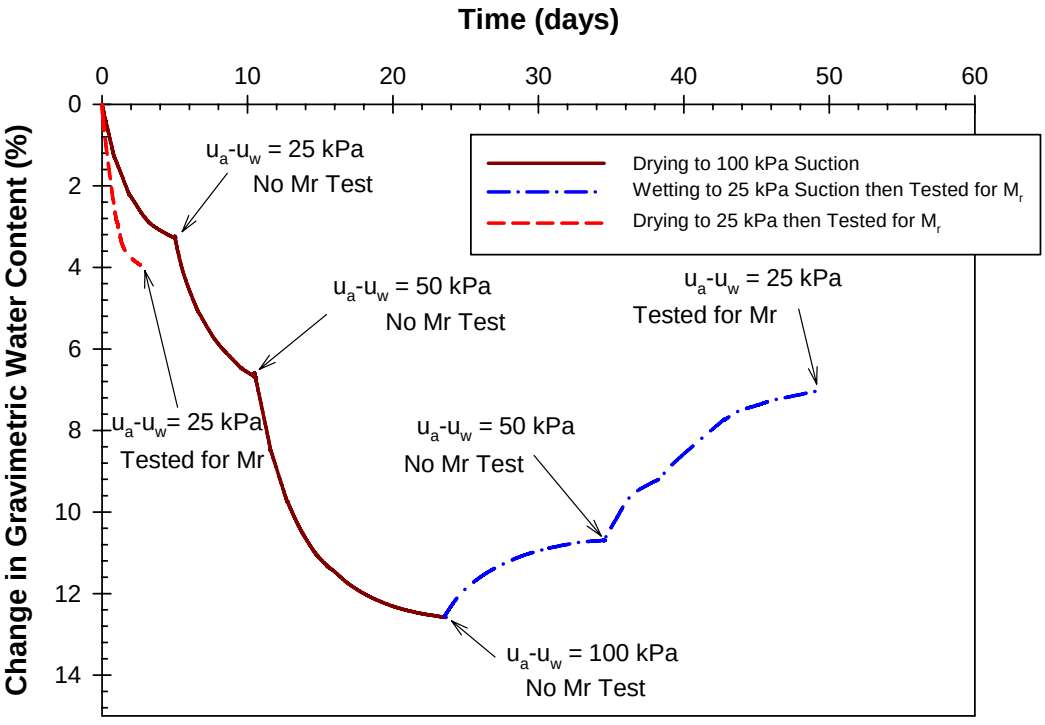

Figure 4.11- Comparison of Water Content Change for both Samples on Drying Curve and Wetting after Drying at target Suction of 25 kPa

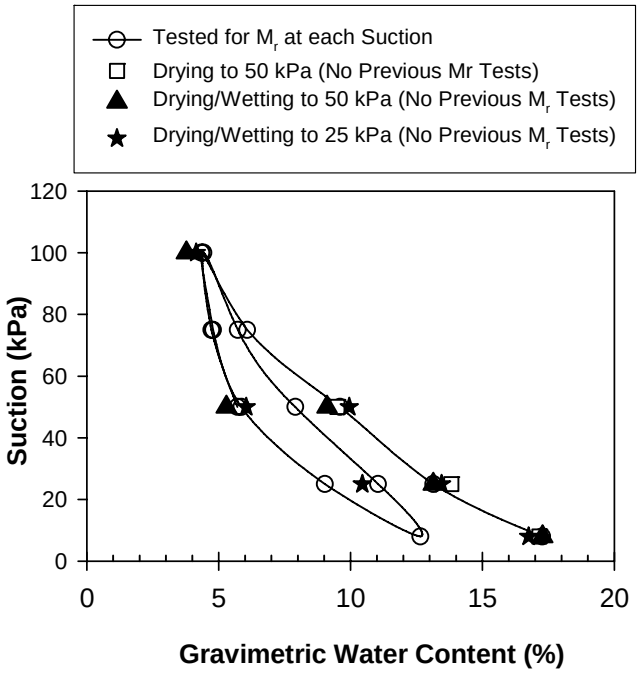

Figure 4.12- Results from M_r Suction Control Tests with no Previous M_r Tests Compared to Results with Previous M_r Tests at each Suction Value

4.4.2.2 Resilient Modulus Results

This section presents results for the tests without previous M_r, which were conducted to check the effect of suction excluding the influence of previous M_r loading history on the results. The M_r values were determined using Equation (4.1) and presented here for a bulk stress of approximately 154.6 kPa (22.5 psi) and at an octahedral stress of 14 kPa (2 psi). Figure 4.13 and Figure 4.14 show the M_r results versus deviator stress (σ_d), for a net confining stress of 41 kPa (6 psi) at matric suction values, on the primary drying (D) and wetting (DW) curve, of 25 and 50 kPa, respectively. In general, results for both drying and wetting tests in those figures indicate that M_r increases slightly and nonlinearly with increasing deviator stress. On the other hand, for all deviator stress values, M_r results on the wetting curves were higher than the values on the drying curves. The Model

parameters and M_r values for the corresponding tests for primary drying (D), and primary wetting (DW) are presented in Table 4.3.

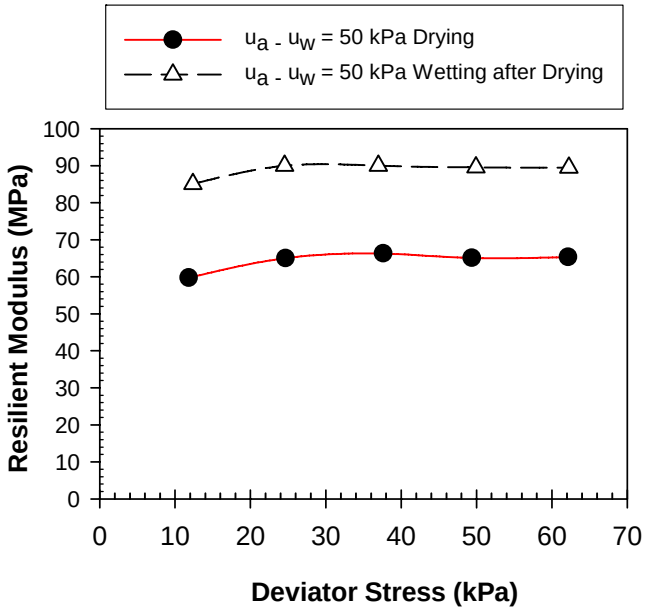

Figure 4.13- Comparison of Resilient Modulus versus Deviator Stress at Net Confining Stress of 41 kPa for Samples not previously Tested for M_r at Suction of 50 kPa

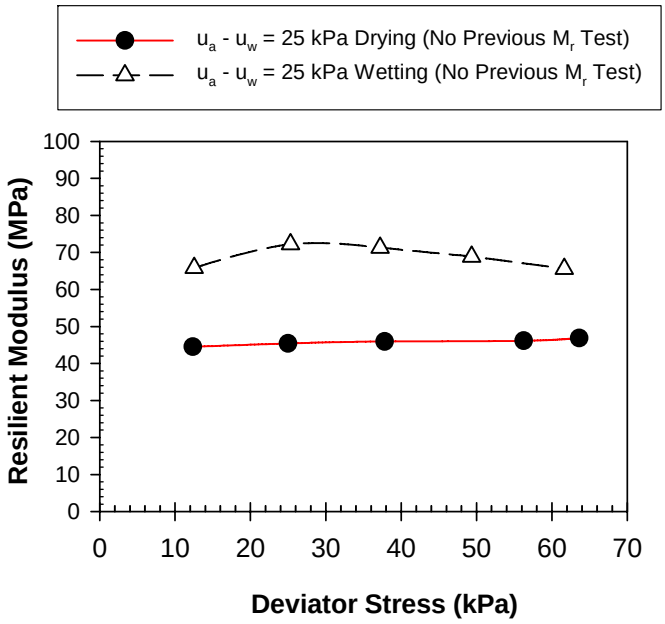

Figure 4.14- Comparison of Resilient Modulus versus Deviator Stress at Net Confining Stress of 41 kPa for Samples not previously Tested for M_r at Suction of 25 kPa

Table 4.3- A Summary of Model Parameters and M_r Values for Tests without Previous M_r

Condition	Suction (kPa)	w(%)	k_1	k_2	k_3	R^2	M_r (Mpa)
Primary Drying	50	9.4	535.2	0.4209	-0.3066	0.946	62.4
Primary Wetting	50	5.3	730.2	0.4818	-0.4105	0.938	86.2
	25	9.8	567.0	0.5921	-0.7960	0.926	66.9

4.4.3 Effect of Suction and Stress History on Resilient Modulus

Figure 4.15 presents the M_r-(u_a-u_w) relationship, known as MRCC, at a bulk stress of approximately 154.6 kPa (22.5 psi) and at an octahedral stress of 14 kPa (2 psi). This figure shows the M_r results from tests conducted continuously on a sample at each target suction superimposed with results from tests performed on similar virgin samples without previous M_r. As noted previously, data for continuous M_r tests in Figure 4.15 indicate that the MRCC relationship of compacted soil, due to wetting and drying, is hysteretic; i.e., M_r values on the wetting curves were higher than those on the drying curves.

Results from three tests without previous M_r (w o/p M_r) were lower than the results from a sample tested continuously (CM_r) at each suction value. This indicates that M_r results are influenced by the continuous stress loading; however, M_r along the wetting curves were still higher than the drying curves for these virgin tests, and therefore indicate that results are also influenced by hysteresis.

Possible reasons for higher M_r on primary wetting (PW) than the primary drying (PD) and secondary drying (SD) curves are discussed in the following paragraph. But before presenting these factors, a brief summary of some related studies on the effect of hysteresis on M_r is first presented.

As mentioned previously, no research has been found in the literature on the effect of suction hysteresis on M_r; some studies have been conducted on the effects of moisture hysteresis on M_r and different conclusions were drawn. For example, Khoury and Khoury

(2009) and Khoury et al. (2009) observed that the M_r-moisture content relationship, for clayey soil, exhibited a hysteretic behavior due to the wetting and drying actions where M_r on the drying curve was higher than that of the wetting curve. Other research studied the effect of suction hysteresis on the shear strength of unsaturated soils, as presented in Sections 3.5.3.2 and 3.6.3.2.

On the other hand, it is interesting to mention that the same behavior (i.e. compared to M_r) of higher shear strength on wetting than drying for unsaturated soils and rough steel interface was observed in this study. A discussion of reasons for such higher strength on wetting than drying is presented in Section 3.10. Those reasons and factors are also applicable to Mr tests; however, some M_r tests underwent additional cyclic deviator stress loading. Therefore, based on the findings from this study, the MRCC relationship can be affected by the following factors: (1) cyclic suction loading on specimens. Figure 4.2 shows the loading patterns used in this study; (2) cyclic deviator stress loading; (3) water-particle contact area and (4) soil type. However, results from the virgin samples tested without previous M_r tests confirm that the possible cyclic stress loading may have a minor effect on the results since: a) a slight difference in M_r was observed on tests with and without previous M_r, and b) the secondary drying resulted in lower M_r values than those of the primary wetting. Therefore, the stiffening effect and the possible water content lubricant effect (at same suction), discussed in Section 3.10 for shear strength, due to cyclic suction (i.e., hysteresis) may be the major factors resulting in the higher M_r for wetting compared to drying. It is worth to mention that this behavior (increased M_r with cyclic suction) for small strain stiffness (G_o) was also reported by Vassallo et al. (2007) among others.

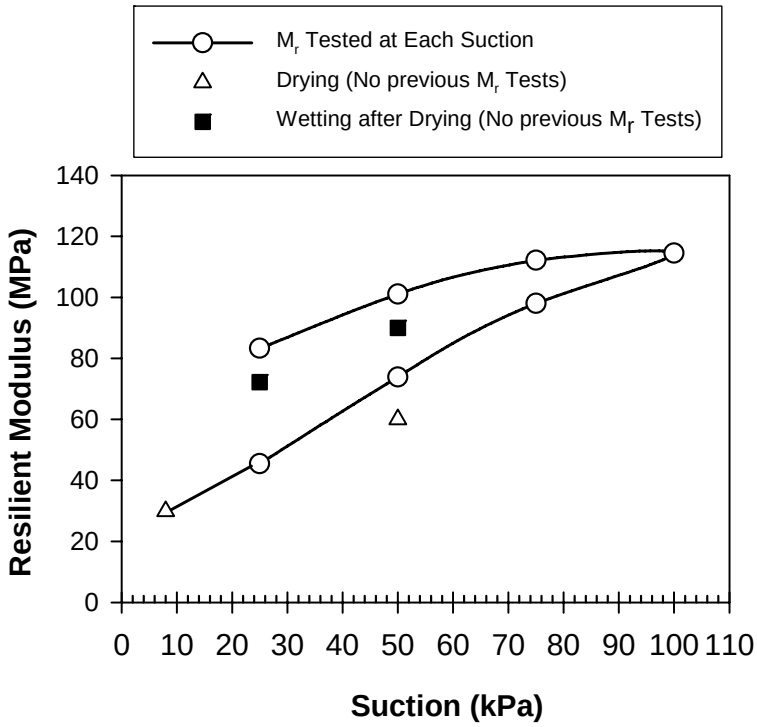

Figure 4.15- Resilient Modulus Characteristic Curve (MRCC) at Net Confining Stress of 41 kPa and Deviator Stress of 28 kPa on Samples with and without previous M_r Tests

4.5 MODELING OF RESILIENT MODULUS (M_r)

As previously discussed in Section 4.2, various research studies have been conducted to predict M_r values with suction. Recent relevant models were presented by Yang et al (2004b), Gupta et al. (2007) and Cary and Zapata (2010) most of which maybe be able to predict M_r values only at a specific suction or due to moisture variations (e.g. Liang et al. 2007), but were not developed to capture the effect of suction hysteresis (drying/wetting) on M_r. In addition, most of these models are based on regression analysis on specific types of soils. Therefore, in this study the results from suction-controlled M_r test including drying and wetting (hysteresis) were used to develop models to predict M_r values due to drying and due to hysteresis (wetting after drying) based on the SWCC.

In this study, M_r results were plotted versus suction and defined as MRCCs (e.g. Figure 4.15). One set of tests were conducted for M_r on fresh samples (virgin tests) at a

given target suction value without any previous M_r tests. This set of tests indicated an increase of M_r with increase of suction along the drying curve, and was modeled using Equation (4.7), which is a modification of the universal model to account for variation of suction.

$$M_R = \left(k_1 p_a \times \frac{\theta_b}{p_a}^{k_2} \times (\frac{\tau}{p_a} + 1)^{k_3} \right) + (\psi - \psi_o)\left(\frac{\theta_d}{\theta_s} \right)^k \quad (4.7)$$

where, the first part $\left(k_1 p_a \times \frac{\theta_b}{p_a}^{k_2} \times (\frac{\tau}{p_a} + 1)^{k_3} \right)$ represents the universal model equation, ψ = suction, ψ_o = low suction corresponding to the M_r test (e.g. wet of optimum), θ_d = volumetric water content along the drying curve, θ_s = volumetric water content (obtained from SWCCs) at zero suction, *k = 1/n*, *n* is a model parameter obtained from Fredlund and Xing (1994) fitting model (Equation 2.4) of SWCC.

The second part $(\psi - \psi_o)\left(\frac{\theta_d}{\theta_s} \right)^k$ of equation (4.7), represent aims at capturing the contribution of suction to the increase in M_r. By conducting an M_r test at any low suction value (defined as ψ_o), the rest of the drying curve can be predicted using the proposed model, which relates to the SWCC. Thus, the initial suction (ψ_o) was subtracted from the suction term (ψ) in the equation; suction is multiplied by the ratio (θ_d/θ_s), which accounts for the change in water content with suction along the drying curve similar to the approach by Vanapalli et al (1996) formulation for the shear strength. Then, the use of this volumetric water content ratio was subjected to the exponent *k*, which relates directly to the SWCC thorugh the parameter '*n*' and describes the rate of suction change

due to change in water content. This exponent has also been used in the prediction equation for shear strength of unsaturated soils and interfaces (Section 3.8.2).

To appreciate the potential of the model to capture the effect of suction increase on M_r, the predicted results along the drying path are plotted together with the experimental data as shown in Figure 4.16. In this figure it is apparent that the model matches the experimental M_r results from the virgin tests.

In an attempt to validate the proposed model, experimental results from the literature by Cary and Zapata (2010) and Yang et al. (2008) were predicted using the proposed equation (Equation 4.7). Comparison between the model prediction and the experimental results from Cary and Zapata (2010) and Yang et al. (2008) for drying tests is shown in Figure 4.17, and Figure 4.18, respectively. These figures indicate that the proposed model predicted well the experimental results.

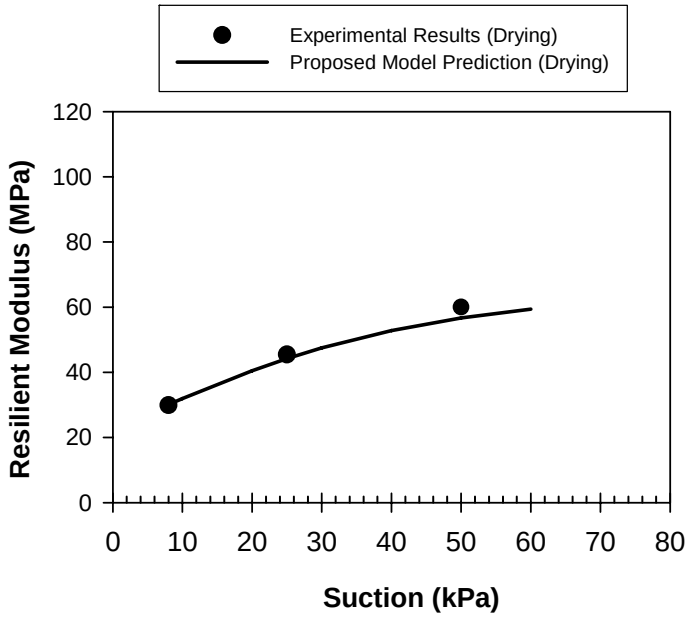

Figure 4.16- Comparison of Model Prediction with the Experimental Results from Virgin M_r Tests along the Drying Curve at Net Confining Stress of 41 kPa and Deviator Stress of 28 kPa

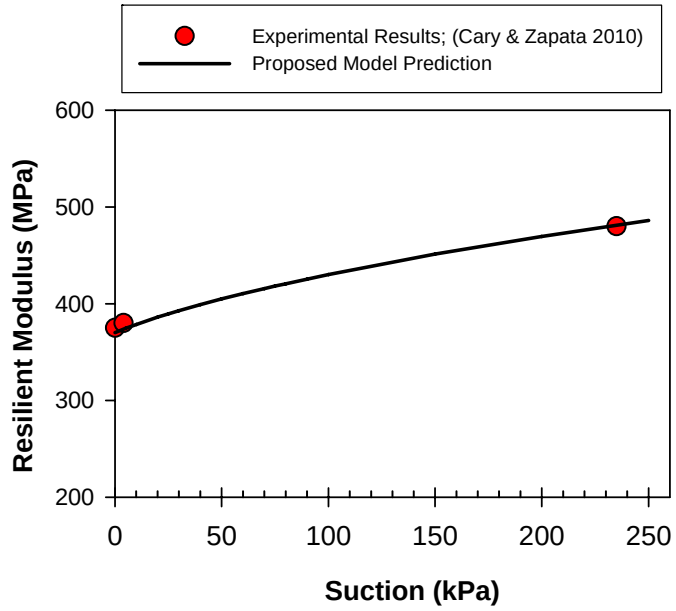

Figure 4.17- Comparison between the Predicted M_r from the Proposed Model and the Experimental Results from Cary and Zapata (2010)

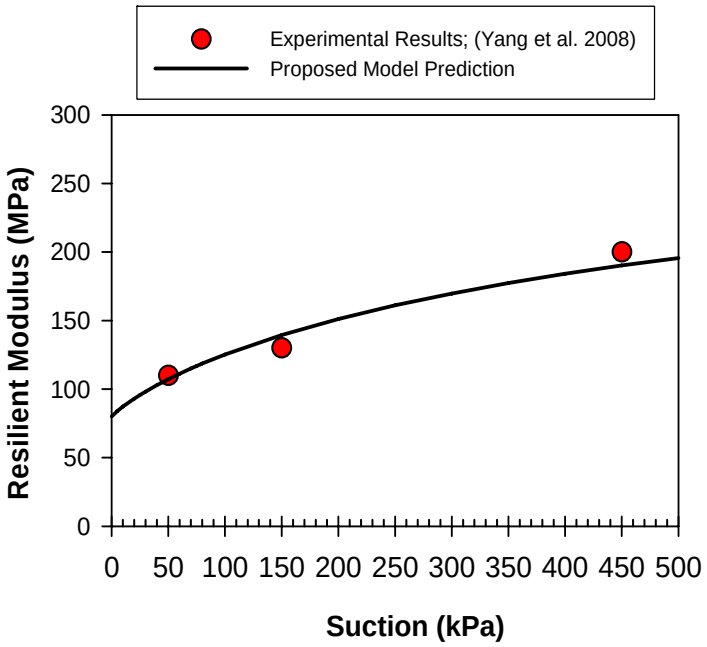

Figure 4.18- Comparison between the Predicted M_r from the Proposed Model and the Experimental Results from Yang et al. (2010)

The model was further expanded to predict the M_r results due to hydraulic hysteresis (wetting after drying). The proposed model is shown as Equation (4.8), from which M_r hysteresis can be predicted by relating directly to the hysteretic behavior of the SWCC.

$$M_R = \left[\left(k_1 p_a \times \frac{\theta_b}{p_a}^{k_2} \times (\frac{\tau}{p_a} + 1)^{k_3} \right) + (\psi - \psi_o) \times \left(\frac{\theta_d}{\theta_s} \right)^k \right] \times (F_{DW}) \quad \textbf{(4.8)}$$

where, $F_{DW} = \theta_d/\theta_w$, θ_d = volumetric water content along the drying curve, θ_w = volumetric water content along the wetting curve corresponding to same suction as for θ_d. The first part of the equation $\left[\left(k_1 p_a \times \frac{\theta_b}{p_a}^{k_2} \times (\frac{\tau}{p_a} + 1)^{k_3} \right) + (\psi - \psi_o) \times \left(\frac{\theta_d}{\theta_s} \right)^k \right]$ represents the M_r prediction along the drying curve, which is multiplied by the factor F_{DW} ($=\theta_d/\theta_w$) to give the values of M_r on the wetting path. This is similar to the formulation presented previously (Section 3.8.2.2) for the shear strength of unsaturated soils and interfaces for wetting after drying tests. Although the stress and loading conditions (i.e. cyclic loading) of M_r tests are different than the direct shear tests (i.e. static loading), the proposed formulation (i.e. the proposed factor F_{DW} for predicting wetting based on drying tests) seems to significantly capture the effect of hysteresis for both tests. Predicted M_r values from the proposed Equation (4.8) compared to the experimental data from virgin M_r tests at two different stress levels are shown in Figure 4.19 and Figure 4.20, and indicate strong agreement between the results. Corresponding model parameters, k_1, k_2 and k_3 are summarized in Table 4.3.

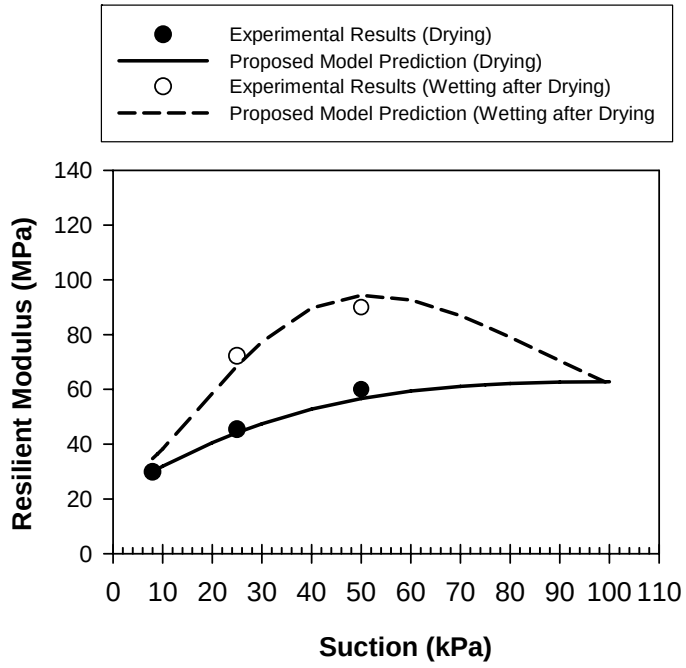

Figure 4.19- Comparison of Model Prediction with the Experimental Results from Virgin M_r Tests for both drying (D) and Wetting (DW) Results at Net Confining Stress of 41 kPa and Deviator Stress of 28 kPa

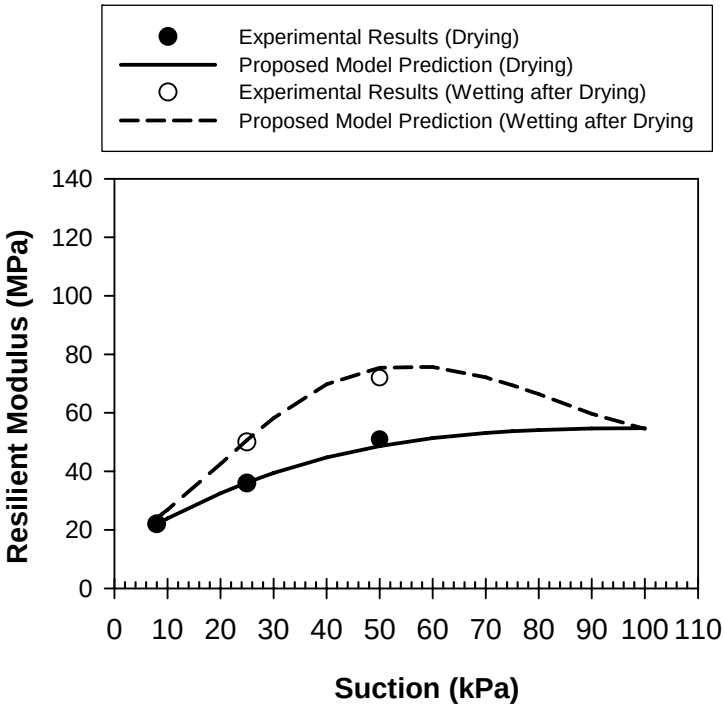

Figure 4.20- Comparison of Model Prediction with the Experimental Results from Virgin M_r Tests for both drying (D) and Wetting (DW) Results at Net Confining Stress of 14 kPa and Deviator Stress of 68 kPa

Another set of test results were obtained from the same sample with continuous M_r tests conducted along drying and wetting. This may best simulate the actual field conditions under seasonal and traffic loading variations, rather than conducting M_r at specific suction on different samples without previous M_r testing. Results from these tests were predicted using the proposed model as shown in Figure 4.21, which indicates that the model underpredicts the experimental results for both drying (D) and wetting (DW) tests. It is believed that the difference between the model prediction and experimental results is related to the hardening effect on samples from the continuous M_r tests at each suction on the same sample (resulting in accumulated net normal stress and deviator stress history) along the drying and wetting paths. Thus, a regression analysis was performed to obtain a reasonable value for the "*k*" parameter to fit the MRCC results for samples subjected to continuous M_r test. For the case of continuous M_r testing, $k = 0.05$ compared to $k = 0.70$ for virgin samples. Predicted M_r values from the proposed Equation (4.8) compared to the experimental data from continuous M_r testing at two different stress levels are shown in Figure 4.22 and Figure 4.23, and indicate strong agreement between the results. Corresponding model parameters, k_1, k_2 and k_3 are summarized in Table 4.2.

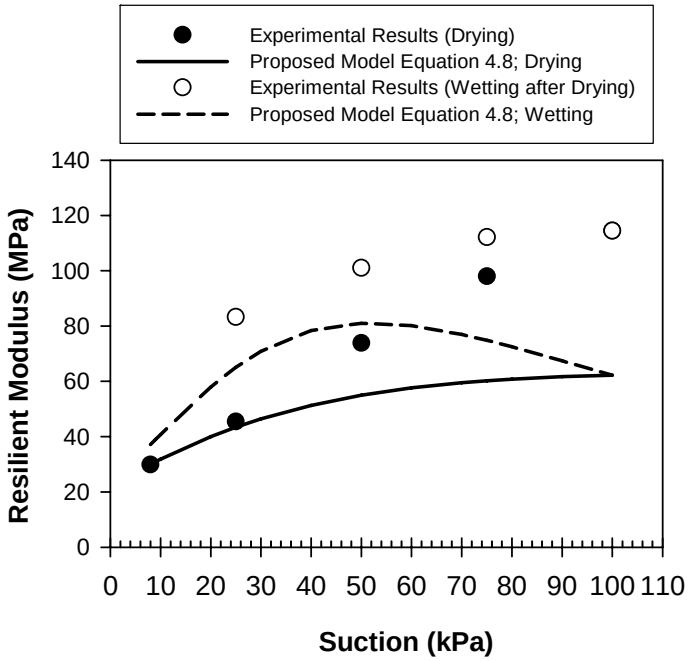

Figure 4.21- Comparison of Model Prediction (Equation 4.8) with the Experimental Results from Continuous M_r Tests for both drying (D) and Wetting (DW) Results at Net Confining Stress of 41 kPa and Deviator Stress of 28 kPa

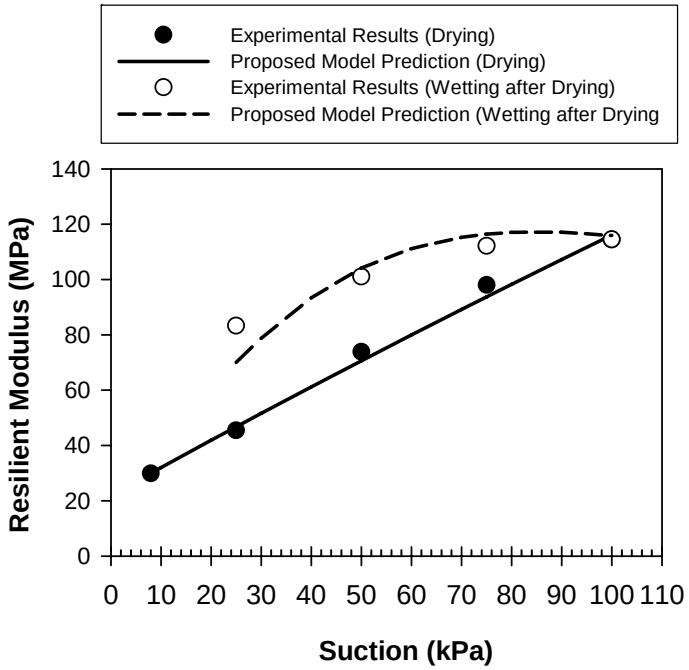

Figure 4.22- Comparison of Predicted MRCC using the Proposed Model (Equation 4.9) with the Experimental MRCC from both Drying and Wetting after Drying Tests at Net Confining Stress of 41 kPa and Deviator Stress of 28 kPa

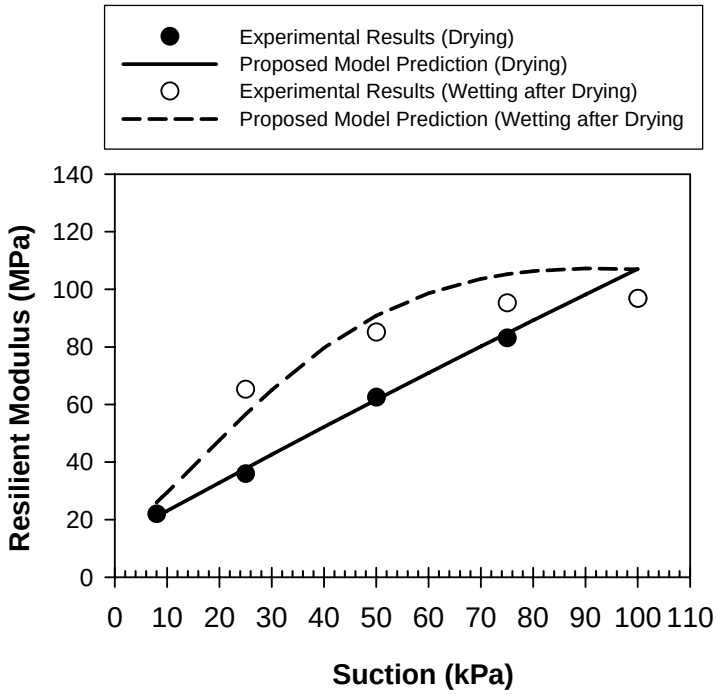

Figure 4.23- Comparison of Predicted MRCC using the Proposed Model (Equation 4.9) with the Experimental MRCC from both Drying and Wetting after Drying Tests at Net Confining Stress of 14 kPa and Deviator Stress of 68 kPa

CHAPTER 5: CONCLUSIONS AND RECOMMENDATIONS

The primary of objective of this research was to study the effect of hydraulic hysteresis (i.e. SWCC suction hysteresis) on the mechanical behavior of unsaturated soils and interfaces (i.e., rough, smooth, and geotextile interfaces) and the resilient modulus (M_r) of fine-grained cohesionless soil. To this end, it is crucial to understand and investigate first the hysteretic behavior. Thus, laboratory tests of SWCCs under different stresses along the drying, wetting, secondary drying, and along scanning curves were performed and presented. Then, suction-controlled direct shear and interface direct shear tests and Mr tests were performed at different suction values along the drying and wetting paths of SWCC. Objectives also included design and manufacturing of a custom made cell for SWCC tests, development of a new approach to decrease testing time for SWCC with hysteresis, investigation of various shear strength models for their applicability to the experimental data, application of an elastoplastic constitutive model based on the results of the laboratory testing of unsaturated rough and geotextile interfaces, development of a relationship between resilient modulus and matric suction hysteresis known as Resilient Modulus Characteristic Curve (MRCC), and development of a model to predict the resilient modulus (M_r) hysteretic behavior from the experimental results by relating it to the SWCC hysteresis. Conclusions and recommendations for future research are summarized in the following sections.

5.1 SOIL WATER CHARACTERISTIC CURVE

SWCC experimental tests were conducted in a custom-made one-dimensional testing cell to examine the coupled mechanical-hydraulic behavior of artificial unsaturated silty soil. Experimental techniques were developed and employed, which proved to be very

valuable in the timely completion of testing. On the other hand, SWCC test results obtained in this study for different stress histories (i.e. under different normal stresses) were used to validate the Muraleetharan et al. (2008) model presented in Miller et al. (2008). Some conclusions follow:

1) Use of an artificial soil composed of crushed silica and glass beads, having a grain size distribution similar to fine sandy silt, enabled a significant number of SWCC tests to be conducted in a relatively short amount of time. The main advantage of this soil is that it has a relatively high hydraulic conductivity but similar suction compared to typical natural soils with similar gradations.

2) A new approach was developed to reduce SWCC testing time. A series of SWCC tests were performed using different sample heights (e.g., 25.4 mm and 6.35 mm). Results indicated that significant time gains (i.e., testing time was reduced by 50 % when the sample height was reduced from 25.4 mm to 6.35 mm) were achieved using relatively thin samples without sacrificing accuracy with respect to volume change measurements.

3) Experimental SWCCs revealed that the air entry value tended to increase as the net normal stress increased, as expected given the decreased void ratio at higher net normal stress. The residual moisture content also increased with increases in net normal stress.

4) As the water contents approached residual saturation the slope of the SWCCs tended to change with increase in net normal stress. The volumetric water content corresponding to a net normal stress of 200 kPa was higher than on the

corresponding curve for 10 kPa net normal stress at the same suction. The constitutive model reported by Miller et al. (2008) appeared to capture this behavior quite well.

5) The constitutive model, reported by Miller et al. (2008), was able to capture the transition from unsaturated to saturated behavior exhibited by the one-dimensional collapse that occurred during sample flooding and subsequent saturated compression prior to conducting the SWCCs.

6) Functional models by Fredlund and Xing (1994) and Feng and Fredlund (1999) were used to fit the primary drying and primary wetting curves. The resulting fit parameters were used for prediction of shear strength and resilient modulus with suction.

5.2 UNSATURATED SOILS AND INTERFACE DIRECT SHEAR TESTS

5.2.1 Soil

A series of suction-controlled direct shear tests were first carried out on an unsaturated fine grained artificial soil. Tests were carried out along the drying (D) curve at different suction (0 kPa, 25 kPa, 50 kPa and 100 kPa) and net normal stress (50 kPa, 100 kPa, 150 kPa and 300 kPa) values. Other tests were performed along the wetting curve after drying (DW) in order to study the effect of hydraulic hysteresis (cyclic suction) on the shearing behavior. These hysteresis direct shear tests were performed at suction values of 8 kPa, 25 kPa and 50 kPa under net normal stresses of 50 kPa and 150 kPa. Some major findings and conclusions are summarized below:

1) The modified direct shear test device performed well and proved to be a suitable device for such testing. The net normal stress and suction were applied at target values without difficulty. This is verified by the fact that the amounts of water drained from comparable test (i.e., change in moisture content), and the magnitude of specimen compression subjected to the same suction and net normal stress values were approximately the same during the equalization phases.

2) In general, during shearing the peak shear strength was achieved followed by an immediate post peak drop in strength for both D and DW tests. A behavior more pronounced with increase in suction.

3) The peak shear strength of soil increased with increase in net normal stress and suction. However, the rate of increase was nonlinear with suction.

4) For a given net normal stress and suction, the peak and post peak shear strength from DW tests were higher compared to D tests. This is believed to be the result of cyclic suction stress loading, which may have induced irrecoverable plastic strains, resulting in sample hardening for wetting tests as compared to drying. Additionally, water may be acting as a lubricant resulting in lower shear strength for test samples D with higher water contents than DW.

5) Both D and DW tests showed a slight initial compression before dilation. Once the strain softening was completed, results showed no further dilation for tests at net normal stresses higher than 50 kPa; while at 50 kPa dilation continued during the rest of shearing.

6) During shearing, results showed that water drained out of samples for both D and DW tests as dilation started; however, although small, the amount for D tests was higher compared to DW tests. This behavior of water draining out of samples contradicts that for saturated soils (i.e., saturated soils that dilate during drained shearing typically experience water flowing into the sample) and is postulated to be related to disruption of menisci and/or non-uniformity of pore water distribution which results in an increase in localized pore water pressures.

5.2.2 Rough and Smooth Steel Interfaces

A series of suction-controlled interface direct shear tests were carried out on rough and smooth steel interfaces. For the rough interface, tests were carried out along the drying (D) curve at different suction (8 kPa, 25 kPa, 50 kPa and 100 kPa) and net normal stress (50 kPa, 100 kPa, and 150 kPa) values. Other rough interface direct shear tests were performed along the wetting curve after drying (DW) to study the effect of hydraulic hysteresis (cyclic suction) on the shearing behavior. These hysteresis tests were performed at suction values of 8 kPa, 25 kPa and 50 kPa under net normal stresses of 50 kPa and 150 kPa. A limited number of tests were performed on smooth interfaces under suction of 50 kPa and net normal stress of 100 kPa and 150 kPa. Some major findings and conclusions are summarized below:

1) During shearing, rough interface D and DW tests exhibited a strain softening behavior following peak shear strength to a post peak shear stress. Strain softening magnitude increased with increase in suction for tests at suction higher than 25 kPa, while no strain softening was observed for 8 kPa suction tests.

2) The rough interface peak shear strength increased with increase in net normal stress and suction. Similar to soil specimens, the rate of increase was nonlinear with suction. Also, the peak and post peak shear strengths from DW tests were higher compared to D tests at a given suction and net normal stress, presumably for the same reasons explained for soil tests.
3) Both D and DW tests showed slight initial compression before dilation. Dilation started as the interface peak shear strength was approached and then ceased, followed by slight compression once the strain softening was completed. Dilation magnitude decreased with increase in net normal stress.
4) Similar to soil specimens, changes in water content for both D and DW rough interface tests were detected during the shearing process. At low suction (i.e. 8 kPa), water flowed into the sample. However, at higher suction water drained out of samples for D tests, but negligible amount (<0.1 %) of water drained into the sample for DW tests. At low suction (i.e 8 kPa), samples behaved more like saturated soils; however, as described for soil specimens (bullet point # 5) at higher suction, it is believed that the menisci between soil particles are disrupted and due to the non-uniformity of pore water distribution an increase in localized pore water pressures resulted in water draining out of samples.
5) More pronounced peak shear strength was observed for rough than smooth interfaces. No strain softening was observed for smooth interfaces; however, a stick-slip behavior was observed.

6) Negligible volume change was observed for smooth interfaces compared to the slight compression then higher dilation for rough interfaces at given suction and net normal stress.

5.2.3 Geotextile Interface

Suction-controlled soil-geotextile interface direct shear tests were carried out along the drying (D) curve at different suction (0 kPa, 25 kPa, 50 kPa and 100 kPa) and net normal stress (50 kPa, 100 kPa, 150 kPa and 300 kPa) values. Some of the findings and conclusions are summarized below:

1) In general, the soil-geotextile interface exhibited slightly higher amounts of strain softening during post-peak shearing as compared to soil specimens. Both types of tests showed a slight initial compression before dilation. Once the strain softening was completed, unsaturated soil-geotextile interfaces showed no further dilation.
2) Generally, increasing net normal stress and suction in the soil-geotextile tests resulted in an increase in the interface peak shear strength. However, the rate of increase was nonlinear with suction. In some cases, the peak shear strength decreased as suction increased from 50 to 100 kPa.
3) Increase in suction resulted in a reduction in the magnitude of horizontal displacement at peak shear strength, a more pronounced strain softening behavior and in most cases, a small decrease in dilation.
4) Small decreases in water content soil-geotextile specimens were detected during the shearing process. A behavior explained by the same reasoning for soils and rough steel interfaces.

5.2.4 Modeling of Unsaturated Soils and Interfaces

Various equations have been used to model the unsaturated soils and interfaces (rough/smooth steel and geotextiles interfaces). First, the extended Mohr-Coulomb failure envelope for the unsaturated interfaces was used in a similar manner to unsaturated soils. But since a non-linear behavior was observed in failure envelopes plotted in the shear stress-suction plane, other exisiting equations based on the SWCC were used to model the experimental results. In addition, existing models seemed to underpredict the results from this study, thus new models based on the SWCC were proposed to predict shear strength with suction for both drying (D) and wetting (DW) tests. These models were also used and validated by predicting some experimental results from the literature. In addition, a general elastoplastic constitutive model was used to simulate the mechanical behavior observed in the experimental results for rough and geotextile interfaces. This model is applicable for constant net normal stress and constant suction conditions. Some of the findings and conclusions are summarized below:

1) Linearity was observed in failure envelopes plotted in shear stress (τ)-net normal stress (σ_n-u_a) plane for both D (tested along primary drying path) and DW (tested alond primary wetting path after drying) tests. Based on linear regression analysis an average value of $\phi_w' = 40^o$ (D) and $\phi_d' = 36^o$ (DW) were determined for the soil used in this study. Similarly, δ_d' and δ_w' were both equal to 32^o for a rough steel interface while $\delta_d' = 32^o$ for a geotextile interface, respectively.
2) Failure envelopes, for both D and DW for all tests (i.e., soils, rough and geotextile interfaces) plotted in τ-(u_a-u_w) plane showed a nonlinear trend for the range of u_a-u_w and σ_n-u_a used in this study.

3) Existing models underpredicted the experimental results for both D and DW tests obtained in this study. A model by Vanapalli et al. (1996) based on the SWCC was modified and the proposed model seemed to favorably predict the shear strength of unsaturated soils and interfaces due to drying and wetting (i.e. hydraulic hysteresis) by relating directly to the SWCC.
4) The model was modified to relate the shear strength along the drying to the SWCC through the factor (exponent $k= 1/n$), where parameter "n" is related to the slope of the inflection point (near the AEV value). This parameter is related to the suction changes due to changes in watcer content, and is influenced by the soil type and the pore size of the sample.
5) The proposed model captured the shear strength behavior due to hysteresis through the factor F_{DW}, which is equal to the ratio of volumetric water contents (θ_d/θ_w, for sand and non-plastic silt where d and w refers to drying and wetting, respectively). This ratio represents the difference in the amount of water between drying and wetting at a given suction; and thus lower shear strength at higher water content (drying) compared to wetting with lower water content for the soil tested in this study.
6) A consistent and unique trend (i.e. bell shape, an increase then decrease with suction) of this ratio (θ_d/θ_w) was observed for different soil types and test conditions.
7) The proposed model predicted well the various shear strength results with suction along the drying curve, obtained from the literature. It was also able to predict the shear strength results from literature due to wetting, although limited

drying/wetting results were found. Note that $F_{DW} = \theta_w/\theta_d$ was used for the shear strength of clayey soils (from literature) due to wetting.

8) Soil behavior due to drying/wetting is believed to be influenced by suction loading history and water-solid contact area. Based on the tests from this study and the preliminary results found in the literature, it is postulated that the behavior due to drying/wetting for each soil type (i.e., soil behaving as sand or clay) maybe dominated more by one or the other. For cohesionless soils, cyclic suction stress (resulting in hardening effect) and the amount of water that may be acting as a lubricant may be the predominant influence resulting in higher shear strength for wetting compared to drying (since $\theta_w < \theta_d$). Thus, the ratio (θ_d/θ_w) is proposed to capture the influence of hysteresis in equations for strength for this type of soil. On ther other hand, for cohesive soils, whose shear strength due to drying/wetting appears lower than drying tests, the solid-liquid interfacical contact area is believed to be the predominant influence on the results. Thus, the ratio (θ_w/θ_d) was used for clayey soils, resulting in lower shear strength for wetting compared to drying

9) Results showed that the general elastoplastic constitutive model was overall capable of capturing the salient response features of unsaturated rough steel and soil-geotextile interfaces. The constitutive model was capable of capturing both the interface peak and the post peak shear strength responses to the increase in the applied suction and net normal stress. Similar to experimental results, the model showed that influence of suction was more pronounced at lower net normal

stresses. In addition, specimen volume change behavior in the interface shear tests was predicted with reasonable accuracy using this model.

5.3 RESILIENT MODULUS

Suction-controlled M_r tests were performed, on compacted samples, along the primary drying, wetting, secondary drying and wetting paths. Two test types were performed to check the effect net normal stress and of cyclic deviatoric stress loading history on the results. The first set of M_r tests were performed on the same sample at each suction (i.e. 25, 50, 75, 100 kPa) value along all different SWCC paths. A relationship between resilient modulus (M_r) and matric suction was obtained and identified as the resilient modulus characteristic curve (MRCC). The second set of M_r tests were performed at selected suction along the SWCC without previous M_r tests (virgin samples) to study the effect of stress loading history on the results.

The conclusions and observations based on the results are summarized as follows:

1) Resilient modulus (M_r) slightly increased with increase in deviator stress (σ_d). This increase seems dependent on suction where a more pronounced increase is observed at higher suction values.

2) Resilient modulus tends to increase with an increase in matric suction. This increase was attributed to the fact that higher soil suction results in stiffening of the specimens.

3) The MRCC exhibited a hysteretic behavior similar to that of the SWCC. For a given suction, M_R values on MRCC on the wetting curve are higher than that on the drying.

4) Duplicate suction controlled M_r tests on the primary drying and wetting paths demonstrate that the MRCC is reproducible to reasonable accuracy.
5) Selected tests (i.e. at specific suction of 25 and 50 kPa, on drying and wetting) were conducted without previous M_r tests on virgin samples. Corresponding M_r values were lower than from the sample tested continuously at each suction value. This indicates that the accumulation of net normal stress and cyclic deviatoric stress loading history has an effect on the results.
6) It is believed that the hardening effect and the possible water content lubricant effect (at same suction), due to cyclic suction (i.e., hysteresis) may be the reason for higher M_r on the wetting compared to drying.
7) A model was proposed to predict M_r along the drying and wetting curves based on the SWCC. The proposed model seemed to predict M_r due to hydraulic hysteresis (i.e. SWCC suction hysteresis, or cyclic suction loading) for all stress levels.

5.4 RECOMMENDATIONS FOR FUTURE RESEARCH

1) Study further the effect of stress loading history on the shearing behavior of unsaturated interfaces by conducting suction-controlled interface direct shear tests following different stress paths from the one presented in this study.
2) The present study used an artificial soil for testing, whose behavior may be different than that of unsaturated natural soils, especially if wetting and drying cycles are involved. Therefore, experimental research should be carried out on different types of materials such as clayey natural soils. However, there exist numerous practical limitations (e.g., excessively long testing time and maximum possible target suction) for testing on natural clayey soils.

3) Compare the influence of hydraulic hysteresis on natural clayey soils to the results on the artificial soil obtained in this study. Develop a further framework and analysis on the effect of hydraulic hysteresis on different type of soils (i.e., natural sands and clay) whose behavior are believed to be significantly different.
4) Use and validate the proposed models from this study to predict shear strength with suction based on the experimental results obtained on natural soils.
5) Modify the general elastoplastic constitutive model for unsaturated interfaces by incorporating the effect of hydraulic hysteresis into the model.
6) Incorporate the constitutive model into finite element (FE) framework for interface boundary value problems.
7) Test methods on fine-grained cohesive soils (e.g. clayey soils) require extremely long equilibrium times to produce changes in suction, which practically prohibits routine examination of the hydraulic hysteresis and its influence on resilient modulus. Thus, future research may overcome this obstacle by possibly developing a miniature suction controlled unsaturated triaxial apparatus compatible with very small samples (e.g., sample height as small as 1"). Such research may be a precursor to advanced testing of unsaturated soils whereby suction controlled resilient modulus tests on fine grained soils will be practical. The equipment will not be limited to resilient modulus testing, but will be fully capable of conducting traditional large strain quasi-static shear tests on soils.
8) Use and validate the proposed M_r model from this study to predict M_r based on the experimental results obtained on natural soils.

9) Develop practical recommendations for incorporating the effects of hydraulic hysteresis (wetting/drying cycles) in determination of design strength and stiffness for geotechnical applications.

REFERENCES:

Abramento, M., and Carvalho, C. S., (1989), "Geotechnical Parameters for the Study of Slopes Instabilisation at Serra do Mar-Brazilian Southeast," *Proceedings of the 12th International Conference on Soil Mechanics and Foundation Engineering*, Rio de Janeiro, Vol. 3, pp. 1599-1602.

Alonso, E.E., A. Gens and Josa, A., (1990), "A Constitutive Model for Partially Saturated Soils," *Géotechnique*, Vol. *40, No. 3*, pp. 405-430.

Alramahi, B., Alshibli, K. A., Fratta, D., and Trautwein, S., (2008), "A Suction-Control Apparatus for the Measurement of P and S-Wave Velocity in Soils," Geotechnical Testing Journal, Vol. 31, No. 1, pp. 1-12.

American Association of State Highway and Transportation Officials (AASHTO), (2002), "Standard specifications for highway bridges," *17th ed. American Association of State Highway and Transportation Officials*, Washington, DC, USA.

American Association of State Highway and Transportation Officials, (AASHTO) (2007), http://www.mrr.dot.state.mn.us/pavement/PvmtDesign/designguide.asp, accessed February, 2008.

American Society for Testing and Materials (ASTM), (2009), Volume 04.13, *Geosynthetics, ASTM International*, W. Conshohocken, PA, USA.

Acar, Y.B., Durgunoglu, H.T., Tumay, M. T., (1982), "Interface Properties of Sand," *Journal of Geotechnical Engineering,* ASCE, Vol. 108, No. GT4, pp. 648-654.

Adamson, A. W., (1990), "Physical Chemistry of Surfaces," 5th Edition, Wiley Interscience, New York.

Bao, C., Gong, B., and Zhan, L., (1998), "Properties of Unsaturated Soils and Slope Stability of Expansive Soils," Keynote Lecture, *Proceedings of the 2nd International Conference on Unsaturated Soils*, Beijing, China, Vol. 1, pp. 71-98.

Barbour, S. L., (1998), "Nineteenth Canadian Geotechnical Colloquium: The Soil Water Characteristic Curve: a Historical Perspective," *Canadian Geotechnical Journal*, Vol. 35, pp. 873-894.

Bear, J., (1972), "Dynamics of Fluids in Porous Media," Dover Publications, Inc., New York.

Berg, R.R.; Christopher, B.R. and Samtani, N.C., (2009), "Design and Construction of Mechanically Stabilized Earth Walls and Reinforced Soil Slopes – Volumes I & 2. NHI Courses No. 132042 and 132043," *U. S. Department of Transportation Federal Highway Administration*, FHWA-NHI-10-024, Federal Highway Administration, Washington, DC, USA.

Billota, E., Foresta V., and Migliaro, G., (2006), "Suction Controlled Laboratory Test on Undisturbed Pyroclastic Soil: Stiffnesses and Volumetric Deformations," *Proceedings of the Fourth International Conference of Unsaturated Soils*, UNSAT 2006, ASCE, Carefree, Arizona, pp. 849-860.

Bishop, A.W., (1959), "The Principle of Effective Stress," *Teknisk Ukeblad*, Vol. 106, No. 39, pp. 859-863.

Blatz, J. A., Graham, J., and Chandler, N. A., (2002), "Influence of Suction on the Strength of Compacted Sand-Bentonite," *Canadian Geotechnical journal,* Vol. 39, pp. 1005-1015.

Boulon, M. and Nova, R., (1990), "Modeling of Soil-Structure Interface Behaviour-A Comparison Between Elastoplastic and Rate Type Laws," *Computers and Geotechnique*, Vol. 9, pp. 21-46.

Bradshaw, A. S. And Baxter, C. D. P., (2006), "Design and Construction of Driven Pile Foundations: Lessons Learned on the Central Artery/Tunnel Project," *U.S. Department of Transportation Federal Highway Administration*, FHWA-HRT-05-159, Federal Highway Administration, McLean, VA, USA.

Brumund, W. F. and Leonards, G. A., (1973), "Experimental Study of Static and Dynamic Friction between Sand and Typical Construction Materials," *Journal of Testing and Evaluation*, JTEVA, Vol. 1, No. 2, pp. 162-165.

Brooks, R.H., and A.T. Corey., (1964), "Hydraulic properties of porous media," *Hydrology Paper 3,* Colorado State Univ., Fort Collins.

BS8006, (1995). British Standard, Code of practice for strengthened/reinforced soils and other fills, BSI.

Cary, C. E., Zapata, C. E., (2010), "Resilient Modulus Testing for Unsaturated Unbound Materials," *Transportation Research Record: Journal of Transportation Research Board*, TRB, Washington D.C.

Ceratti, G. A., Gehling, W. Y. Y., and Nunez, W. P. (2004), " Seasonal Variations of Subgrade Soil Resilient Modulus in Southern Brazil," *Transportation Research Record: Journal of Transportation Research Board*, No. 1874, TRB, Washington D.C., pp. 165-173.

Chiu, C. F., and Ng, C. W. W., (2003), "A State-Dependent Elastoplastic Model for Saturated and Unsaturated Soils," *Geotechnique*, Vol. 53, pp. 809-829.

Christopher, B.R., Zornberg, J.G. and Mitchell, J.K., (1998), "Design Guidance for Reinforced Soil Structures with Marginal Soil Backfills," *Sixth International Conference on Geosynthetics*, Atlanta, GA, USA, 1, pp. 797-804.

Clough, G. W., and Duncan, J. M., (1971), "Finite Element Analyses of Retaining Wall Behavior," *Journal of the Soil Mechanics and Foundations Division,* ASCE, Vol. 97, No. SM12, pp. 1657-1673.

Cui, Y. J., and Delage, P., (1996), "Yielding and Plastic Behavior of Unsaturated Compacted Silt," *Geotechnique*, Vol. 46, No. 2, pp. 291-311.

Dafalias, Y.F. and E.P. Popov, (1975), "A Model of Nonlinearly Hardening Materials for Complex Loading," *Acta Mechanica*, *21*, pp. 173-192.

Dafalias, Y.F. and E.P. Popov, (1976), "Plastic Internal Variables Formalism of Cyclic Plasticity," *Journal of Applied Mechanics*, *43*, pp. 645-651.

Desai, C. S., (1980), "A General basis for Yield, Failure and Potential Functions in Plasticity," *International Journal of Numerical and Analytical Methods in Geomechanics*, Vol. 4, pp. 361-375.

Desai, C. S. and Faruque, M. O., (1984), "Constitutive Model for (Geological) Materials," *Journal of Engineering Mechanics Division*, ASCE, Vol. 110, No.9, pp. 1391-1408.

Desai, C. S., Drumm, E. C., and Zaman, M. M., (1985), "Cyclic Testing and Modeling of Interfaces," ASCE, *Journal of Geotechnical Engineering*, Vol.111, No.6, pp.793-815.

Desai, C. S., and Fishman, K. L., (1991), "Plasticity-Based Constitutive Model with Associated Testing for Joints," *Int. j. of Rock Mech. Min. Sci. & Geomech. Abstr*. Vol. 28, No.1, pp. 15-26.

Desai, C. S., Somasundaram, S., Frantziskonis, G., (1986), "A Hierarchical Approach for Constitutive Modelling of Geologic l Materials," *International Journal of Numerical and Analytical Methods in Geomechanics*, Vol. 10, pp. 225-257.

Drumm, E. C., and Desai, C. S., (1986), "Determination of Parameters for a Model for the Cyclic Behaviour of Interfaces," *Earthquake Engineering and Structural Dynamics*. Vol. 14, pp.1-18.

Drumm, E.C., Reeves, J.S., Madgett, M.R., and Trolinger, W.D., (1997), "Subgrade Resilient Modulus Correction for Saturation Effects," *Journal of Geotechnical and Geo-environmental Engineering*, Vol. 123, No. 7, 1997.

Edris, E. V., Jr., and Lytton, R. L. (1976). "Dynamic Properties of Subgrade Soils including Environmental Effects." *Texas Transportation Institute Rep. No. TTI-2-18-74-164-3*, Texas A&M Univ., College Station, Texas.

Elias, V., Christopher, B.R. and Berg, R.R., (2001), "Mechanically Stabilized Earth Walls and Reinforced Soil Slopes-design and Construction Guidelines," *FHWA-NHI-00-043*, Federal Highway Administration, Washington, DC, USA.

Escario, V., and Juca, J.F.T., (1989), "Strength and Deformation of Partly Saturated Soils," *Proceedings of the 12th ICSMFE*, Vol.1, pp.43-46.

Escario, I., and Saez, J., (1986), "The Shear Strength of Partly Saturated Soils," *Geotechnique*, Vol. 36, pp. 453-456.

Evgin, E. and Fakharian, K., (1996), "Effect of Stress Path on Interface Behaviour," *Canadian Geotechnical Journal*, Vol. 33, No. 6, pp. 853-865.

Fakharian, K. and Evgin, E., (1996), "An Automated Apparatus for Three-Dimensional Monotonic and Cyclic Testing of Interfaces," *Geotechnical Testing Journal*, Vol. 19, No. 1, pp. 22-31.

Fakharian, K. and Evgin, E., (2000), "Elasto-Plastic Modelling of Stress-Path-Dependent BNehavious of Interfaces," *Int. J. Num. and Anal. Meth. Geomech.*, Vol. 24, pp. 183-199

Faris, M. M., Pinheiro, M., and Neto, M. P. C., (2006), "An Elastoplastic Model for Unsaturated Soils under General Three-Dimensional Conditions," *Soils and Foundations*, Vol. 46, No. 5, pp. 613-628.

Feng, M. and D.G. Fredlund (1999), "Hysteretic influence associated with thermal conductivity sensor measurements," Proceedings from Theory to the Practice of Unsaturated Soil Mechanics, in associated with 52nd Can. Geotech. Conference and Unsaturated Soil Group, Regina.

Fleming, I.R., Sharma, J.S., and Jogi, M.B. (2006), "Shear Strength of Geomembrane-Soil Interface under Unsaturated Conditions," *Geotextiles and Geomembranes*, 24, pp. 274-284.

Fredlund, D.G., Morgenstern, N.R., and Widger, R.A., (1978), "The Shear Strength of Unsaturated Soils," *Canadian Geotechnical Journal*, Vol. 15, No. 3, pp. 313-321.

Fredlund, D.G., and Rahardjo, H. (1993), "Soil Mechanics of Unsaturated Soils," John Wiley and Sons, NY.

Fredlund, D.G., and Xing, A., (1994), "Equations for the Soil Water Characteristic Curve," *Canadian Geotechnical Journal*, Vol. 31, pp. 521-532.

Fredlund, D.G., and Xing, A., and Huang, S., (1994), "Predicting the Permeability Function for Unsaturated Soils using the Soil Water Characteristic Curve," *Canadian Geotechnical Journal*, Vol. 31, pp. 533-546.

Frost, J.D. and Han, J., (1999), "Behavior of Interfaces between Fiber-Reinforced Polymers and Sands," *ASCE J. of Geotechnical and Geoenvironmental Engineering*, 125(8), pp. 633-640.

Galage, C. P. K., Uchimura, T., (2006), "Effects of Wetting and Drying on the Unsaturated Shear Strength of a Silty Sand Under Low Suction," *Proceedings of the Fourth International Conference of Unsaturated Soils*, UNSAT 2006, ASCE, Carefree, Arizona, pp. 1247-1258.

Garven, E. A., and Vanapalli, S. K., (2006), "Evaluation of Emperical Procedures for Predicting the Shear Strength of Unsaturated Soils," *Fourth International Conference of Unsaturated Soils*, UNSAT 2006, ASCE, Carefree, Arizona, pp. 2570-2592.

Gallipoli, D., A. Gens, R. Sharma and J. Vaunat (2003), An elasto-plastic model for unsaturated soil incorporating the effects of suction and degree of saturation on mechanical behavior, *Géotechnique,*53(1), 123-135.

Gan, J. K. M., Fredlund, D. G., and Rahardjo, (1988), "Determination of Shear Strength Parameters of an Unsaturated Soil Using Direct Shear Test," *Canadian Geotechnical journal*, Vol. 25, No. 8, pp. 500-510.

Geiser, F., Laloui, L., and Vulliet, L., (2000), "Modelling the Behaviour of Unsaturated Silt," *Experimental Evidence and Theoretical Approaches in Unsaturated Soil*, Rotterdam: Balkema, pp. 155-175.

Goodhue, M.J., Edil T.B., and Benson, C.H., (2001), "Interaction of Foundry Sands with Geosynthetics," *ASCE J. of Geotechnical and Geoenvironmental Engineering*, 127(4), pp. 353-362.

Gourc, J. P., Reyes-Ramirez, R. and Villard, P., (2004), "Assessment of Geosynthetics Interface Friction for Slope Barriers of Landfill," *GeoAsia 2004*, pp. 116-149.

Guan, G. S., Rahardjo, H., and Choon, L. E., (2010), "Shear Strength Equations for Unsaturated Soil under Drying and Wetting," *Journal of Geotechnical and Geoenvironmental Engineering,* Vol. 136, No. 4, pp. 594-606.

Gupta, S, Ranaivoson, A., Edil, T., Benson, C., and Sawangsuriya, A, (2007), "*Pavement Design Using Unsaturated Soil Technology,"* Minnesota Department of Transportation, St. Paul, Minnesota, pp. 1-104.

Hamid, T.B., (2005), "Testing and Modeling of Unsaturated Interfaces," *Ph.D Dissertation*, *School of Civil Engineering and Environmental Science*, University of Oklahoma, Norman, Oklahoma.

Han, K.K., Rahardjo, H., and Broms, B.B., (1995), "Effect of hysteresis on the shear strength of a residual soil," *Proceeding of the first international conference on unsaturated soils*, Paris, 2, pp. 499–504.

Hamid, T. B., and Miller, G. A., (2008), "A Constitutive Model for Unsaturated Soil Interfaces," *International Journal for Numerical and Analytical Methods in Geomechanics*, Vol. 32, pp. 1693-1714.

Hamid, T.B., and Miller, G.A., (2009), "Shear Strength of Unsaturated Soil Interfaces," *Canadian Geotechnical Journal*, Vol. 46, No. 5, pp. 595-606.

Ho, K.M.Y., Ng, C.W.W., Ho, K.K.S. and W.H. Tang (2006), "State-dependent Soil-water Characteristic Curves (SDSWCCs) of Weathered Soils," *Proc. of UNSAT 2006*, *ASCE*, pp. 1302-1313.

Hu, L. and Pu, J., (2004), "Testing and Modeling of Soil-Structure Interface," *Journal of Geotechnical and Geoenvironmental Engineering*, Vol. 130, No. 8, pp. 851-860.

IFAI, (2009), "Geosynthetics Specifier Guide," *Industrial Fabrics Association International*.

Karube, D. and K. Kawai (2001), "The role of pore water in the mechanical behavior of unsaturated soils," *Geotechnical and Geological Engineering,* 19, 211-241.

Kayadelen, C., Tekinsoy, M. A., Taskiran, T., (2007), "Influence of Matric Suction on Shear Strength Behavior of a Residual Clayey Soil," *Environmental Geology*, Vol. 53, Issue 4, pp.891-901.

Khalili, N., and Khabbaz, M. H., (1998), "Unique Relationship for χ, for the Determination of the Shear Strength of Unsaturated Soils," *Geotechnique*, Vol. 48, No. 5, pp. 681-687.

Kishida, H. and Uesugi, M., (1987), "Tests of Interface Between Sand and Steel in the Simple Shear Apparatus," *Geotechnique*, Vol. 37, No. 1, pp. 45-52.

Khoury, N. N., Brooks, R., Zaman, M., Khoury, C. N., (2009), "Variations of Resilient Modulus of Sub-grade Soils with Post-Compaction Moisture Contents," *Transportation Research Record: Journal of the Transportation Research Board.* Transportation Research Board of the National Academies, Washington D.C.

Khoury, C. N., Khoury, N. N., (2009), "The effect of Moisture Hysteresis on Resilient Modulus of Subgrade Soil," *Eighth International Conference on the Bearing Capacity of Roads, Railways, and Airfields*, Champaign, Illinois, USA.

Khoury, C., N., Miller, G. A., and Hatami, K. (2010), ″ Unsaturated Soil-Geotextile Interface Behavior, ″ *Geotextiles and Geomembranes Journal*, in press.

Khoury, N. N., and Zaman, M., (2004), "Correlation Among Resilient Modulus, Moisture Variation, and Soil Suction for Subgrade Soils," *Transportation Research Record. 1874*, Transportation Research Board, Washington, D.C., 99–107.

Khoury, N. N., Zaman, M., Nevels, J. B., and Mann, J. (2003). "Effect of soil suction on resilient modulus of subgrade soil using the filter paper technique." *Proc., Transportation Research Board,* National Research Council, Washington, D.C.

Koerner, R.M., (2005), "Designing with Geosynthetics," *5th Edition Pearson Prentice Hall*, Upper Saddle River, NJ, USA.

Kohgo, Y., (2008), "A Hysteresis Model of Soil Water Retention Curves Based on Bounding Surface Concept," *Soils and Foundations*, Vol. 58, No. 5, pp. 633-640.

Kohgo, Y., Nakano, M., and Miyazaki, T., (1993), "Theorethical Aspects of Constitutive Modelling for Unsaturated Soils," *Soils and Foundations*, Vol. 33, No. 4, pp. 49-63.

Kung, J. H. S., Lin, H. D., Yang, S. J. and Huang. W. H., (2006), "Resilient Modulus and Plastic Strain of Unsaturated Cohesive Subgrade Soils." *The 4th International Conference on Unsaturated Soils*, ASCE, Arizona, Vol. 1, pp. 541-552.

Larson, G., and Dempsey, B. J. (1997). "Integrated climatic model, Version 2.0." *Rep. No. DTFA MN/DOT 72114*, Univ. of Illinois at Urbana- Champaign and Newmark Civil Engineering Laboratory, Urbana, Ill.

Lawson, C., (2005), "Geosynthetic Reinforced MSE Walls and Slopes with Fine grained Fills: International Perspectives," *NAGS 2005/GRI-19 Conference*, Las Vegas, Nevada, USA.

Lee, I. M., Sung, S. G., Cho, G. C., (2005), " Effect of Stress State on the Unsaturated Shear Strength of a Weathered Granite," Canadian Geotechnical Journal, Vol. 42, pp. 624-631.

Leong, E. C., Rahardjo, H., (1997), "Review of Soil Water Characteristic Curve Equations," *Journal of Geotechnical and Geoenvironmental Engineering*, ASCE, Vol. 123, No. 12, pp 1106-1117.

Li, X.S., (2007a), Thermodynamics-based constitutive framework for unsaturated soils 1: Theory, *Géotechnique*, *57(5)*, pp. 411-422.

Li, X.S., (2007b), "Thermodynamics-based Constitutive Framework for Unsaturated Soils 2: A Basic Triaxial Model," *Geotechnique*, *57(5)*, pp. 423-435.

Liang, R. Y., Rabab'ah, S., and Khasawneh, M., (2007), "Predicting Moisture Content-Dependent Reislient Modulus of Cohesive Soils Using Soil Suction Concept," *Journal of Transportation Enigneering*, ASCE, Vol. 134, No. 1.

Likos, W. J., and Lu, N., (2004), "Hysteresis of Capillary stress in Unsaturated Granular Soil," *Journal of Engineering Mechanics*, Vol. 130, No. 6, pp. 646-655.

Lu, N. and Likos, W.J., (2004), *Unsaturated Soil Mechanics*, Wiley, New York.

Lu, N. and Likos, W.J., (2006), "Suction Stress Characteristic Curve for Unsaturated Soil," *Journal of Geotechnical and Geoenvironmental Engineering*, Vol. 132, No. 2, pp. 131-142.

Macari, E. J., Hoyos, L. R., and Arduino, P., (2003), "Constitutive Modeling of Unsaturated Soil Behavior under Axisymmetric Stress States using a Stress/Suction-Controlled Cubical Test Cell," *International Journal of Plasicity*, Vol. 19, pp. 1481-1515.

Marshal, T. J., Holmes, J. W., Rose, C. W., (1996), *Soil Physics*, third edition. Cambridge: Cambridge, University Press.

Matsuoka, H., Sun, D., Kogane, A., Fukuzawa, N., and Ichihaea, W., (2002), "Stress-Strain Behaviour of Unsaturated Soil in True Triaxial Tests," Cana*dian Geotechnical Journal*, Vol. 39, pp. 608-619.

Mendoza, C. E., and Colmenares, J. E., (2006), "Influence of Suction on the Stiffness at Very Small Strains," *Proceedings of the Fourth International Conference of Unsaturated Soils*, ASCE, Carefree, Arizona, pp. 529-540.

Miller, G. A. and Hamid, T. B., (2007), "Interface Direct Shear Testing for Unsaturated Soil. *Geotechnical Testing Journal, Vol. 30, No.3.*

Miller, G. A., Khoury, C. N., Muraleetharan, K. K., Liu, C., and Kibbey, T. C. G. (2008), "Effects of Solid Deformations on Hysteretic Soil Water Characteristic Curves: Experiments and Simulations," *Water Resources Research Journal, 44, W00C06, doi:10.1029/2007WR006492.*

Mitchell, J.K. and Zornberg, J.G., (1995), "Reinforced Soil Structures with Poorly Draining Backfills. Part II: case histories and applications," *Geosynthetics International*, Vol. 2, No. 1, pp. 265-307.

Motan, S. E., and Edil, T. B., (1982), "Repetitive-Load Behavior of Unsaturated Soils," *Transportation Research Record*, No. 872, Washington, D.C., pp. 41-48.

Muraleetharan, K.K., Liu, C., Wei, C.F., Kibbey, T.C.G. and Chen, L., (2008), "An elastoplastic framework for coupling hydraulic and mechanical behavior of unsaturated soils," *Int. J. Plasticity*, 25, 473-490.

Musser, S.W. and Denning, C., (2005), "Deep patch road embankment repair application guide," *United States Department of Agriculture Forest Service*, Technology & Development Program 7700. Transportation Management, October 2005, 0577 1204-SDTDC.

Navayogarajah, N., (1990), "Constitutive Modeling of Static and Cyclic Behavior of Interfaces and Implementation in Boundary Value Problems," Ph.D. Dissertation, Department of Civil and Engineering Mechanics, University of Arizona, Tucson, USA.

NCMA, (2002), "Design Manual for Segmental Retaining Walls," 2nd Edition, *National Concrete Masonry Association*, Herndon, VA, USA.

Navayogarajah, N., Desai, C. S., and Kiousis, P.D., (1992), "Hierarchical Single Surface Model for Static and Cyclic Behaviour of Interfaces," *Journal of Engineering Mechanics*, ASCE, Vol. 118, No.5, pp. 990-1011.

Ng., W. W. and Pang, Y.W., (2000), "Influence of Stress State on Soil-Water Characteristics and Slope Stability," *Journal of Geotechnical and Geoenvironmental Engineering*, *126(2)*, pp. 157-166.

Ng, C. W. W., Xu, J., Yung, S. Y., (2009), "Effects of Wetting-Drying and Stress Ratio on Anisotropic Stiffness of an Unsaturated Soil at Very Small Strains," *Canadian Geotechnical Journal*, Vol. 46, pp. 1062-1076.

Nishimura, T., Hirabayashi, Y., and Fredlund, D. G., (1999), "Influence of stress History on the Shear Strength Parameters of an Unsaturated Statically Compacted Soil," *Canadian Geotechnical Journal*, Vol. 36, pp. 251-261.

Nishimura, T., and Fredlund, D. G., (2002), "Hysteresis Effects Resulting from Drying and Wetting under Relatively Dry Conditions," *Proceeding of the third international conference on Unsaturated soils*, Recife, Brazil, pp.301-305.

Oberg, A., and Sallfours, G., (1997), "Determination of Shear Strength Parameters of Unsaturated Silts and Sands Based on the Water Retention Curve," *Geotechnical Testing Journal*, Vol. 20, pp. 40-48.

Oloo, S. Y. and Fredlund, D. G., (1996), "A method for determination of ϕ^b for Statically Compacted Soils," *Canadian Geotechnical Journal*, Vol. 33, No. 2, pp. 272- 280

Pham, H. Q., Fredlund , D.G., and Brabour, S. L., (2003), "A Practical Hysteresis Model for the Soil-Water Characteristic Curvefor Soils with Negligible Volume Change," *Geotechnique*, Vol. 53, No. 2, pp. 293-298.

Pham, H. Q., Fredlund , D.G., and Brabour, S. L., (2005), "A Study of Hysteresis Models for Soil Water Characteristic Curves," *Canadian Geotechnical Journal*, Vol. 42, No. 6, pp. 1548-1568.

Potyondy, J. G., (1961), "Skin Friction between Various Soils and Construction Materials," *Geotechnique*, Vol. 11, No. 4, pp. 831-853.

Powel, W., Keller, G.R. and Brunette, B., (1999), "Applications for Geosynthetics on Forest Service Low-Volume Roads," *Transportation Research Record,* 1652, pp. 113-120.

Ramberg, W. and Osgood, W. R., (1943), "Description of Stress-Strain Curves by Three Parameters," *Technical Note 902, National Advisory Committee for Aeronautics*, Washington, D.C.

Rampino, C., Mancuso, C., and Vinale, F., (2000), "Experimental Behavior and Modeling of an Unsaturated Compacted Soil," *Canadian Geotechnical Journal*, Vol. 37, pp. 748-763.

Rassam, D. W., and Cook, F. J., (2002), "Predicting the shear strength envelope of Unsaturated Soils," *Geotechnical Testing Journal*, Vol. 25, pp. 215-220.

Rassam, D. W., and Williams, D. J., (1999), "A Relationship Describing the Shear Strength of Unsaturated Soils," *Canadian Geotechnical Journal*, Vol. 36, pp. 363-368.

Romero, E., A. Gens, and A. Lloret (1999), "Water permeability, water retention and microstructure of unsaturated compacted Boom clay," *Engineering Geology*, 54, 117–127.

Sandri, D., (2005), "Drainage Recommendations for MSE Walls Constructed with Marginal Fills," *NAGS 2005/GRI-19 Conference*, Las Vegas, Nevada, USA.

Sharma, R. S., and Bukkapatnam, A. T., (2008), "An Investigation of Unsaturated Soil Stiffness," The 12th International Conference of International Association for Computer Methods and Advances in Geomechanics (IACMAG), Goa, India.

Sharma, J. S., Fleming, I.R., and Jogi, M.B., (2007), "Measurement of Unsaturated Soil-Geomembrane Interface Shear-Strength Parameters," *Canadian Geotechnical Journal*, Vol. 44, pp. 78-88.

Shemsu, K. A., Kiyama, S., Aoyama, S., Kobayashi, A., (2005), "Experimental Study of the Effect of Cyclic Suction Loading on Shearing Behavior of Collapsible Soils," *Proceedings of the International Symposium on Advanced Experimental Unsaturated Soil Mechanics*, Trento, Italy, pp. 235-241.

Sheng, D., Fredlund, D. G., and Gens, A., (2008), "A New Modelling Approach for Unsaturated Soils using Independent Stress Variables," *Canadian Geotechnical Journal*, Vol. 45, pp. 511-534.

Sia, A.H.I. and Dixon, N., (2007), "Distribution and Variability of Interface Shear Strength and Derived Parameters," Geotextiles and Geomembranes, 25(3): 139-154.

Silva, C. H. C., Ortiz, O. F. P, Fratta, D., and Macari, E. J., (2002), "Mechanical Response of Unsaturated Particulate Materials- AStiffness Assessment study under Controlled Matric Suction," *Proceedings of the International Mechanical Engineering Congress and Exposition (IMECE)*, New Orleans, Louisana.

Seed, H. B., and Chan, C.K., (1959), "Structure and Strength Characteristics of Compacted Clays," *Soil Mechanics and Foundation Division*, ASCE, Vol. 85, No. SM5, pp. 87-128.

Stulgis, R.P., (2005), "Full-scale MSE Test Walls," *NAGS 2005/GRI-19 Conference*, Las Vegas, Nevada, USA.

Sun, D.A., D.C. Sheng, H.B. Cui and S.W. Sloan, (2007a), "A Density-dependent Elastoplastic Hydro-mechanical Model for Unsaturated Compacted Soils," *International Journal for Numerical and Analytical Methods in Geomechanics*. *31*, pp. 1257-1279.

Sun, D. A., Sheng, D., and Sloan, S. W., (2007b), "Elastoplastic Modelling of Hydraulic and Stress-Strain Behaviour of Unsaturated Soils," *Mechanics of Materials*, Vol. 39, pp. 212-221.

Tarantino, A. and S. Tombolato (2005), "Coupling of hydraulic and mechanical behaviour in unsaturated compacted clay," *Géotechnique*, 55(4), 307–317.

Tekinsoy, M. A., Kayadelen, C., Keskin, M. S., and Soylemez, M., (2004), "An Equation for Predicting Shear Strength Envelope with Respect to Matric Suction," *Computers and Geotechnics*, Vol. 31, No. 7, pp. 589-593.

Thu, T. M., Rahardjo, H., and Leong, E. C., (2006), "Effects of Hysteresis on Shear Strength Envelopes from Constant Water Content and Consolidated Drained Triaxial Tests," *Proceedings of the Fourth International Conference of Unsaturated Soils*, ASCE, Carefree, Arizona, pp. 1212-1222.

Thu, T. M., Rahardjo, H., and Leong, E. C., (2007), "Elastoplastic Model for Unsaturated Soil with Incorporation of the Soil Water Characteristic Curve," *Canadian Geotechnical Journal*, Vol. 44, pp. 67-77.

Topp, G. C., (1971), "Soil Water Hysteresis in Silty Loam and Clay Loam Soils," *Water Resources Research Journal*, Vol. 7, No. 4, pp. 914-920.

Uesugi, M. and Kishida, H., (1986), "Frictional Resistance at Yield Between Dry Sand and Mild Steel," *Soils and Foundations*, Vol. 26, No. 4, pp. 139–149.

Van Genuchten, (1980), "A Closed Form Equation for Predicting the Hydraulic Conductivity of unsaturated soils," *Soil Science Society of American Journal*, Vol. 44, pp. 892–898.

Vanapalli, S.K., Fredlund, D.G., and Pufahl, D.E., (1999), "The Influence of Soil Structure and Stress History on the Soil Water Characteristic Curve of a Compacted Till," *Geotechnique*, 49, No. 2, pp. 143-159.

Vanapalli, S.K., Fredlund, D.G., and Pufahl, D.E., (2001), "Influence of Soil Structure and Stress History on the Soil Water Characteristics of a Compacted Till," *Geotechnique*, Discussion. Vol. LI, 6, pp. 573-576.

Vanapalli, S.K., Fredlund, D.G., Pufahl, D.E., and Clifton, A.W. (1996), "Model for the Prediction of Shear Strength with Respect to Soil Suction," Canadian Geotechnical Journal, 33, pp. 379-392.

Vassallo, R., Mancuso, C., Vinale, F., (2007), "Effects of net stress and suction history on the small strain stiffness of a compacted clayey silt," *Canadian Geotechnical Journal*, Vol. 44, pp. 447-462.

Vilar, O. M., (2006), "A Simplified Procedure to Estimate the Shear Strength Envelope of Unsaturated Soil," Canadian Geotechnical Journal, Vol. 43, pp. 1088-1095.

Wei, C. (2001), "Static and Dynamic Behavior of Multiphase Porous Media: Governing Equations and Finite Element Implementation," *Ph.D. Dissertation, University of Oklahoma*, Norman, Oklahoma.

Wei, C. and M.M. Dewoolkar, (2006), "Formulation of Capillary Hysteresis with Internal State Variables," *Water Resources Research*, *42*, W07405.

Wei, C. and K.K. Muraleetharan, (2002a), "A Continuum Theory of Porous Media Saturated by Multiple Immiscible Fluids: I. Linear Poroelasticity," *Int. J. Eng. Sci.*, *40(16)*, pp. 1807-1833.

Wei, C. and K.K. Muraleetharan, (2002b), "A Continuum Theory of Porous Media Saturated by Multiple Immiscible Fluids: II. Lagrangian Description and Variational Structure," *Int. J. Eng. Sci.*, *40(16)*, pp. 1835-1854.

Wheeler, S.J., R.S. Sharma and M.S.R. Buisson (2003), "Coupling of hydraulic hysteresis and stress-strain behavior in unsaturated soils," *Géotechnique*, *53(1)*, 41-53.

Wiebe, B., Graham, J., Tang, G. X., and Dixon, D., (1998), "Influence of Pressure, Saturation, and Temperature on the Behaviour of Unsaturated Sand-Bentonite," *Canadian Geotechnical journal,* Vol. 35, pp. 194-105.

Xu, Y. F., (2004), "Fractal Approach to Unsaturated Shear Strength," *Journal of Geotechnical and Geoenvironmental Engineering*, Vol. 130, No. 3, pp. 264-273.

Yang, H., Rahardjo, H., Leong, E. C., and Fredlund, D. G., (2004a), "A Study of Infiltration on Three Sand Cpillary Barriers," *Canadian Geotechnical Journal*, Vol. 41, pp. 629-643.

Yang, S. J., Huang. W. H., and Tai, Y. T., (2004b). "Variation of Resilient Modulus with Soil Suction for Compacted Subgrade Soils." *Proc., Transportation Research Board,* Annual Meeting, Washington, D.C.

Yang, S. R., Lin, H. D., Kung, J. H. S., Huang, W. H., (2008), "Suction-Controlled Laboratory Test on Resilient Modulus of Unsaturated Compacted Subgrade Soils," *Journal of Geotechnical and Geo-environmental Engineering*, Vol. 134, No. 9, pp. 1375-1384.

Yoshimi, Y. and Kishida, T., (1981), "Friction between Sand and Metal Surface," *Proceedings, 10th International Conference on Soil Mechanics and Foundation* Engineering, Vol. 1, pp. 831-834.

Yuan, D. and Nazarian, S., (2003), "Variation in Moduli of Base and Subgarde with Moisture," CD-ROM, *Transportation Research Board of the National Academies*, Washington D.C.

Zeghal, M. and Edil, T. B., (2002), "Soil Structure Interaction Analysis: Modeling the Interface," *Canadian Geotechnical journal*, Vol.39, pp. 620-628.

APPENDIX A: ELASTOPLASTIC CONSTITUTIVE MODEL PARAMETERS

DETERMINATION AND PHYSICAL MEANING OF THE MODEL PARAMETERS

(1) Ultimate or Failure Parameter, γ(s):

Parameter γ(s) represent the ultimate shear stress state of interface, which is related to net normal stress (σ_n- u_a), suction (through parameter R(s)) and interface roughness (R_n).

As shown in Equation 3.17, $\gamma(s)^{1/2} = \dfrac{\tau_p}{\sigma_{net} + R(s)} = \mu_{p1} + \mu_{p2} R_n$, thus the slope of ($\tau_p$) versus ($\sigma_n$ + R(s)) will give $\gamma(s)^{1/2}$, which is related to R_n through the material parameters μ_{p1} (intercept) and μ_{p2} (slope) of $\gamma(s)^{1/2}$ versus R_n, as shown in Figure A.1 (obtained from the experimental results of rough, smooth and geotextile interfaces).

The value $\gamma(s)^{1/2}$ can be thought of in a similar manner as *tan* ϕ in the Mohr Coulomb failure criteria, for a given interface roughness.

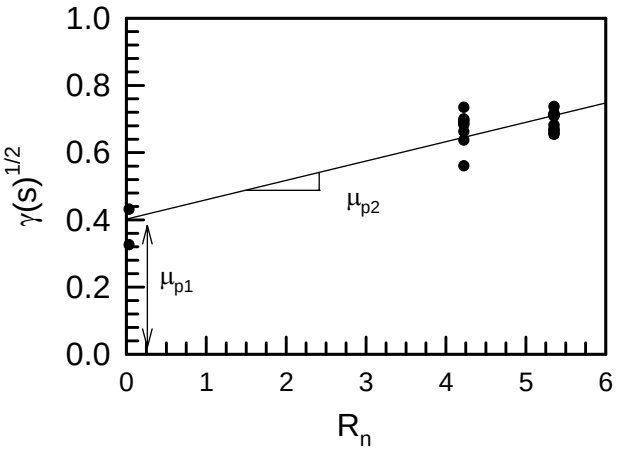

Figure A.1- Plot of $\gamma(s)^{1/2}$ vs R_n from the Experimental Results for Determination of μ_{p1} and μ_{p2}

(2) Bonding Stress R(s):

R(s) represents the increase in the strength of the unsaturated interface with the increase in suction; it can be thought as the value of effective cohesion in the net normal stress-shear stress plane. Since the shear strength was non-linear with change in suction, R(s) was related to suction as follows:

$$R(s) = \lambda_1(s)(u_a - u_w)^2 + \lambda_2(s)(u_a - u_w) + \lambda^*$$

where $\lambda^* = \lambda_1 R_n + \lambda_2$, thus for each interface λ^* is plotted versus R_n which provides parameters λ_1 (slope) and λ_2 (intercept).

(3) Phase Change Parameter (n):

The parameter *n* represents the phase change point, which permits transition of volumetric behavior from compression to dilation. In other words, *n* is related to a state of stress at which the material passes through a state of zero volume change. As reported by Hamid and Miller (2008), the phase change parameter expression used in this study is the modified form of the expression proposed by Wathugala (1990).

$$[\gamma_t^{1/2} / \gamma(s)^{1/2}] = [(n-2)/n]^{1/2}$$

where, $\gamma(s)^{1/2}$ is the slope of the ultimate line and $\gamma_t^{1/2}$ is the slope phase change line.

(4) Hardening Parameter (ξ_D^*, a and b):

The parameter ξ_D^* is represents the prepeak (or hardening phase) and postpeak (or softening phase) on interface (Navayogaraga 1990). ξ_D^* is equal to the value of ξ_D when shear stress reaches its peak value (i.e., when $\tau = \tau_p$).

Miller and Hamid (2008) reported that the experimental results show that ξ_D^* is not only dependent on roughness, but its value also changes with change in suction, similarly to what was observed in this study. Therefore, ξ_D^* was expressed as follows:

$$\xi_D^* = \left[\xi_{D1}^* + \xi_{D2}^* \left(R_n + R(s)/P_a\right)\right]$$

P_a is the atmospheric pressure. Parameters ξ_{D1}^* and ξ_{D2}^* represent the slope and intercept of ξ_D^* versus $\left[R_n + \left(R(s)/P_a\right)\right]$ plot, respectively as shown in Figure A.2 obtained from the experimental results of rough, smooth and geotextile interfaces.

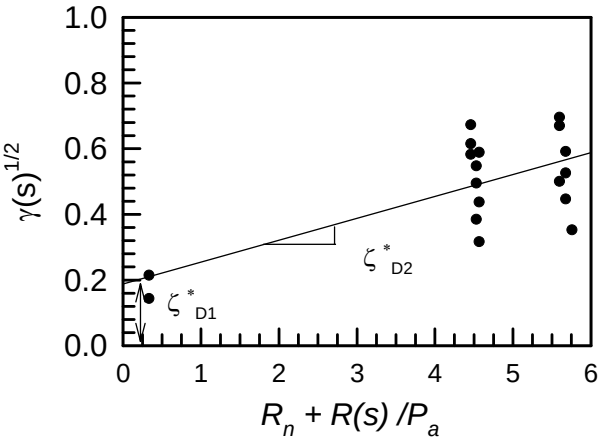

Figure A.2- Plot of $\gamma(s)^{1/2}$ vs $\left[R_n + \left(R(s)/P_a\right)\right]$ from the Experimental Results for Determination of ξ_{D1}^* and ξ_{D2}^*

Hardening parameters '*a*' and '*b*' are the slope and intercept of the best fit line between $[\{\ln\gamma(s) - \ln\alpha(s)\}/\ln\{(\xi_D^* - \xi_D)/\xi_D^*\}]$ versus $[\xi_v/\ln\{(\xi_D^* - \xi_D)/\xi_D^*\}]$ plot, as shown in Figure A.3 for a typical rough interface test. Data points are selected between 0 to ξ_D^* (or 0 to τ_p) to generate this plot. Parameters '*a*' and '*b*' are computed for each interface (rough, smooth or geotextiles) and suction value, and the averages are used for

prediction. These hardening parameters (i.e., *a* and *b*) control the compression and dilation of the interface and also the transition of the shear stress from peak to post peak. High values of both parameters result in increased dilation and decreased compression of interface behavior.

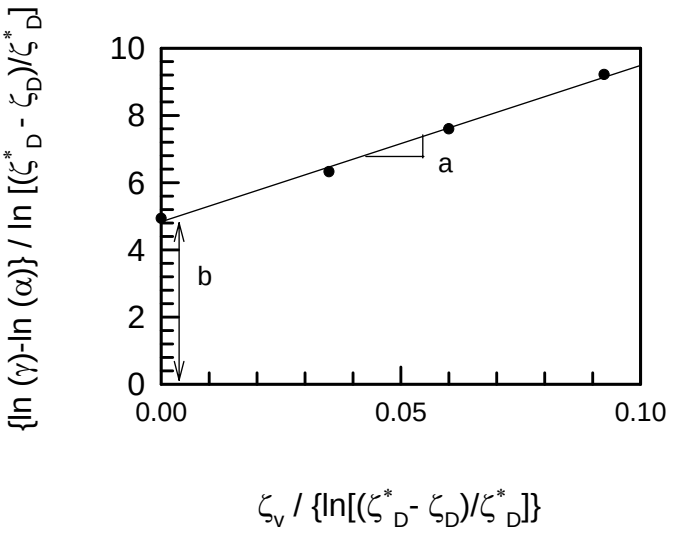

Figure A.3- Typical Plot of Rough Interface Tests Results for Determination of '*a*' and '*b*'

(4) Non-Associative Parameter (κ):

Non-associative parameter κ is defined as the plastic incremental ratio described by Navayogarajah (1990) and used by Miller and Hamid (2008) and is given and computed as follows:

$$\kappa = -[\gamma(s)]^{-1/2} * (dv^p / du^p)\Big|_{\xi_D = \xi_D^*}$$

where dv^p and du^p are the plastic displacements normal and tangential to the shearing surface, respectively.

Parameter κ for unsaturated interfaces tested in this study seemed to be related to the normalized roughness, and suction as follows:

$$\kappa = [\kappa_1 + \kappa_2 \{R_n + (R(s)/P_a)\}]$$

Where, parameters κ_1 and κ_2 can be computed as the intercept and slope of κ vs. $[R_n + R(s)/P_a]$ plot, respectively (Figure A.4).

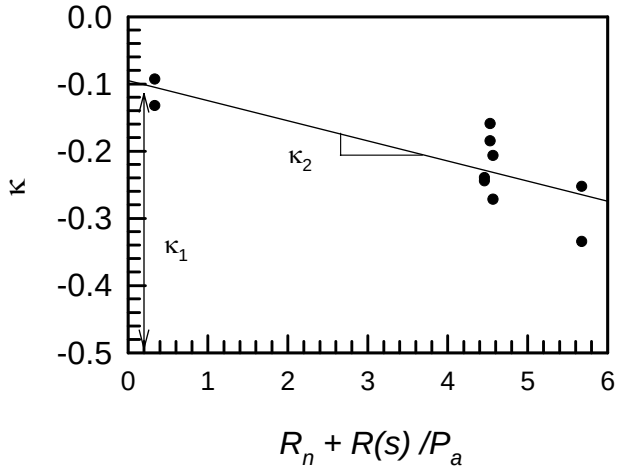

Figure A.4- Plot of κ vs $\left[R_n + \left(R(s)/P_a\right)\right]$ of Experimental Results for Determination of κ_1 and κ_2